A biogeography of the mesopelagic community

Roland Hudson Proud

Declarations

I, Roland Hudson Proud, hereby certify that this thesis, which is approximately 45,000 words in length, has been written by me, and that it is the record of work carried out by me, or principally by myself in collaboration with others as acknowledged, and that it has not been submitted in any previous application for a higher degree.

I was admitted as a research student in November, 2012 and as a candidate for the degree of PhD in November, 2013; the higher study for which this is a record was carried out at the University of St Andrews and the University of Tasmania between 2012 and 2016.

Date 01/04/2016 signature of candidate

I hereby certify that the candidate has fulfilled the conditions of the Resolution and Regulations appropriate for the degree of PhD at the University of St Andrews and that the candidate is qualified to submit this thesis in application for that degree.

Date 01/04/2016 signature of supervisor

I hereby certify that the candidate has fulfilled the conditions of the Resolution and Regulations appropriate for the degree of PhD at the University of Tasmania and that the candidate is qualified to submit this thesis in application for that degree.

Data 01/04/2016 signature of supervisor

In submitting this thesis to the University of St Andrews I understand that I am giving permission for it to be made available for use in accordance with the regulations of the University Library for the time being in force, subject to any copyright vested in the work not being affected thereby. I also understand that the title and the abstract will be published, and that a copy of the work may be made and supplied to any bona fide library or research worker, that my thesis will be electronically accessible for personal or research use unless exempt by award of an embargo as requested below, and that the library has the right to migrate my thesis into new electronic forms as required to ensure continued access to the thesis. I have obtained any third-party copyright permissions that may be required in order to allow such access and migration, or have requested the appropriate embargo below.

The following is an agreed request by candidate and supervisor regarding the publication of this thesis:

Embargo on all or part of print copy for a period of 1 year on the following ground: Publication would preclude future publication

Embargo on all or part of electronic copy for a period of 1 year on the following ground: Publication would preclude future publication

Date 01/04/2016 signature of candidate

Date 01/04/2016 signature of the supervisor

Abstract

There are a large number of research vessels and fishing vessels equipped with echosounders plying the world ocean, making continual observations of the ocean interior. Developing data collation programmes (e.g. Integrated Marine Observing System) and automated, repeatable analyses techniques enable the upper c. 1,200 meters of the world ocean to be sampled routinely, and for their characteristic deep scattering layers (DSLs) to be compared. Deep scattering layers are comprised of zooplankton (e.g. euphausiids) and fish, particularly myctophids or lantern fish, and comprise the majority of sub-surface biomass. Here we present, by the analysis of a global acoustic dataset, a mesopelagic biogeography of the sea. This was accomplished by (i) the collation and processing of a global active acoustic dataset, (ii) the development of a standardised and automated method of sound scattering layer (SSL) extraction and description, (iii) the derivation of the environmental drivers of DSL depth and biomass, (iv) the definition of a mesopelagic biogeography based on the drivers of DSL metrics and (v) the prediction, using output from the NEMO-MEDUSA-2.0 coupled model, of how the metrics and biogeography may change by 2100. Key findings include, the development of the Sound Scattering Layer Extraction Method (SSLEM) the inference that primary production, water temperature and wind stress are key drivers in DSL depth and biomass and that mesopelagic fish biomass may increase by 2100. Such an increase is a result of increased trophic efficiency from the shallowing of DSLs and rising water temperatures, suggesting, that as the climate warms the ocean is becoming more efficient. The biophysical relationships and biogeography derived here, serve to improve our understanding of mesopelagic mid-trophic level dynamics in open-ocean ecosystems. This will aid both fisheries and conservation management, which now adopt more holistic approaches when monitoring and evaluating ecosystem health and stability.

Acknowledgements

I would like to thank my supervisors, Andrew Brierley, Martin Cox and Simon Wotherspoon for their support and council. In particular, I would like to thank Andrew Brierley, for helping me, on a regular basis, in my understanding of ocean ecosystem function and providing me with many opportunities to collaborate with other scientists across different fields; this has led to my current position as a research fellow at the University of St Andrews.

I would also like to thank the Australian Antarctic Division (AAD), for partly funding the project and for all the help and guidance I received from various members of staff there including the team that I was proud and honoured to be a part of that took to the Southern Ocean on board the R/V Polarstern in August 2013: including, Simon Jarman, Rob King, Mark Milnes, Klaus Meiners and Elwood Mantel. I would also like to thank Martin Cox for securing my place on the expedition.

I would like to thank the Trans-Antarctic Association for funding my travel arrangements for field work on board the Polarstern.

I would also like to thank the crew and scientist on board the Polarstern. It was my first experience of at-sea field work and one that will stay with me for my entire life.

I would like to thank the Marine Alliance for Science and Technology (MASTS) they funded my travel to and from the international acoustics symposium in 2015 (SOME acoustics) without which I would not have been able to attend and present my work.

I would like to acknowledge the help of the Integrated Marine Observing System data centre (IMOS) and in particular, Tim Ryan, for advice and calibration training.

I would like to thank Rick Towler of NOAA for providing vital code for the pre-processing of the acoustic data.

I would like to thank Phil Hosegood for providing the SMILES EK60 data.

I would like to give thanks to the students, namely Katie Kirk, Katie Wurtzell and Laura Hobbs whom attended the Marine Bioacoustics workshop in Friday Harbor, Marta D'Elia from the Florida International University and Sam Gordine, Mirko Semler, Chris Mueller & Moritz Wiesel from the University of St Andrews, for taking the time to help with the validation of the Sound Scattering Layer Extraction Method (SSLEM).

Finally, I would like to thank my examiners, Dr Lars Boehme and Dr Jonathan Watkins for helpful comments and instruction.

Contents

List of Acronyms 1
List of Symbols 5
Chapter 1: General Introduction 9
1.1 Introduction 10
1.2 The mesopelagic region of the water-column 13
1.2.1 Zooplankton of the mesopelagic zone 15
1.2.2 Mesopelagic fish 16
1.2.3 Acoustic detection of mesopelagic fish 17
1.3 Sound Scattering Layers 20
1.4 Ocean Provinces 23
1.5 Aims 25
Chapter 2: Acquisition and pre-processing of a global acoustic dataset 27
2.1 Acoustic Data Collection 28
2.2 Acoustic Data Collation 29
2.3 Ocean Variables 33
2.4 Pre-processing of Acoustic Data 34
2.4.1 Data partition 34
2.4.2 Environmental Parameters and calibration 35
2.4.3 Volume Backscattering Strength 36
2.4.4 Masks, filters and thresholds 37
2.4.5 Seabed interruption 39
2.4.6 Mean Volume Backscattering Strength 40
Chapter 3: A method for identifying Sound Scattering Layers and extracting key characteristics 41
3.1 Introduction 42
3.1.1 Rainforest canopies and the pelagic water-column 42
3.1.2 The acoustic image 43
3.1.3 Aims 43
3.2 Materials and Method 45
3.2.1 Acoustic data 45
3.2.2 SSL extraction method (SSLEM) 46
3.2.3 Validation framework 56

3.3 Results 57
3.3.1 SSLEM Validation 57
3.3.2 SSL Metrics 61
3.4 Discussion 64
3.4.1 Sound Scattering Layer Extraction Method (SSLEM) 64
3.4.2 SSLEM parameterisation 64
3.4.3 SSLEM Results 65
3.4.4 SSLEM Applications 65
3.4.5 Summary 66
Chapter 4: Pelagic Regimes: Statistically distinct regional-scale biological water-column structures 67
4.1 Introduction 68
4.1.1 Primary production 68
4.1.2 Regional oceanography 70
4.1.3 Diel Vertical Migration 71
4.1.4 Geographical and temporal variance of the Deep Scattering Layer 72
4.1.5 Aims 73
4.2 Materials and Methods 74
4.2.1 SSLEM, SPDs and SPMs 74
4.2.2 Estimating DSL depth and NASC 77
4.2.3 Grouping the data: SPD distance, MDS and K-means 77
4.2.4 Pelagic regimes 78
4.2.5 Temporal analysis of Pelagic Regimes 79
4.3 Results 80
4.3.1 Cluster Selection 80
4.3.2 Pelagic Regimes 81
4.3.3 Spatial distribution of pelagic regimes 83
4.3.4 Pelagic regime descriptors 85
4.3.5 Temporal Variability at local scales 85
4.4 Discussion 87
4.4.1 Method 87
4.4.2 Water-column structure 88
4.4.3 Spatial and temporal patterns of pelagic regimes 89
4.4.4 Implications and conclusions 90
Chapter 5: A present estimate of global mesopelagic fish biomass 91

5.1 Introduction 92
5.1.1 Drivers of deep scattering layer depth 92
5.1.2 Drivers of deep scattering layer biomass 94
5.1.3 Acoustic estimates of biomass 95
5.1.4 Aims 97
5.2 Materials and Methods 98
5.2.1 Estimating mesopelagic fish NASC values 98
5.2.2 Estimating mesopelagic fish biomass 98
5.2.3 Weighted linear regression 101
5.2.4 Explanatory variables 102
5.3 Results 105
5.3.1 Regression model results 105
5.3.2 Optimum weighted linear regression models for Z_{PDSL} and MFB 106
5.3.3 Explanatory variables 108
5.3.4 Global Z_{PDSL} and MFB 110
5.4 Discussion 112
5.4.1 Deep scattering layer depth 112
5.4.2 Deep scattering layer biomass 113
5.4.3 Implications 114
5.4.4 Conclusions 115
Chapter 6: A biogeography of the mesopelagic community 117
6.1 Introduction 118
6.1.1 Surface provinces 118
6.1.2 Pelagic coupling 119
6.1.3 Trophic flow in marine ecosystems 119
6.1.4 Predicting change in the ocean 120
6.1.5 Aims 121
6.2 Materials and Methods 123
6.2.1 Mesopelagic Classes 123
6.2.2 Multiple models 124
6.2.3 Trophic Efficiency 124
6.2.4 NEMO-MEDUSA-2.0 125
6.3 Results 127
6.3.1 K-means model results and model selection 127

6.3.2 Mesopelagic Biogeography 130
6.3.3 Global predictions of Z_{PDSL}, MFB and TE 133
6.3.4 Global change in the pelagic ocean 135
6.3.5 Pelagic Ecosystem resilience 137
6.4 Discussion 139
6.4.1 Mesopelagic biogeography 139
6.4.2 Predicted change in the ocean 140
6.4.3 NEMO_MEDUSA-2.0 predictions 140
6.4.4 Implications 141
6.4.5 Conclusions 142
Chapter 7: Conclusions 143
7.1 Summary 144
7.2 Implications of results 146
7.2.1 Pelagic regimes 146
7.2.2 Biophysical drivers of DSL depth and biomass 147
7.2.3 Mesopelagic biogeography 150
7.3 Future Directions 153
7.3.1 Data collaboration and SSLEM 153
7.3.2 Data analysis 154
7.3.3 Mesopelagic fish distribution and Target Strength 154
7.3.4 Future work 155
7.4 Concluding remarks 157
Bibliography 159
Appendix A: Disclaimer of collaborative contributions 176
Appendix B: Derivation and definition of acoustic variables 177
Appendix C: Deep Scattering Layers: A history 179
Appendix D: Myctophidae relationships 185
Appendix E: Ocean Phenomenon 187

List of Acronyms

AAD	Australian Antarctic Division
ADCP	Acoustic Doppler Current Profiler
AMT	Atlantic Meridional Transect
BAS	British Antarctic Survey
BIC	Bayesian Information Criterion
BIOT	British Indian Ocean Territory
BNL	Background Noise Level
BODC	British Oceanographic Data Center
CI	Confidence Interval
CMIP	Coupled Model Intercomparison Project
CPA	Change Point Analysis
CZCS	Coastal-Zone Color Scanner
DO	Dissolved Oxygen
DSL	Deep Scattering Layer
DVM	Diel Vertical Migration
ENSO	El-Nino Southern Oscillation
FV	Fishing Vessel
IMOS	Integrated Marine Observing System
ISSG	Indian South Subtropical Gyre Province
LL	Log-Likelihood
MB	Mesopelagic Biogeography
MC	Mesopelagic Class
MDS	Multi-Dimensional Scaling
MESOPP	Mesopelagic Southern Ocean Prey and Predators
MF	Mesopelagic Fish
MFB	Mesopelagic Fish Biomass
MFP	Mesopelagic Fish Production
MLD	Mixed Layer Depth
MODIS	Moderate Resolution Imaging Spectrometer
MPA	Marine Protected Area

List of Acronyms

MPM	Mesopelagic Model
MVBS	Mean Volume Backscattering Strength
MZ	Migrant Zone
NASA	National Aeronautics Space Administration
NASC	Nautical Area Scattering Coefficient
NEMO	Nucleus for European Modelling of the Ocean
NGDC	National Geophysical Data Center
NODC	National Oceanographic Data Center
NPTG	North Pacific Tropical Gyre Province
OBIS	Ocean Biogeographical Information System
OMZ	Oxygen Minimum Zone
OPR	Ocean Pelagic Regimes
PA	Percentage Assigned
PAR	Photosynthetically Active Radiation
PER	Pelagic Ecosystem Resilience
PERG	Pelagic Ecology Research Group
PF	Polar Front
POM	Particulate Organic Matter
PP	Primary Production
PPR	Polar Pelagic Regime
PR	Pelagic Regime
pTL	per Trophic Level
RCP	Representative Concentration Pathway
RMSE	Root-Mean-Square Error
RV	Research Vessel
SEAPODYM	Spatial Ecosystem and Populations Dynamics Model
SHAPES	Shoal Analysis and Patch estimation system algorithm
SIMFAMI	Species Identification Methods from Acoustic Multi-frequency Information
SMILES	Surface Mixed Layer Evolution at Sub-mesoscales Cruise
SNR	Signal-to-Noise Ratio
SODA	Simple Ocean Data Assimilation

List of Acronyms

SONA	Southern Ocean Network of Acoustics
SONAR	Sound Navigation & Ranging
SP	Surface Province
SPD	Sound Scattering Layer Probability Distribution
SPM	Sound Scattering Layer Probability Map
SSL	Sound Scattering Layer
SSLEM	Sound Scattering Layer Extraction Method
SST	Sea Surface Temperature
ssT	Sub-Surface Temperature
SSTC	South Subtropical Convergence Province
STCZ	Subtropical Convergence Zone
TE	Trophic Efficiency
TL	Trophic Level
TS	Target Strength
TVG	Time-Varied Gain
UNESCO	United Nations Educational, Scientific and Cultural Organization
UTAS	University of Tasmania
VGPM	Vertically Generalized Production Model
WLR	Weighted Linear Regression

List of Symbols

Commonly used Symbols

S_V	Volume Backscattering Strength
TS	Target Strength
Z_{PDSL}	Depth of the primary deep scattering layer component
ssT_{PDSL}	Water temperature at the depth of the primary deep scattering layer component
τ	Wind stress

Chapter 1

N_v	numerical density of acoustic targets

Chapter 2

c	sound speed
G_0	transducer peak gain
P_r	received power
P_t	transmitted power
R	Range
$S_a$correction	Simrad correction factor
α	absorption coefficient
λ	wavelength
τ	pulse duration
Ψ	equivalent beam angle

Chapter 3

μ	mean MVBS over simple analysis window
μ_1	mean MVBS over split analysis window/column towards sea-surface
μ_2	mean MVBS over split analysis window/column towards seabed
CPA_{int}	Unit time of CPA analysis
CPA_{max}	Maximum absolute value of CPA cumulative sum
d_1	depth range of split analysis window/column towards the sea-surface
d_2	depth range of split analysis window/column towards the seabed
px	acoustic pixel
r	row number of acoustic pixel being evaluated

R	Total number of rows
ssl	Boolean variable, indicating if acoustic pixel is within (1) or outside of an SSL (0)
X	space/time extent of simple analysis window
Z	depth extent of simple analysis window
ΔZ	mean depth change of SSL over unit time

Chapter 4

μ	Cluster or centroid of K-means model
D	Dissimilarity matrix
d	variable of K-means dataset
D	Number of variables in K-means dataset
$dist_{AB}$	Relative distance measure between two SPDs
K	Number of clusters selected for K-means analysis
N_{min}	Total sample effort per cell
P	Number of MDS dimensions
$Pr_{z,MVBS}$	probability of observing a SSL at depth (z) and MVBS level (ml)
SSL_{min}	Total SSL observation time
x	sample of variable d
X	Number of samples in K-means dataset
z	Depth of SSL
$P(x\|u)$	Probability of sample x belonging to cluster μ
Z_{DSL}	Depth at which DSL observation is statistically most likely to occur
s_A	Nautical area scattering coefficient
s_{SSL}	Nautical area scattering coefficient, including backscatter from just SSLs
s_{epi}	Nautical area scattering coefficient, including backscatter from just SSLs in the epipelagic zone (0 – 200m)
s_{meso}	Nautical area scattering coefficient, including backscatter from just SSLs in the mesopelagic zone (200 – 1200m)
ML	vector containing ml (level of SSL backscatter at depth) values
ml	level of SSL backscatter at depth
Z	vector containing SSL depths

Chapter 5

Z_{1028}	Depth of the 1028kgm^{-3} seawater density isopycnal
Z_{SDSL}	Depth of the secondary deep scattering layer component
Z_P	euphotic depth
s_{MF}	Nautical area scattering coefficient, including backscatter from just SSLs (> -80 dB re 1m^{-1}) in the mesopelagic zone (200 – 1200m)
N_{MF}	Number of mesopelagic fish
σ_{MF}	acoustic cross-section of a mesopelagic fish
w_{MF}	weight of a mesopelagic fish
pop_{CW}	population of mesopelagic fish
a	A vector containing age classes of a mesopelagic fish population
A	A vector containing abundance values for each age class of a mesopelagic fish population
L	A vector containing length values for each age class of a mesopelagic fish population
w	A vector containing weight values for each age class of a mesopelagic fish population
TS_{sb}	Target strength of a swimbladdered mesopelagic fish
TS_{wsb}	Target strength of a mesopelagic fish without (or fat invested) swimbladder
TS_{pop}	Mean target strength of a population of mesopelagic fish, with mean calculated in linear domain
w_{pop}	Mean weight of a population of mesopelagic fish
β	Regression coefficient
x	Regression explanatory variable
E(Y)	Expected value of Y
wSSE	Weighted sum of squared residuals
W	Weights for weighted linear regression
w_i	individual weight, of sample i, for weighted linear regression
ρ_{PDSL}	Density of seawater at the depth of the deep scattering layer
Z_{ML}	Mixed layer depth

Chapter 6

P/B	Ratio of biological production over biomass
M	Number of K-means clusters or centroids

List of Symbols

N	Number of samples in the K-means model
ΔBIC	Change in the Bayesian Information Criterion between two K-means models
t	Trophic level
ΔTE	Change in trophic efficiency between two time periods

Chapter 1: General Introduction

This PhD project involved a collaboration between the University of St Andrews, the University of Tasmania (UTAS) and the Australian Antarctic Division (AAD). The principle aim of the project was to define and characterise a mesopelagic (200m – 1000m) biogeography of the world ocean, using active acoustic data. The idea was conceived by Professor Andrew Brierley and offered as a cotutelle between the named institutes, the majority of the funding originating from UTAS and the AAD.

1.1 Introduction

Photosynthetic primary production drives most of the ecosystems on earth. Laws of conservation of energy underpin the pyramids of biomass and numbers inherent in the trophic structuring of most of those ecosystems. Ecological theory might therefore lead us to expect that ecosystems with similar primary production, and similar numbers of food-chain links, would have similar arrangements at equivalent higher trophic levels. In his seminal '*Ecological geography of the sea*' Alan Longhurst (1998) offered an ecological geography of the pelagic ecosystem of the surface waters of the world ocean based on satellite observations of chlorophyll and regional oceanography. He defined statistically-distinct biogeographic provinces with characteristic phytoplankton production regimes. Following ecological theory, we might therefore reasonably expect that ecosystems in the water-columns underlying these distinct provinces should themselves be distinct, that mesopelagic biogeography should map on to biogeography of surface production. Satellite oceanography revolutionised our understanding of the spatiotemporal variability in processes at the ocean surface, but knowledge of the ocean interior has lagged considerably (Webb et al., 2010).

The mesopelagic region hosts mid-trophic level organisms that generally form the centre pieces of open-ocean food-webs. It is now recognised that in order to conserve species diversity and marine habitats, holistic approaches to conservation and fisheries management must be adhered to. Mid-trophic levels species are currently poorly understood (Lehodey et al., 2010), under-protected (Game et al., 2009) and are potentially on the brink of becoming a commercially important fishery (St John et al., 2016), influenced by recent findings that mesopelagic fish biomass could be 10 times any previous estimate (Irigoien et al., 2014). In light of a rapidly changing climate, a growing human population and greater food demands, a better understanding of mesopelagic population structure and dynamics are required.

This study attempts to assess Longhurst's geographical partitions for mesopelagic studies, determining whether or not oceanographic surface expressions such as sea-surface temperature and primary production map onto mesopelagic community structures. The mesopelagic cannot be directly observed using optics, as in Longhurst's partition, since visible light does not penetrate far into the ocean (intensity decreases to 1% of its surface value at c. 100m). Instead, sound waves, which can travel for hundreds of meters in seawater (at low frequencies: <200 kHz) are used to indirectly observe mid-water communities.

The most commonly used instruments in active acoustics are split-beam echosounders that typically operate between 18 and 200 kHz. Echosounders consist of a transducer (Fig 1.1b - produces and receives sound waves) that is hull-mounted to a vessel (both fishing and research), fixed to a pole or housed by a towed body and a transceiver (Fig 1.1a - controls frequency/amplitude of sound wave) which outputs to and receives data from, a computer that is connected to a display (Fig 1.1c). Sound pulses or pings, typically milliseconds in duration, are produced by the transducer every couple of seconds (depending on maximum recording depth), and organisms (or anything that has a different density to seawater) in the water-column scatter the sound, which is then detected by the same transducer, digitised and recorded. A single ping's worth of data, contains a number of sampled depths (dependent on the minimum sampling volume and by extension the pulse length), each one associated with a date and time stamped (received) power value. This information is recorded, converted into backscattering intensities (essentially logarithmic power ratios of the transmitted and received sound intensities) such as the volume backscattering coefficient (S_v – see Appendix B and Equ 2.1) and then displayed on screen as an echogram (Fig 1.1c & Fig 1.5) or acoustic image, where features such as the seabed and fish schools can be readily identified.

The mesopelagic has been studied via echosounders since the end of World War II (Lyman, 1948). A ubiquitous feature of echograms recorded over the past 70 years, is the Sound Scattering Layer (SSL – see Fig 1.5), a vertically discrete aggregation of organisms (see Appendix C for a history of SSLs). The main tasks of this project were to collate as much echosounder data together as possible, specifically EK60 (Simrad, Horten, Norway) data (most common) recorded at 38 kHz (to enable observation down to 1200m), develop a standardised method of quantifying the SSLs and to determine drivers of SSL depth and biomass to enable us to characterise the mesopelagic region and describe a biogeography.

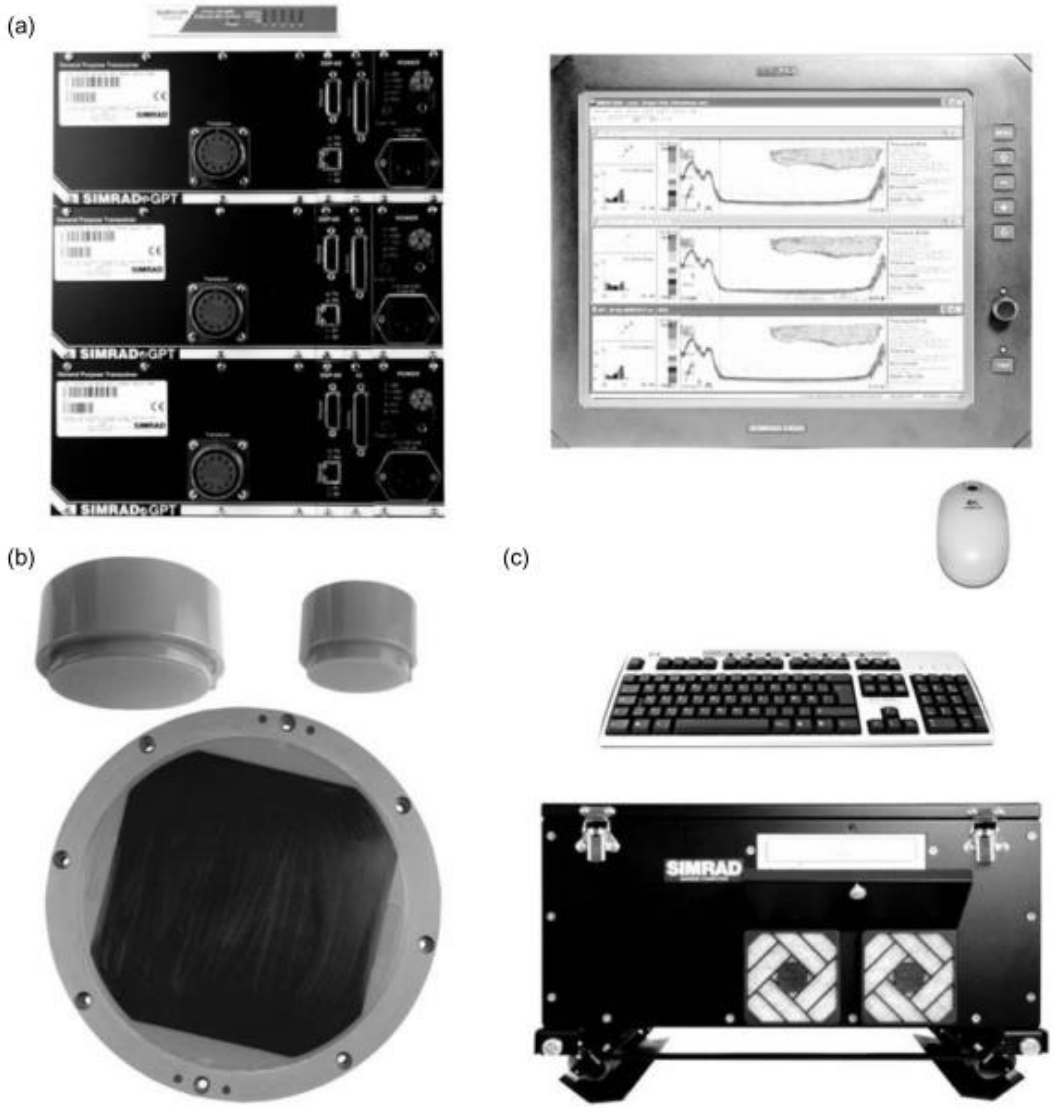

Figure 1.1: Echosounder setup: a.) three transceivers; b.) 3 different sized transducers (38, 120 and 200 kHz); c.) Computer display. Figure taken from Fisheries Acoustics (Simmonds & MacLennan 2005).

1.2 The mesopelagic region of the water-column

The mesopelagic zone is usually defined as encompassing the depth range between 200 and 1,000 meters (Fig 1.2); or more formally, from the depth that photosynthesis ceases, to the depth that prey can no longer be visually identified by down-welling irradiance (Robinson et al., 2010). Physically, it can be described as the region that extends from the mixed-layer depth (MLD: position of seasonal thermocline) to the far extent of the permanent thermocline (see Fig 1.2), which can reach depths of up to 1500 m. The mesopelagic, is relatively cold (mean of around 6°C), high in inorganic nutrient concentrations, subject to a continuous surface-borne flux of particulate organic matter (POM) or 'marine snow', dark and inhabited by bacteria, protists, archaea, viruses, zooplankton and nekton (Koppelmann et al., 2008). The larger multi-cellular organisms break down into Cephalopods (squid), Cnidarians (jellyfish), mesopelagic fish (such as lanternfish and bristlemouths) and a host of zooplankton species (mainly copepods, amphipods and euphausiids), of which, their dietary preference may change with their environment, switching between carnivory to particle feeding, for example (Robison, 1984). Mesopelagic organisms dwell in complete darkness almost their entire lives, for some, this provides protection from visual predators (Hays, 2003), whilst others are trackers, simply following the paths of their prey (Kinzer, 1969). The majority of the animals form distinct layers that are on average, vertically static during the daytime. The depth of the DSL is believed to be photo-regulated (Boden & Kampa, 1967; Clarke and Backus, 1964) but other evidence suggest their depth is dependent upon the depth of plankton (Auster et al., 1992) or the density structure of the water-column (Godø et al., 2012). At night, a large proportion migrate to the surface at speeds that are related to their depth (Ariza et al., 2016), but are limited by maximum swim speed, related to size and species, and buoyancy controls; some swimbladdered fish need to regulate internal gas exchanges during migration, limiting their speed (Nelson, 2006). Once at the surface, remaining under the cover of darkness, the organisms feed, normally stratified into several depth ranges, dependent upon positioning of prey, before returning to the mesopelagic region before dawn (Brierley, 2014). This daily movement, that is known as daily vertical migration (DVM), is thought to be the largest migration by biomass on the planet (Hays, 2003); some species, such as jellyfish that are tactile hunters, have been observed to perform migrations to the surface during the daytime and return to depth at night (Brierley, 2014). Importantly, DVM provides the transfer of energy, carbon and nutrients between the surface and deep sea, the so-called biological pump; contrary to this theory, it has been observed that fish returning to a relatively oxygen poor

mesopelagic zone after feeding at the surface, regurgitate their consumed prey before descending (Holton, 1969).

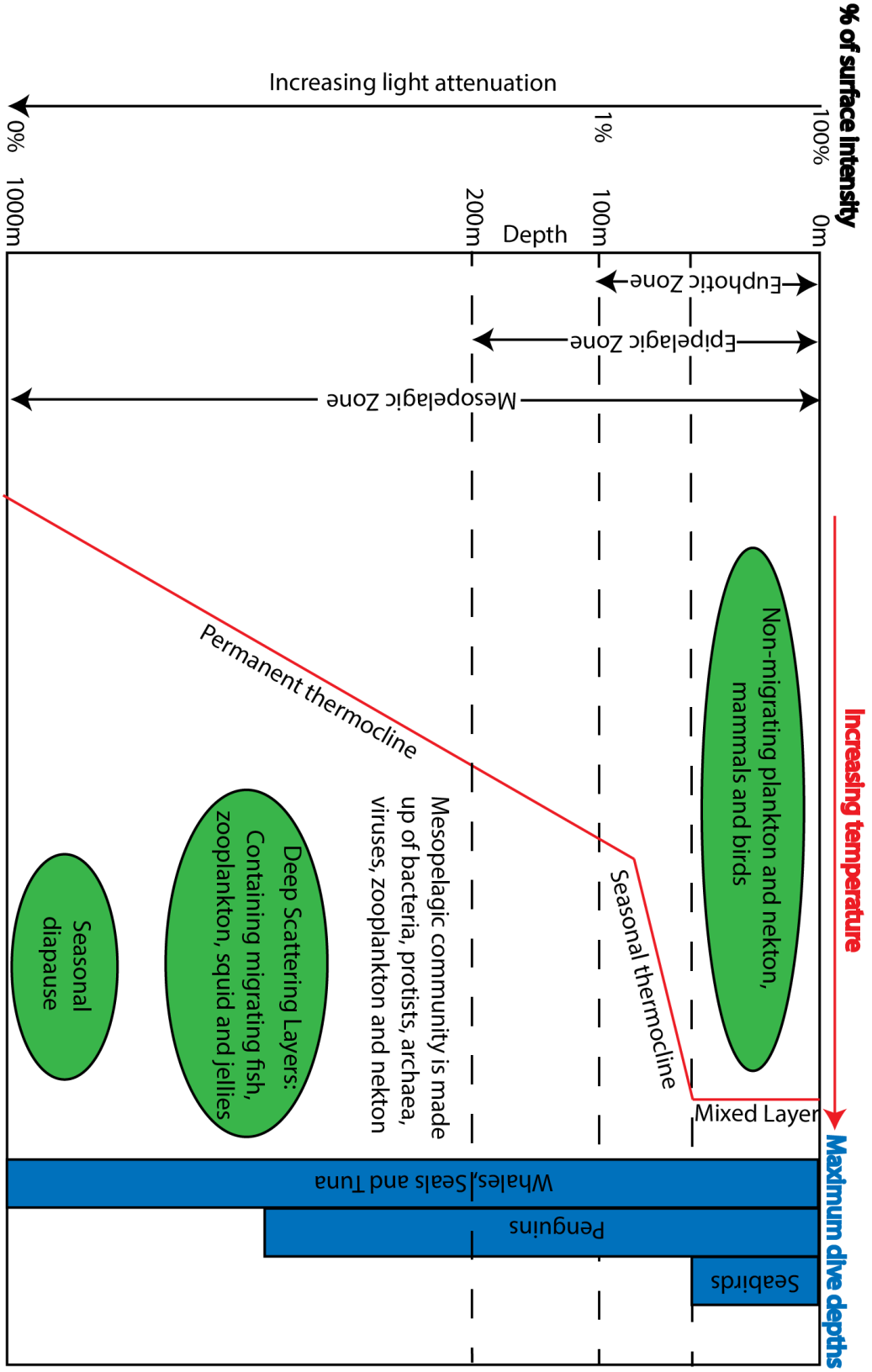

Figure 1.2: Schematic view of the water-column during daytime down to a depth of 1000m. Green ellipses represent biota and blue bars the maximum dive depths of marine predators.

1.2.1 Zooplankton of the mesopelagic zone

The majority of mesopelagic biomass is in the form of fish and their prey (zooplankton). Siphonphores (Fig 1.3e) and in-particular, physonects, formed from colonies of zooids, were once thought to dominate the acoustic response field of mesopelagic communities, due to their gas inclusions (Barham, 1963) which produce relatively strong acoustic echoes, along with the swim-bladders of lanternfish (Barham, 1966). The diet of the lanternfish consists of copepods (Fig 1.3a), the most abundant multi-cellular organism on the planet (even more so than insects), the euphausiid (Fig 1.3b), more commonly known as krill, that often form dense swarms (Watkins & Murray, 1998) especially in polar regions (e.g. Brierley et al., 1997; Hewitt et al., 2002; Jarvis et al., 2010), amphipods (Fig 1.3c: such as hyperiids) and pteropods (Fig 1.3d) (Pakhomov et al., 1996).

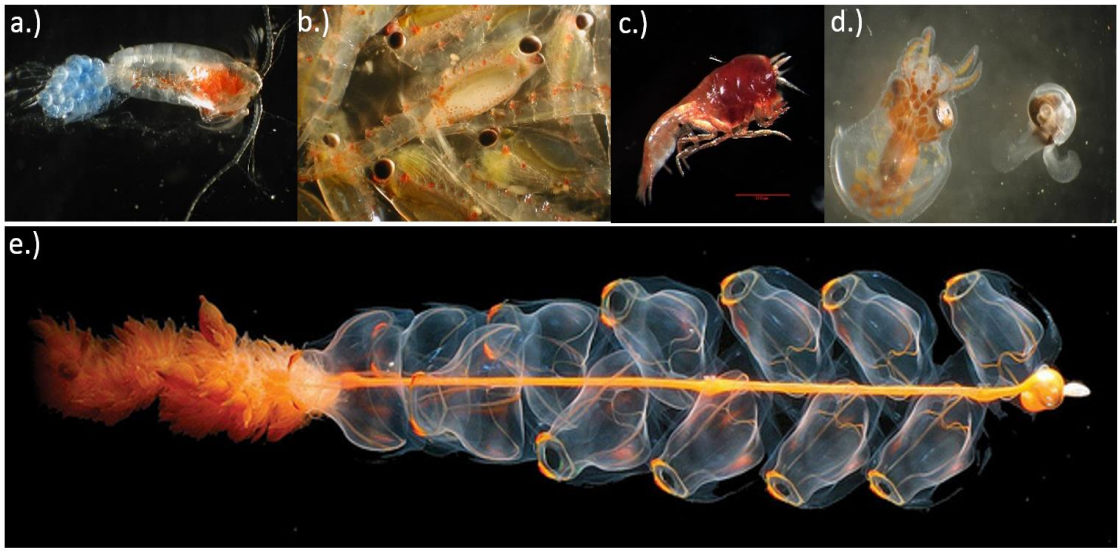

Figure 1.3: Zooplankton of the mesopelagic: main prey items of mesopelagic fish such as lanternfish: a.) Copepod as seen under a microscope with eggs; b.) Euphausiids (krill). Credit: Matt Wilson/Jay Clark, NOAA NMFS AFSC; c.) Amphipod. Credit: Hidden Ocean 2005 Expedition: NOAA Office of Ocean Exploration; d.) Pteropod (right) alongside an octopus larvae. Credit: Matt Wilson/Jay Clark, NOAA NMFS AFSC; e) Siphonophore in an Arctic region off Alaska (2007). Credit: Hidden Ocean Expedition 2005/NOAA/OAR/OER.

Zooplankton species that inhabit the mesopelagic zone are normally translucent or are partially covered by red pigments (Fig 1.3). Red light is readily absorbed in sea water and so these species are hidden in the deep (appearing to be black) from the majority of predators;

some species are able to emit red light and can detect their prey over small distances (Bone & Moore, 2008).

1.2.2 Mesopelagic fish

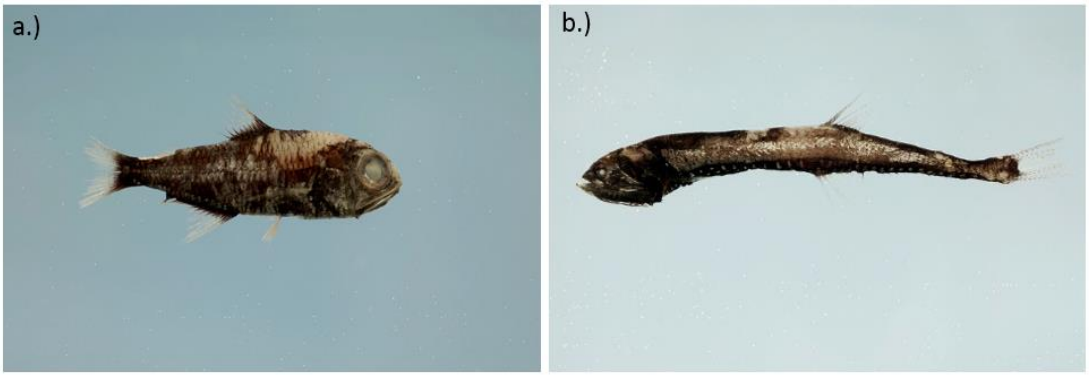

Figure 1.4: The two families of dominant mesopelagic fish, the myctophid and the gonostomatid. These two were found in the Gulf of Mexico: a.) Wisner's lanternfish (*Myctophum selenops*); b.) Elongated bristlemouth. Credit: SEFSC Pascagoula Laboratory. Collection of Brandi Noble, NOAA/NMFS/SEFSC.

Gonostomatidae (Fig 1.4b), commonly referred to as bristlemouths, are a relatively small family of small bony fish (32 species: www.fishbase.org), but are numerically abundant; in particular, the cyclophone genus, thought to be the most abundant vertebrate in the world (Nelson, 2006). They join the Family Myctophidae (Fig 1.4a), known commonly as lanternfish (due to bioluminescence), a much more diverse (248 recorded species: www.fishbase.org) and ubiquitous species group (www.fishbase.org), in being the bulk of the mesopelagic fish biomass, estimated at between 1 (Gjøsaeter & Kawaguchi, 1980; Lam & Pauly, 2005) and 15 billion tonnes (Irigoien et al., 2014).

Myctophids are visual predators, eating very little at depth during the daytime and are often found amongst their prey in mixed assemblages within DSLs (Auster et al., 1992). Like most mid-water fish, myctophids produce their own light via chemical reactions, known as bioloumineseence. The mechanism is believed to provide a method of intra-species communication, species identification and also provide a defence mechanism at depth by mimicking the intensity of down-welling daylight, in order to avoid appearing as silhouettes to any lurking predators below (Bone & Moore, 2008). Larval periods of tropical/subtropical myctophids range from 28 - 40 days with maximum growth rates in the juvenile stage of between 0.2 – 0.35 mm d^{-1} (Gartner, 1991); which are similar to epipelagic fish (0-200m) such

as anchovies. Feeding, reproduction and development of myctophids has been observed to take place in shallow waters at night, making them similar to shallow water species (Gartner, 1991). Acoustic response of mesopelagic fish changes in accordance to the morphology of the swimbladder, whether it is absent, inflated or not inflated and its fat content (Neighbors & Nafpaktitis, 1982). Myctophids have euphysoclistous swimbladders meaning that the connection between the often gas-filled organ and the gut of the fish is closed in early development stages (as opposed to physostomes, where it remains open) and its volume is regulated by internal gas exchanges (Bone & Moore, 2008). Studies have shown that its growth and functional capacity can change species-to-species and geographically (Edwards et al., 2010) over the course of its life cycle. Myctophids have been observed to start investing heavily in lipid (fats) resources after just a few months (Edwards et al., 2010), filling their swim bladder (and/or muscles) with fats and oils that in some cases, reduces the organ to the point where it loses its functional use. Juvenile myctophids generally have gas filled swimbladders, whereas larger and older adult fish, which are less abundant, are more likely to have fat invested swimbladders (Butler & Pearcy, 1972). Fats, attained through feeding, come in the form of wax esters and triglycerides. The less dense of the two, wax esters, have been linked to neutral buoyancy in older larger mesopelagic fish, whilst triglycerides are more likely to function as an energy store (Neighbors & Nafpaktitis, 1982; Phleger et al., 1997). Neutral buoyancy of mesopelagic fish can be achieved, either by swimbladder regulation (via gas-exchange) or by reducing body density by altering water and lipid content (Neighbors & Nafpaktitis, 1982).

1.2.3 Acoustic detection of mesopelagic fish

The sampled depth of echosounders increases with decreasing frequency (Table 1.1). This is because sound-waves lose energy via beam spreading (proportional to the square of the incident frequency) and to heat via frictional forces and molecular relaxation as the wave propagates through the water-column (MacLennan & Simmonds, 2005).

Frequency (kHz)	Wavelength (cm; sound speed = 1500 ms^{-1})	Approximate Range (m)	Absorption coefficient (dB/km; S = 35 ppt, T = 10°C, pH = 8)
18	8.3	3000	2.76
38	4	1200	10.1
70	2.1	700	23.6
120	1.25	400	38.7
200	0.75	200	54.3

Table 1.1: Echosounder frequency relationships to sampled range. Absorption coefficients calculated from Francois and Garrison (1982). S is salinity and T is water temperature.

For a given incident frequency, the acoustic backscatter of a single organism is called its Target Strength (TS – see Appendix B for derivation). A single organism effectively has a TS distribution that varies with orientation and frequency of the incident wave. In addition, a species size, shape and density profile affect the scattering strength and consequently different species can produce similar values of TS. The relationship between frequency and the size of the organism complicates matters further. At certain frequencies, species (dependent on size) resonate producing relatively high peaks in backscatter, effectively biasing estimations of biomass (Godø et al., 2009). These resonant peaks have been mainly associated with the swimbladder of fish, an organ that, due to its high density contrast, is particularly receptive to acoustic insonification and is often considered to dominate the acoustic response field (Stanton et al., 2012). Swimbladders are believed to have four main uses: it can provide buoyancy; act as a sensory organ; provide respiratory support or produce sound (e.g. Harden Jones & Marshall, 1953; Alexander, 1966). Swimbladder models therefore need to be functionally specific in order take into account these different mechanisms – buoyancy being the normal assumption and simplest to model.

Estimates of the TS of myctophids vary largely by over a factor of 100 (Irigoien et al., 2014), from between -73.8 dB re $1m^2$ (Yasuma et al., 2009) to -50 dB re $1m^2$ (Kloser et al., 1997). The difference arises due to the presence/absence of a gas-filled swimbladder; where an absence includes those that are empty or fat invested. Gas-filled swimbladders are relatively strong sound scatterers, as the density and sound speed of the gas is very different to the surrounding medium. It has often been observed that myctophid populations are well-mixed in

terms of their swimbladder states (Butler & Pearcy, 1972; Yasuma et al., 2009) but studies in Polar Regions have often shown higher proportions of fish with higher fat contents (Phleger et al., 1997) when compared to lower latitudinal observations. Since zooplankton are typically weak scatterers (Stanton & Chu, 2000; Stanton et al., 1996b), a mixed population of bony fish that have varied swim bladders states are expected to dominate the acoustic response field of the mesopelagic region at large scales.

To measure TS in the field requires that the species of interest, i.e. the target, is individually resolvable, meaning no other scatterer can be present within the minimum sampling volume (see Appendix B). This requirement is not normally satisfied and so a technique of analysis called echo integration is applied (MacLennan & Simmonds, 2005), where the total backscatter energy over each sampled volume is determined, yielding an S_V value. Given a known TS of the individual targets within a sampled volume, the volumetric numerical density, N_V, may be calculated using:

$$N_V = 10^{(S_V - TS)/10} \quad (1.1)$$

A mean value of S_V can be calculated over a finite volume to yield a Mean Volume Backscattering Strength (MVBS – see Appendix B) and nautical area scattering coefficient (NASC – see Appendix B), a linear measure of scattering. Numerical density of sound scattering layers (SSLs), comprising of organisms of known TS, can be determined over a particular area by application of Equation 1.1. Recently, a global estimate of mesopelagic fish biomass was made using the backscatter recorded in the mesopelagic region and a median value of TS for myctophids from available models (Yasuma et al., 2003; Yasuma et al., 2006; Yasuma et al., 2009), yielding a value of mesopelagic fish biomass (between -40deg and 40deg latitude) of between 12 and 15 billion tonnes (Irigoien et al., 2014); considerably larger than estimates made using data collected by ocean trawls (1 billion tonnes).

1.3 Sound Scattering Layers

Sound Scattering Layers (SSLs) or Deep Scattering Layers (DSLs) are vertically discrete (100s of m or less) water column aggregations of organisms that can extend horizontally over 1,000s of km (Kloser et al., 2009). The layers (Fig 1.5) are comprised of pelagic organisms (organisms of the water column, as opposed to benthic organisms that live on or in the seabed), primarily zooplankton and small fish (cm to 10s cm), living together in distinct communities. When insonified, these organisms produce a distinct echo that, depending upon depth and incident acoustic frequency, can stand out prominently as scattering layers above background noise (MacLennan & Simmonds, 2005; Watkins & Brierley, 1996). Such layers have been known since the mid-20th century when naval sonars detected signals thought initially to be echoes from the sea bed: the depths of the echoes however changed with time of day and it became apparent that these 'false bottoms' were in fact biological in origin (Brierley, 2014).

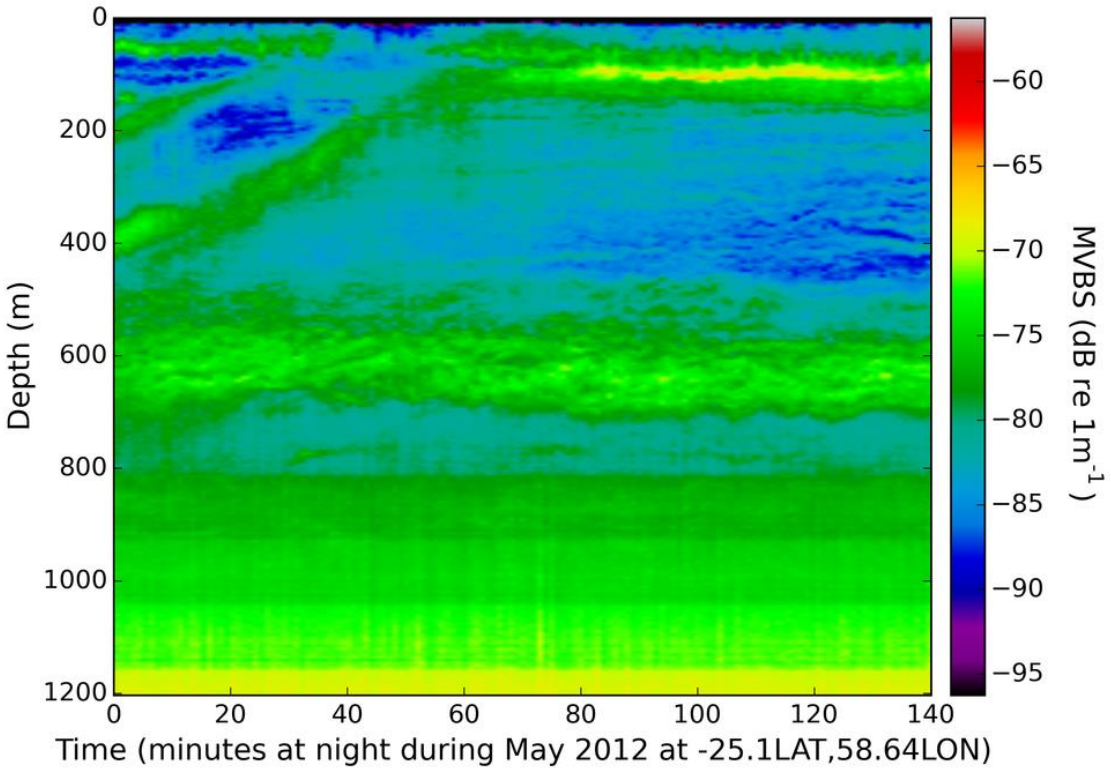

Figure 1.5: Night-time accent of a Deep Scattering Layer (DSL). A component of the mesopelagic community migrates vertically at night to feed; a resident DSL remains at 600m during the night. Beyond 800m deep, the time-varied gain from the echosounder makes it difficult to resolve biological signal. Data downloaded from www.imos.au (IMOS, 2013); image taken from www.soundscatterinlayers.com.

The organisms that comprise SSLs are responsible for the transport of vast quantities of carbon (increasing particle export by up to 40% - Bianchi, 2013) from the surface to the deep sea (the biological pump) via DVM. They thus play an important role in atmosphere-ocean interactions, and in the global biogeochemical cycle. SSL scales can vary from the micro, at vertical resolutions of centimetres over timescales of a fraction of a minute (Holliday et al., 2003; McManus et al., 2003, 2005) to pan-oceanic (Anderson et al., 2004; Kloser et al., 2009; Irigoien et al., 2014). The former, so called 'microlayers' provide an explanation for the 'paradox of the plankton' where high species diversity occurs in what at first glance may appear to be a homogenous volume of water. Biological vertical structure means that the water column is in fact far from homogenous. Its physical properties can change dramatically over just a few cm's or meters enabling the discrete formation of aggregates at specific depth ranges (Longhurst, 1998). In this way, SSLs show the water column divided into multiple vertically discrete habitats. Despite the importance of SSLs to ocean and earth-system function, there is no accepted standard method for identifying or classifying them. This in turn has hampered comparative or integrative studies of SSLs.

Some quantitative research has already been carried out on SSLs. Regional structure of SSLs has been identified by comparing total water-column backscattering strength at sites across the Pacific and Atlantic Oceans, in the Caribbean, Labrador, Norwegian and Mediterranean Seas and in Baffin Bay (Chapman et al., 1974) and also in the Atlantic and North Western Pacific using depth-frequency structure of backscattering strength (Andreeva et al., 2000; Tarasov 2002). Biomass estimates of SSLs have also been made at the basin scale using both echo counting and echo integration techniques, in the Tasman Sea for example (Kloser et al., 2009). More recently, a method was developed to extract SSLs (Cade & Benoit-Bird, 2014), that required input parameters such as an acoustic threshold intensity and minimum separation distances between SSLs to be defined a priori.

Research on SSLs has, however, typically been qualitative. The depth structure of SSLs has been observed to vary over large spatial scales in both longitude and latitude (Kloser et al., 2009), across ocean basins (Anderson et al., 2004) in the Irminger Sea and across fronts (Nicol et al., 2000; Kawaguchi et al., 2010) in the Southern Ocean. Studies at oceanic features have also shown characteristic behaviour, such as bulges in SSLs at continental shelves (Jarvis et al., 2010) off East Antarctica and bowl-like SSL features forming under eddy structures (Godø et al., 2012) in the Norwegian Sea.

Conversely, discrete, biological aggregations - schools, shoals and swarms - have been quantitatively defined. The fisheries acoustic community has wrestled for years over the question of what, as seen in an acoustic record, is a school, and some standard identification and description protocols have been agreed (Reid & Simmonds 1993; Reid 2000). The importance of particular school metrics for school identification has differed between studies; for example Coetzee (2000), using the Shoal Analysis and Patch estimation system algorithm (SHAPES: Barange, 1994), identified morphological aspects to be the chief descriptor; Lawson (2001), identified school energetics and water-column position as the most important parameters.

The reason for this lack of a quantitative definition is related to the nature of the data collected and lack of automated processing techniques available for analysis. Narrowband single frequency processed acoustic data are 3-dimensional, space/time vs. depth vs. scattering intensity, typically recorded in the open ocean from research vessels at time intervals of 2 seconds averaging over 75 cm depth intervals over the observable water-column (dependent on frequency). A 5-day cruise, covering 1200 nautical miles (at a nominal 10 knots cruise speed) observing down to a depth of 1000 meters, equates to over a billion backscatter intensity values (c. 6GB/day). Subsequently an immense quantity of data has amassed that is both difficult to analyse and store. It is only in recent decades, with the advent of the digital era that cataloguing and analysing such data has become plausible. Since the standardisation of calibration techniques (Foote et al., 1983; Foote, 1983a, 1983b) software packages like Echoview (Myriax, Hobart, Australia) and LSSS (Korneliussen et al., 2006) have facilitated the processing and analysis of multi-frequency inter-survey acoustic data. The cost of these products has imposed restrictions on scientific analysis in the more general community, since raw data files recorded by the instruments of different manufacturers are not of a common data format and hence difficult to manipulate. A suite of processing techniques available are through these packages, but with advances in statistical approaches and image processing, an increasing number of tools are becoming available to interrogate raw echosounder data.

1.4 Ocean Provinces

Mary Sommerville in her Physical Geography (1862 – 70) made the first real attempt at partitioning the ocean, when she described her 9 latitudinal 'homo-zoic' zones. This was followed much later by a geography that was based on plankton studies (Steur, 1933). In fact, partitioning in this way via distributions of phytoplankton (Semina, 1997) and zooplankton (Alvarino, 1965; Briggs, 1974; Brinton, 1962), became quite popular, affording the term zoogeographic barriers. Before Longhurst's description of the surface provinces, there were several others defined (Backus, 1986; Beklemishev, 1976; McGowan, 1971) and notably that of Reid et al (1978) which bears the closest resemblance (Longhurst, 1998); the work of Margalef (1997) is also noteworthy. Despite the plethora of available partitioning techniques and resultant geographies, it was the work of Alan Longhurst that was most well-received by the scientific community.

An ocean province/biome or ecological region, is an area of the ocean that displays a set of characteristics (biological, chemical or physical) that distinguishes itself from other areas, of a similar scale, in a numerically significant manner, so that it is unique and is not like any other ocean area. In the first instance, the ocean can be easily divided into 3 areas based on temperature and proximity to land mass and those are the Coastal (shallower than 200m) biome, the Polar biome (poleward of the sub-tropical fronts) and the rest of the ocean, divided further by Longhurst, into the Trades and Westerlies biomes, in accordance with the tropical and temperate wind systems.

Longhurst (1998) described 54 ocean provinces (pelagic provinces shown in Fig 1.6), derived from spatiotemporal patterns of chlorophyll, regional oceanography (frontal positions, mixed-layer depth), photic depth and surface nutrient fields. Global partition, enables the study of change in the ocean at large scales, particular changes influenced by increased rates of global warming (Brander, 2007). The provinces themselves were constructed from data observed and collected within the euphotic zone (illuminated region) of the ocean, where primary production (PP) can be estimated remotely by satellites and is limited by seasonal variations in light and surface nutrients (Longhurst, 1998). What is not clear, is how these global surface partitions relate to the deeper communities, those of the mesopelagic region. Some attempts have been made recently at partitioning the deeper region (UNESCO, 2009) but none that are based on direct observations, rather inferences made using surface properties.

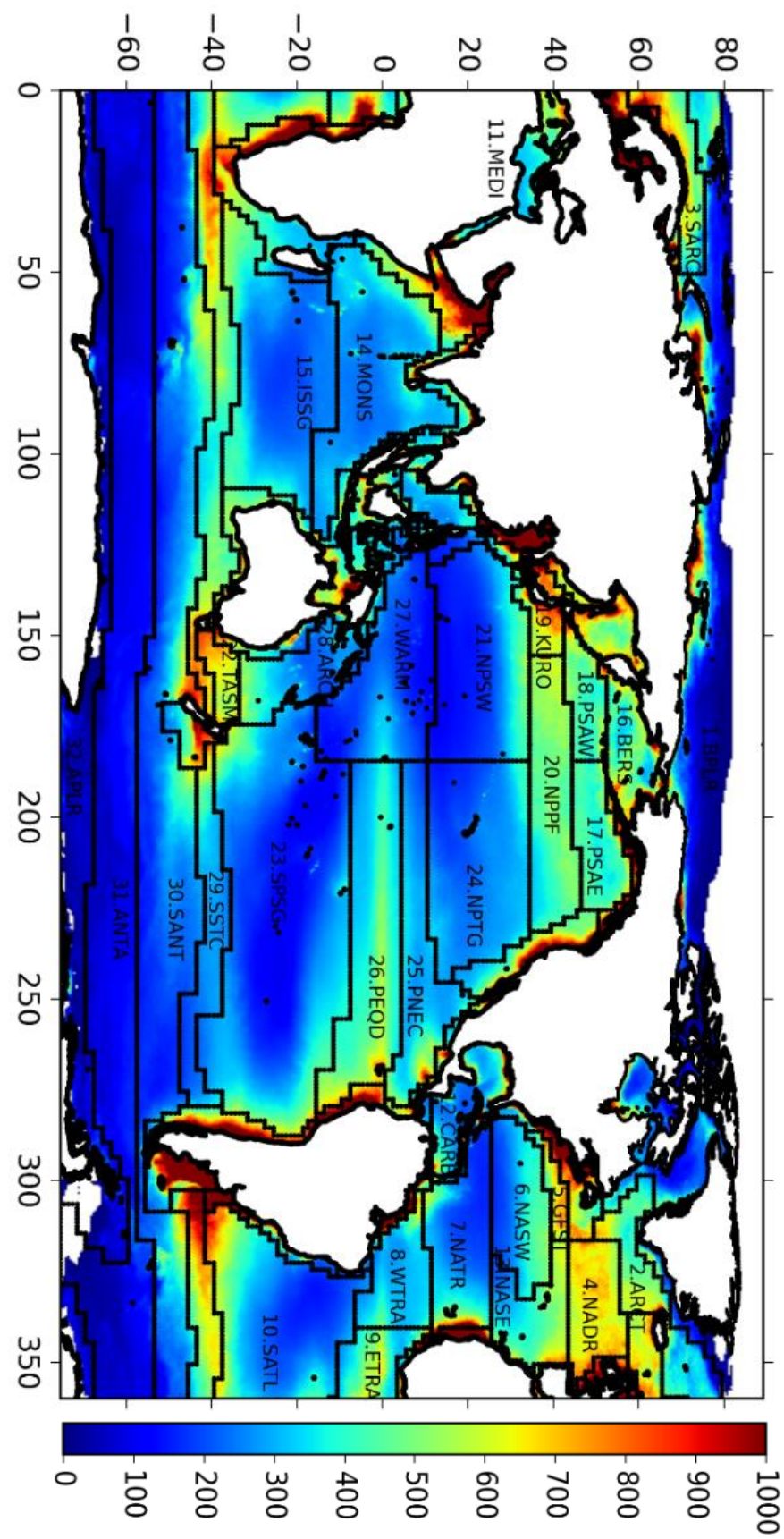

Figure 1.6: Longhurst pelagic ocean provinces and mean annual primary production (mg C/day/m^2). Pelagic province short-names are indicated and numbered (Longhurst, 1998).

1.5 Aims

From the initial review of literature and data availability, it was clear that a description, based on observation, of the mesopelagic community was plausible. The project required the acquisition of a global dataset of acoustic data, the development of a Sound Scattering Layer (SSL) extraction methodology and the derivation of a mesopelagic biogeography. To this end, the aims were as follows:

- Acquire/collect 38 kHz EK60/ES60 data to provide representative coverage of most of the Longhurst ocean provinces (Ch 2).
- Develop a standardised and automated method of SSL extraction and description (Ch 3).
- Derive geographically distinct SSL arrangements (Ch 4).
- Determine drivers of mesopelagic biomass and depth from environmental variables (Ch 5).
- Derive a mesopelagic biogeography, characterised by the drivers of mesopelagic biomass and depth (Ch 6).

Chapter 2: Acquisition and pre-processing of a global acoustic dataset

A large volume of active acoustic data were required in order to satisfy the first aim of the project of obtaining data coverage across the majority of the Longhurst pelagic provinces (see 1.5 and Fig 1.6). These data were mainly acquired through data centres (Table 2.1) but some were collected during the course of this PhD.

2.1 Acoustic Data Collection

EK60 data were recorded in-situ on a 9-week expedition on board the R/V Polarstern between August and October 2013 (see Fig 2.1 for cruise track). The vessel was equipped with 5 hull-mounted echosounders operating at 18, 38, 70, 120 and 200 kHz, which were continuously recording for the majority of the expedition. A calibration was conducted close to South Georgia (Fig 2.1), using the standard method (Foote, 1983), but due to bad weather conditions and problematic equipment, only the 38 and 120 kHz transducers were calibrated accurately. In this project, we were only interested in performing echo integration, as opposed to echo-counting which involves resolving single targets (for more information, see MacLennan & Simmonds, 2005), using the 38 kHz data and therefore the only relevant calibration parameters were the transducer peak gain (28 dB re $1m^{-1}$) and the Sa correction value (-0.57 for a pulse duration of 1.024 ms), which contribute to the calibration constant term in the calculation of the volume backscattering strength (S_V: Equ 2.1).

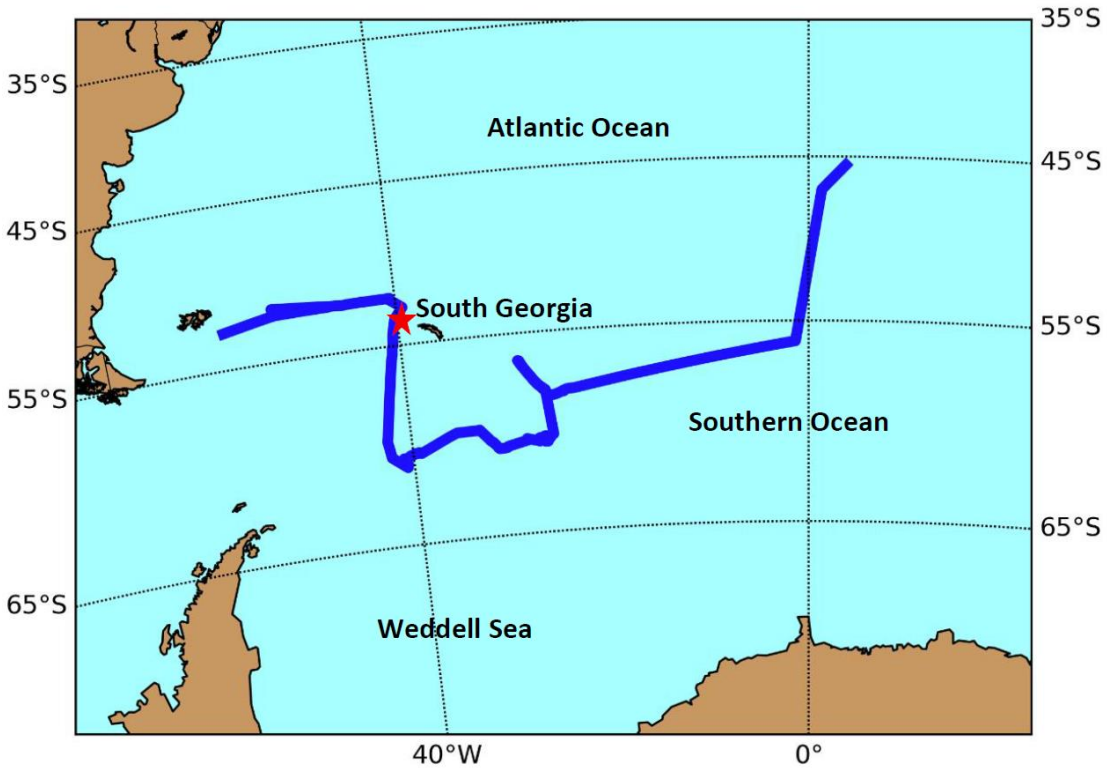

Figure 2.1: Cruise track of the R/V Polarstern (Aug – Oct 2013). Calibration site marked by red star.

2.2 Acoustic Data Collation

Available EK60 acoustic data (Table 2.1 and Fig 2.2) were collated from the British Oceanographic Data Centre (BODC, 2014) the Integrated Marine Observing System (IMOS, 2013), British Antarctic Survey (BAS), the Pelagic Ecology Research Group (PERG) and from a recent cruise on the RRS James Clark Ross, Surface Mixed Layer Evolution at Sub-mesoscales Cruise (SMILES, 2015).

Source	Ship/Cruise	Region	Time Period
PERG	HICEAS10	Central N. Pacific	AUG - DEC 2010
PERG	R/V Nansen	S.W. Indian Ocean	NOV - DEC 2009
PERG	R/V Polarstern	Southern Ocean Atlantic Sector	AUG - OCT 2013
PERG	R/V Lance	Arctic Ocean	JUL 2009
PERG	R/V Lance	Arctic Ocean	DEC 2012
IMOS	R/V Southern Surveyor	Tasman Sea	JUN – AUG 2012/13
IMOS	R/V Kaharoa	Tasman Sea	JUL – AUG 2008
IMOS	FV Southern Champion	S.W Indian Ocean	JAN – MAR,SEP 2010/11
IMOS	FV Janas	Southern Ocean Pacific Sector	APR-MAY, AUG,NOV 2012/13
IMOS	FV Rehua	Tasman Sea	JUN 2013
IMOS	FV Austral Leader II	S.W Indian Ocean/ Southern Ocean	FEB, APR-MAY,JUL-SEP,DEC 2011 – 2013
IMOS	FV Will Watch	S.W/Central Indian Ocean	Exc. JAN,NOV 2011 2012

PERG	RRS James Cook/JC011	N. Atlantic	JUL – AUG 2007
PERG	RRS James Cook/JC037	N. Atlantic	AUG – SEP 2009
BODC	RRS James Cook/JC050	N.E Atlantic/ Greenland Sea	JUL – AUG 2010
BODC	RRS James Cook/JC066	S.W Indian Ocean	NOV – DEC 2011
PERG	RRS James Cook/JC080	Southern Ocean Atlantic Sector	Dec – JAN 2012/13
BODC	RRS James Cook/JC087	N. Atlantic	MAY – JUN 2013
BAS	RRS James Clark Ross/JR161	Southern Ocean Atlantic Sector	OCT –DEC 2006
BAS	RRS James Clark Ross/JR177	Southern Ocean Atlantic Sector	DEC – FEB 2007
BAS	RRS James Clark Ross/JR179	Southern Ocean Atlantic Sector	FEB – APR 2008
BODC	RRS James Clark Ross/JR195	Southern Ocean Atlantic Sector	NOV 2009
PERG	RRS James Clark Ross/JR210	Arctic Ocean	AUG 2008
BODC	RRS James Clark Ross/JR211	Arctic Ocean	AUG – SEP 2008
BODC	RRS James Clark Ross/JR218	N. Atlantic	OCT 2008
SMILES	RRS James Clark Ross/JR311	Southern Ocean	MAY 2015

Table 2.1: Summary of acoustic data. PERG – Pelagic Ecology Research Group; IMOS – Integrated Marine Observing System, BODC – British Oceanographic Data Centre; BAS – British Antarctic Survey and SMILES - Surface Mixed Layer Evolution at Submesoscales Cruise.

In total, more than 40 surveys worth of data recorded at 38 kHz between 2006 and 2015 were obtained. For each survey, where available, the most appropriate calibration parameters (latest available, conducted in a similar environment to the survey location) were applied and in-situ sound speed values were estimated (Roquet et al., 2015) from a climate re-analysis dataset (2.2.2). Only pelagic regions were considered, away from continental shelves where the depth of the sea bed was at least 800m. The spatial coverage of the data included 14 of the 32 pelagic provinces, covering all the major ocean basins, except for the South Atlantic. The data were partitioned into 3196 acoustic images or echograms, to enable efficient processing; the data volume was equivalent to over 380 days of continuous recording.

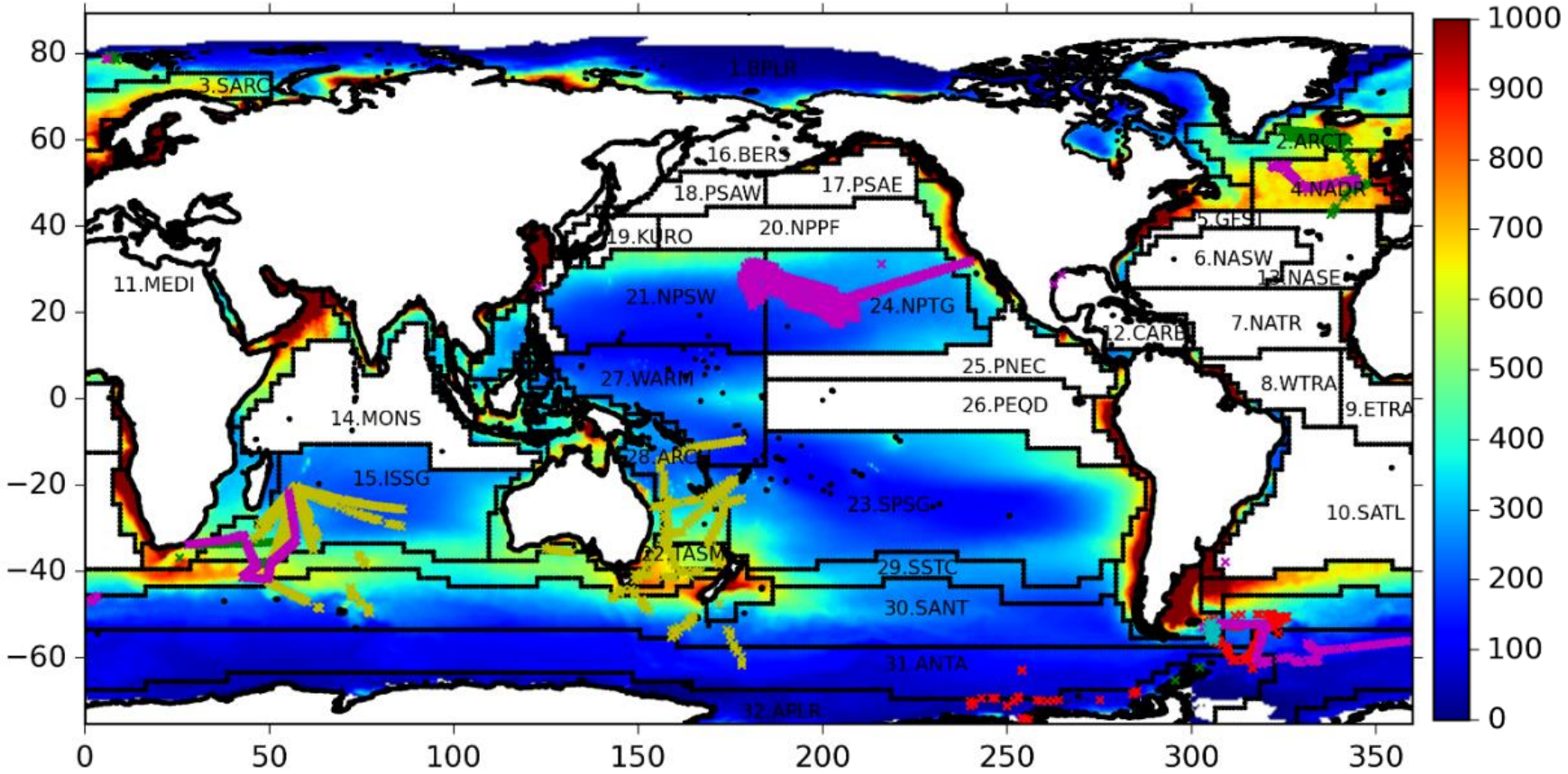

Figure 2.2: Longhurst pelagic ocean provinces and mean annual primary production (PP – mg C/day/m^2: calculated from data downloaded from http://www.science.oregonstate.edu/ocean.productivity/index.php). Pelagic province short-names are indicated and numbered (Longhurst, 1998). PP is shown for the 14 provinces that were covered by the EK60 data. Surveys tracks of the collected acoustic data are shown, the colour of which indicates source of the data: red – IMOS; green – BAS; black – BODC, purple – PERG and cyan – SMILES.

2.3 Ocean Variables

To determine the drivers of the mesopelagic community metrics (depth and biomass), we obtained a wide range of physical variables, along with rates of primary production (PP), at a global scale. Ocean variables, for the period between 2005 and 2008, were obtained from the Simple Ocean Data Assimilation (SODA version 2.2.4) product (Carton et al., 2000), including wind stress, temperature, salinity, current velocities and sea-surface height, as gridded monthly averages. PP was downloaded via the Ocean Productivity website (http://www.science.oregonstate.edu/ocean.productivity/index.php), where PP had been estimated using the Vertically Generalized Production Model (VGPM: Behrenfeld & Falkowski, 1997). The VGPM uses values of chlorophyll concentration, inferred from spectral power distributions measured by spectroradiometers (MODAS) on-board earth-orbiting satellites (Aqua and Terra), available light and photosynthetic efficiency (which is a function of temperature) to estimate values of net PP. There are several variants of the VGPM model, such as the Eppley-VGPM (Morel, 1991) and the Carbon-based Production model (CbPM: Behrenfeld et al., 2005), but here we used the standard product. PP values were re-calculated at the same temporal (monthly averages) and spatial resolution (0.5°) as the SODA dataset. For the period between 2090 – 2100, we used output from a coupled climate model with both a physical and biological component, the physical component comprised of version 3.2 of the Nucleus for European Modelling of the Ocean (NEMO: Madec, 2008) and the ecosystem component, the intermediate complexity global ecosystem model, MEDUSA-2.0 (Yool et al., 2013), referred to together as NEMO-MEDUSA-2.0, under the Representative Concentration Pathways (RCP) 8.5 scenario, surface forcing as per UKMO's HadGEM2-ES model. The RCP 8.5 scenario was used to explore the 'worst-case' climate scenario, elevating CO_2 concentrations to 1000ppm by 2100; other scenarios were not tested due to time restrictions of the project, but should be considered in future work. There was insufficient data to look at global seasonal variances, instead, we sought to ascertain long-term global trends in mesopelagic metrics that would be related to long-term regional properties. To support this analysis, variables were averaged over each time period (2005 - 2008 and 2090 – 2100) to reduce the significance of seasonality and high-frequency components.

2.4 Pre-processing of Acoustic Data

Raw acoustic data output from the ER60 software v2.4.3 (Kongsberg Maritime AS, Horten, Norway - the software used during EK60 operation) consists of 3 file types, .raw files (5 – 100Mb) containing timestamped power values, by ping and sample depth (along with a host of other data such as GPS coordinates, sounder configuration and calibration parameters), a .bot file, containing estimated seabed depths determined by an algorithm embedded in the ER60 software and an index file (.idx). To enable automatic processing of the .raw files, a python package, namely pyecholab (Towler, 2015), was adapted to enable processing. The .raw files were read in sequentially and pre-processed on a desktop computer, taking approximately 3 months and 6 computer crashes. The output of this process consisted of 3,196 data arrays, of Mean Volume Backscattering Strength (MVBS – see Appendix B) values, binned into 5m depth by 1-minute time cells. The raw data were subject to a number of pre-processing adjustments, refinements, filters, masks and thresholds to remove noise from a variety of sources (Fig 2.3). These processes are outlined in the remainder of this chapter.

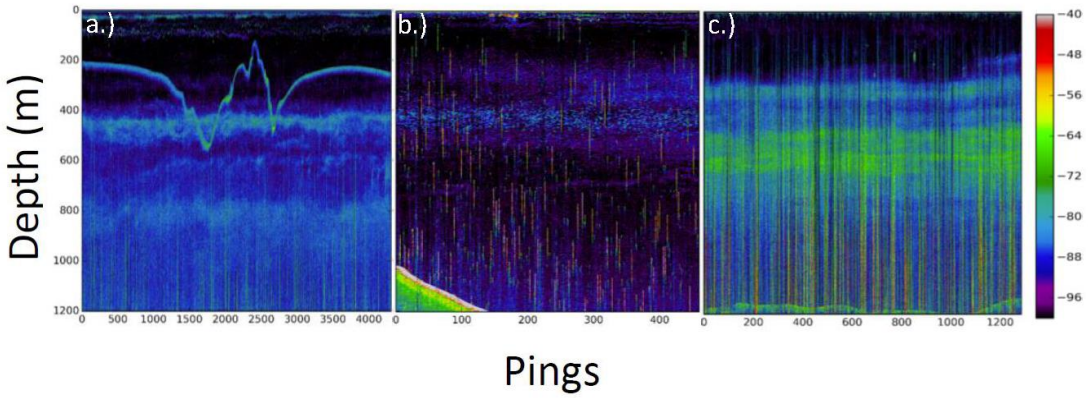

Figure 2.3: Echograms (MVBS – dB re $1m^{-1}$) showing examples of different types of noise inherent in the acoustic dataset: a.) Lagged seabed echo (FV Southern Champion); b.) Interference from other acoustical instruments (JR211); c.) Attenuated and amplified pings (FV Austral Leader II).

2.4.1 Data partition

The data could not be processed in large (more than a single day's worth of continuous recording) volumes, as it required an unreasonably large amount of RAM (16 GB was sufficient to process 24 hours' worth of data – approx. 1bn values). This was not a problem, since the diel nature of SSLs meant that their water-column arrangement would predictably change

around dusk and dawn each day. It was therefore practical and reasonable to partition the data, in the first instance, by day/night period, using local sunrise/sunset times; by doing so, vertical migrations of organisms were always found at the beginning or end of the image segments (Fig 1.5). Pelagic surveys, from which most of the data was obtained, normally involve a multi-disciplinary operations schedule and acoustic data collection is often interrupted or halted, parameters such as ping rate are sometimes changed and levels of ship noise vary significantly. For any interruption lasting more than 10 pings, the data were further segmented, similarly, this was also applied in instances where any of the recording parameters were altered. Data were not used if the recording depth reduced to below 800m and any segmented images that were smaller than 30 minutes in length (minimum acceptable length, in this study, of a regional scale SSL) were also removed. Only data recorded underway, travelling at speeds greater than 4 knots were considered for analysis. This avoided using data collected on-station, during ship operations that are a considerable source of noise. This imposed restriction meant that the minimum distance covered by a SSL over a 30-minute period was 3.704 km and the minimum distance between pings, for a 2 second ping-interval, was 4.1m; the majority of ship surveys were conducted at speeds greater than 8 knots, yielding a minimum distance of 7.408 km. The minimum distances covered by SSLs were deemed acceptable for regional scale study, since they were much larger than the sizes of ephemeral biological structures, such as fish schools.

2.4.2 Environmental Parameters and calibration

In order to compare acoustic records from two different surveys data require calibration using a standardised technique. In common practice, Foote et al's (1983) standard target method is usually implemented, where a spherical target of known acoustic response, usually made out of tungsten carbide and typical dimeter of 38.1 mm, is moved throughout the acoustic beam, produced by the transducer, typically at a distance of between 15 and 30m (MacLennan & Simmonds, 2005). The resultant backscatter is recorded and compared to the expected values, from which, a beam model (ER60: Single Target Detection) fits certain calibration parameters such as transducer gain and beam width; for more on this see (MacLennan & Simmonds, 2005). Ideally, calibration should take place in-situ and the survey environment should not change significantly. However, this is rarely the case for extensive pelagic surveys that move through different water masses, which have distinctly different temperatures; an environmental factor that is known to affect calibration parameter values (Demer & Renfree,

2008). A further complication is that the electro-acoustic efficiency of a transducer can change over time and with temperature and unevenly across its face, so regular calibrations are required to detect faulty quadrants and variation in response due to deformation. Calibration parameters for the data collected here were obtained where possible and the latest values were used. Errors inherent from incorrect calibration parameters for fully functioning transducers are normally small (when calibrations are made regularly) and were deemed not to be significant for a study of this scale; for instance, since there were over 40 surveys worth of data collected, under and over-estimation due to incorrect transducer gain values would be expected to be distributed normally (ICES, 2015) and would cancel each other out when calculating mean values over large regions. Errors inherently caused by environmental changes, affecting sound speed (c) and water-column absorption (α), were however, compensated for. We used mean seasonal values of ocean temperatures, pressure and salinity from SODA to calculate in-situ values of c (Roquet et al., 2015) and α (Francois & Garrison, 1982). Mean values were calculated for each image and applied to the raw data, correctly updating the values of the pulse length. One further change was made to the calculated range, to account for the positioning of the transducers relative to the water's surface. These values ranged between 3 and 7 meters and varied from ship to ship; for instances where a value could not be obtained a mean of 5m was used.

2.4.3 Volume Backscattering Strength

Data collected using an ES60 echosounder is embedded with a systematic triangular wave error (courtesy of SIMRAD) that can cause a deviation in the underlying raw values of +/- 0.5 dB; originally identified by Ryan and Kloser (2004). This error was removed before converting the power values.

The received power was converted to volume backscattering strength (S_V) using Equation 2.1

$$S_V(R, P_r) = P_r + 20logR + 2\alpha R - 10log\left(\frac{P_t G_0^2 \lambda^2 c\tau\psi}{32\pi^2}\right) - 2 \times S_a correction \quad (2.1)$$

where R is the range (m), P_r is the received power (dB re $1m^{-1}$), α is the absorption coefficient (dB/m - Francois and Garrison, 1982), P_t is the transmitted power (W), G_0 is transducer peak gain, λ is wavelength (m), c is sound speed (m/s), τ is pulse duration (s), ψ is the equivalent beam angle and S_a is the Simrad correction factor.

S_V is expressed in units of dB re $1m^{-1}$, dB referring to the decibel, calculated by taking the log base 10 of the original value and multiplying by a factor of 10; when quoting dB units, it is standard practice to reference the original units, in this case $1m^{-1}$. S_V is calculated by taking the dB of the received power (term1 of Equ 2.1) adding the two transmission loss terms, the time-varied-gain (TVG – term2) and the loss due to seawater absorption (term 3) and then subtracting a calibration constant (terms 4 and 5). The TVG adds gain to the signal, to compensate for that which is lost (mainly to heat) as the beam propagates and spreads: sound is a mechanical wave and does work on its environment.

2.4.4 Masks, filters and thresholds

Once the data was converted to S_V values, the unwanted signal (noise) was removed. In this project the signal was defined as the scatter produced by regional scale (persisting for at least 30 mins) SSLs, meaning all other sources of scatter, for example, fish schools, ship noise and ephemeral SSLs were considered to be noise. A minimum threshold was applied, to mask data values below -110 dB re $1m^{-1}$, which would be considered weak backscatter for even the smallest of fluid filled zooplankton (Stanton & Chu, 2000), and values that were above -30 dB re $1m^{-1}$, a level that is often associated with the seabed. To remove ambiguity around the extent of the near-field (a region close to the transducer, dependent upon frequency and beam angle, where acoustic response is difficult to model) the first 5 m of each ping were also masked – this would be of small consequence for DSL study but significant for small-scale studies such as krill biomass estimates (Brierley et al., 1997; Cox et al., 2011; Hewitt et al., 2004). Background noise was assessed for each of the processed images and removed using the technique described by De Robertis & Higginbottom (2007); a region (usually deeper than 1500m for a 38 kHz transducer) dominated by noise is used to estimate a noise value at depth, then, by using the relationship between depth and TVG, the level of noise is calculated at each depth level up to the surface and removed, similar to the method described by Watkins and Brierley (1996). Noise amplified and attenuated signal (Fig 2.3c & Fig 2.4a) was masked via a filter, designed specifically for SSL analysis. For each row of S_V values (of constant range from the transducer), a median value was calculated and assumed to be signal either from within a SSL or outside; attenuated and noise amplified values would lie either side of the median as long as the majority of the values were signal. Any values along the row that were found to be +/- 10dB either side of the median were then masked, i.e. removed from further analysis. This filter proved effective at masking very noisy regions of acoustic images (see Fig 2.4), including

those containing interference from other active acoustic devices (see Fig 2.3b). This method did not work for rows of data where > 50% of the sample was dominated by noise (Fig 2.5), since the calculated median could be amongst either the attenuated or amplified backscatter values and hence part of the signal region would then be removed erroneously. These images were identified (Fig 2.5), where the total proportion of noise was more than 30% (a relatively conservative value) and removed from the analysis.

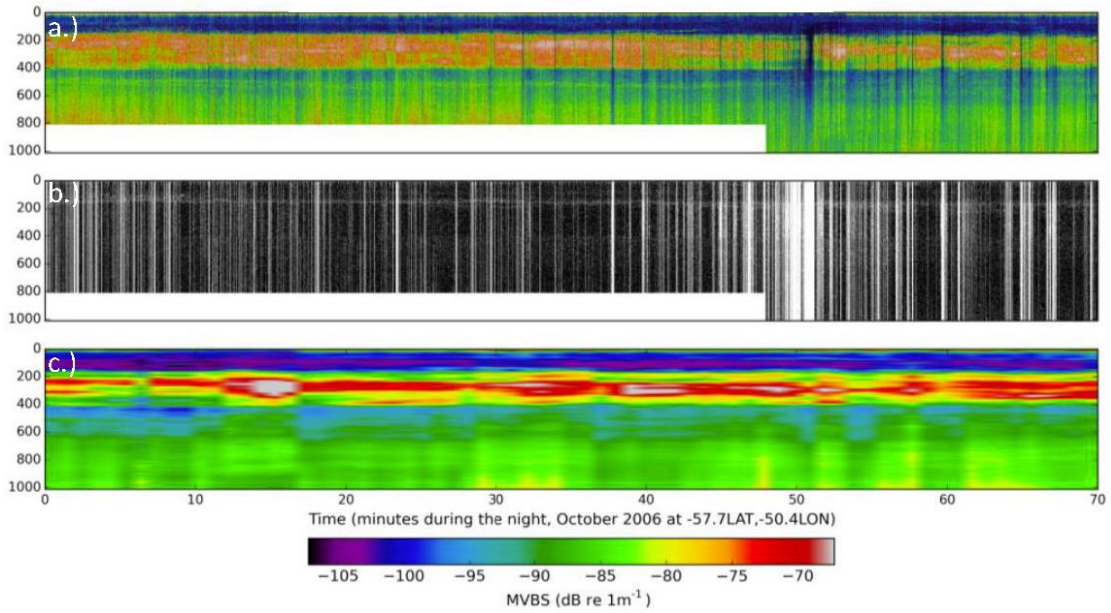

Figure 2.4: Application of Sound Scattering Layer (SSL) filter. Echograms show sampled depth by time. Example taken from JR311 expedition: a.) Original acoustic image; b.) Noise mask; c.) Integrated data.

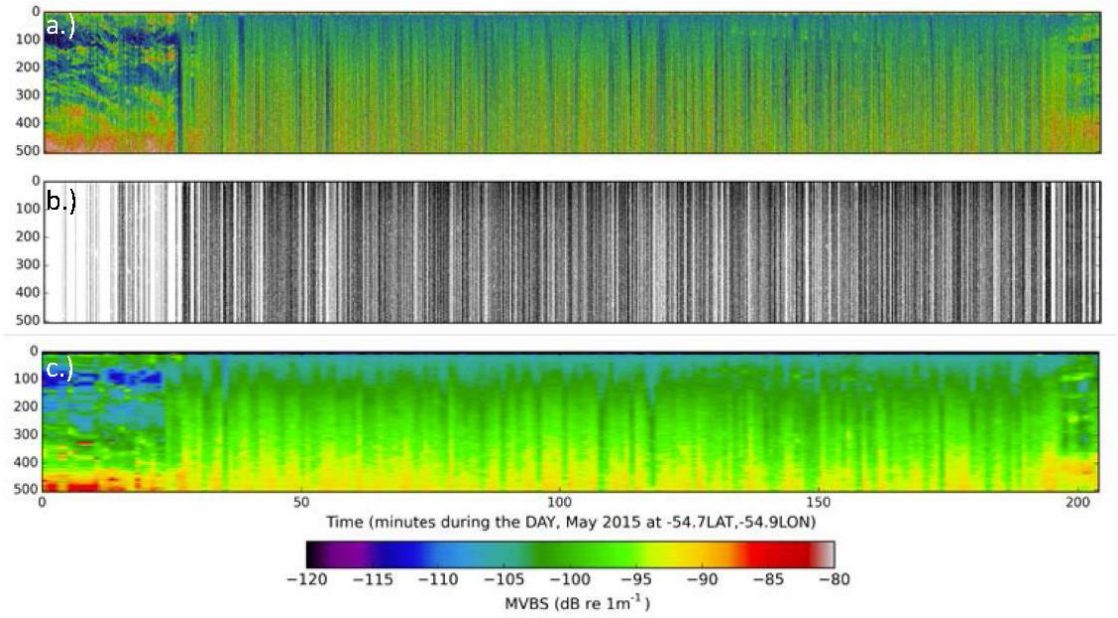

Figure 2.5: Noise dominated acoustic image (sampled depth by time). The Sound Scattering Layer filter removes signal (LHS) in this instance as the image is dominated by noise. Example taken from JR311 expedition. a.) Original acoustic image; b.) Noise mask; c.) Integrated data. This data was not used in the analysis of SSLs.

2.4.5 Seabed interruption

The seabed produces a relatively large backscattering response, as it is a solid and has a high acoustic impedance for a soundwave travelling through a fluid medium (MacLennan & Simmonds, 2005). The threshold applied to the data (see previous section) removes the feature partially, but is still apparent. A simple algorithm was developed to detect persistent strong backscatter values (> -40dB, substantially larger than the strongest DSLs) and to identify images for visual checks to be made; where a seabed was present, the image was excluded. A second problem that arises from seabed scatter, are multiple reflections between the seabed and surface boundary, resulting in a false bottom echo (Fig 2.3a) appearing at some depth (dependent upon actual seabed depth and ping interval) and is markedly weaker than the original since it has travelled much further (and not been correctly compensated for by the TVG). This can cause problems since they can resemble SSLs or fish schools, but are normally easy to spot (organisms usually move with purpose in the water-column, vertically or horizontally, whereas false seabed echoes deviate unnaturally). There has been some recent development of methodologies to deal with these features, but they are applicable at the recording stage – not the processing stage (Renfree & Demer, 2015). For this study, each

image that was processed was plotted and viewed, images that appeared to include a false seabed echo were excluded from the rest of the analysis; it is impossible to objectively conclude that all were removed, but the vast majority were, and any remnants left, would not cause any significant changes to the results.

2.4.6 Mean Volume Backscattering Strength

Each image at this stage consisted of between 20 million and 250 million data values. Before the data could be analysed further (Ch 3), they were volume integrated into larger cells that were 5m in depth by 1 minute in time. The mean of the volume integration was calculated, the Mean Volume Backscattering Strength (MVBS – Appendix B), reducing the grid size, whilst maintaining an adequate scale for regional SSL analysis; regional SSLs are typically 10's to 100's of meters vertically and can extends for 1000's of km. Images that were particular noisy would end up with large regions full of masked values. To enable a cleaner SSL extraction, these regions were removed and the resulting two sections merged; this assumed that regional scale SSLs don't vary significantly over time periods of the order of minutes. The resultant dataset consisted of 3196 cleaned images, ready for SSL extraction and description.

Chapter 3: A method for identifying Sound Scattering Layers and extracting key characteristics

This method was published in May 2015 in Methods in Ecology and Evolution:

Proud, R., Cox, M. J., Wotherspoon, S., & Brierley, A. S. (2015). A method for identifying Sound Scattering Layers and extracting key characteristics. *Methods in Ecology and Evolution*, *6*(10), 1190-1198.

This chapter is an expansion of that publication.

We developed an automated and reproducible method for Sound Scattering Layer (SSL) identification and characterization, the SSL Extraction Method (SSLEM). It functions independently of echosounder frequency and the spatial scale (vertical and horizontal) of the data. Here we demonstrate the SSLEM through its application to identify SSLs in data gathered to a depth of 1,000 m using 38 kHz hull-mounted echosounders in the South West Indian Ocean and Tasman Sea. SSLs were identified in the water-column as horizontally extensive echoes that were above background noise. For each identified SSL a set of 9 quantitative 'SSL metrics' (describing their shape, dynamics and acoustic backscattering distribution) were calculated, enabling inferences to be made concerning the spatial arrangement, distribution and heterogeneity of the biological community. The method was validated by comparing its output to a set of visually-derived SSL metrics that were evaluated independently by 8 students. The SSLEM outperformed the by-eye analysis, identifying three times the number of SSLs and with greater validity; 95% of SSLs identified by the SSLEM were deemed valid, compared to 75% by the students.

3.1 Introduction

There are parallels between the pelagic and tropical rain forest ecosystems, in as far as both have vertical (depth) layered structure that with increasing depth is increasingly light-limited. The sea surface, like the forest canopy, can be studied remotely by satellites and yield estimates of biomass and primary production (PP) (Longhurst, 2003; Anderson, 2012). The sea bed is a physically-fixed entity and organisms living there, like organisms and vegetation of the forest floor, are amenable to study because they are constrained by a two-dimensional environment. The ocean interior, however, is physically dynamic, and its inhabitants – pelagic organisms including zooplankton and fish – have freedom to move in three dimensions so the dynamics of the sometimes-dense layers of mid-trophic level communities are poorly understood (Lehodey et al., 2010). Developments in forest sampling can perhaps guide developments in ocean sampling.

3.1.1 Rainforest canopies and the pelagic water-column

In an effort to improve understanding of rainforest interiors, the 'RAINFOR' project (Malhi et al., 2002) that was established over a decade ago initialised a network of sampling sites for Amazonian rainforest ecosystems. As part of the initiative, field measurements of the forest interior were taken and the data related back to satellite information in order to gain a more complete picture of the ecosystem and to provide the capability to validate remotely-sensed data. Since the rainforest covers less than 7% of the earth's surface (Bierregaard et al., 1992; Wilson, 1994), a network of sites can provide a representative sample. The ocean on the other hand, covers over 71% of the earth's surface and therefore makes it extremely difficult, logistically and financially to study the pelagic community by in-situ biological sampling alone. The required greater spatial coverage for the ocean can be achieved by using active acoustic sampling techniques (scientific echosounding) to rapidly observe large volumes of the ocean, from ship-based instruments routinely used on both research and fishing vessels. These acoustic data can help reveal the spatial structure of pelagic communities: many marine organisms scatter sound waves in a characteristic fashion (dependant on the frequency of the incident wave and anatomy of the organism) such that 'remote sensing' by echosounder can provide community insight. These data could then be linked back to remotely sensed PP data at the surface, acquired from online resources such as the National Oceanographic Data Centre (NODC, www.nodc.noaa.gov) and validated by biological point samples, available from, for example, the Ocean Biogeographical Information System (OBIS, www.iobis.org). Acoustic

survey data already exist in vast quantities, with wide geographic coverage, leading to the possibility that a method capable of identifying and characterising pelagic communities, found within sound scattering layers (SSLs), would, akin to the RAINFOR project, potentially enable deep ocean processes to be inferred from satellite observation of the surface, yielding a more complete understanding of ocean ecosystem function. To achieve this, first a repeatable technique to identify and parameterise SSLs, extracted from echograms, is required.

3.1.2 The acoustic image

An echogram (Fig 1.5) is a form of image, an acoustic image, that details, for a specific frequency and resolution (depth by time), the scattering response (intensity) of the water-column, down to a depth that is dependent upon signal-to-noise ratio (and therefore incident frequency), over a period of time. The image can represent a static position (time-series) or a transect at speed across a region (survey). The image itself is made up of two principal components, signal (subject to study) and noise (the remainder). In order to process the image, the signal needs to be identified and the majority of the noise removed, to enable useful metrics to be extracted. Image processing techniques, using thresholds and filters can be used to differentiate between strong/weak backscatter for example and image segmentation used to identify continuous regions of signal within echograms (schools/layers). The problem with the acoustic image is that the scatter from organisms can vary by up to a factor of a million (between a large fish and small copepod for example at 38 kHz) meaning that thresholds are redundant when they are applied to more than one environment/situation; for example, applying the same threshold to identify mesopelagic fish (small weak scatterers, mean of -60 dB re $1m^2$:Irigoien et al., 2014) to tropical mid-water fish such as small tuna (strong scatterers, -46 dB re $1m^2$: Doray et al., 2006; Doray et al., 2007), would result in a significant oversight in the spatial distribution and abundance of the tropical fish. In order to establish an automatic and standardised method of SSL extraction, the technique must use relative values, which are derived from each environment/acoustic image.

3.1.3 Aims

No standardised objective approach exists for defining SSLs, rendering comparisons between studies and between water-column communities and the environment difficult beyond the merely descriptive. The lack of a consistent analytical approach was identified by Handegard et al. (2013) as hindering marine ecosystem monitoring and management. Our overarching goal

was to develop a standardised analysis method to extract biological layers consistently from underway-acoustic survey data. We illustrate the utility of our method here by identifying SSLs from data observed at 38 kHz in the South West Indian Ocean and Tasman Sea. Application of this method will lead to a better understanding of mid-trophic level communities, within and across oceanic boundaries at varying spatial and temporal scales.

3.2 Materials and Method

3.2.1 Acoustic data

The acoustic data used in this study were a subset of the 38 kHz acoustic data described in Chapter 2, originally obtained from the Integrated Marine Observing System (IMOS, www.imos.au, downloaded on 1st June 2013) data centre. 38 kHz data were suitable for SSL observations because the moderately low attenuation rate (5 - 10 dB/km: Ainslie & McColm 1998) enables deep water-column penetration (up to 1500m) and because the wavelength is appropriate for detection of many of the fish and plankton species of the order of cm's that inhabit the layers. Data had been collected by research vessels (RV) *Southern Surveyor* and *Aurora Australis*, as well as several fishing vessels (FVs) including the *Southern Champion*, *Janas*, *Rehua*, *Austral Leader II* and *Will Watch*. Data were granted by the Marine National Facility and processed by the Commonwealth Scientific and Industrial Research Organisation (CSIRO) Oceans and Atmosphere Flagship as part of the IMOS Bio-Acoustic Ships of Opportunity (BASOOP) Program. The data totalled 24 transects covering wide areas of the South West Indian Ocean and Tasman Sea (Fig 3.1). Transect length ranged from 200 NM to 1800 NM and included 24hr (day/night) coverage across all seasons between 2009 and 2012. The spatial coverage of the tracks included 2 of the 4 major global ocean biomes as described by Longhurst (1998) - the Trades and Westerlies - and also spanned major frontal zones and boundaries including the Subtropical Convergence Zone (STCZ) and the Polar Front (PF).

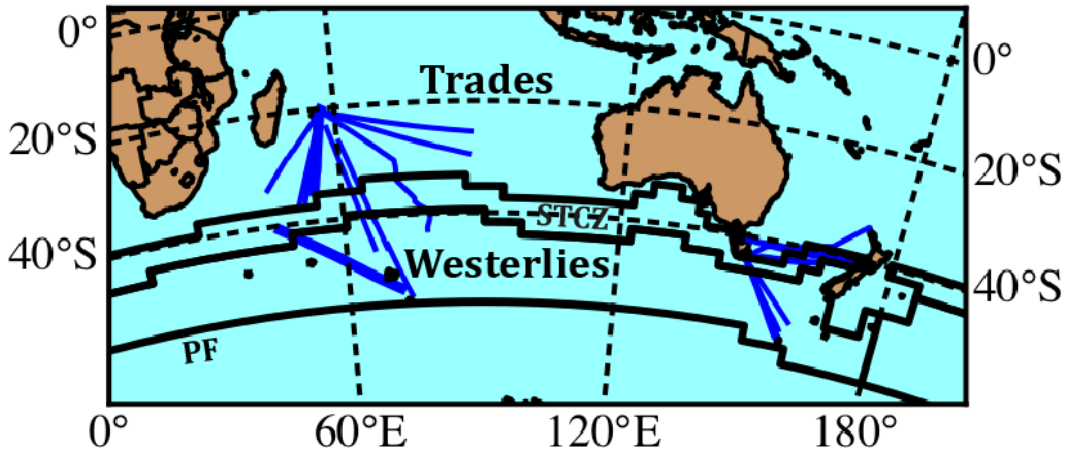

Figure 3.1: Map showing ship transect lines (blue) for acoustic data extracted from the Integrated Marine Observing System (IMOS) data centre. Mean positions of the Subtropical Convergence Zone (STCZ) and Polar Front (PF) are marked as well as two Longhurst Biomes, the Trades and the Westerlies, separated by the northern boundary of the STCZ.

3.2.2 SSL extraction method (SSLEM)

Our objective was to provide a method that would function over the range of bio-acoustical echosounder frequencies in common (and likely future) use, over horizontal scales from bays to oceans, and on vertical scales that encompass microlayers (Holliday et al., 2003) upwards to tens and hundreds of m. The common observational frequency band (18 to 200 kHz) spans the Rayleigh and geometric scattering regions for most zooplankton and nekton. This means that small changes in frequency can result in large changes in backscattering intensity and hence in SSL descriptors. Layers only become apparent acoustically when they can be distinguished from background noise (sufficiently high signal-to-noise ratio – SNR). SNR is a function of organism packing density, acoustic Target Strength, depth, insonification frequency and power, and environmental conditions (Simmonds & MacLennan, 2005). SSL appearance may also be influenced by sampling resolution (Korneliussen et al., 2008): for transect data resolution is determined by ping rate, beam angle, depth and ship speed. The geographic scale of data is an important consideration as there are many oceanic processes that occur over different spatial and temporal scales, from micro-turbulence to decadal oscillations. A robust general method should be capable of resolving features of interest at the scale of the study being conducted, and for the organisms of interest in the environment in which they exist.

The SSL extraction method (SSLEM) is based upon detection of a contrast in MVBS (Berge et al., 2014) between pixels within SSLs (relatively high MVBS signal) and background pixels outside (relatively low MVBS noise). For a simple SSL analysis, using a window of depth range Z and time/space extent X, one could identify a vertically 'static' SSL surrounded by empty water by selecting pixels for which MVBS intensities were greater than the mean, μ, over the entire window. Under such a scheme, for any acoustic pixel (px) within the analysis window,

$$ssl = \begin{cases} 1, & px > \mu \\ 0, & px \leq \mu \end{cases} \quad (3.1)$$

where *ssl* is a Boolean variable, taking a value of 1 for pixels that are deemed to belong to an SSL and 0 for those that are not. This simple process, useful as an introduction to the method, assumes that the SSL is completely contained by the analysis window and the surroundings are made up of pixels with low MVBS that is attributable to background noise. This may not be the case; for example, a transition between depth intervals that exhibit a difference in background noise (inherently caused by time-varied gain (TVG) amplification of background noise) would yield a layer-like boundary of *ssl* pixels. To ensure that SSLs were surrounded by lower intensity MVBS (both towards the surface and the seabed), the depth interval of the analysis window was divided into two equal values, d_1 and d_2, and pixels were only deemed a SSL pixel (*ssl* value of 1) when their MVBS value was larger than both the MVBS means, μ_1 and μ_2, over each of the two regions of the split window (Fig 3.2a), yielding a new equation for *ssl*:

$$ssl = \begin{cases} 1, & (px > \mu_1)\ AND\ (px > \mu_2) \\ 0, & otherwise \end{cases} \quad (3.2)$$

where μ_1 and μ_2, are calculated over the regions X by d_1 and X by d_2 respectively, and where d_1 is equal to d_2.

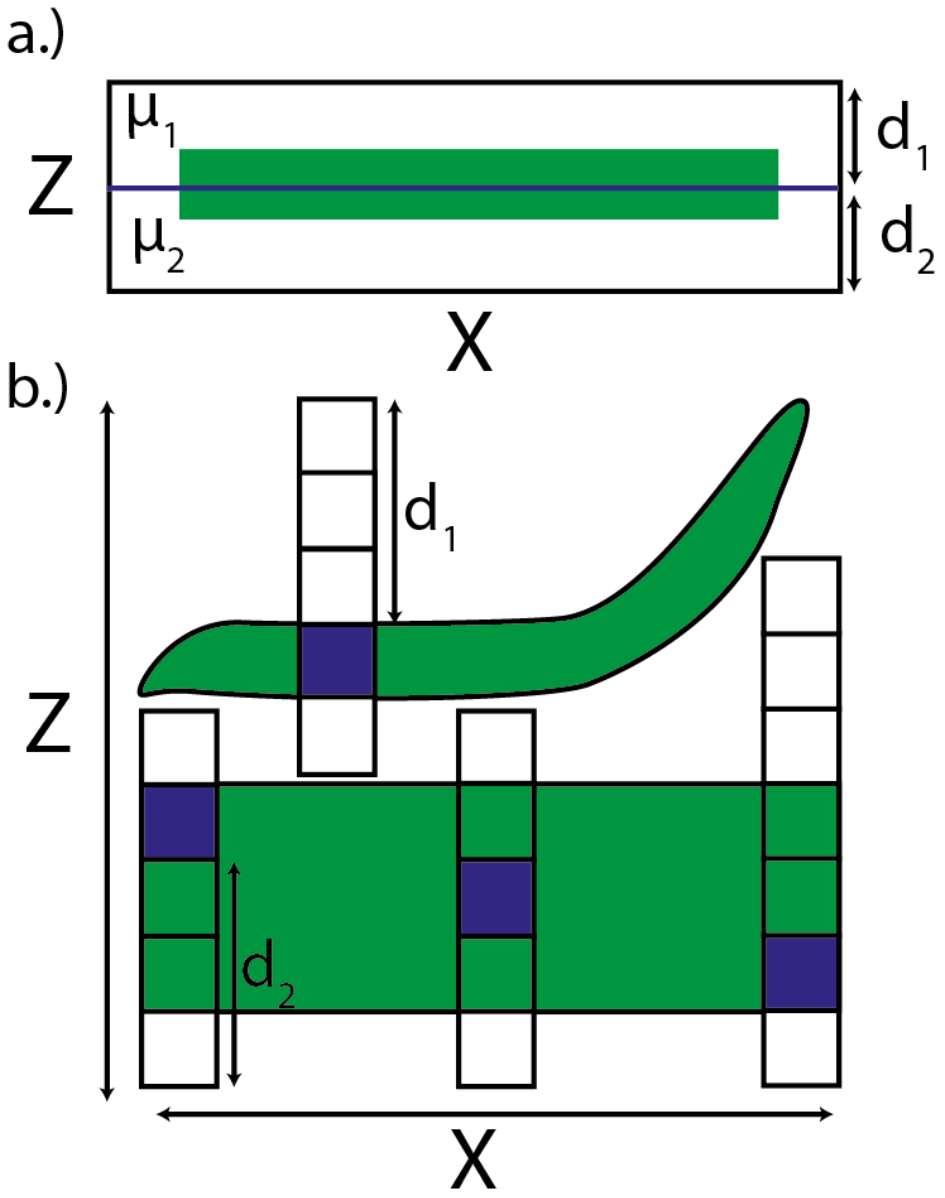

Figure 3.2: Identification of Sound Scattering Layer (SSL) pixels, where green features indicate relatively high intensity SSLs, white background indicates low intensity noise (or empty water) and blue cells represent the SSL pixel being evaluated. a.) Simple SSL analysis window: only vertically static SSLs separated by a distance larger than d_1 or d_2 are detected b.) Dynamic SSL analysis column: a column is moved pixel by pixel through the image, where at each step the column size ranges from the minimum (5 pixels in length; where d_1 and d_2 are both equal to 2 pixels plus the pixel being evaluated) up to the full vertical extent of the Z axis, by stepping through all the possible values for each of the two parameters, d_1 and d_2; in doing so, SSLs of varying separation distances and vertical behaviours are captured.

In practice, using a fixed analysis window does not capture all SSLs, since they are rarely vertically static: they may for instance oscillate with internal wave activity or migrate vertically. To accommodate this, an analysis column one pixel wide was used instead of a window. The column was moved pixel-by-pixel through the image evaluating the pixel at the centre of the column at each step, such that μ_1 and μ_2 were calculated over the specific column (single point in time-series), not the entire window, bounded either side of the central pixel by the depth ranges d_1 and d_2. For constant values of d_1 and d_2 this approach would only work if all SSLs had the same thickness and were separated by distances larger than the size of d_1 or d_2: this is not the case. To overcome this problem, the depth ranges d_1 and d_2, for each pixel evaluated, were varied in size from 2 pixels in height (this minimum, rather than 1, was used to avoid flooding the image with incorrectly assigned *ssl* pixels when analysing highly variable or 'noisy' images) up to the vertical extents of the image (Fig 3.2b). Then, for any pixel within an image, evaluated using a dynamic column,

$$ssl = \begin{cases} 1, & \left(\sum_{d_1=2}^{r-1} \sum_{d_2=2}^{R-r} (px > \mu_1) \; AND \; (px > \mu_2) \right) > 0 \\ 0, & otherwise \end{cases} \quad (3.3)$$

where r is equal to the row number of the pixel being evaluated and R equal to the total number of rows within the image; consequently, the first and last two rows of each image are not processed. Each pixel thus has multiple opportunities (for varying d_1 and d_2 values) to be attributed an SSL pixel. This ensured that both vertically static and migrant SSLs of varying thicknesses and separation distances would all be identified.

On occasions when no SSL was present in the analysis column, pixels would sometimes erroneously be designated as SSL pixels as a result of the backscatter from individual or diffuse arrangements of organisms, tightly packed schools or swarms, variation of the physical properties of sea water, or by natural variation inherent within the data. The variable, SSL_{min}, which designated a fixed minimum horizontal extent for SSLs (measured in space/time units), was therefore introduced to enable the identification of only those SSLs that were relevant to the scale of process being studied e.g. from ocean basin scale (large SSL_{min}) down to krill swarms (small SSL_{min}: Watkins et al. 1990). In spite of this precaution, the natural variation within the data still sometimes produced SSLs. These incorrectly identified SSLs, termed 'phantom SSLs' (Fig 3.3) were removed in post processing (3.3.1) by analysis of SSL signal-to-noise ratios; SSLs were removed where the mean SSL MVBS (signal) was smaller than the

maximum background MVBS value (noise) by analysing the pixels immediately surrounding the layers.

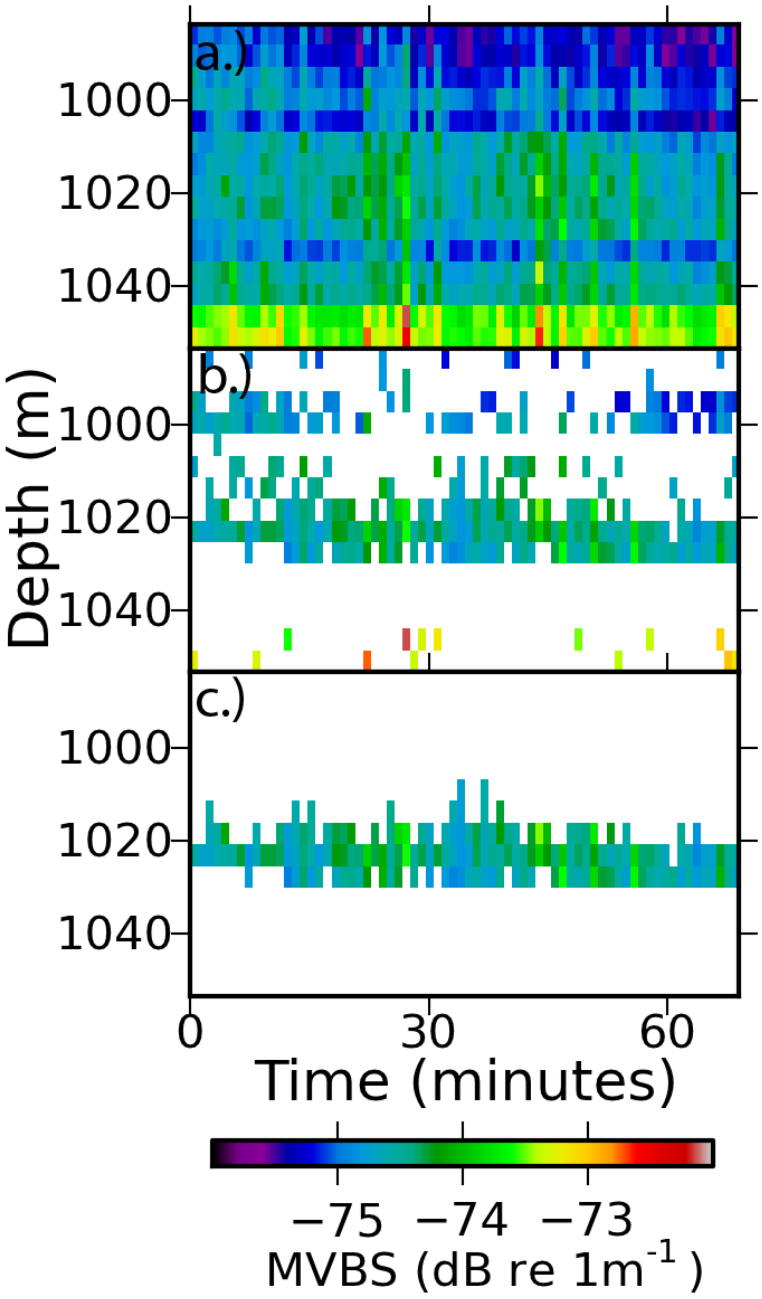

Figure 3.3: Phantom Sound Scattering Layer (SSL) extracted from FV *Austral Leader II* transect during May 2012, where SSL_{min}, the minimum horizontal resolution of SSLs, was set to 60 minutes a.) acoustic image segement; b.) SSL pixels identified by the method. c.) Extracted phantom SSL: MVBS values of the SSL are similar to that of the surrounding background.

The SSL pixels identified were used to generate an SSL mask (Fig 3.4b) that bounded pixels that were connected, termed SSL features. These features were not classified as SSLs at this point, as a single feature could consist of several merged SSLs. Features smaller than SSL_{min} were removed and internal gaps smaller than SSL_{min} within accepted features were filled (Fig 3.4c).

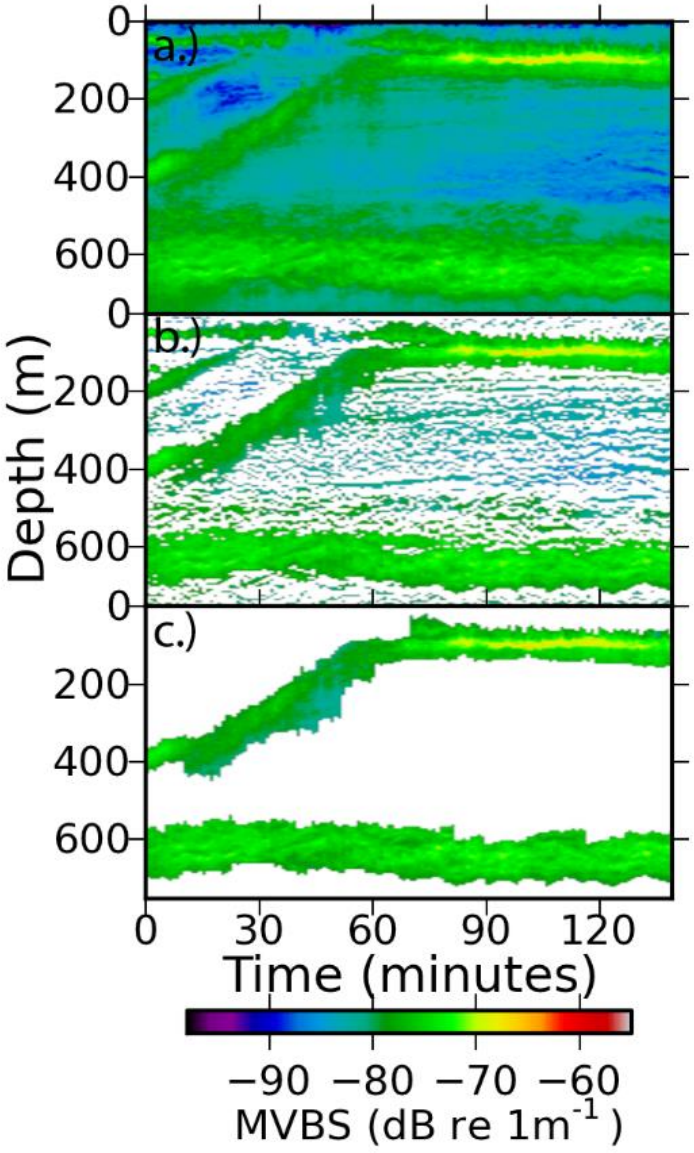

Figure 3.4: Processed acoustic image, from FV *Austral Leader II* transect during May 2012, where SSL_{min}, the minimum horizontal resolution of Sound Scattering Layers (SSLs), was set to 60 minutes. a.) Original acoustic image at a resolution of 5m in depth and 1 minute in time. b.) Masked image: only pixels that are deemed to be potential SSL pixels are shown. c.) SSLs identified after removing features smaller than SSL_{min} and filling SSL internal gaps (that are smaller than SSL_{min}).

Each feature was then segmented into individual SSLs which existed over a discrete depth range at each point along a time-series. This was achieved by implementing a region-based image segmentation process. A simple growing algorithm moved column by column through the image, initialising new regions (that would eventually grow into individual SSLs) within features where SSLs merged or split (Fig 3.5). SSLs identified in this process that were smaller than SSL_{min} were ignored and not analysed further.

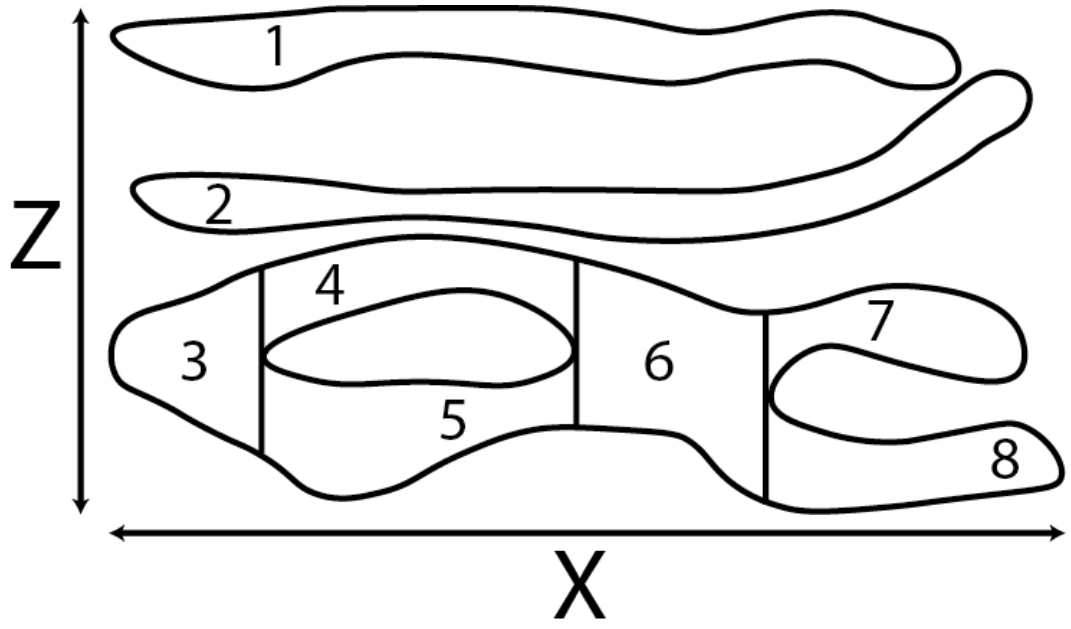

Figure 3.5: Segmentation of Sound Scattering Layers (SSLs) features into individual SSLs. Each SSL was assigned a unique index value.

Vertically static SSLs were separated from upwardly or downwardly-migrating SSLs by application of a Change Point Analysis (CPA: Page 1954). CPA can detect the existence of multiple trends within a time series by analysing the cumulative deviation from the mean over time. The CPA was conducted using a time-series of the mean depth change, ΔZ, over a selected time interval, CPA_{int}, across each SSL (Fig 3.6). The choice of CPA_{int} is related to the size of SSL_{min}. For a relatively large value of SSL_{min} (> 4 hours for example) a large CPA_{int} value can be chosen and will reduce the likelihood that undulating SSLs, caused by internal waves, would be incorrectly segmented. For small values of SSL_{min}, a CPA_{int} value should be selected to provide enough samples (>10) for the CPA to be conducted appropriately. The deviation of ΔZ from its mean was calculated (Fig 3.6b), followed by the cumulative sum of this deviation (Fig

3.6c), the most significant point of change was indicated by the largest absolute value (Fig 3.6c – black line), and quantified by the range, CPA_{max}, of the cumulative sum values. A confidence interval (CI) was calculated by determining the percentage of 1000 bootstrapped samples of ΔZ that yielded a CPA_{max} value smaller than the original CPA_{max} value. Where a significant change occurred (95% CI), indicating that a SSL changed from simply varying in depth around a static mean to exhibit migrant behaviour (increasing/decreasing depth), SSLs were separated into migrant and static components (Fig 3.6).

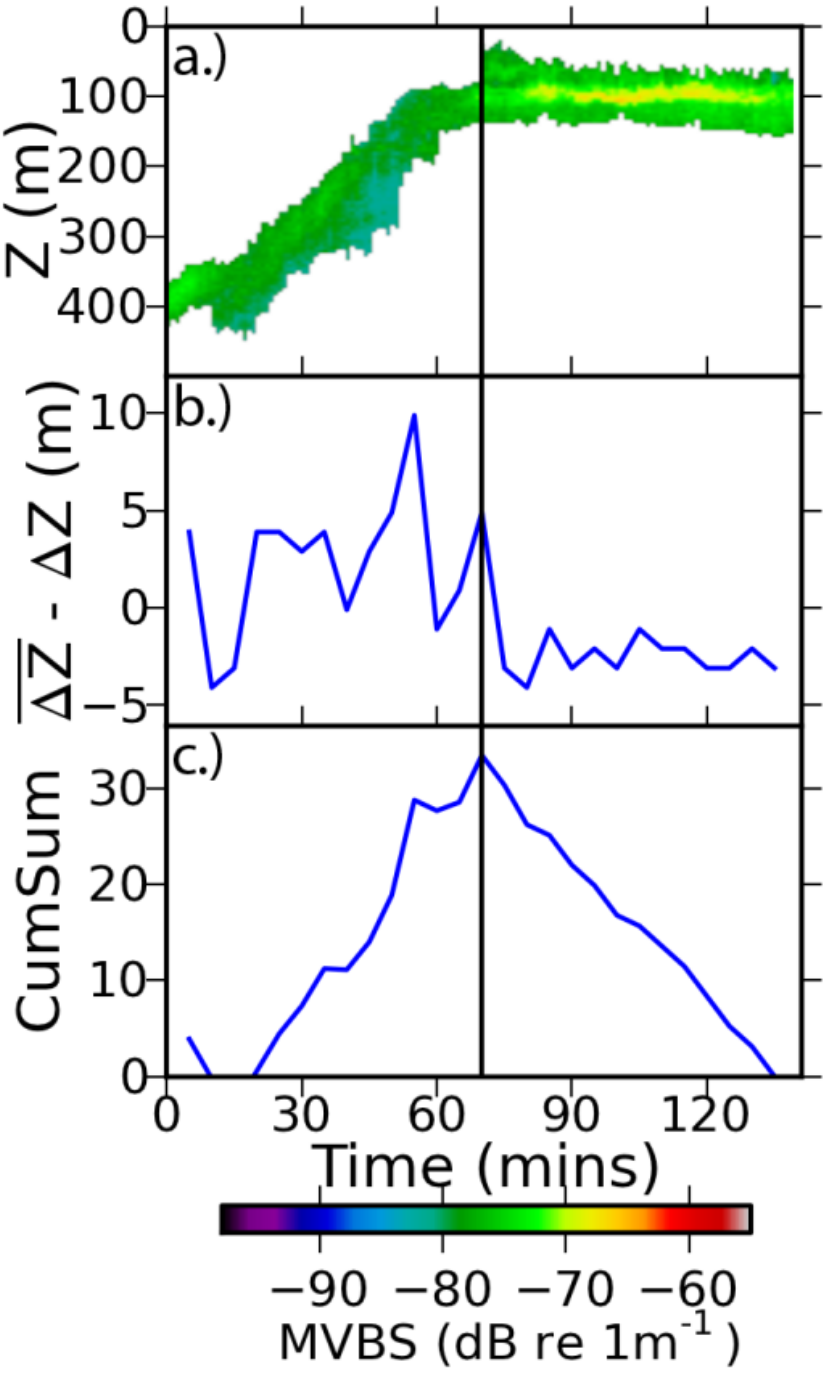

Figure 3.6: Change Point Analysis of mean Sound Scattering Layer (SSL) depth – SSL taken from the example image in Figure 3.4. The vertical black line at 70 minutes - the maximum point of the cumulative sum of b.) - indicates the point of separation of a static SSL and a migrant SSL. a.) SSL depth b.) The overall mean depth change of SSL minus each mean depth change in the time-series (binned at 6 min intervals) plotted in time c.) Cumulative sum of b: the maximum value indicates the most significant point of change.

The CPA was conducted iteratively, until no further statistically significant change (95% CI) within an image segment could be detected: this ensured that multiple migrations, during a diel cycle for example, would all be separated. Multiple migrations were unlikely to occur in this study since at an earlier stage we partitioned the data into separate day and night segments.

For each individual SSL identified a set of SSL metrics were evaluated (Table 3.1). The depth, duration, MVBS, MVBS standard deviation, MVBS range and layer thickness described spatial extent and backscatter distribution. The vertical velocity and depth range were used to identify and describe migratory layers. The Background Noise Level (BNL) was used to quantify the maximum level of noise surrounding the SSL. The maximum value was taken to ensure that it would be greater than the mean MVBS value of SSLs consistent of natural variation within the data (phantom SSLs).

SSL metric	Definition	Unit
Depth	mean depth	m
Depth range	Max(depth) – Min(depth)	m
MVBS	MVBS over entire SSL	dB re $1m^{-1}$
MVBS range	Max(MVBS) - Min(MVBS)	dB re $1m^{-1}$
MVBS STD	standard deviation of MVBS	dB re $1m^{-1}$
Thickness	mean SSL thickness	m
Vertical velocity	(change in depth)/time	ms^{-1}
Background Noise Level (BNL)	Max (MVBS) of background pixels surrounding SSL	dB re $1m^{-1}$
Duration	length of SSL duration	(H:M:S)

Table 3.1: Sound Scattering Layer (SSL) metrics: summary metrics for individual SSLs. The unit dB re $1m^{-1}$ represents 10 times the log base 10 value of a variable with units of m^{-1}, in this case the mean volume backscattering coefficient (Simmonds & MacLennan, 2005), that is relative to a reference level of $1m^{-1}$. Underlying MVBS values were first transformed into linear units, before summary metrics were calculated and then back-transformed into log units.

The SSL metrics were analysed to gain objective insight into the nature of SSLs within the study region, enabling inferences concerning the pelagic community (spatial arrangement, distribution and heterogeneity) to be made.

3.2.3 Validation framework

In order to examine the efficacy of our automated SSL identification technique versus the principal present approach, adopted by most acoustic-trawl surveys when assessing fish stocks – visual scrutinisation (which may be subjective and prone to between-operator inconsistencies) - we designed a validation framework to examine potential differences between SSLs determined by the SSLEM and visually scrutinised acoustic images. If visual scrutiny gave highly variable results, this would illustrate the difficulty likely to be encountered in comparative studies and the requirement of an automated method.

The validation was conducted using a subset of the IMOS data. Images from this subset were published online at www.soundscatteringlayers.com. Independent visual scrutiny was performed autonomously by a group of 8 students, all of whom had attended an acoustic data collection and processing summer school (www.depts.washington.edu/fhl/) and were either PhD candidates at the University of St Andrews or the Florida International University. Each student estimated 3 SSL metrics, namely the depth, MVBS and thickness for all SSLs they could identify that persisted for a time period longer than 1 hour. Each student considered 10 images selected randomly from a set of 50. The results of the visual scrutiny were compared to those from SSLEM (3.3.1).

3.3 Results

Sound Scattering Layers (SSLs) that persisted for time periods longer than 1 hour (SSL_{min} = 60 minutes; change-point-analysis time interval (CPA_{int}) = 6 minutes: see 3.2.2 for definitions) were identified and extracted from the IMOS dataset (3.2.1) using the SSL extraction method (SSLEM). SSLs were extracted at these setting in order to conduct a regional analysis of the study area, ensuring that only persistent and therefore characteristic SSLs were identified. In total, 2064 SSLs were extracted from 264 images that were on average 3.4 hours in length; an example of the identification of SSLs for an IMOS image is given in Fig 3.4. 108 phantom SSLs (3.2.2) that were identified in the validation procedure were removed. For each SSL, SSL metrics described in Section 3.2.2 were determined and relationships found between select SSL metrics explored (3.3.2).

3.3.1 SSLEM Validation

SSL Metrics that were estimated by the students from SSLs visually identified were mapped back on to the original acoustic images for comparison with the SSLEM identified SSLs. Each visually identified SSL was categorised as being a valid/invalid SSL identification. This process was mirrored using the output from the SSLEM, where phantom SSLs (3.2.2) were visually identified after extraction and deemed to be invalid SSLs comprised of background noise. The students identified 211 SSLs from 80 images. For the same SSLs that were identified by more than 6 of the students from the same image, mean ranges of the estimated metrics were calculated (Table 3.2).

Method	Mean depth range (m)	Mean MVBS range (dB re $1m^{-1}$)	Mean thickness range (m)	< SSL_{min} (%)	Noise (%)	TVG (%)	Valid (%)	Invalid (%)
SSLEM	0	0	0	0	5.2	0	94.8	5.2
VISUAL	26.3	4.8	53	5.7	8.5	10.4	75.4	24.6

Table 3.2: Summary of method output versus visual scrutiny for identification of Sound Scattering Layers (SSLs). Columns definitions from left to right: Method – method of SSL identification; Mean depth range, Mean MVBS range & Mean thickness range – mean ranges of values for the depth, MVBS and thickness metrics for repeat estimations of the same SSLs; < SSL_{min} – percentage of SSLs identified smaller than the pre-set minimum value; Noise – percentage of SSLs consistent of background noise (including phantom SSLs); TVG – percentage of SSLs made up of 'layer-like' noise bands amplified by time-varied gain (TVG); Valid – number of correctly identified SSLs; Invalid – number of incorrectly identified SSLs. Percentages and means are to 1 d.p.

Of the three SSL identification fields in Table 3.2 (< SSL_{min}, Noise & TVG), the Time-Varied-Gain (TVG) field contained the largest proportion of the student's misclassification of SSLs. The TVG increases the amplitude, as a function of time (or depth for a fixed sound speed) of the echo return and serves to amplify both signal, when organisms are present, and the background in an empty pixel, which appears in the acoustic image as depth dependent noise (Simmonds & MacLennan, 2005). This essentially limits the useful (range over which signal dominates noise) range of the instrument and causes visible, layer-like bands to form at the far extent of this range. These layers can resemble SSLs during visual scrutiny, but not to the SSLEM; normally TVG is removed in pre-processing but can just as easily be removed afterwards (e.g. Watkins & Brierley, 1996).

The SSLEM identified, on average, over 3 times the number of SSLs per acoustic image than the group of students. Whereas the SSLEM output included no variance between repeat identifications and characterisations of SSLs from the same image, the overall mean standard deviation of the number of SSLs identified per image for the students was 0.54. This is in fact quite low, and demonstrates that although the students identified fewer SSLs, the group broadly did agree on the number of SSLs per image. Metric estimates by the students were, however, notably large, especially the mean MVBS range (4.8 dB re $1m^{-1}$) that is equivalent to

a factor 3 change in the linear domain. The SSLs identified by the SSLEM were also much more likely to be valid (94.8%), i.e. not phantom SSLs, than those identified by the students (only 75.4% valid), who misidentified SSLs a quarter of the time (Table 3.2). The SSLEM extracted a total of 108 incorrect SSLs, all of which were considered to be phantom SSLs (3.2.2).

Phantom SSLs form by the naturally occurring variation in the data. They are an artefact of the SSLEM, and hence not detected by visual scrutinisation. This variability is of no consequence within SSLs, but can cause false SSL identification outside (i.e. in empty water - Fig 3.3). In order to remove phantom SSLs, the Background Noise Level (BNL) metric was used to identify SSLs that had low signal-to-noise ratios or more accurately, low BNL-to-MVBS ratios. SSLs that had a MVBS value that was smaller than the maximum BNL were identified as being phantom SSLs (black points in Fig 3.7). Removing these SSLs from the results increased the validity of the automated method, for the data analysed in this study, to 100%.

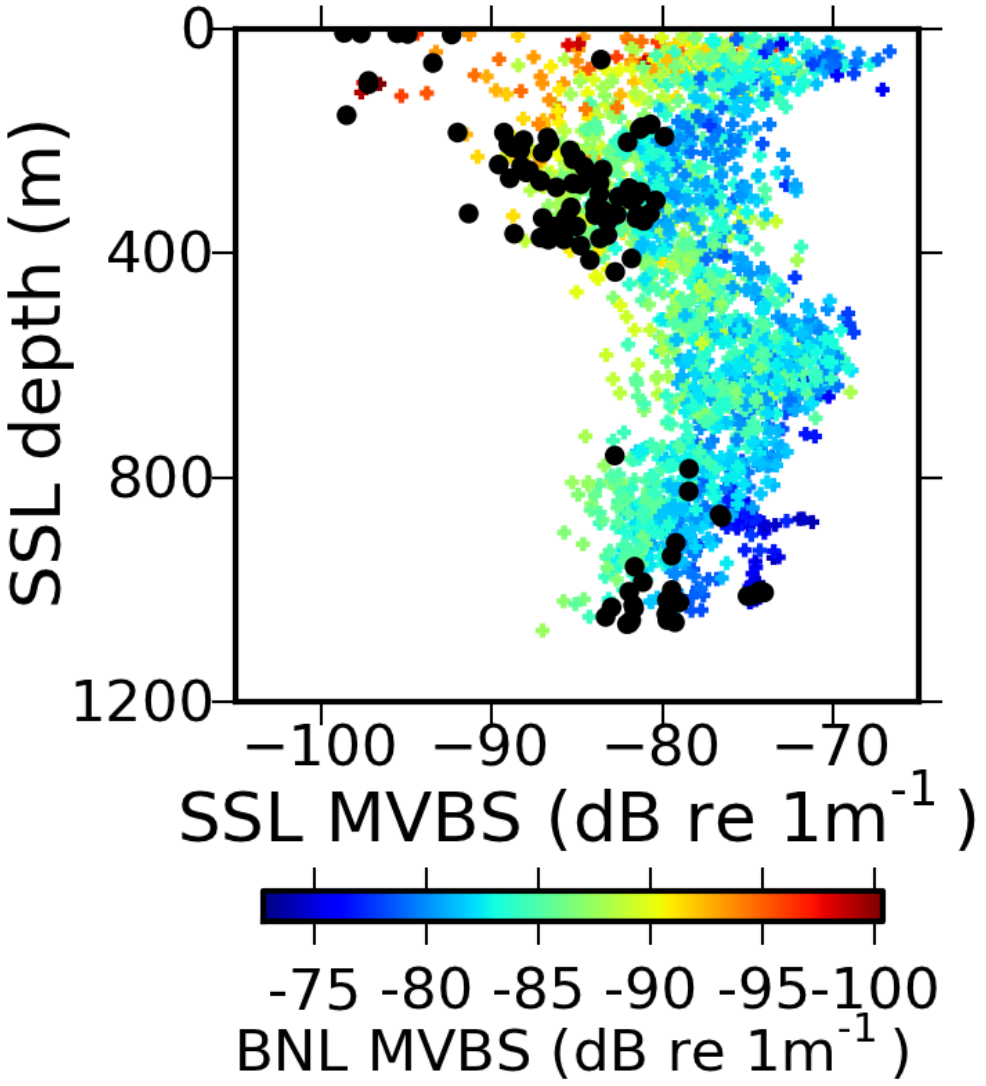

Figure 3.7: Background Noise Level (BNL) for Sound Scattering Layers (SSLs) extracted from the IMOS dataset by SSL depth and MVBS. Black points represent phantom SSLs (incorrectly assigned SSLs) identified where BNL > SSL MVBS.

Phantom SSLs are apparent throughout the entire water-column, except for the region between 400m and 800m. In this depth region within the study location of the South West Indian Ocean and Tasman Sea, strong and broad SSLs were persistently present (Fig 3.9), meaning that SSLs dominated, excluding the possibility of phantom SSLs forming at the same depth.

3.3.2 SSL Metrics

The SSLEM output a total of 1956 valid (non-phantom) SSLs from the IMOS data. Each SSL was summarised by a set of 9 SSL metrics (Table 3.1). The vertical velocity (W), SSL depth range and SSL duration (Fig 3.8) metrics aid in the identification of migrant SSLs; applying appropriate thresholds to each of these variables enable static and migrating SSLs to be separated.

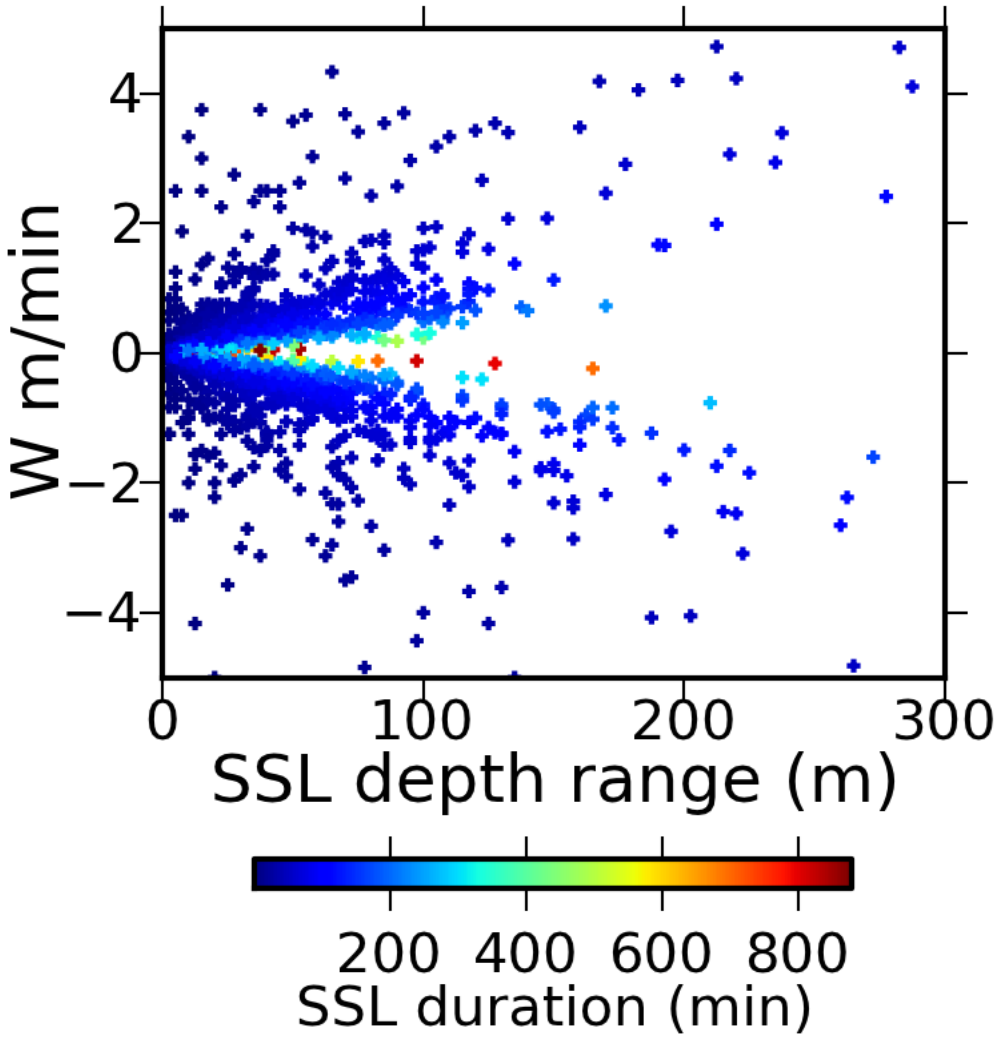

Figure 3.8: Migratory Sound Scattering Layer (SSL) metrics extracted from the IMOS dataset, where W is the mean vertical velocity of each SSL.

SSLs clustered around the origin (Fig 3.8 - 0, 0) are almost vertically static. Migrant SSLs begin to appear as the SSL depth range increases and the split between ascending/descending SSLs is evident from the decrease/increase in W. It is unlikely that the depth change of SSLs that

persist for periods longer than 3-4 hours are truly migrating with purpose in a diel sense. It is more probable that depth change over the extended period is related to changes in water mass properties, for example because SSLs are associated with isopycnals that are gradually increasing/decreasing with depth (Godø et al., 2012).

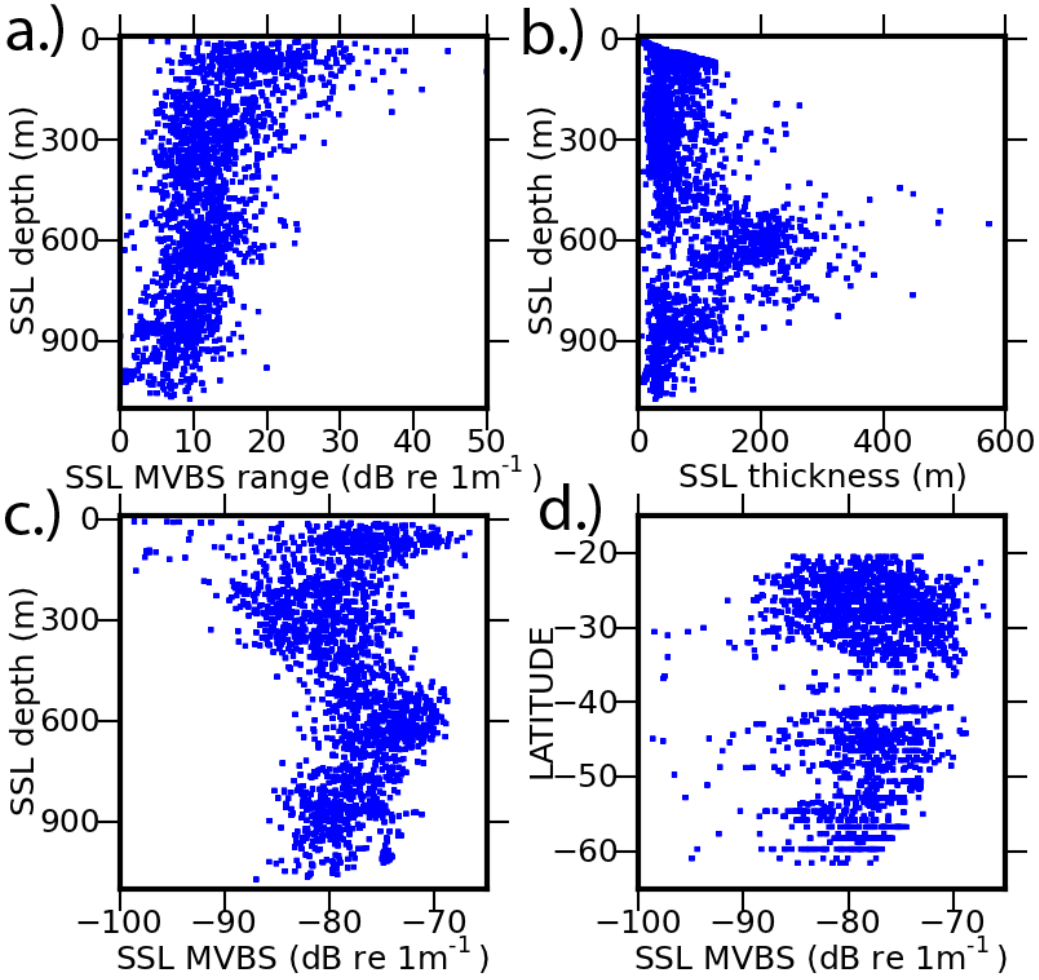

Figure 3.9: Sound Scattering Layer (SSL) metrics extracted from the IMOS dataset. a.) Water column heterogeneity: MVBS range serves as a proxy for biological complexity; b.) SSL thickness as a function of depth; c.) Depth distribution of MVBS; d.) Latitudinal distribution of MVBS.

Physical characteristics of SSLs provide biological/ecological insight into pelagic community dynamics. For example, the MVBS range increased towards the surface (Fig 3.9a) suggesting that the biological community becomes more complex/heterogeneous in the epi-pelagic region; this could be caused by an increase in species diversity or a larger range of the

orientations of organisms, caused by feeding for example. The broadest SSLs lie within the central portion of the mesopelagic region of the water-column (Fig 3.9b). The highest MVBS values (a proxy for increased biomass/abundance) occurred within the water-column at depths of around 600m and at the surface (Fig 3.9c) and also geographically towards 40° south (Fig 3.9d). This is consistent with the fact that the zone is the highly productive Subtropical convergence zone (see Fig 3.1; as identified by Longhurst 1998) where previous work has revealed an enhanced prey-field (Boersch-Supan et al., 2012).

3.4 Discussion

3.4.1 Sound Scattering Layer Extraction Method (SSLEM)

The Sound Scattering Layer (SSL) Extraction Method (SSLEM) was demonstrated here using data observed at a single frequency, 38 kHz. However, the method is independent of frequency and is entirely appropriate for use with other frequencies. The main differences that would occur would be subject to the characteristics of the incident frequency, for example, reduced depth range and increased resolution at higher frequencies (Simmonds & MacLennan 2005).

The efficacy of the SSLEM was examined by comparing output from that of visually scrutinised data (Table 3.2). The comparison demonstrated that the SSLEM method is more effective at identifying SSLs (3.3.1). Visually scrutinised images were subject to SSL misclassification, under classification and sample variation, whereas the SSLEM output was perfectly repeatable, with zero variance between repeat extractions of SSLs and metrics.

Merged vertically static and migrant SSLs were separated by an application of a change-point analysis (3.2.2). Analysis of the derived SSL metrics revealed water-column and geographical trends (Fig 3.9). Summarising these data into discrete metrics offers a method of standardised analysis for assessing variability in biological communities in the water-column. Importantly, acoustic survey data can now be condensed down from millions of values to a set of community descriptors that can be easily stored, shared and analysed.

3.4.2 SSLEM parameterisation

SSLEM requires two parameters, SSL_{min}, which sets the minimal SSL length, either in time or space and CPA_{int}, which sets the interval over which data are averaged for the CPA analysis. SSLEM can extract SSLs at any spatial or temporal scale, as SSL_{min} reduces, more and more ephemeral features, such as schools, swarms and micro-layers (often caused by sharpe changes in physical/biological structure) will be extracted, along with large features such as DSLs. At this stage, a maximum SSL duration parameter could easily be added and set to extract features over a specific range (e.g. from SSL_{min} to SSL_{max}). The value of CPA_{int} is set with consideration of system dynamics. For example, selecting a small value for this parameter could lead to SSLs being segmented at the peaks and troughs of internal wave structures, or break larger DSL structures into smaller pieces where small-scale protrusions exist (from

feeding events for example). A good recipe to follow would be to try various setting and analyse the output, consider what is important in your study and then adjust the parameters appropriately.

3.4.3 SSLEM Results

Results from SSLEM were summarized in Figure 3.9, allowing trends between SSL metrics to be analysed. The decrease in SSL MVBS range from the surface to the deep, maybe an artefact caused by decreasing levels of SNR with increasing depth, rather than a consequence of decreasing species diversity. At the study scale, general properties of the water-column are apparent, such as the DSL, a broad (200m, see Fig 3.9b) relatively strong (-80 to -70 dB re $1m^{-1}$, see Fig 3.9c) feature sitting at around 600m (Figure 3.9b) and also geographical trends, such as lower MVBS at higher latitudes (Fig 3.9d), a consequence of lower abundances of fish, which are relatively strong sound scatterers when compared to zooplankton, such as euphausiids, which are prevalent in polar regions. These trends could be assessed at smaller scales, by region and season for example, but this is beyond the scope of this study, which looks to assess long-term global trends.

3.4.4 SSLEM Applications

Analysis of the ocean's SSLs will enable the study of the ocean's mid-trophic structure, providing a global prey field that would be invaluable to predator-prey ecologists. SSL depths could be used to gauge energy expenditure of diving mammals (Boersch-Supan et al., 2012; Walters et al., 2014) and spatial arrangements of prey-fields that could be incorporated into existing biophysical models (for example, SEPODYM: Bertignac et al., 1998; Lehodey et al., 1998). Monitoring the structure of SSLs over long time periods could reveal climatic influences and the knock-on effects for SSL inhabitants (Lehodey et al., 2003). Spatially distinct formations of SSLs made up of diverse communities are likely to be distinguished and characterized by SSL metrics, allowing the division of regionally distinct biological communities (Longhurst, 1998). Whilst the SSLEM does not resolve communities at the species level, such as the Species Identification Methods from Acoustic Multi-frequency Information (SIMFAMI: Gajate et al., 2004) project, the SSLEM offers an alternate and simpler approach for fisheries and conservation management regimes to assess and monitor open ocean ecosystem health and stability (Korneliussen et al., 2008; Handegard et al., 2013).

3.4.5 Summary

The SSLEM presented here is directly applicable to all acoustic images (produced from any vessel/platform), including echograms output from Acoustic Doppler Current Profilers (ADCPs). The method works across the full range of frequencies (limited only by SNR) used in marine active acoustics (1 kHz – 1 MHz), yet only requires data output from a single frequency sounder to yield useful results. SSLEM is based upon simple image processing routines which enable automated processing and the evaluation of large (> 100 GB) acoustic datasets. Furthermore, it naturally lends itself to more complex multi-frequency analysis (Jarvis et al., 2010). Unlike other methods (e.g. Cade & Benoit Bird, 2014), the SSLEM was built to facilitate automated processing of data in a standardised fashion that would vary only with consideration of the resolution and scale of the study in mind. It is our hope that its introduction will enable the analysis of a wealth of data that is immediately available, offering insights into the biological structure of the world's ocean. The derived SSL metrics provide a means to summarise the extracted layers, making them readily available for a wide range of analysis. Importantly, the SSLEM offers the opportunity to study the structure of the mid-trophic communities in the ocean and will aid in improving our understanding of an ocean ecosystem.

Chapter 4: Pelagic Regimes: Statistically distinct regional-scale biological water-column structures

The Sound Scattering Layer Extraction Method (SSLEM: Ch 3) was applied to a large acoustic dataset, comprised of 3196 processed acoustic images (Ch 2) or echograms, covering 104,688 km (2.6 times the circumference of the Earth), collected within 14 of the 32 Longhurst pelagic provinces (Fig 1.6), extracting more than 40,000 Sound Scattering Layers (SSLs) in total. SSL metrics (depth, height and MVBS) were used to describe local (300 by 300 km scale) water-column communities via SSL probability distributions (SPDs). Using the SPDs, the depth of the primary component of the Deep Scattering Layer (DSL), which was likely to be consistent of myctophids, was derived. The SPDs naturally clustered together forming six distinct pelagic regimes. Each regime, essentially a probability distribution that described the chance of observing a particular pelagic community, was characterised by spatial SSL structure, SSL scattering strength and diel vertical migration (DVM) behaviour. Despite the pelagic regimes being clustered independently and consistent of both multi-seasonal multi-annual data, they naturally grouped together spatially, providing evidence that the mesopelagic community exists in spatially well-defined regions, similar to the ocean provinces described by Longhurst (1998).

4.1 Introduction

From the sea-surface to 1000 meters deep, the pelagic water-column can generally be divided into two regions, the epipelagic (0 – 200 m) and mesopelagic (200 – 1000 m). The epipelagic, contains a surface mixed-layer, which is illuminated, isothermal and variable in depth, providing a suitable habitat for primary production (PP), which is usually bounded by a steep seasonal thermocline. The mesopelagic is consistent of a much colder, darker and denser environment and is inhabited in the majority by layers of zooplankton and small bony fish, both of which, generally migrate daily to the surface at night to feed via diel vertical migration (DVM). The mesopelagic can be studied using acoustics: layers that occupy discrete depth ranges within this region are known as Deep Scattering Layers (DSLs). The depth of the DSL varies geographically and over time (Kloser et al., 2009). This variance is thought to be predictable since recorded depths of DSLs have been linked to environmental drivers such as density (Godø et al., 2012), light intensity (Hays, 2003) and oxygen concentration (Bianchi et al., 2013; Klevjer et al., 2016) and their biomass has been linked to primary production (Irigoien et al., 2014). These relationships, although not fully understood, indicate that globally, the mesopelagic community may split in to a discrete number of distinct ecological regions, akin to the surface ocean provinces described by Longhurst (1998), which were based on PP and regional oceanography.

4.1.1 Primary production

The rate of primary production (PP) for a sample of seawater can be directly measured via the ^{14}C stable isotope method (Nielsen, 1952), but global estimates are usually inferred from models such as the Vertically Generalized Production Model (VGPM: Behrenfeld & Falkowski, 1997), that consider relationships between PP and chlorophyll concentration. Chlorophyll concentrations are inferred from data collected by radiometers that are built into earth orbiting satellites. The Nimbus-7 satellite that was launched on October 24th, 1978 (NASA), recorded data using the Coastal Zone Colour Scanner (CZCS) and contributed to the first observation based estimate of global PP of 45-50 Gt C year^{-1} (Longhurst et al., 1995). PP varies widely both geographically and over time: mean seasonal levels of PP predicted via the VGPM using MODIS and SeaWiFS data obtained via the ocean productivity website (http://www.science.oregonstate.edu/ocean.productivity/index.php) are shown in Fig 4.1.

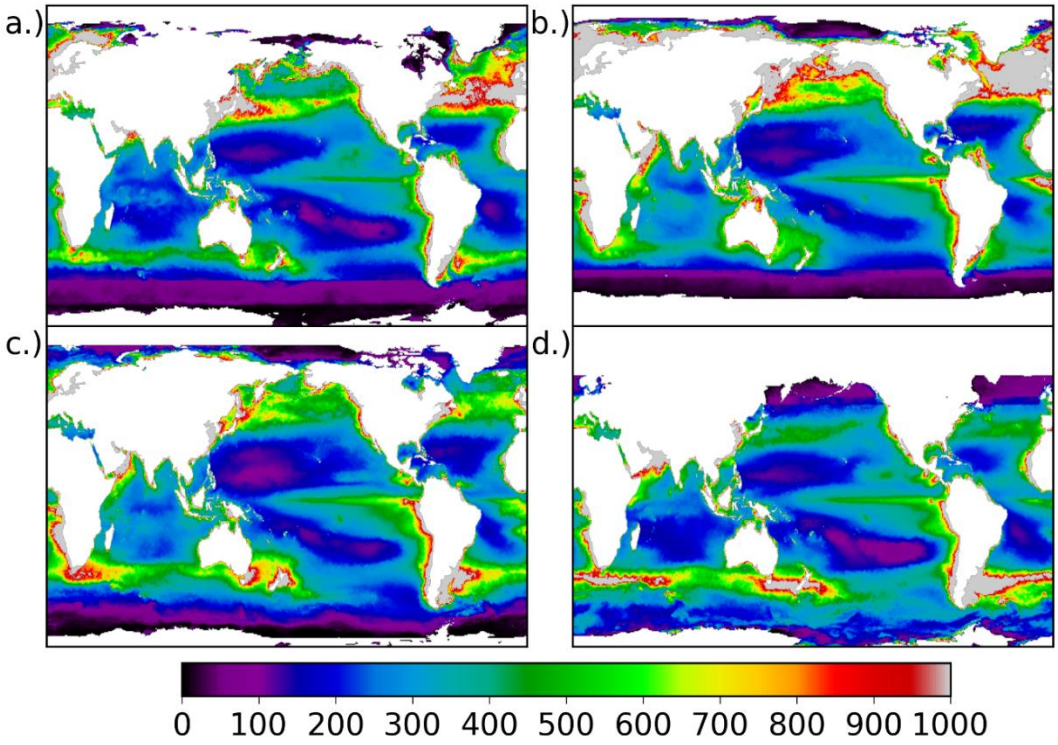

Figure 4.1: Primary production (mg C day^{-1} m^{-2}) based on the VGPM using chlorophyll and SST from MODIS, photosynthetically available radiation (PAR) from Sea WiFS and euphotic depth derived using the method described by Morel & Berthon (1989). Seasonal (northern hemisphere) averages between 2010 and 2015: a.) Spring; b.) Summer; c.) Autumn; d.) Winter.

The inferred values of net PP are dependent upon models and therefore are associated with model errors which vary regionally (Behrenfeld & Falkowski, 1997). Photosynthetic efficiency varies as a function of temperature in the VGPM, but will also vary with phytoplankton community composition. Values of PP may be underestimated where strong deep chlorophyll maximums (DCMs: elevated levels of PP in the subsurface, normally aligned with nutriclines) occur, since only the radiance from the upper surface is being considered by the model. For global scale analysis, these errors are acceptable, as a trade-off for high spatial and temporal coverage, but may be inappropriate for smaller-scale studies. Although there are several variants of the VGPM (see 2.2), here we use the standard product for our global analysis.

Variation in PP gives cause for global partitioning of the ocean into ecological regions, such as those derived by Longhurst (1998). Both surface and deeper communities are limited by PP, which is a function of light intensity, temperature and nutrient availability (via mixing), therefore where major changes in these properties occur, such as at oceanic fronts, PP regime shifts are often observed.

4.1.2 Regional oceanography

Water masses meet at oceanic fronts that physically partition the ocean into regions; at smaller scales, eddies and filaments act in the same way. In the open ocean, frontal regions are often associated with relatively high levels of production (Longhurst, 1998) usually a result of complimentary water mass mixing where the frontal habitat, sometimes known as an ecotone (from Odin, 1971 or Shelford, 1963), gains the compositional advantages of both adjoining water masses (either converging or diverging); an example of this is where nutrient rich, iron poor subantarctic water converges with nutrient poor, iron rich subtropical waters at the southern subtropical convergence zone. They are identified by shifts in water temperature and density, akin to atmospheric fronts. SST (Fig 4.2), acts as a proxy for surface frontal features, but often water-column profiles of density structure are required to reveal the complete picture.

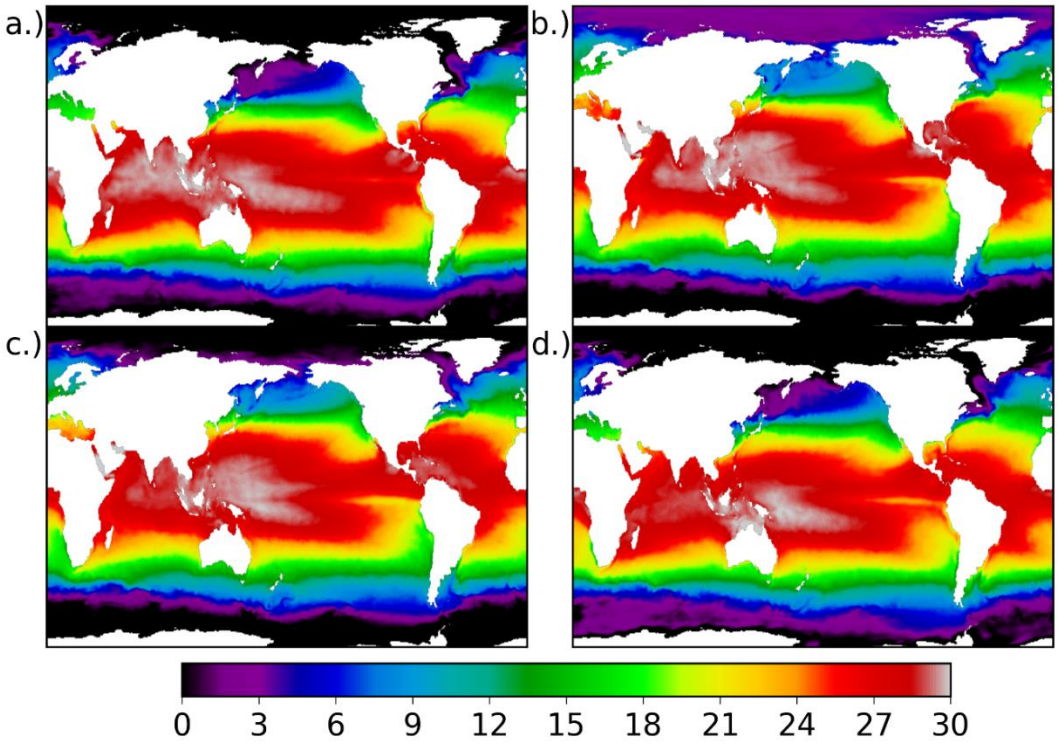

Figure 4.2: Sea-surface temperature (SST; °C) output from the simple ocean data assimilation (SODA) product. Seasonal (northern hemisphere) averages taken over the period from 2000 to 2008: a.) Spring; b.) Summer; c.) Autumn; d.) Winter.

Coupled with seasonal variation in PP (Fig 4.1), and mixing depths, the ocean naturally divides into distinct regions. The surface provinces are linked to the mesopelagic community by diel vertical migration (DVM).

4.1.3 Diel Vertical Migration

Diel vertical migration (DVM) is a ubiquitous phenomenon in the oceans. Zooplankton (0.2 – 20mm) and small mesopelagic fish (<15cm) migrate between the surface and deeper dark waters following low light-level isolumes, so as to remain in a certain, size-specific, level of darkness, to reduce risk of predation from visual predators (Hays, 2003). As dusk or dawn approaches, isolumes shift and the organisms follow, which has led to the opinion that changes in light intensity trigger the event (Ringelberg, 1999). Importantly, the daily movements and rest periods at depth provide transport of carbon and nitrogen (via respiration and excretion) from the surface to deep water (Schnetzer & Steinberg, 2002). The residing depth of zooplankton may be dependent upon their perceptibility by planktivorous fish (Hays, 1995; De Robertis et al., 2000), meaning small zooplankton reside shallower in the water-column (Fiksen & Carlotti, 1998; Sekino & Yamamura, 1999). Additionally, well-nourished organisms have been observed to spend less time at the surface feeding when compared to underfed specimens (Hays et al., 2001). Carnivorous zooplankton such as some copepods, track their prey throughout the diel cycle and are relatively undisturbed by fluctuations in light intensity, using tactile stimuli to hunt for prey; although the predation pressure on the copepods is likely to change with light intensity as mesopelagic fish that predate on copepods, such as myctophids, are visual predators. Naturally, the mesopelagic fish track their zooplankton prey, forming discrete layers that are often formed of specimens of similar sizes, that increase with depth (Auster et al., 1992); zooplankton have also been observed to aggregate by species and development stage (Tarling et al., 2001). Other, larger predators, such as Tuna and swordfish, track their migrating prey, but don't exhibit DVM, often returning to shallower waters (to warm) during the daytime (Dagorn et al., 2000; Robison, 2009). Feeding on the mesopelagic fish are air-breathing vertebrates such as King penguins and elephant Seals, preferentially feeding during the day/night depending on aspects such as ambient light levels at depth, their visual acuity and the ability of their prey to escape (Hays, 2003). Essentially the migrating mass is formed of organisms that reduce risk of predation and prolong their survival by remaining in dark conditions (subject to oxygen content) and a

community of followers that predate upon them. Key drivers in depth are therefore light level and perceptibility, which are related to either the organism or the prey of an organism.

4.1.4 Geographical and temporal variance of the Deep Scattering Layer

Environmental barriers, such as Oxygen Minimum Zones (OMZs) and thermoclines can limit the depth range of species, but can also offer a haven from predators for those that are more adapted (Klevjer et al., 2012). Oceanic features such as eddies, Gyres, currents and fronts affect DSL depth. Eddies that evolve at coarse scales (10 – 100kms) can provide a rich feeding habitat, driven by continual upwelling of nutrients and internal warmer waters, shifting the DSL structure, forming bowl shape features directly beneath the epicentre (Godø et al., 2012); this behaviour is thought to be a consequence of lethargic fish following paths of constant density. Oceanic fronts at the sea surface, that are regions of increased production, have been associated with sharp rises in DSL depth (Nicol et al., 2000), which could be related to reduced light penetration from increased PP at the surface. Mesopelagic communities often appear in the form of multiple DSLs and their arrangement normally shifts at twilight to form distinct day and night patterns. DSL stratification is related to the physical structure of the water-column, dividing predators and their prey, and also into groupings of organisms that preferentially seek distinct or extreme habitats to increase their survival probability. Due to their complex nature and form, point observations of DSL depth and vertical arrangement that are often reported in DSL studies are not adequate when investigating the drivers of these variables.

At high latitudes, the dependence on DVM of the DSLs reduces and seasonal migrations (to deeper waters) take president in population dynamics (Rabindranath et al., 2010). Where the DVM signal is stronger at lower latitudes, seasonal variation controls the strength of DSLs (Urmy et al., 2012). Topographical features like seamounts, continental shelves and Ridges offer pathways for ocean currents and drive increased faunal activity. As expected, bulges in DSLs develop at these locations (Letessier et al., in press); especially at shelves where shallow conditions restrict vertical spacing and ocean currents rise out of basins to induce concentrated activity (Jarvis et al., 2010). A study by Anderson et al. (2004) in the Irminger Sea captured the temporal and spatial variance of DSLs across a topographically rich region. Backscatter strength varied at the shelf, across the basin, at the mid-Atlantic ridge and was shown to vary with both season and depth; the importance of seasonality was also highlighted and diapause noted as a key contributor in its reduction during winter months.

4.1.5 Aims

PP regimes and physical oceanic barriers such as fronts form surface provinces that interact with the mesopelagic community, formed of DSLs, via DVM. The spatial unity between the two regions remains unknown. Here we investigate the coherence between the surface and mesopelagic environment by deriving characteristic water-column forms, pelagic regimes, based on SSL metrics extracted using the SSLEM, and analysing their properties, comparing their geographical extents to the surface provinces derived by Longhurst (1998).

4.2 Materials and Methods

It was apparent following the development of SSLEM (Ch 3) and the extraction of SSLs from the acoustic dataset (see 2.1) that mesopelagic communities were inherently dynamic (highly variable in depth and MVBS: Fig 3.9) and that a probability distribution would be required to describe them at large scales (> 100 km's). SSL probability distributions (SPDs – see 4.2.1), characterised the regional-scale water-column, providing a means of determining the probability that any specific instance (or acoustic realisation) of a pelagic community would be observed. SPDs were formed of a set of discrete probability values for specific SSL depth-MVBS pairs that were visually represented using SSL probability maps (SPMs – see 4.2.1). SPMs provide insight into community dynamics, spatial structure and biomass. SPDs were used to calculate the principal depth of the DSL and total backscatter (4.2.2) and were also, merged by likeness (4.2.3) to form distinct pelagic regimes (4.2.4).

4.2.1 SSLEM, SPDs and SPMs

Each acoustic image was pre-processed by extracting and parameterising the biological components (SSLs) of the water-column using the Sound Scattering Layer Extraction Method (SSLEM: Ch 3). Approximately 40,000 SSLs were extracted in total, ranging from 30 minutes in length to 6 hours. Each SSL was summarised by a set of 3 key metrics, SSL depth, thickness and MVBS.

A uniformly spaced 2-dimesional grid with a cell-resolution of 300 by 300 km's was constructed to represent the surface area of the pelagic ocean; this scale was deemed appropriate as it allowed for adequate spatial coverage (over 7% of the ocean's surface) and intra-cell sample effort (> 1 day). Within each cell, the ensemble of observed SSLs, described by SSL metrics were combined to form two separate SSL Probability distributions (SPDs), one representing the daytime arrangement and the other, the night-time. The SPDs were formed of 240 separate probability distributions, each one representing a 5m depth interval between 0 and 1200m. The depth probability distributions were simplified into a set of 31 discrete probabilities (Equ 4.1) each one describing the probability of a particular value of MVBS (-110 dB re $1m^{-1}$ to -50 dB re $1m^{-1}$ by 2dB re $1m^{-1}$) occurring at a particular depth (0 to 1200 m by 5 m); including a probability that no SSL would be present.

$$Pr_{z,ml} = \frac{SSLmin_{z,ml}}{Nmin_{z,ml}} \quad (4.1)$$

Where $Pr_{z,ml}$ is the probability of an SSL at a particular depth, z (belonging to a vector of discrete depths, Z, ranging between 0 and 1200 m at 5 m intervals) and MVBS level, ml, (belonging a to a vector of discrete MVBS levels, ML, ranging from -110dB re $1m^{-1}$ to -50dB re $1m^{-1}$ at intervals of 2dB re $1m^{-1}$), occurring, $SSLmin_{z,ml}$ the number of minutes where an SSL of a particular ml and z was observed and $Nmin_{z,ml}$, the total number of minutes (sample effort) recorded within each grid cell.

The SPDs conveyed the probability of any possible spatial distribution of SSLs, day and night, of any given MVBS to be determined, but importantly, also conveyed the most likely arrangement of regional-scale SSLs that would occur for each cell. The SPD can be visually represented by SSL probability maps, SPMs: see Fig 4.3b for an example. Since day and night periods were separated at local sunrise/sunset times, migrating layers appear as weak (due to changes in organism orientation during DVM), low probability (occurring only around dusk and dawn) features within the migrant zone (200 – 400 m see Fig 4.3) for both day and night SPDs.

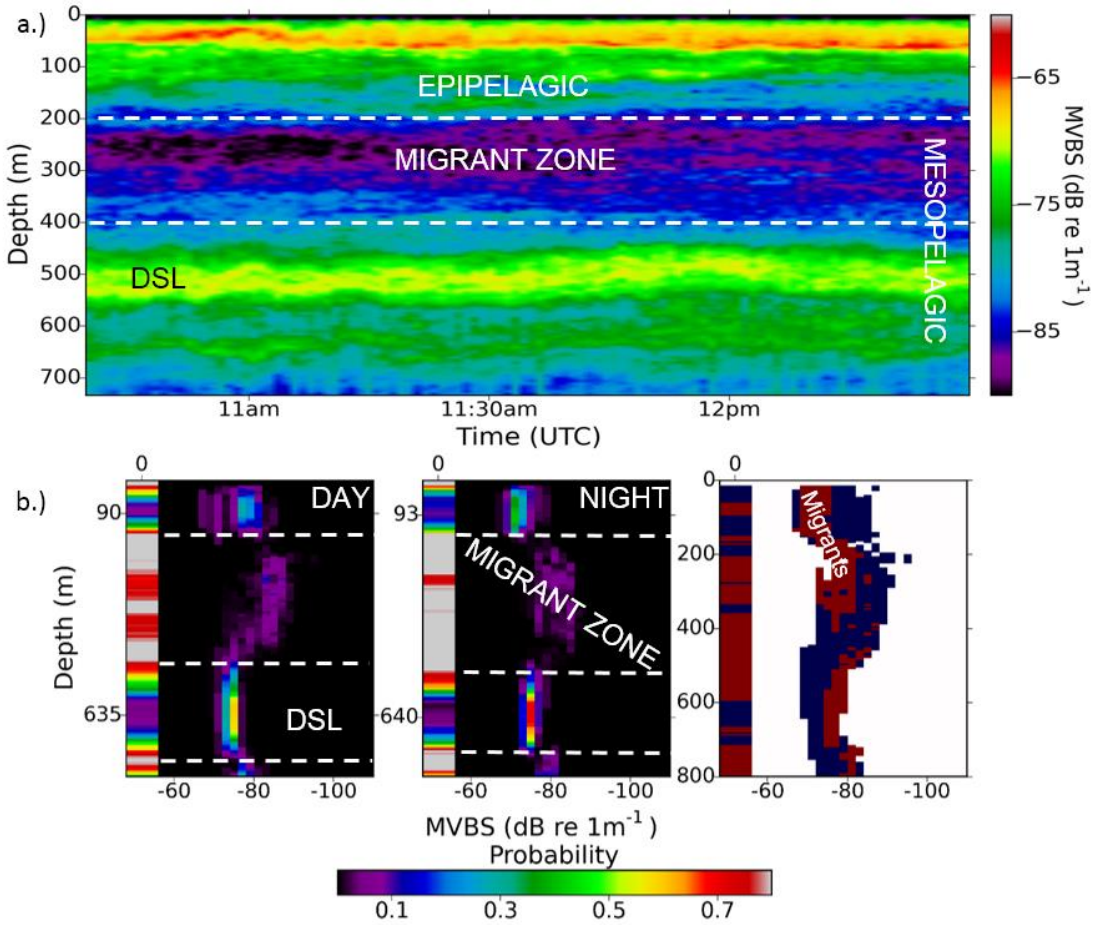

Figure 4.3: A typical acoustic view of the water-column.

a.) A typical water-column profile, with a resident daytime surface scattering layer contained within the epipelagic (0 – 200 m) and a deep scattering layer (DSL) at around 525m within the mesopelagic zone (200 – 1000 m); data recorded using a 38 kHz echosounder on the HICEAS10 cruise, observed on the 10th August 2010 in the N. Pacific close to Hawaii (26.5°S, -141°E).

b.) An example Sound Scattering Layer (SSL) Probability Map (SPMs) based on SSL probability distributions (SPD) for a single geographical cell (300 by 300 km). Left-hand plot shows the daytime SPM, centre the night-time and the RHS represents the change in probability between day and night, coloured red if the probability is higher during the night and blue during the day. For the day and night SPMs, a probability is given at each depth and MVBS level. In this example, the most common occurrence of SSLs occur between 400 and 800m and at the surface. There is a clear increase in probability and scattering strength at the surface during the night indicating DVM. The first column of each SPM, gives the probability of observing no SSL at that depth and acts as a proxy for expected SSL spatial arrangement.

4.2.2 Estimating DSL depth and NASC

The probability of a SSL being observed at a particular depth (Pr_z), during the day or night, was defined as:

$$Pr_z = \sum_{i=1}^{30} Pr_{z,ML[i]} \quad (4.2)$$

Where i is an index value that cycles through the different values of MVBS in the ML vector. To determine the depth of the principle or most commonly occurring DSL component (Z_{DSL}) for the SPD, the maximum value of Pr_Z from within the mesopelagic depth range (200 – 1200m) was calculated:

$$Pr_{Z[40:240]} = \{Pr_{Z[40]}, Pr_{Z[41]}, Pr_{Z[42]} \dots, Pr_{Z[240]}\} \quad (4.3)$$

$$Z_{DSL} = \arg\max(Pr_{Z[40:240]}) \quad (4.4)$$

DSLs are known to form in complex depth arrangements that can change over time and space (Anderson et al., 2005; Kloser et al., 2009). If these arrangements are driven by physical drivers (or biological), then it is reasonable to assume that the most commonly observed depth of the DSLs (Z_{DSL}), is also related to these drivers.

A form of the nautical area scattering coefficient (NASC or s_A; Maclennan, 2002) was calculated that isolated SSL scattering energy, per square nautical mile (nmi^2), over the epipelagic (s_{epi}) and the mesopelagic (s_{meso}) region for each cell of the uniform grid (during the daytime) that data were available for:

$$s_{epi} = \sum_{j=0}^{40} \left(\sum_{i=0}^{30} \left(Pr_{Z[j],ML[i]} \times 10^{(MVBS[i]/10)} \right) \right) \times 4\pi \times 1852^2 \quad (4.5)$$

$$s_{meso} = \sum_{j=40}^{240} \left(\sum_{i=0}^{30} \left(Pr_{Z[j],ML[i]} \times 10^{(MVBS[i]/10)} \right) \right) \times 4\pi \times 1852^2 \quad (4.6)$$

4.2.3 Grouping the data: SPD distance, MDS and K-means

A distance measure was derived to determine the similarity between each SPD. Since the SPDs were all constructed from a set of discrete probabilities, with values between 0 and 1 and one

value per depth/MVBS bin, a simple matrix subtraction could be used to calculate a relative distance measure:

$$dist_{AB} = \sum abs(\boldsymbol{A} - \boldsymbol{B}) \quad (4.7)$$

where **A** and **B** are 2-dimensional arrays (SPDs) and $dist_{\mathbf{AB}}$ is a relative distance measure between **A** and **B**.

Using equation 4.7, a 300 by 300 dissimilarity matrix **D** was constructed, holding the pairwise distances between all the SPDs. To reduce the data down into a smaller number of dimensions to improve computational efficiency of further analysis, classical multi-dimensional scaling (MDS) was applied. From the resulting configuration matrix, an appropriate number of dimensions P was assigned by evaluating values of stress. A k-Means clustering algorithm was applied to the resultant reduced dataset, to determine the natural number of groupings or clusters that were evident within the data. The algorithm was run for a range of cluster frequencies (2 – 20), where at each step the Log-likelihood (LL) value was determined (Equ's 4.8 & 4.9) to allow for model assessment.

$$P(x|u) = \frac{e^{-\sum_{d \in D}(u_d - x_d)^2}}{\sum_u e^{-\sum_{d \in D}(u_d - x_d)^2}} \quad (4.8)$$

$$LL = \sum_{x \in X} log\ max\ (P(x|u)) \quad (4.9)$$

Where $P(x|u)$ is the probability of sample x belonging to model μ, for the set of X samples and D variables.

4.2.4 Pelagic regimes

SPDs were merged to form new SPDs with larger spatial coverage by matrix addition. This operation was carried out by adding the underlying data (SSLmin – see Eqn.4.1) of all the SPDs in each group together, and then determining a new set of probabilities by applying new values of Nmin to Equ 4.1; this accounted for differences in sample effort between cells. The groups of SPDs were termed, 'pelagic regimes', that were essentially distinct water-column classes, formed of a set of geo-referenced cells. Where these cells clustered together naturally, ocean regions were formed. A local neighbourhood filter (3 x 3 cells) was passed over the grid filling in empty cells with a pelagic regime class-index, where a class majority was found.

4.2.5 Temporal analysis of Pelagic Regimes

A temporal analysis was conducted to ascertain the variance over time of regional SPDs. This could only be carried out where multiple observations were made during different months and years within the same cell. In these instances, for each cell, all the SPDs were grouped together to form a local regime, from which, the most probable DSL depth-MVBS pair was calculated for both the day and night. These probabilities were then compared to the individual SPDs that made up each group, to assess change in the form of the dominant DSL.

4.3 Results

In total, over 40,000 SSLs were extracted from the acoustic survey data via the SSLEM (see Ch 3), summarised by a set of metrics (depth, thickness and MVBS) and binned into cells over a uniform grid (cell size: 300 by 300 km) representing the pelagic ocean. SSLs metrics were sub-divided within each cell into day and night sets (4.2.1). In total, 300 unique cells were formed, consistent of 300 sets of day and night SSL metrics. SSL probability distributions (SPDs) were determined for each set (4.2.1). Distances between cell SPDs were calculated (Equ 4.7) and the resultant dissimilarity matrix reduced by application of classical MDS. K-means was applied and using calculated values of the Log-Likelihood (Equ 4.9), a six cluster model was deemed an appropriate selection (4.3.1). Each cluster was formed of a discrete number of SPDs, these were merged together (4.2.4) to form distinct pelagic regimes (4.3.2), characterised by their common DSL depth (Z_{DSL}), SSL NASC-type values (s_{epi} and s_{meso}) and geographical distribution (4.3.2 to 4.3.4). The temporal variation of individual cells, or local regimes, were analysed (4.3.5) to ascertain the variation over large timescales of DSLs.

4.3.1 Cluster Selection

The MDS analysis indicated that for a stress value of 0.1, providing a good representation of the data, 37 dimensions were required (Fig 4.4a); using the associated eigenvalues, the lower dimensional representation of the data accounted for 72% of the variance. The clustering analysis was performed using the reduced dataset. An elbow-like feature was apparent when fitting six clusters (Fig 4.4), increasing the value of the LL away from the decreasing trend. This feature indicated that there was a better than expected fit, a natural well in the data, when clustering with six centres. As the number of clusters increased, particularly towards 18, more and more of these features appeared, suggesting that the data is fractal in nature and has many different levels of groupings. Since in this study we are interested in regional-scale trends, taking the first natural grouping was appropriate. For the six cluster model, 89% of the SPDs were assigned to a cluster with a probability (Equ 4.8) that was at least twice the value of the next best selection, indicating a good fit.

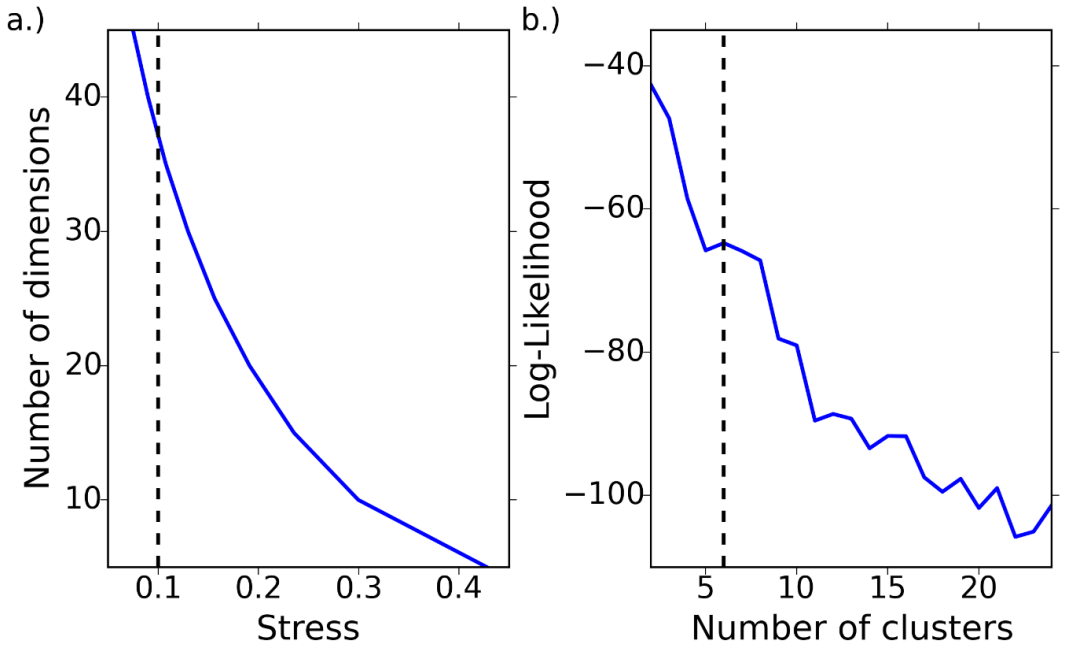

Figure 4.4: Model selection criteria. a.) Multi-dimensional Scaling results, 37 dimensions were chosen at a stress level of 0.1; b.) K-means clustering results, six clusters were selected (indicated by a black dashed line) where an elbow in the trend increased the value of the Log-Likelihood significantly.

4.3.2 Pelagic Regimes

300 SPDs were generated and grouped by cluster analysis into six clusters (4.3.1). They were merged (4.2.4) and plotted as SPMs (Fig 4.5) representing six distinct pelagic regimes, labelled numerically PR1 to PR6.

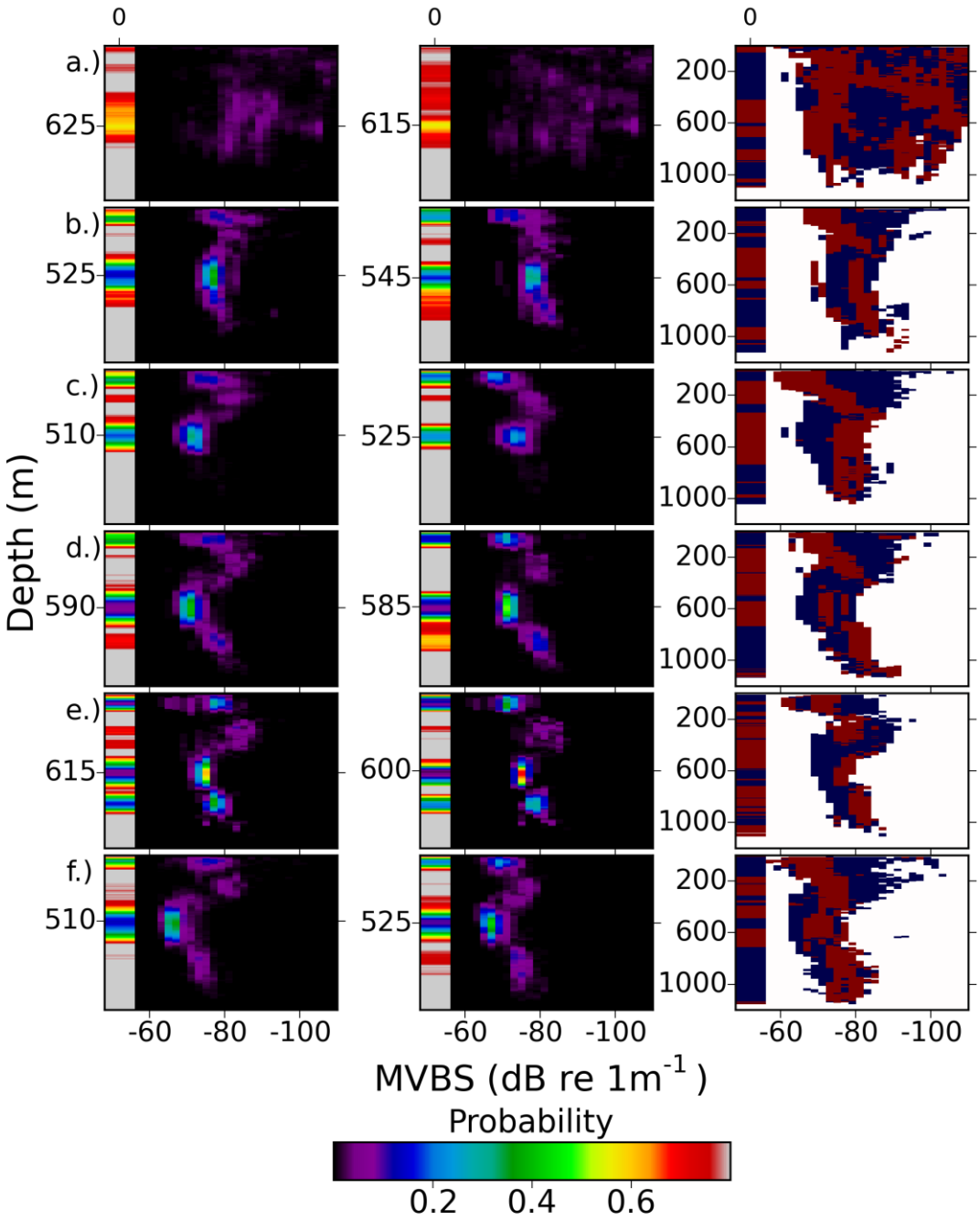

Figure 4.5: Sound Scattering Layer Probability Maps for each of the six pelagic regimes (PR1 to PR6). Columns 1 and 2 contain day and night SPMs. The first column of each SPM represents the probability that no SSL is observed at a given depth. The final column of the figure, contains composite plots, indicating when the probability is largest: during the day (blue), during the night (red) or no change (white). The most commonly observed deep scattering layer depths are indicated.

The SPDs were plotted in depth/MVBS space (SPMs: Fig 4.5), where black regions within the SPMs indicate areas in that space where no SSL has been observed. As the number of observations and hence probability of observing a particular SSL increases, features begin to appear. The first column yields the probability of no SSL being observed and is a good indicator of the most likely depth of SSL observation, importantly, this enables Z_{DSL} to be estimated.

As the DSL depth deepens, the temperature of the habitat decreases and by extension slows metabolic rates and reduces trophic efficiency (Gascuel et al., 2008); a depth difference of around 100m between PR 2, 3 & 6 and the other PRs, is therefore likely to reduce production for any given rate of PP. PR1 yields a broad shallow (probability wise) map, suggesting the SSLs vary substantially in both depth and MVBS and that no common structure is apparent (at this scale); this behaviour is likely to be accounted for by a large amount of zooplankton SSLs, which are relatively weak scatterers at 38 kHz. The other PRs are much more distinct in structure owing to their inherent compact trunk like features formed in the SPMs. MVBS values of these stronger PRs vary widely, by up to a factor of 10 (PR6 the strongest around -65 dB re $1m^{-1}$) and can serve as a proxy for biomass. The most common structure appears to be a two-tiered DSL arrangement (PR4, 5 & 6), where the primary or most common DSL resides shallower and a weaker component is deeper in the water-column around 800/900 m. Column 3 of Fig 4.5 indicates that in all but one case (PR1) there is an increase in backscatter at the surface and a decrease in the mesopelagic region, as would be expected for DVM. PR1 shows an increase in the mesopelagic, meaning that potentially deeper layers (> 1200m) reside in this regime that migrate up from the bathypelagic during the night. Finally, the region between the surface layers and the DSL components contains the scatter from migrating organisms. It is characteristically weaker than other components (PR2-6), this is likely to be related to changes in packing density, orientation and swimbladder volume as the organism's swim towards the surface. However, PR2 does not show a substantial decrease in migratory scatter, remaining fairly constant through the region; suggesting perhaps an absence of swimbladdered fish.

4.3.3 Spatial distribution of pelagic regimes

PR classes were plotted geographically (Fig 4.6) and fell naturally into distinct regions. PR1, was located mostly in Polar Regions, lying poleward of 40° latitude in both hemispheres. PR5 formed a single region within the S. Indian Ocean. The other PRs occurred at mid to low latitudes forming sub-regions both north and south of the equator.

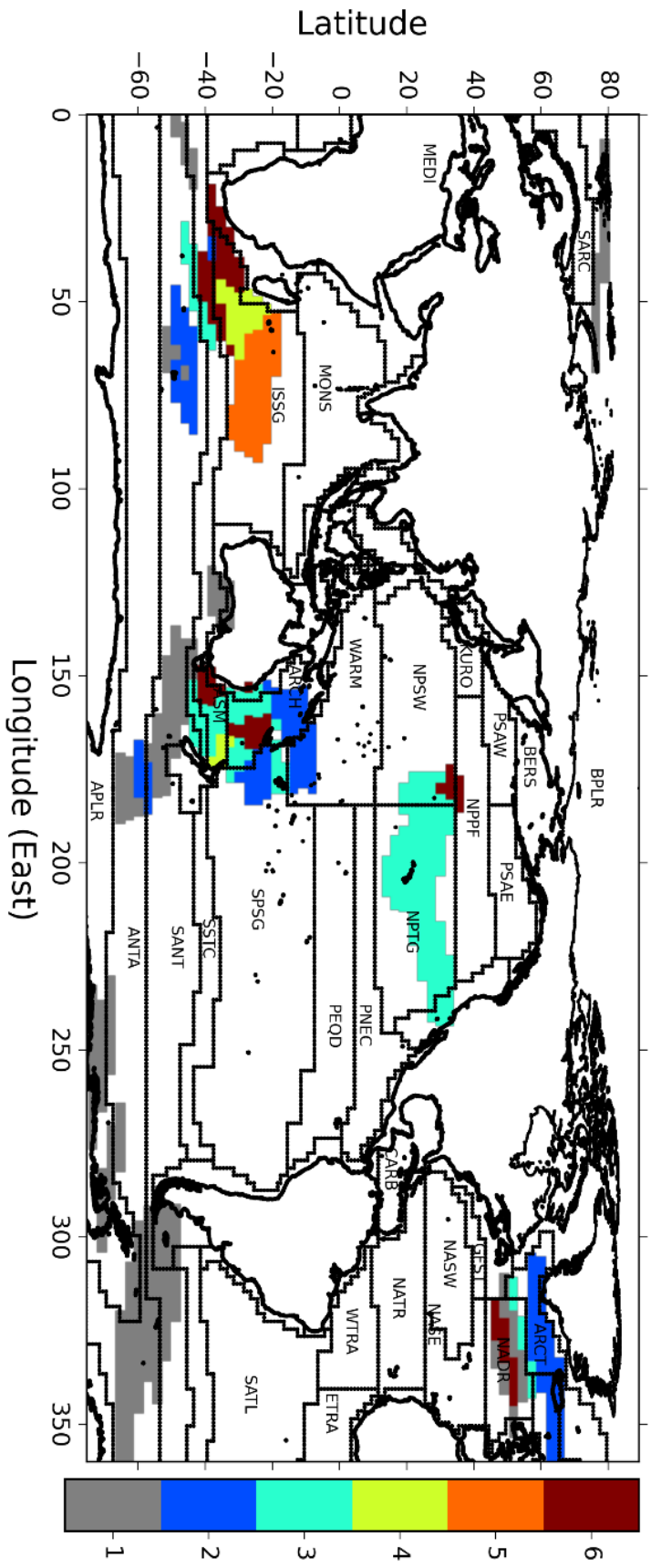

Figure 4.6: Geographical distribution of pelagic regimes (PR1-6). Longhurst pelagic ocean provinces are shown, labelled by short-name (Longhurst, 1998).

The spatial unity of the PRs, provide evidence that pelagic communities are distinct at the regional scale and exhibit DSL characteristics that allow them to be distinguished from one another (Z_{DSL}, MVBS etc.). Though there is some coherence between the surface provinces and the PRs (NPTG), there is evidently disunity between the two (ISSG).

4.3.4 Pelagic regime descriptors

The PRs were characterised by a set of metrics that quantified their distinct properties and were given appropriate labels (Table 4.1); the metrics did not describe DVM.

		Daytime				Night-time			
PR	Label	Z_{DSL} (m)	s_{meso} (m^2 nmi^{-2})	Pr_{DSL}	s_{epi} (m^2 nmi^{-2})	Z_{DSL} (m)	s_{meso} (m^2 nmi^{-2})	Pr_{DSL}	s_{epi} (m^2 nmi^{-2})
6	MP-I	510	2707	0.87	139	525	2196	0.91	474
4	MP-II	590	1103	0.94	143	585	848	0.93	367
3	MP-III	510	687	0.82	121	525	391	0.77	651
5	MP-IV	615	516	0.95	232	600	368	0.97	500
2	MP-V	525	287	0.86	44	545	217	0.84	279
1	Polar	625	94	0.43	19	615	151	0.45	35

Table 4.1: Pelagic regime (PR) metrics and descriptions. MP-I to MP-V – mesopelagic production classes; Z_{DSL} – common deep scattering layer (DSL) depth; s_{meso} – nautical area scattering coefficient (NASC) for SSLs found within the mesopelagic region (200 – 1200m); Pr_{DSL} – probability of observation of a DSL at Z_{DSL}; s_{epi} – NASC values for SSLs found within the epipelagic region (0-200m).

The PRs were labelled by their daytime s_{meso} values (MP-I to MP-V: high to low NASC values) and in one case, by geographical distribution (polar PR). Interestingly, s_{meso} did not correlate with s_{epi} (total backscatter in the epi-pelagic: 0 – 200m), indicating that trophic efficiency may vary between PRs.

4.3.5 Temporal Variability at local scales

The data were partitioned geographically and temporally by year and month. Where multiple SPDs existed for the same spatial cell, the most probable DSL (described by depth and MVBS) was predicted for a merged SPD of all the temporal partitions and compared to the individual

component SPDs. The results indicate that in the majority of cases, there is no change in the dominant DSL over time for at least one of the two diel states and that the daytime DSL state is more stable (Fig 4.7).

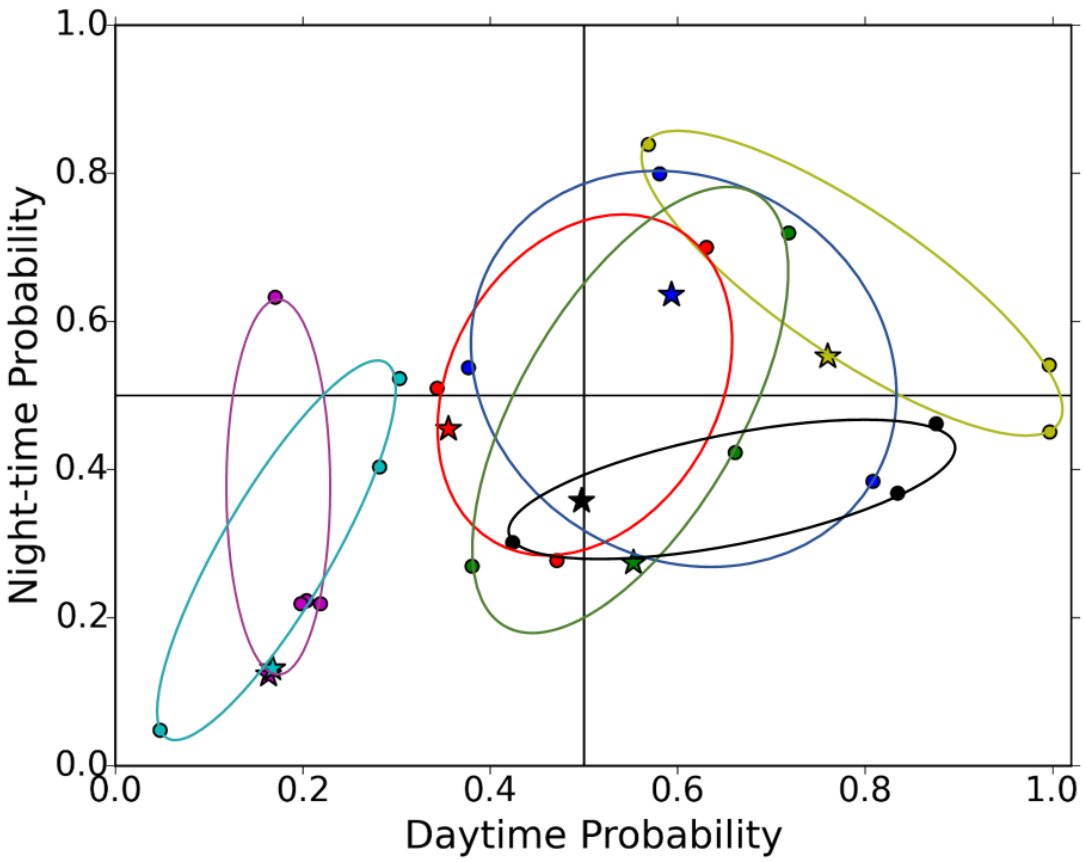

Figure 4.7: Temporal variability of spatially explicit Deep Scattering Layer distributions. Each colour represents a different spatial location where multiple observations of SSLs were made over a number of different time periods (binned by year and month). The star indicates the day and night probability of observing the most commonly observed DSL (defined by depth and MVBS) over all the time periods merged together, the points represent the probabilities for individual time periods. The variance of each group of points is illustrated by an ellipsoid of the same colour. Points located in the top half of the plot indicate that the DSL associated with the probabilities is the dominant (most probable of any arrangement) during the night, anywhere in the cell, similarly, those points found in the RHS, are dominant during the day.

4.4 Discussion

4.4.1 Method

The sound scattering layer extraction method (SSLEM) was implemented to extract regional scale (> 30minutes) sound scattering layers (SSLs), meaning that fish schools, that can have extremely large backscatter values (> -40 dB re $1m^{-1}$) would be excluded. Studies of scattering layers that don't incorporate such methods will undoubtedly incur errors and produce overestimates of total layer backscatter (Irigoien et al., 2014). If the fish school component was quantified, it could go some way towards estimating predation pressure. The analysis was conducted using data recorded at 38 kHz, partly due to it being the most commonly used frequency (data abundant) in pelagic echosounding and also as the collection range (a function of noise) extends to the far extent of the mesopelagic region. The study was partly limited by the range of the echosounders, which varied survey to survey (due to variability in sea-state and ship noise), using lower frequency data (18 kHz) would enable deeper ranges, but such data are comparatively sparse; fishing vessels collect data at 38 kHz and provide a large quantity of the available acoustic data. Due to the variable nature of DSLs, probability distributions were derived (SPDs) in order to determine likely water-column arrangements, easily visualised via probability maps (SPMs). These maps, along with their descriptors (Table 4.1) provide insight into regional ecology, quantifying depths of the mesopelagic community and providing NASC values which give some insight into biomass. The six pelagic regimes derived here were an example of this, clustering the distributions into distinct biological profiles of the water-column. The method selected the first deviation in the LL, but other levels could have been selected, resulting in lower intra-regime variability but at the cost of a reduced sample size. The PRs described here serve to illustrate the characteristic forms of the biological water-column and highlight, via their spatial distribution, that the likely drivers of these characteristics are based on environmental variables. We calculated a common depth for the mesopelagic region (Z_{DSL}), which in all cases was the depth of the shallowest and strongest DSL (Fig 4.5) and likely made up of stronger/more abundant scatterers of the mesopelagic, the swimbladdered fish; the deeper DSL component perhaps is formed of weaker scatterers such as squid, larger and older fish that have fat invested swimbladders (Butler & Pearcy, 1972) or zooplankton.

4.4.2 Water-column structure

The PRs differed in their structure (based on depth and MVBS), providing some insight into the underlying biological communities themselves. Surprisingly, although DVM was evident in all PRs by an increase in MVBS at the surface during the night-time (table 4.1), resident DSLs and surface SSLs were apparent for both day and night states (Fig 4.5), meaning that some proportion of the community would remain behind, while others would actively migrate. This could be explained by either a permanent/temporary (e.g. diapause) resident mesopelagic community or by a community made up of intermittent/opportunistic migrators that may selectively perform DVM, based on some environmental property (predation pressure/food availability/season). There was a clear distinction between the polar regime (PR1) and the other classes, in that it was significantly more variable in MVBS. It might be that the polar regime is not best represented at 38 kHz (dominated by weaker scatterers) or that it requires further segmentation into smaller classes; alternatively, it may indeed be indicative of the nature of this regime. Polar Regions do not contain schooling fish, the environment is much colder (see Fig 5.2) and metabolic rates are comparatively slow and life cycle stages longer, reducing survival probability of larvae and hence lowering the biomass transfer efficiency. Primary production (PP) cycles are unimodal and a lot of organisms partake in diurnal migrations to deeper waters during times of low PP. These environment traits lower production rates, reducing mesopelagic fish biomass and SSL density, meaning that there are layers formed solely from zooplankton species (providing the weakest SSLs: < -80 dB re $1m^{-1}$). In the remainder of the PRs, there are four well-defined components to the water-column, a surface community in the epipelagic that changes day to night when migrators come and go, a migratory zone between the shallowest DSL and the surface community, which is relatively weak in MVBS due to changes in scattering response during migration, the primary DSL component, defined as the shallowest and strongest layer, followed by a secondary weaker DSL component, which is sometimes absent. Mesopelagic fish have been observed to stratify in the water-column, where groups of larger fish take deeper positions (Auster et al., 1992). Larger myctophids are likely to have weaker target strengths (TS) than small juveniles that have gas-filled swimbladders (Butler & Pearcy, 1972) which could explain the difference in MVBS between the two DSL components; the juvenile fish may also be following their zooplankton prey (copepod), meaning they aggregate with the zooplankton forming stronger SSLs, whereas older, more well-nourished fish remain deeper, to reduce predation risk from deep diving air-breathing vertebrates. These distinct water-column structures could be

analysed further and form the basis of a separate study, by taking a closer look at day-to-night change and DVM dynamics for example, but such analysis was deemed to beyond the scope of this project.

4.4.3 Spatial and temporal patterns of pelagic regimes

Biological water-column variability can be very high on smaller spatial and temporal scales (e.g. feeding activity within the epipelagic during the night, involving a wide variety of predator-prey interactions and feeding strategies), with more data this could be investigated, but this was not part of this study, which concentrates on regional (province-scale) trends over long time periods (years).

The PRs naturally grouped together spatially forming distinct regions (Fig 4.6), even though there seemed to be an element of temporal variation (Fig 4.7: seasonally and annually). The two ellipsoids, each representing a single 300 by 300 km cell, occupying the low-probability region of Figure 4.7 (coloured purple and cyan) indicate that DSL depth and density in these regions are highly variable. The vertical orientation of the ellipsoids suggests that for some seasons, the night-time DSLs properties stabilize. These two cells were both found in the Polar Regions and belong to PR1 (Fig 4.5), which explains the high variability. The more stable night-time DSLs are likely to be formed of a seasonally dependent resident DSL community, which is perhaps formed of immigrant mesopelagic fish.

The data contained repeat surveys within the same locations for different years and seasons. Despite this, the derived mean community structures (quantified by SPDs) were distinguishable from other regional water-column structures. The spatial extent of these regions, correlated to some extent with the surface provinces derived by Longhurst (1998) but this varied province to province, where some were highly variable such as the ISSG province. The disunity between the two partitions, is related to the biological depth structure of the water-column (particularly the mesopelagic), which seems to be variable over the surface provinces. This is not surprising since there isn't a linear relationship between sea-surface temperatures and sub-surface temperature (affecting growth of mesopelagic organisms via metabolism), due to differences in deep water mass structure. Taking into account the physical structure of the deeper community, as well as surface production, is likely to provide a partitioning of the ocean that is more in sync with pelagic communities.

4.4.4 Implications and conclusions

From the results of this study, we conclude that a biogeography of the pelagic ocean, taking into account the mesopelagic region, should include consideration of sub-surface properties such at temperature that may affect mesopelagic biomass and depth. Partitioning in this way, is a step closer to obtaining a more holistic impression of the pelagic ecosystem, relating the lower trophic levels to the mid-trophic level fish species. In addition, by considering the impact on these communities by ocean predators such as seals (DSL fishers) and schooling fish and also by fishing activity, we will be able to obtain a better understanding of pelagic ecosystem function.

Chapter 5: A present estimate of global mesopelagic fish biomass

Acoustic deep scattering layers (DSLs; so-called 'false bottoms') are prominent features of the ocean's dark mesopelagic zone (200m – 1,500m depth). They contain high biomasses of lantern fish (Family Myctophidae), which undertake pronounced vertical migrations towards the surface at night to feed. Fish migrate back to depth at dawn, and respire and excrete there, transporting carbon and nutrients downwards into the ocean interior (Hays, 2003). How the characteristics of these ecologically important DSLs vary spatially, what the drivers of variability may be, and consequences for DSLs of environmental change are unknown. Here we show that variability in DSL depth and mesopelagic fish biomass across the global ocean can be explained very well in terms of regional surface primary production, mixing intensity and temperature and estimate the global fish biomass to be 11,250 +/- 3750 million tonnes. Previous work has suggested that DSL depth was driven principally by light intensity, which will be invariant on evolutionary timescales. The discovery here of coupled biophysical drivers opens the way to use existing models to explore future scenarios for the hidden world of DSLs.

5.1 Introduction

Fisheries and conservation management regimes now adopt more holistic approaches when implementing planning and monitoring protocols, which consider ecosystem impacts (Lehodey et al., 2008). Accurate estimates of biomass are required not only for the commercially important fish stocks but of other trophic levels, including mid-trophic species that inhabit the mesopelagic region (Handegard et al., 2013). Present estimates of mesopelagic fish biomass (MFB) vary substantially. The first attempt at mapping global distribution of mesopelagic fish was made in 1980 (Gjøsaeter & Kawaguchi, 1980), estimating a value of 945 Million tonnes (Mt), calculated by summing up biomass estimates (density multiplied by surface area) of 15 large FAO areas (excluding Polar Regions), using data collected by ocean trawls; consequently, due to known net avoidance issues, this is likely an underestimate of the true value. This estimate was later amended using modern software (e.g. Arc GIS) by Lam & Pauly (2005) to a value of 999 Mt. Recently, using a median TS value for mesopelagic fish from available acoustic models and a single transects worth of EK60 38 kHz data (traveling through the Pacific, Atlantic and Indian Oceans, between -40°S and 40°N), Irigoien et al. (2014), estimated a median value of between 11,000 and 15,000 Mt, with minimum and maximum estimates of 4,707 and 618,432 Mt respectively. This most recent estimate, based on a relationship between PP and mesopelagic fish biomass (R^2 = 0.46), has rapidly increased interest in re-opening the mesopelagic fishery (St John et al., 2016). In order to obtain more reliable estimates, a better understanding of the drivers of deep scattering layer (DSL) depth and biomass are required.

5.1.1 Drivers of deep scattering layer depth

The depths of DSLs vary substantially geographically (Kloser et al., 2009) and can form arrangements of multiple layers. A sound scattering layer probability distribution (SPD: 4.2.1) formed from a global dataset of SSLs (see 2.1) was plotted (Fig 5.1) showing that the most commonly observed daytime depth of DSLs is 525m; this depth deepens slightly at night to 545m. By visual scrutiny of the SSL probability maps, the water-column can be broken down into 4 ecological components: a surface component (0m - 200m), a weak migratory component (200m – 400m), a strong, relatively shallow, primary DSL component (Z_{PDSL}: 400m – 700m) and a weak, relatively deep, secondary DSL component (Z_{SDSL}: 700m – 900m).

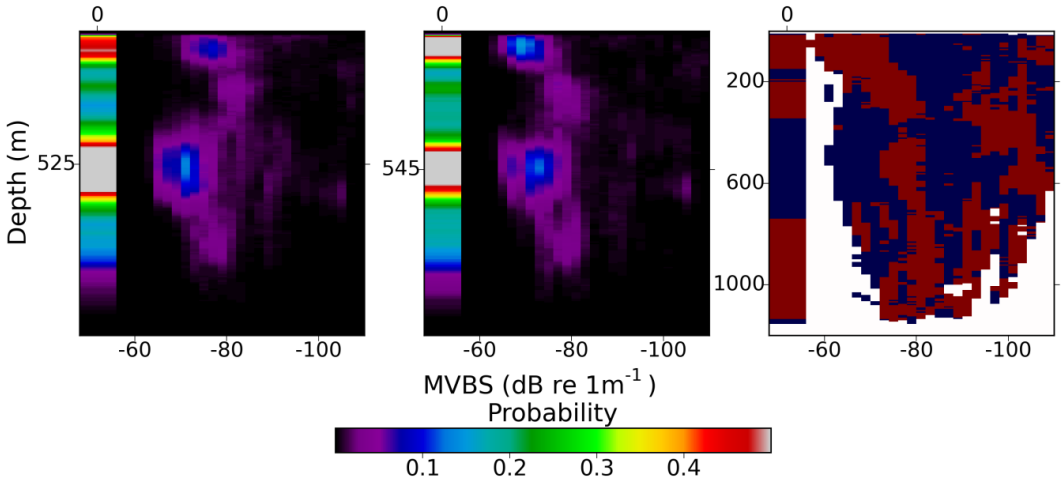

Figure 5.1: Sound Scattering Layer (SSL) Probability Map (SPM), formed from a global dataset of SSLs (see Ch 4). The first column represents the daytime arrangement, the second, the night time arrangement and the final column represents the change in probability between day and night, coloured red if the probability is higher during the night and blue during the day. The most commonly observed DSL depth is indicated in both the daytime and night time arrangements. The first column of each SPM, indicates the probability of observing a SSL at that depth and acts as a proxy for expected SSL spatial arrangement.

The primary DSL component covers a larger area of the SPM than the secondary and also has much larger probability values. The primary appears to be unimodal, suggesting that the most common formation is a singular DSL, followed by the less likely scenario of a dual DSL formation with a secondary weaker DSL component. As to why there are two components (or more) is likely to be related to predation by large air-breathing invertebrates or to changes in water-column properties, such as oxygen content (Bianchi et al., 2013). The strongest backscatter is expected to be produced by swimbladdered fish (Kloser et al., 2002; MacLennan & Simmonds, 2005; Stanton, 2009). Since the primary DSL is characteristically strong, it can be inferred that it contains a proportion, probably the majority, of the mesopelagic fish population and that its depth (Z_{PDSL}), will be characteristic of environmental drivers. Known environmental drivers that influence DSL depth are light intensity (Hays, 2003), lower light levels provide a haven from visual predation, oxygen content, mixed-layer depth, temperature and PP (Bianchi et al., 2013) and less frequently observed, water density (Godø et al., 2012). Light intensity varies as a function of depth (Johnsen, 2014), water clarity (particulate matter content) and sea-state and is often quantified by the euphotic depth (Z_P) at which, light

intensity has fallen to 1% of its surface value. Light penetration varies with changes in PP and wind-driven mixing and also by local effects such as cloud cover.

5.1.2 Drivers of deep scattering layer biomass

In the pelagic ocean, growth and reproduction (and therefore biomass) are dependent upon food availability, predation pressure and water temperature. In the mesopelagic region the temperature is naturally lower than at the surface, but the relationship between the two variables is not linear (Fig 5.2) and is dependent upon deep water mass structure.

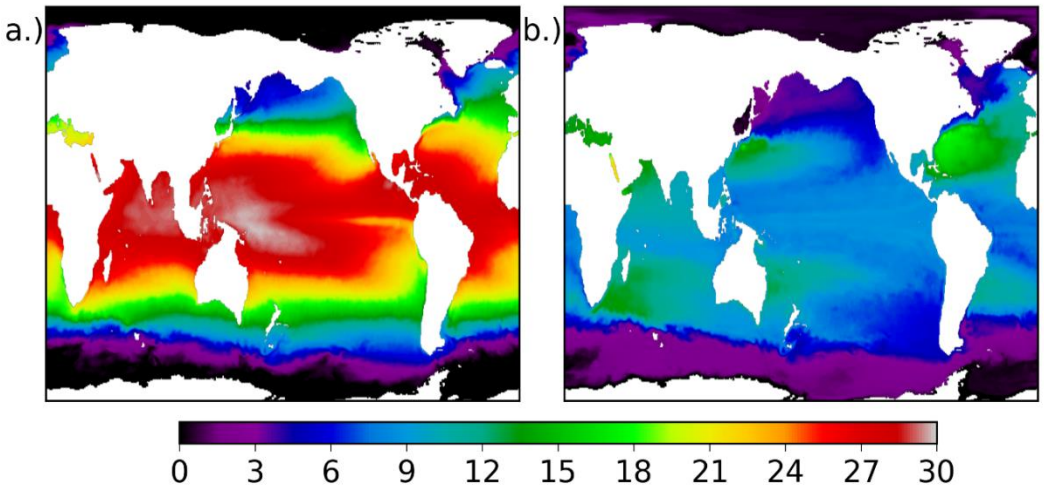

Figure 5.2: Water temperature (°C) a.) Sea-surface temperature (SST) and b.) Sub-surface temperature (ssT at 450m).

It not clear which environment (surface/deep) mesopelagic fish life cycles adhere to, as they have been observed to exhibit growth rates that are similar to epipelagic fish (Gartner, 1991), but at the same time, are known to digest their consumed prey at depth (Holton, 1969). Interestingly, where there are significantly reduced oxygen levels at their daytime depth, myctophids have been observed to regurgitate food after feeding at the surface before migrating to depth, presumably to reduce oxygen consumption while digesting (Holton, 1969). To date, studies have derived fairly weak relationship between MFB and PP (Irigoien et al., 2014), where sub-surface temperatures (ssT) are not considered as a variable, mainly due to an unknown DSL depth. Using Z_{PDSL}, ssT could be inferred and used to parameterise DSL density/biomass functions (Fennel & Rose, 2015).

5.1.3 Acoustic estimates of biomass

Acoustic estimates of biomass rely on prior knowledge of the organism's Target Strength (TS) to length relationship and frequency-length distribution, usually obtained from net/trawl data (Benoit et al., 2008) and acoustic models (Stanton et al., 1996; Yasuma et al., 2009; Yasuma et al., 2006). Errors in biomass calculation are normally caused by, but are not limited to, overestimation due to the presence of stronger scatterers (relative to your target/s species), over-estimation due to resonant scattering of fish swimbladders, or biased catch data, arising from net avoidance, leading to underestimation.

The acoustic response of a gas-filled swimbladder can be more than 10,000 times the strength of the scattering response of zooplankton, such as copepods for example (Stanton, 2009), making estimations of zooplankton biomass in mixed assemblages very difficult; such is the case that is found in the majority of DSLs. There are also large variances in backscatter encountered between different sizes of swimbladders, TS values can vary by more than a factor of 10 at 38 kHz (Kloser et al., 2002), and these variances are not always synonymous with the size of the organism (Fig 5.3); for example, the degree of allometric growth of the swimbladder organ varies across species of the ubiquitous Myctophidae family (Yasuma et al., 2009).

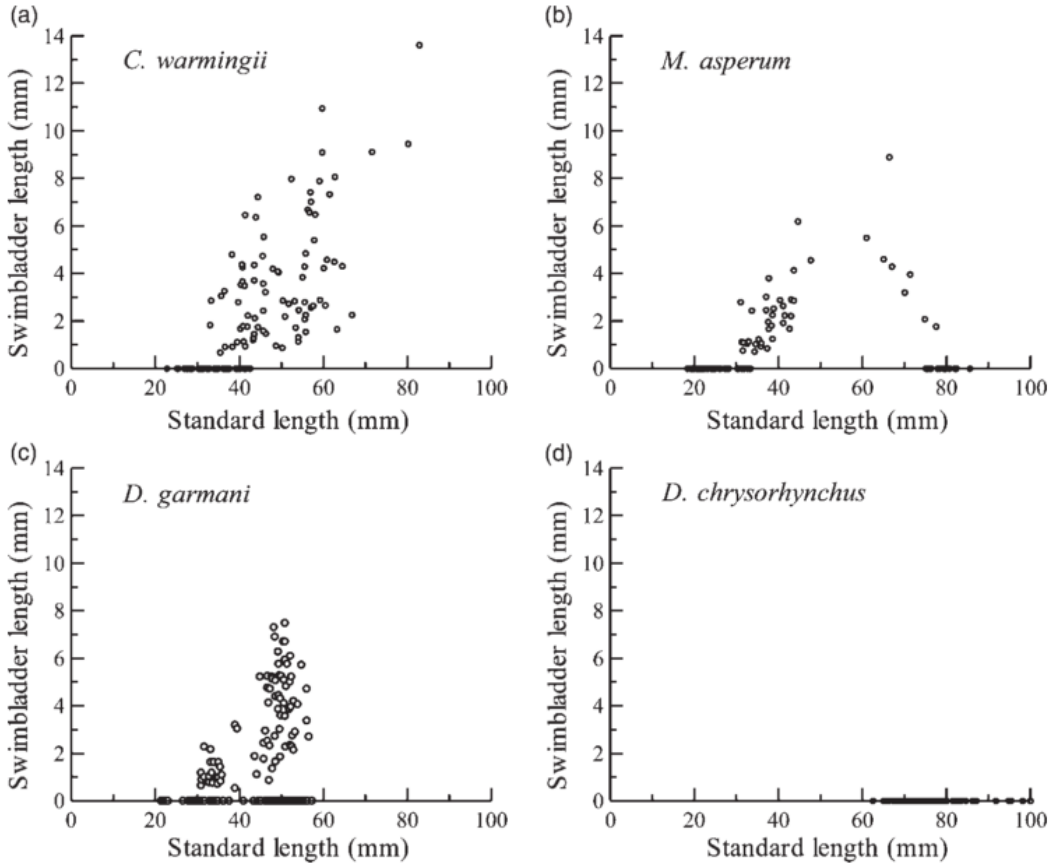

Figure 5.3: Swimbladder length versus fish length of four species of the Myctophidae family caught in the Northwest Pacific: a.) *Ceratoscopelus warmingii*; b.) *Myctophum asperum*; c.) *Diaphus garmani*; d.) *Diaphus chrysorhynchus*. Figure taken from Yasuma et al. (2009).

Many commercially important species do not dominate the acoustic response field and hence are harder to detect using acoustics. This problem has been tackled by detecting species that hold some relationship to the targeted species. A recent example of this was performed by Ressler et al (2012), where Pollock were observed to be inversely proportional to the acoustically 'opaque' euphausiids species on the Bering Sea shelf. Resonant scattering from gas bladders (elevating signal strength and therefore biomass estimations) often occurs at low incident frequencies (< 18 kHz) but has been observed at 38 kHz, for very small fish deep in the water-column, with gas bladder diameters smaller than 0.4mm (Benfield et al., 2003). When validating acoustic biomass estimates, net/trawl data is used. It is almost impossible to determine the degree of net avoidance (without the aid of videography), as it is variant across species, size, depth and time of day. Methods have been applied, such as efforts to stun euphausidds with strobe lighting (Mcclatchie et al., 2000), but larger organisms at depth, such as mesopelagic fish, are more difficult to trap, since they react to light differently (Bone &

Moore, 2008). Estimations of biomass have also been made using a wide variety of models. Kloser (2009) compared the results of biomass estimates in the Tasman Sea calculated using acoustics (16–29 g m^{-2}), net sampling (1.6 g m^{-2}), two ecological models (0.5–3 g m^{-2}) by Lehodey (2004) and Fulton, Smith, & Punt (2005) and an Ecopath model by Griffiths et al (2010) (45g m^{-2}), categorically demonstrating the variance between methods and underlining the need for more accurate techniques.

5.1.4 Aims

Where the TS-length and length-weight relationships of an organism are known, its acoustic response dominant and probability of resonant scatter low, reliable estimates of biomass can be calculated without the requirement of in-situ catch data. The mesopelagic biomass, is considered to be formed of mainly Myctophidae sp. and Cyclothone sp., bony swimbladdered fish that dominate the acoustic response field (over-shadowing weakly scattering zooplankton, jellyfish and squid) and a recent study (Irigoien et al., 2014) has estimated global mesopelagic fish biomass (MFB) values using acoustic data recorded by a 38 kHz echosounder and known TS relationships of the fish (Torgersen, 2001; Yasuma et al., 2006; Yasuma et al., 2009).

Here, we estimate the mean value of mesopelagic fish Target Strength (TS) and weight by creating a pseudo-population of a ubiquitous myctophid species, *Ceratoscopelus warmingii.* We then determine biophysical drivers of the Z_{PDSL} and MFB, using a number of variables related to light intensity and biomass, in order to estimate the total MFB in the global pelagic ocean.

5.2 Materials and Methods

Following Section 4.2.1, 300 sound scattering layer (SSL) probability distributions (SPDs) were derived. The SPDs represent local pelagic regimes (300 by 300 km in spatial extent), based on SSL metrics (depth, MVBS and height). The 300 SPDs covered 14 of the 32 pelagic surface provinces (SPs) described by Longhurst (1998). Here, we take the SPDs, merge them within each SP, estimate mesopelagic fish biomass (MFB: see 5.2.2) and depth of the primary DSL component (Z_{PDSL}: see 4.2.2) and relate them, by weighted linear regression (WLR: see 5.2.3), to environmental variables (5.2.4), in order to make global predictions of MFB (5.3).

5.2.1 Estimating mesopelagic fish NASC values

In order to estimate the total amount of scatter produced by mesopelagic fish (MF), a threshold was applied to remove DSLs from the analysis with a mean MVBS value smaller than -80 dB re $1m^{-1}$; effectively setting the minimum packing density of mesopelagic fish within a DSL to 0.011 targets m^{-3}, using the average TS of myctophids (-60.6dB re $1m^2$) from Irigoien et al. (2014). This would remove DSLs that were zooplankton dominated or had diffuse arrangements of MF. Dense mixtures of zooplankton and MF are not resolvable using a single acoustic frequency, however, scattering strengths of zooplankton are typically significantly smaller than that of MF (Stanton, 2009); it would be considered unlikely to have both high densities of MF and zooplankton within a single DSL, as the MF would naturally consume its zooplankton prey when in close contact. From Equation 4.6 the NASC value for MF (s_{MF}) over the mesopelagic region is:

$$s_{MF} = \sum_{j=40}^{240} \left(\sum_{i=15}^{30} \left(Pr_{Z[j],ML[i]} \times 10^{(MVBS[i]/10)} \right) \right) \times 4\pi \times 1852^2 \quad (5.1)$$

The SPDs within each of the SPs were merged and values of Z_{PDSL} and s_{MF} were calculated (Equ's 4.4 & 5.1).

5.2.2 Estimating mesopelagic fish biomass

The estimated total scattered energy for all individual mesopelagic fish found within DSLs (per nautical square mile) is represented by s_{MF} and therefore:

$$\frac{s_{MF}}{4\pi} = N_{MF} \times \overline{\sigma_{MF}} \quad (5.2)$$

where N_{MF} is the number of mesopelagic fish and $\overline{\sigma_{MF}}$, is the mean acoustic cross section (MacLennan & Simmonds, 2005). $\overline{\sigma_{MF}}$ is a measure of the backscattered energy of each individual target, commonly referred to as the target strength (TS) when in its decibel form: TS = $10\log_{10}(\sigma_{MF})$. It follows that mesopelagic fish biomass (MFB) is calculated as:

$$MFB = \frac{s_{MF}}{4\pi \times \overline{\sigma_{MF}}} \times \overline{w_{MF}} \quad (5.3)$$

where $\overline{w_{MF}}$, is the mean weight of each target. In order to estimate $\overline{\sigma_{MF}}$ and $\overline{w_{MF}}$ we produced a pseudo-population of *Ceratoscopelus warmingii* sp. (pop_{CW}) a ubiquitous myctophid species found across all latitudes except within the arctic region (Fig 5.4: www.fishbase.org) and the subject of much study (Pakhomov et al., 1996; Takagi et al., 2006; Yasuma et al., 2009), to represent a mesopelagic fish population; growth and TS relationships for *C.warmingii*, along with those for other species of Myctophidae found in the literature, are listed in Appendix D.

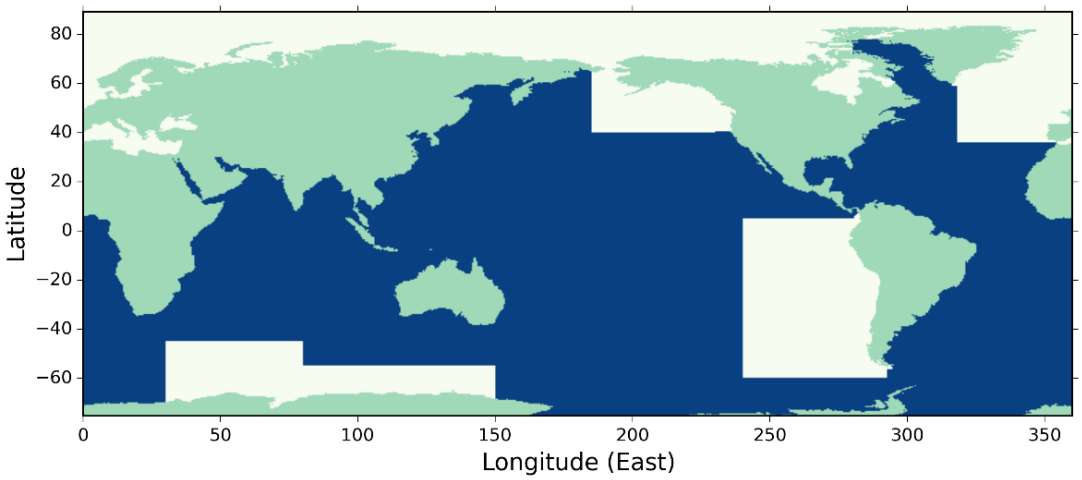

Figure 5.4: Distribution of the myctophid sp. *Ceratoscopelus warmingii* (blue). Data taken from www.fishbase.org.

The presence/absence and state (fat content) of the swimbladder are responsible for the strength of backscatter from a MF (Yasuma et al., 2009). This value is known to vary by over a factor of 100 (Irigoien et al., 2014), yet observations of DSLs show fairly uniform and constant values of MVBS (Proud et al., 2015), with variance far below the expected variance of TS values, meaning the inhabitants must be well-mixed in terms of their TS. The individual TS values are then dependent upon season (food availability: fat content; and temperature: metabolic rates) and ontogenetics. Juvenile mesopelagic fish are the most abundant and most

likely to have gas-filled swimbladders (strong scatterers) whereas older specimens, are fewer and have had time to accumulate larger quantities of lipids (Butler & Pearcy, 1972; Young et al., 1988). Longevity and growth rates vary widely in Myctophidae sp. (Takagi et al., 2006), and the *C.warmingii* sp. falls somewhere in the middle in terms of population dynamics, making them a good candidate to represent the MF population.

Assuming a 60 day period for larval and metamorphosis stages (Hayashi et al., 2001) and a maximum age of 3 years (*C. warmingii* stops growing after around 500 days: Takagi et al., 2006) lengths for each age-class of pop_{CW}, from an age of 60 days up to 3 years in increments of 1 day, were estimated following Takagi et al., (2006):

$$L = 80.8\big(1 - \exp\big(-0.00769(a - 34.4)\big)\big) \quad (5.4)$$

where L is the body length (mm) of the fish and a is the age-class in days. To estimate abundance (A) of each age-class, we use the relationship from Young et al., (1988):

$$A = \exp\left(-0.132\left(\frac{a}{30}\right) + 10.209\right) \quad (5.5)$$

To estimate weight of each age-class, we use the length-weight relationship derived by Pakhomov et al., (1996):

$$w = 0.0004(L^{3.361}) \times \left(\frac{1}{0.217}\right) \quad (5.6)$$

where w is the weight of the individual (mg). Since we expect the proportion of fish that are missing/have fat invested swimbladders (reducing TS), to increase with age, we set the proportion of fish with gas-filled swimbladders to uniformly decrease from 1 to 0 over the population age range, gradually increasing the proportion of fish without swimbladders in the population. TS relationships were obtained from Yasuma et al. (2009):

$$TS_{sb} = 26.3log_{10}(L) - 78.1 \quad (5.7)$$

$$TS_{wsb} = 49.4log_{10}(L) - 112.2 \quad (5.8)$$

where TS_{sb} is the TS of a MF with a swimbladder and TS_{wsb} without. Application of the above equations produced a mean TS value for each age group in the population (Fig 5.5).

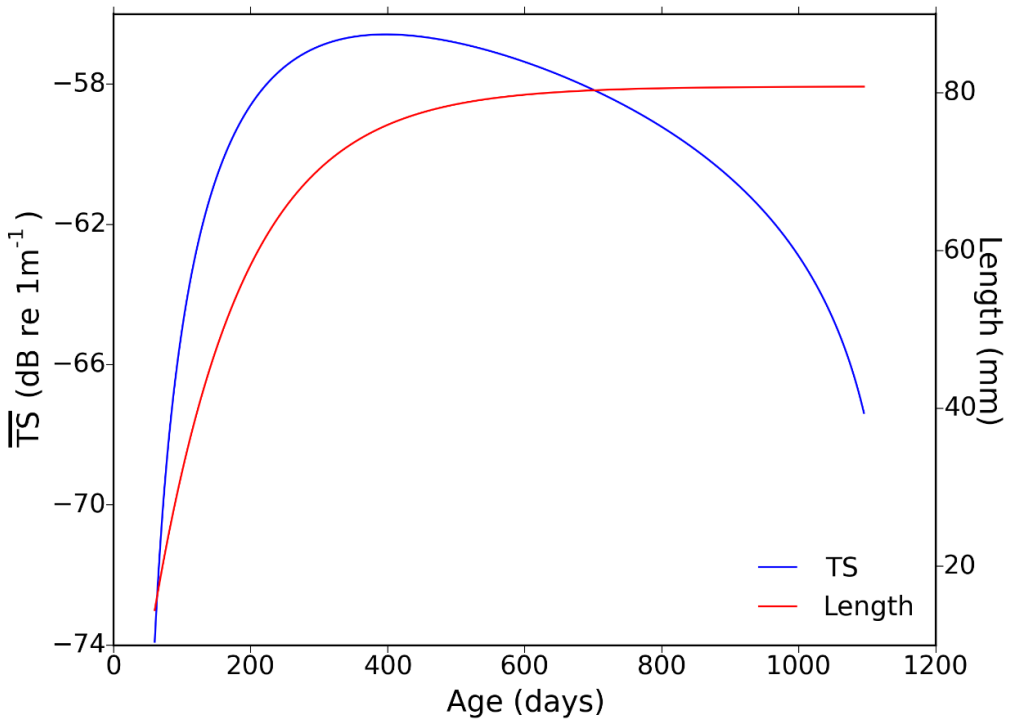

Figure 5.5: Age vs mean Target Strength (TS) vs length for a pseudo-population of mesopelagic fish.

Average values of TS and w were calculated over the entire population, resulting in a population TS mean ($\overline{TS_{pop}}$) of -59 dB re 1m^2 and a mean population w ($\overline{w_{pop}}$) of 2.06 grams; this yields a dB/Kg value of -32.14, which is smaller than the median value derived by Irigoien et al., (2014) of -30.8, but larger than their average value, -34.6. For a population where all targets were assumed to have gas-filled swimbladders, $\overline{TS_{pop}}$ increased to -57.4 dB re 1m^2. Substituting these values into Equation 5.3 we obtain an estimation for MFB (mg/nmi^2):

$$MFB = 1.302e9 \times s_{MF} \quad (5.9)$$

5.2.3 Weighted linear regression

The ordinary multi-linear regression formula can be expressed as:

$$E(Y) = \beta_0 + \beta_1 x_1 + \beta_2 x_2 + \cdots + \beta_k x_k \quad (5.10)$$

where E(Y) is the expected value of Y given values of the explanatory variables x_1 - x_k with coefficients β_1 – β_k respectively. Normally, to estimate the coefficients, the sum of squared residuals (SSE) is calculated and minimized, but for the case where each value of the

dependent variable is given a weighting, the weighted sum of squared residuals (wSSE) is determined:

$$wSSE = \sum_{i=1}^{n} w_i (y_i - \hat{y}_i)^2 \quad (5.11)$$

$$wSSE = \sum_{i=1}^{n} w_i \left[y_i - \left(\widehat{\beta_0} + \widehat{\beta_1} x_{i,1} + \widehat{\beta_2} x_{i,2} + \cdots + \widehat{\beta_k} x_{i,k} \right) \right]^2 \quad (5.12)$$

where the weights sum to 1 and are calculated using the original weight values (W_i) :

$$w_i = W / \sum_{i=1}^{n} W_i \quad (5.13)$$

and the error quantified by the root-mean-squared error (RMSE):

$$RMSE = \sqrt{wSSE}$$

For the weighted linear regressions (WLR), each dependent variable, Z_{PDSL} and MFB, were weighted differently. Z_{PDSL} was weighted by the probability of observation (Pr_z), calculated via Equation 4.2. The Pr_z value represented how likely it was that a particular depth region would be occupied by an SSL. For regions where the DSLs were highly variable (Polar Regions – see 4.3) low values of Pr_z would be obtained, reducing their weight in the regression analysis. For MFB, the WLR was weighted by SP spatial coverage i.e. the proportion of cells within each SP that data were obtained for. Spatial variance of the explanatory variables within each SP is expected and so the greater the coverage, the more likely it is that a true mean value for the SP is estimated.

5.2.4 Explanatory variables

Explanatory variables (Table 5.1) were selected based on prior knowledge and known relationships between the dependents and the environment (food availability, light intensity, water density, temperature) and data availability. The majority of variables were taken from the SODA (Carton et al., 2000) dataset and all were averaged over the period 2005 – 2008, to yield mean states of each variable (gridded at the same scale as the SPDs: uniformly with cell size of 300 by 300 km), in order to represent the oceans present state; acoustic dataset collection period (2006 – 2015).

Variable name	symbol (units)	Description	Source
primary production	PP (mg C m^{-2} day^{-1})	PP derived from VGPM using MODIS data	http://www.science.oregonstate.edu/ocean.productivity/index.php
wind stress	τ (N m^{-2})	Magnitude of surface wind stress	SODA (Carton et al., 2000)
sub-surface temperature	ssT_{PDSL} (°C)	Temperature at Z_{PDSL} depth	SODA (Carton et al., 2000)
sea-surface temperature	SST (°C)	Temperature at sea surface	SODA (Carton et al., 2000)
isopycnal1028	Z_{1028} (m)	Depth of the 1028 kg m^{-3} isopycnal	SODA (Carton et al., 2000)
sub-surface density	ρ_{PDSL} (kg m^{-3})	Density at Z_{PDSL} depth	SODA (Carton et al., 2000)
photic depth	Z_P (m)	Depth of the 1% isolume (RE surface illumination)	Longhurst (1998)
mixed-layer depth	Z_{ML} (m)	Depth at which density has reduced by 0.125 kg m^{-3}	SODA (Carton et al., 2000)

Table 5.1: Summary of the environmental variables used as explanatory variables in weighted linear regressions predicting change in mesopelagic fish biomass and deep scattering layer depth (primary component).

PP has already been associated with mesopelagic NASC values and more tentatively, biomass (Irigoien et al., 2014). Mesopelagic organisms will be affected by their habitat temperature (Fennel & Rose, 2015), which is split between the surface (SST) and the subsurface (ssT_{PDSL}). Light penetration (Z_P) changes with sea state (proxy: τ) and water clarity (proxy: PP), but also will be influenced by smaller scale variables, including cloud cover. The water-column density structure (proxies: Z_{1028}/ρ_{DSL}) is a function of pressure, temperature and salinity and shifts in

accordance with the depth of the mixed layer (Z_{ML}). Mean values of the explanatory variables were calculated for each SP and used to explain the variability in Z_{PDSL} and MFB.

5.3 Results

Sound Scattering Layer (SSL) probability distributions (SPDs, see 4.2.1) were calculated for each of the 14 Longhurst (1998) pelagic surface provinces (SPs) that data were available for (see Fig 2.1). The depth of the primary DSL (Z_{PDSL}) and the mesopelagic fish biomass (MFB) per square nautical mile were calculated for each SP (5.2). Ocean variables were averaged over each of the 14 provinces (5.2.4) and were used to construct weighted multilinear regression models (5.3.1) to explain the variance in Z_{PDSL} and MFB (5.3.2). Values of Z_{PDSL} and MFB were predicted for the other 16 pelagic provinces allowing a global prediction of MFB to be made (5.3.4).

5.3.1 Regression model results

For each dependent variable, weighted linear regressions (WLRs) were performed for various combinations of the explanatory variables (Table 5.2) that were averaged over each SP. For MFB, the proportion of cells within each SP that contained acoustic data was used for the weighting, for Z_{PDSL}, the probability of observation of a DSL (at Z_{PDSL}) was used. Not all combinations of the explanatory variable were tested, only those that were deemed appropriate given prior knowledge of relationships between the variables; also, using variable combinations involving strong correlations were avoided when possible, such as using both ssT_{PDSL} and SST at the same time. An outlier was identified for the MFB dependent variable leading to two further regressions (see MFB* in Table 5.2) where the outlier was left out.

Dependent variable	Explanatory variables	p-values	R^2
MFB*	PP, ssT_{PDSL}	0.017, 0.0001	0.87
MFB*	PP, SST	0.002, 0.03	0.651
MFB	PP, ssT_{PDSL}	0.1, 0.01	0.653
MFB	ssT_{PDSL}	0.001	0.58
MFB	PP, ρ_{PDSL}	0.06, 0.05	0.54
MFB	PP, SST	0.01, 0.12	0.47
MFB	PP	0.01	0.39
MFB	SST	0.19	0.07
Z_{PDSL}	PP, τ	0.01, 0.001	0.68
Z_{PDSL}	PP, τ, Z_{ML}	0.1, 0.01, 0.75	0.65
Z_{PDSL}	τ, Z_{ML}	0.001, 0.06	0.58
Z_{PDSL}	τ	0.005	0.459
Z_{PDSL}	τ, Z_P	0.007, 0.776	0.414
Z_{PDSL}	PP, ssT_{PDSL}	0.16, 0.21	0.23
Z_{PDSL}	Z_P	0.752	-0.07

Table 5.2: Weighted linear regression results. Z_{PDSL} is the primary deep scattering layer (DSL) depth and MFB is mesopelagic fish biomass. MFB* are regression results with an outlier (SSTC province) removed. Adjusted values of R^2 are given.

No relationship was found between Z_{PDSL} and Z_P (R^2 = -0.07), suggesting that light intensity is not a key driver of Z_{PDSL}. A better relationship for predicting MFB was found when using the ssT_{PDSL} over the SST, with R^2 values of 0.58 and 0.19 respectively. The variance in Z_{PDSL} and MFB were best explained by regression models with 2 explanatory variables, which were PP and τ in the case of Z_{PDSL} and PP and ssT_{PDSL} for MFB.

5.3.2 Optimum weighted linear regression models for Z_{PDSL} and MFB

Optimum models were selected for each of the dependent variables, by assessing p-values and adjusted R^2 values recorded in Table 5.2, yielding two multi-linear relationships:

$$\widehat{MFB} = -19{,}560 + 47 \times PP + 5{,}430 \times ssT_{PDSL} \quad (5.14)$$

$$\widehat{Z_{PDSL}} = 483.8 + 1272 \times \tau - 0.143 \times PP \quad (5.15)$$

where $\widehat{Z_{PDSL}}$ (R^2 = 0.68, RMSE = 28m) is the predicted depth of Z_{PDSL} and $\widehat{MFB}$ (R^2 = 0.65, RMSE = 20,221) the predicted value of MFB. The errors are calculated by taking the root of the mean-squared error for each regression model and do not consider errors associated with the estimation of environmental variables, or MFB. We make the assumption that since these values are calculated as means over large areas and for long time periods (large sample size), that errors are distributed normally and naturally reduce the uncertainty in these values (see 7.2.2 for a more detailed explanation of MFB error). $\widehat{MFB}$ is a function of PP and ssT_{PDSL}, which is reasonable since PP is a proxy for available prey biomass of MF and ssT_{PDSL} controls metabolic rates and therefore growth and reproduction. $\widehat{Z_{PDSL}}$ is a function of PP and τ, both of which act as proxies for light penetration in the water-column. Interestingly, Z_{PDSL} deepens, with increasing values of τ, which is counter-intuitive for a layer depth that is driven by light intensity. The deepening could be attributed to larger mixing depths (associated with increased wind stress) that deepen the subsurface density structure and therefore the DSLs.

For the MFB regression, an outlier was identified, the SSTC province (see Fig 2.1), which when removed, improved the model significantly (R^2 = 0.87, RMSE = 10,022). The SSTC province is a frontal zone between subtropical and subantarctic waters that forms a ring around the northern extent of the Southern Ocean. It is perhaps not surprising that the value of MFB was underestimated for this province, since data observations were made in the highly productive regions of the zone (S.W Indian Ocean and south Tasman Sea) as opposed to areas of low productivity in the S. Pacific sector (see Fig 2.1); the SSTC had the highest variability in PP (σ^2 = 31,145), which was significantly larger than the mean variance over the other provinces ($\overline{\sigma^2}$ = 9,411). For the WLR model without the SSTC province we have:

$$\widehat{MFB} = -19{,}940 + 40.3 \times PP + 5{,}513 \times ssT_{PDSL} \quad (5.16)$$

Predicted values were compared with observations for each of the WLR models (Equ's 5.14 – 5.16) and the root-mean-sqaured error (RMSE) values were calculated as confidence limits (Fig 5.6); RMSE was used over the more traditional method of using t-values as the population size (32 provinces) was known and is not significantly larger than our sample size (14 provinces).

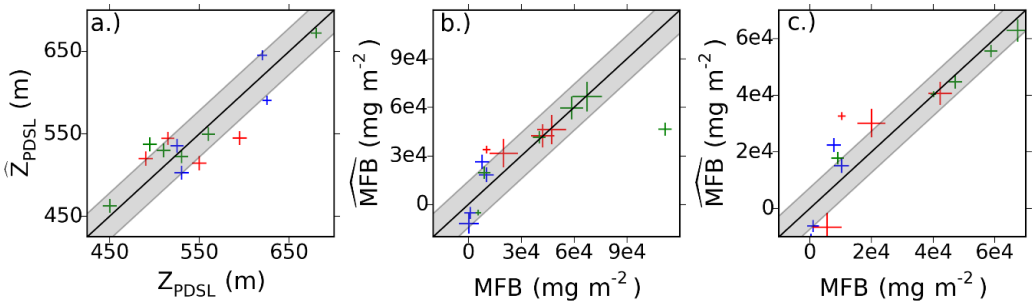

Figure 5.6: Weighted linear regressions (WLRs) predicting primary deep scattering layer depth (Z_{PDSL}) and mesopelagic fish biomass (MFB). Grey regions indicate extent of RMSE for each regression model. Z_{PDSL} weighted by probability of observation and MFB weighted by sample size (spatial coverage within surface province). a.) Z_{PDSL}, $R^2 = 0.68$, RMSE = 28m; b.) MFB, outlier (SSTC province) included, $R^2 = 0.65$, RMSE = 20,221 mg m^{-2}; c.) MFB, outlier excluded, $R^2 = 0.87$, RMSE = 10,022 mg m^{-2}. Cross size represents relative weighting between samples. Colors for a. & b. represent Longhurst Biome: Red = Trades; Green = Westerlies and blue = Polar.

The outlier was removed (due to large variance in PP values across the province) from the analysis. Equation 5.15 was used to predict values of Z_{PDSL} in order to be able to estimate values of ssT_{PDSL} in all of the SPs. MFB was then predicted for each SP by substituing the predicted values of ssT_{PDSL} along with PP values into Equation 5.16.

5.3.3 Explanatory variables

Z_{PDSL} and MFB were related to three environmental variables, PP, ssT_{PDSL} and τ (Fig 5.7).

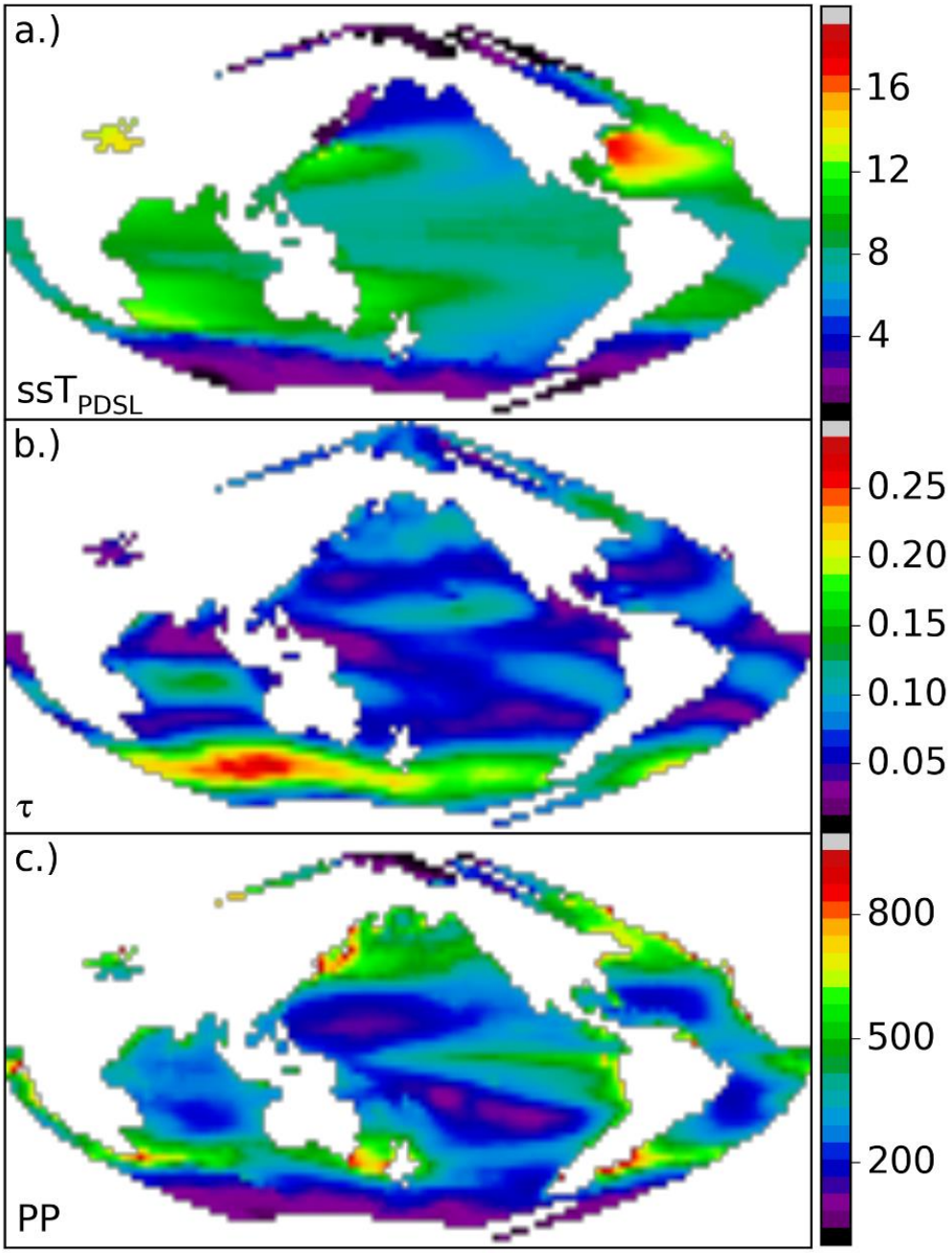

Figure 5.7: Explanatory variables for the optimum weighted linear regression models explaining both the primary deep scattering layer depth and mesopelagic fish biomass. Units: ssT_{PDSL} (°C); τ (Nm^{-2}) and PP (mg $Cm^{-2}day^{-1}$).

Mean global values of the explanatory variables were calculated, yielding values of 319 mg $Cm^{-2}day^{-1}$ for PP, 7.2 +/- 0.28 °C for ssT_{PDSL} and 0.084 Nm^{-2} for τ. Sub-surface temperatures peak in the north Atlantic at around 18° and are smallest in the Polar Regions. Wind stress values are most prominent in the Southern Ocean, peaking in the Indian Ocean sector and fall close to 0

at the equator and around mid-latitudes. Primary production increases in frontal regions between sub-polar and sub-tropical waters and close to coast lines, notable troughs in PP are observed both in the north and south Pacific and at high latitudes.

5.3.4 Global Z_{PDSL} and MFB

Values of Z_{PDSL} and MFB were predicted using equations 5.15 and 5.16 for all 32 surface provinces (Fig 5.8).

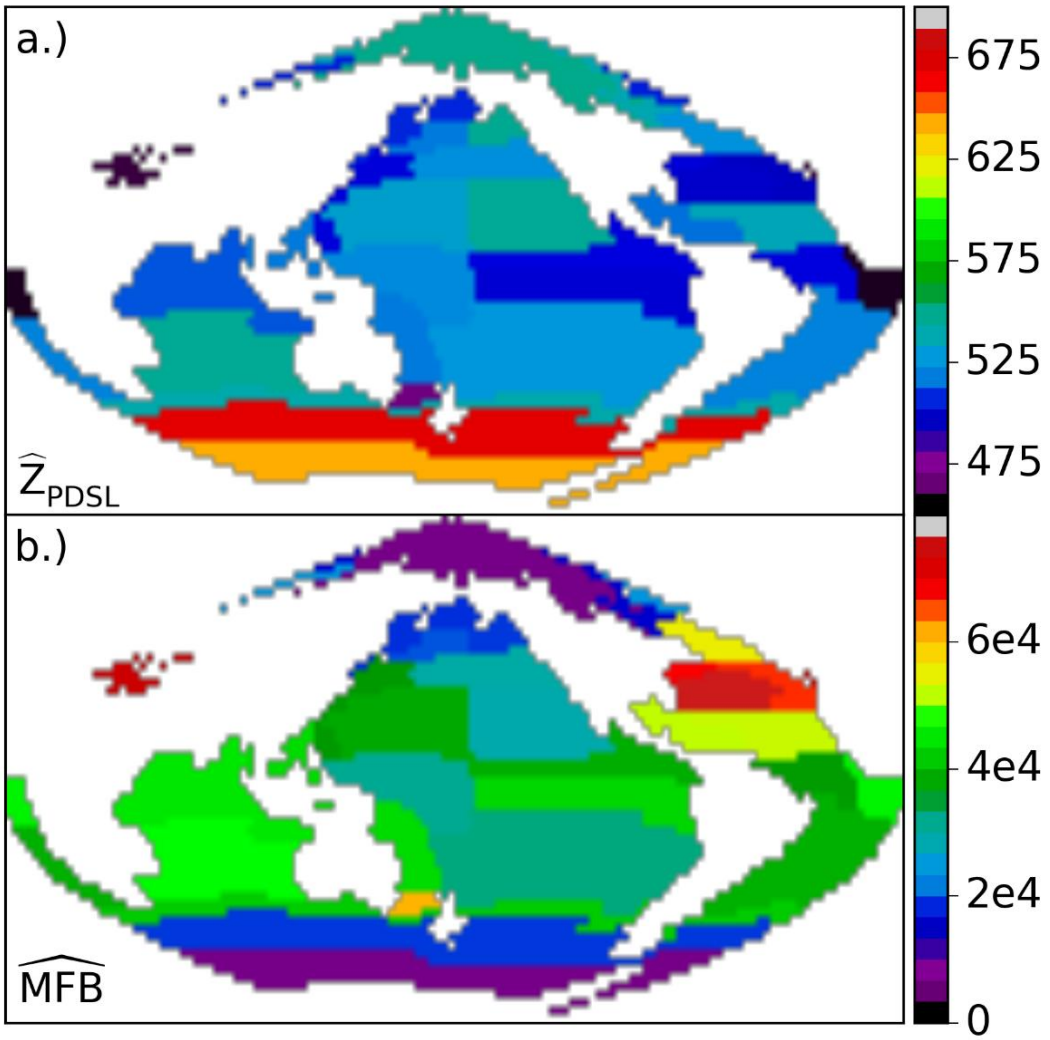

Figure 5.8: Predicted values of primary deep scattering layer depth (Z_{PDSL}, m) and mesopelagic fish biomass (MFB, mg m^{-2}) for each of the 32 pelagic Longhurst surface provinces.

The global MFB of the pelagic ocean was estimated to be 11,250 +/- 3750 Million tonnes (Mt) and the average Z_{PDSL} value (during the daytime) was 510m +/- 28m. The largest values in MFB

correlate with high sub-surface temperatures (North Atlantic for example) and deep DSLs are found in regions with strong wind-driven mixing (Southern Ocean).

5.4 Discussion

We predicted the change in the present depth of the primary deep scattering layer component (Z_{PDSL}), across the Longhurst surface provinces (SPs). From this depth, we were able to infer subsurface temperature from the SODA dataset and together with PP values, predict values of mesopelagic fish biomass (MFB). The methodology makes two large assumptions: firstly, when estimating the value of Z_{PDSL}, it is assumed that the mesopelagic fish population resides in the majority, within a relatively strong (> -80 dB re $1m^{-1}$), primary DSL component and secondly, that mean values of target strength (TS) and weight of the mesopelagic fish population can be estimated from a pseudo-population of myctophids, constructed using life-history traits and TS models of the geographically diverse species *Ceratoscopelus warmingii*, from the literature.

5.4.1 Deep scattering layer depth

Evidence suggests that larger myctophids dwell deeper in the water-column (Auster et al., 1992) and produce lower levels of backscatter (smaller target strength), since lipid content increases with age (Butler & Pearcy, 1972) and lipid invested swimbladders, are generally (when not resonant) weaker acoustic targets (Yasuma et al., 2009). The secondary DSL component, which resides deeper in the water-column and is characteristically weaker in scattering strength, could be formed of the larger mesopelagic fish. Larger zooplankton, potential prey of the larger mesopelagic fish, have also been known to reside deeper in the water-column too (Kinzer, 1969). The larger the organism, the higher its perceptibility, therefore larger organisms reside in lower light levels; this can also depend on colour, large red pigmented amphipods for example, may be able to reside shallower and avoid detection just as easily. As myctophids grow in size their pupils become larger and have a higher sensitivity to changes in light, allowing them to mimic lower light levels of down welling irradiance and occupy deeper depths (de Busserolles et al., 2013); this mechanism enables them to escape predation from lurking visual predators below them, as they would appear as silhouettes otherwise – incidentally, lanternfish are not very good at matching the light intensity when compared to other meso-/bathy-pelagic fish such as Hatchetfish (Bone & Moore, 2008). The depth of the fish population may follow that of its prey and further, follow the size stratification as well. More than 60% of the variability in depth estimates could be explained by simple models including just PP and wind stress. Increases in PP, shallow the Z_{PDSL}, this makes sense for a light driven DSL, where either the community as a whole/majority reacts to decreased light intensity by shallowing or a subset of the community, perhaps the

zooplankton, react and the fish follow. As wind stress increase, Z_{PDSL} deepens, which is counter-intuitive for a depth driven by light intensity, since increased mixing reduces light penetration. Deep water-column mixing entrains nutrient rich water into the mixed-layer which increases PP – but this effect is already accounted for in the PP variable. There was no relationship found between Z_{PDSL} and photic depth (R^2 = -0.07), suggesting that light intensity may not be the principle driver of Z_{PDSL}. Depth also could be driven by the density of the organisms (lipid/water content of either zooplankton or fish) in relation to the density of the water-column. Increased PP, would naturally reduce density by increasing lipid contents and result in shallowing – which is observed. Increased wind stress, may increase the kinetic energy demands of the community and reduce lipid stores and therefore increase depth. The Z_{PDSL} was selected as the DSL depth variable, as it was the strongest and most commonly observed component of the DSL; the secondary deeper component was not always resolvable (Fig 4.5). It may be prudent to consider the two component depths separately; it is expected that the drivers would be the same (with different regression coefficients), since they always appear close to each other and follow the trend that the strongest scattering layer is shallowest (Fig 4.5). Not all the variance in Z_{PDSL} could be explained (only 65%), other sources of variance could be related to local atmospheric effects (cloud cover), morphological factors, related to the specific inhabitants of the mesopelagic communities, oxygen content (related to PP and mixing) and oxygen demand (temperature and biomass).

5.4.2 Deep scattering layer biomass

A value of 11,250 +/- 3750 Mt was predicted for the global pelagic MFB. This prediction is similar to a value arrived at in another study using a similar method (Irigoien et al., 2014) finding median values of between 11,000 and 15,000 Mt, using a much smaller dataset (a single transect) and geographical range (-40°S to 40°N). The largest estimates of MFB were found in the N. Atlantic of around 70,000 mg m^{-2} (or 35 fish m^{-2} by applying a mean weight of 2 grams). This prediction correlates with studies that have observed relatively strong DSLs in the region (Anderson et al., 2005; Fennel & Rose, 2015). The variability in MFB was explained by just PP and sub-surface temperature, this is perhaps not surprising since food web theory and observed ranges of trophic efficiency (TE) suggest that biomass in higher trophic levels will be c. 10% of the level below and this will increase with increasing temperatures (Gascuel et al., 2008). MFB values were predicted using estimated values of mesopelagic fish TS and weight from a pseudo-population of myctophids and applying them to the backscatter recorded from

the entire mesopelagic region, which included both components of the DSL, the strong shallow component and the weak deeper component. Since the two components are likely to be made up of different size/age aggregates of mesopelagic fish, the assumption of a community TS will underestimate biomass in the case of larger fish aggregates (large lipid reserves, small TS) and overestimate in the case of small young fish (gas-filled swimbladders, strong TS). But as the estimates are made over the entire region, a mean community values is reasonable. There are 248 recorded species of myctophids (www.fishbase.org) and there will be large variance in their TS-length distributions. Here we selected a common species that has been intensely studied and therefore life-history traits are well understood. More work needs to be done to assess regional variance in the TS of mesopelagic fish. The ssT_{PDSL} value was determined at the primary component of the DSL, since it was the strongest layer and was always present. If larger fish do dwell in the secondary component and in sufficient density, then the ssT_{PDSL} value should be changed to a mean community depth when more than one DSL component is predicted/observed, alternately, they could be considered separately.

5.4.3 Implications

Relating DSL depth and biomass to biophysical drivers will improve the parametrisation of the forage components of ecosystem and population models, such as the spatial ecosystem and population dynamics model (SEAPODYM: Lehodey et al., 2008; Lehodey, 2004). It will also allow depths to be estimated and predicted using coupled climate models, such as the Coupled Model Intercomparison Project 5 (CMIP5) suite of models. Understanding the variability in DSL depths will aid in determining energy expenditures of deep-diving air-breathing vertebrates such as elephant seals (Boersch-Supan et al., 2012) and King penguins (Bost et al., 2015). Mesopelagic fish biomass was related to PP and ssT_{PDSL}, meaning that trophic efficiency between phytoplankton and mesopelagic fish is dependent upon temperature (Gascuel et al., 2008). It follows that as the ocean warms, mid-trophic level fish biomass will increase for any given PP value. An increase in wind stress correlates with a deepening DSL, which is contrary to what has been observed previously (Klevjer et al., 2016). Perhaps this implies that wind stress acts as a proxy for another unknown variable or that increased kinetic energy expenditure plays an important role in the spatial arrangement of the mesopelagic community.

5.4.4 Conclusions

Using the relationships derived here, DSL depths and MFB values were estimated and yielded a global MFB of 11,250 +/- 3750 Mt. The provinces, derived from surface properties, were adequate, but not optimal in partitioning the ocean for mesopelagic studies, as they do not consider subsurface properties; such as the disunity between sea surface and sub surface temperatures (Fig 5.1). A mesopelagic biogeography could be defined by forming regions that were based on the explanatory variables derived here. Regional variances in TE are likely to be related to ssT_{PDSL} and could be predicted for future scenarios by using output from coupled climate-ecosystem models such as NEMO-MEDUSA-2.0.

Chapter 6: A biogeography of the mesopelagic community

A mesopelagic biogeography was derived from drivers of deep scattering layer (DSL) depth and mesopelagic fish biomass, specifically, primary production, wind stress and water temperature. Gridded values of each of the environmental drivers were clustered into 22 distinct classes that formed the geographical boundaries of the mesopelagic provinces. Using output from a coupled climate-ecosystem model (forced by the HadGEM2-ES earth system model under the RCP 8.5 climate scenario), NEMO-MEDUSA-2.0, we predict that mesopelagic fish biomass may increase from 9 billion tonnes (bt) to 11.05 bt by 2100. This unexpected result arises because of greater mean trophic efficiency (TE), increasing on average by 1.8% per trophic level (TL) between primary production (TL: 1) and mesopelagic fish production (TL: 3.2). Using predicted ΔTE as a proxy for future resilience of pelagic ecosystems to anthropogenic impact, we highlight regions that may potentially require increased management in order to sustain healthy (diverse and abundant) pelagic ecosystems. The changing mesopelagic landscape, may offer an increasing source of fish protein for a growing human population (expected to increase to 11bn by 2100): this is an example of climate change having a positive impact on food security.

6.1 Introduction

A biogeography, partitions a region into areas that are biologically distinct, such that variation, in some well-defined population metrics, within each area is smaller than it is between. These distinctions can be made directly from biological observations, of community composition for example, or inferred from environmental properties that are known to drive certain biological processes, such as temperature and food availability. No such biogeography exists for the mesopelagic region of the water-column (200 – 1000 m), a consequence of the difficulty inherent in sampling an environment that is in the dark. Recently, alongside developments in computer technology, performance and data storage, a vast quantity of echosounder data has become available to the scientific community, collected by research/fishing vessels that have been ploughing the oceans for decades. Echosounder data provides the necessary information to extract key biological metrics, such as spatial arrangement, behaviour and biomass (when the inhabitants' target strengths are known) from observations of mesopelagic communities (e.g. Cox et al., 2011; Irigoien et al., 2014; Klevjer et al., 2016; Proud et al., 2015). Analysis of these data, can help us understand how mesopelagic communities change geographically and by extension provide the required information to define a mid-water biogeography, akin to the sea-surface provinces described by Longhurst (1998) that have markedly advanced our understanding of pelagic ecosystems.

6.1.1 Surface provinces

The surface provinces described by Longhurst (1998: see Fig 2.1) each belong to a specific biome, of which there are 4 in total. The first partition, the coastal biome, segregates regions on or close to the continental shelves (including shallow seas) that are influenced by coastal/island processes and land-runoff. The second biome, divides the ocean by temperature at the sub-polar fronts into the Polar biome and two oceanic biomes that follow the positions of the two low-to-mid latitudinal wind-systems, yielding the Trades and Westerlies biomes. Biomes are then divided primarily by primary production (PP) type, of which there were 6 cases, defined by the phase, frequency and amplitude of phytoplankton blooms throughout the annual cycle, derived from observations of chlorophyll concentration (a proxy for PP) from the coastal zone colour scanner (CZCS) taken from the Nimbus-7 satellite (NASA). Oceanic features provided the natural boundaries between provinces and physical properties, such as photic depth, mixed-layer depth and temperature, provided characteristics, resulting in a

partition of 54 distinct provinces, 32 of which, were off the continental shelf and their bottom depths extended beyond the mesopelagic region.

6.1.2 Pelagic coupling

In the open-ocean, surface provinces are linked to a deeper habitat, the mesopelagic region (200 – 1000 m), by diel vertical migration (DVM), in the same way that forests are linked to caves, inhabiting bats. The cave, alike to the mesopelagic region, is dark and protects its residents from predators during the daytime. At night, the inhabitants, leave their darker dwellings and make their way towards food; whereas mesopelagic fish are visual predators, bats, akin to cetaceans, use echolocation once outside the cave to then find their prey. In the case of the water-column, there are vast differences between environmental properties of the surface and the mesopelagic, particularly in temperature, pressure and also in nutrient and oxygen content. These changes form barriers or clines that are often used to the advantage of the biological community (e.g. Webster et al., 2015). The mesopelagic is somewhat sheltered or buffered from changes related to atmospheric conditions and it is likely that it is relatively more stable, or more homogeneous, than its surface counterpart; an observed decrease in biological complexity (a proxy for diversity) for example, was observed in SSLs extracted in Chapter 3 (Fig 3.9).

6.1.3 Trophic flow in marine ecosystems

The speed and quantity at which biomass flows through trophic levels (trophic kinetics) is now considered to be of paramount importance when studying ecosystem function, especially in the context of fisheries science (Pitcher & Cochrane, 2002; Cury et al., 2003). Trophodynamics are studied and simulated using models such as Ecopath with Ecosim (EwE: Christensen & Pauly, 1992; Walters et al., 1997) , and Ecotroph (Gascuel, 2005), which are based on predator-prey interactions and ontogenetic changes. Gascuel et al. (2008) showed how the ratio of production over biomass (P/B) can be used as a metric for trophic flow and derived an empirical relationship, based on data from FishBase (www.fishbase.org) and published Ecopath models, between P/B, trophic level and water temperature.

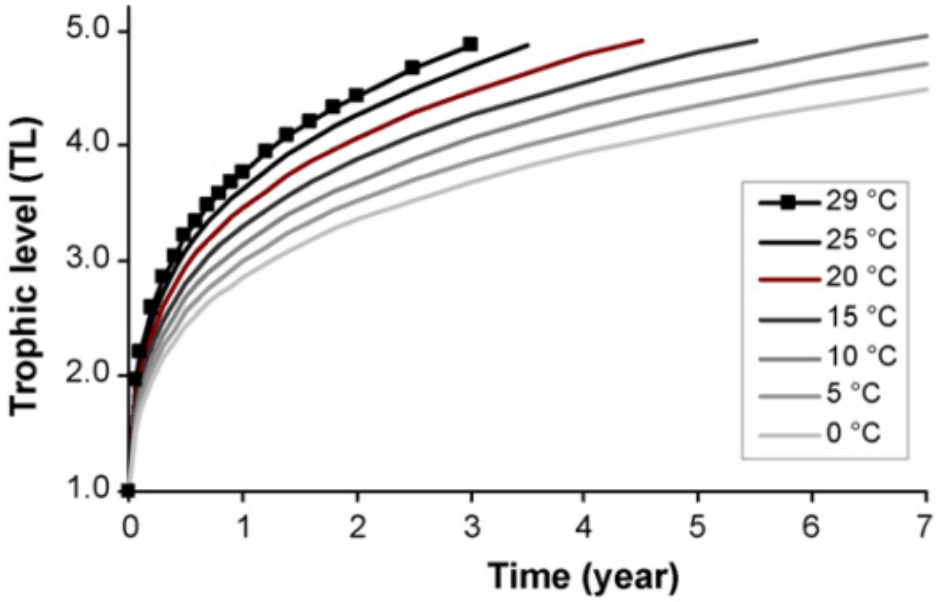

Figure 6.1: Trophic flow by temperature taken from Gascuel et al., (2008). Time can be interpreted as mean age of biomass.

As mass (carbon) flows through a food web in the most traditional sense, increasing in trophic level, its trophic speed reduces, taking in some cases more than 7 years to transfer from phytoplankton to apex predators such as Orcas (Fig 6.1). Trophic efficiency (TE), is an important metric of ecosystem resilience, since it quantifies how efficient a system is operating. Flow between PP and mesopelagic fish (trophic level 3.2: www.fishbase.org) is likely to vary geographically and over time. This quantity is related to water temperature and therefore DSL depth, and other environmental properties such as nutrient availability and turbulence along with predation pressure. Determining TE of pelagic systems and predicating its change could provide valuable insight to conservation management when planning the future spatial distribution of marine protected areas (MPAs) i.e. identifying those systems that have the least resilience to change and setting into action plans to protect them.

6.1.4 Predicting change in the ocean

Atmospheric CO_2 content is increasing rapidly as a consequence of anthropogenic activity post-industrial revolution (IPCC, 2013). The burning of 'fossil fuels', land use change and cement production, has raised CO_2 levels from 280ppm to 400ppm, an unprecedented rise that is larger than the observed changed between the previous glacial and inter-glacial periods (Yool et al., 2013). It is predicted that this level could rise to 1000ppm by 2100 (Houghton et al.,

2001) and that the increased warming of the ocean will dramatically change its physical state, affecting circulation and stratification, which some predict, will decrease its productivity (Boyce et al., 2010, 2012). Furthermore, increased levels of dissolved inorganic carbon in the ocean is altering its pH level, increasing its acidity (by 30% since the industrial revolution: Orr et al., 2005), and impacting $CaCO_3$ forming organisms such as pteropods and coccolithophores, which use the calcite/aragonite to form structures such as cellular walls, shells and skeletons (Doney et al., 2009). Natural mitigation processes are occurring that are actively curbing the increase in CO_2, such as the solubility pump, that draws CO_2 into the ocean interior via amplified CO_2 dissolution in the surface combining with deep-water formation, accounting for as much as 30% of anthropogenic emissions (Key et al., 2004), the biological pump, where organisms are aiding in the vertical transportation of carbon in the ocean via DVM (increasing particle export by up to 40% - Bianchi, 2013) and terrestrial processes such as the 'fertilisation effect' where plants are able to sequest more CO_2 per unit volume of water intake (van Minnen et al., 2009). Undoubtedly though, the physical changes in the ocean will significantly impact pelagic ecosystems. In order to understand how these changes will affect communities, a plethora of climate and ecosystems models have been developed to predict, under certain conditions, the likely change of our climate. Leading institutions have produced models as part of the Coupled Model Intercomparison Project 5 (CMIP5), including the HadGEM2-ES earth-system model (UKMO), which was used to force the coupled climate-ecosystem model, NEMO-MEDUSA-2.0. The ecosystem component of this model, MEDUSA, is formed of an intermediate complexity ecosystem model that divides the plankton community into two groups: small fast-growing plankton representing the microbial loop and large slower growing microphytoplankton and mesozooplankton (Yool et al., 2013). As the ocean warms and acidifies, community structure changes. Given that the mesopelagic community is driven by predictable biophysical drivers (see Ch 5), coupled climate-ecosystem models can be used to predict how they may change in the future.

6.1.5 Aims

Here we aim to define a mesopelagic biogeography based on the drivers of deep scattering layer (DSL) depth and mesopelagic fish biomass (MFB), which take into account sub-surface temperature structure along with surface PP and mixing. We then aim to revise the regression relationship derived in Chapter 5, by using the new mesopelagic partition as opposed to using Longhurst's surface provinces and predict values of MFB and regional trophic efficiency (TE) for

each mesopelagic province, calculating a revised global value of MFB. Using output from the coupled climate-ecosystem model, NEMO-MEDUSA-2.0, we will then predict how DSL depth, MFB and TE may change by 2100.

6.2 Materials and Methods

The depth of the primary DSL component (Z_{PDSL}) is a function of primary production (PP) and wind stress (τ) and the mesopelagic fish biomass (MFB) is a function of water temperature at Z_{PDSL} (ssT_{PDSL}) and surface PP. In order to derive a mesopelagic biogeography, the pelagic ocean was partitioned based on the drivers of MFB (as ssT_{PDSL} is a function of Z_{PDSL}) by applying the K-means clustering algorithm to define a number of mesopelagic classes (MC: 6.2.1 and 6.2.2) using the uniform grid defined in section 4.2.1. Using an extensive acoustic dataset (see 2.1) values of Z_{PDSL} and MFB were estimated for each MC data were available for. Weighted Linear regression was re-applied (as in Ch 5) to estimate a new coefficient for the MFB model (see Equ 5.9). Trophic efficiency values were inferred (6.2.3) from an empirical relationship from Gascuel et al. (2008) and predictions of Z_{PDSL}, MFB and TE for 2100 were made using data output from the coupled climate-ecosystem model, NEMO-MEDUSA-2.0 (6.2.4).

6.2.1 Mesopelagic Classes

Normalised mean values of the descriptors of the MFB regression (PP, ssT_{PDSL}) were grouped together into a number of clusters, each one defined by their respective cluster variable means (centroid values), using the K-mean clustering algorithm based on Euclidian distances. Each centroid (consistent of a mean PP and ssT_{PDSL} value) defined a separate mesopelagic class (MC). The clustering algorithm was applied, to determine the natural number of groupings or c that were evident within the data. The algorithm was run for a range of cluster frequencies (3 – 35), where at each step the Bayesian Information Criterion (BIC – Equ 6.1) was determined from the Log-likelihood (LL – see Equ 4.9) value, following the method by Anderson et al. (2007) to allow for model assessment:

$$BIC = -2 * LL + \big((M-1) * \log(N)\big) \quad (6.1)$$

where M is the number of centroids or cluster centers and N is the number of samples. The BIC conveys the goodness of fit of a particular K-means-model, as more clusters are added, there is more choice and therefore the maximum probability of at least some of the samples naturally reduces (see Equ 4.8), decreasing the LL and increasing the BIC; the BIC carries a penalty for number of clusters, see RHS of Equation 6.1. As the data approaches a 'natural well' where a better than average fit is achieved the change in BIC (ΔBIC) reduces to a minimum (Fig 6.3a) before increasing once more when the cluster frequency is incremented, forcing the model to fit back into a more unnatural state.

6.2.2 Multiple models

Multiple K-means models would be expected to fall into natural data wells in the cluster frequency range (3 – 35). To determine the model that best represented the data, we analysed the relationships of MFB with the explanatory variables (PP, ssT_{PDSL}), for each separate model. As the number of clusters increases, the intra-cluster variance (of the explanatory variables) reduces, but at the same time, the population size (total number of clusters) increases with respect to the sample size (number of clusters included in the regression) and the sample effort per cluster reduces. As the number of clusters is reduced, intra-cluster variance increases and the population size and sample effort per cluster reduces. This means that as the cluster number changes, across the models, the variance of the dependent variable (MFB) that is explained (quantified by an adjusted R^2 value) will change, as a consequence of the sample effort varying within and between clusters (some cluster arrangements will suit the data better than others). Therefore, although we expect the R^2 values to vary, as we alter the scale by increasing/decreasing cluster number, this change is not necessarily a consequence of scale, but maybe related to the spatial and temporal distribution and the sample effort per cluster of the acoustic dataset. By maximising the R^2 values for the dependent variable, we ascertain the best available estimate for the regression model coefficients; the scale will also be appropriate but not perhaps optimal or indeed characteristic of the relationship. Along with the R^2 values, the regression constants were recorded and analysed (Fig 6.3c). The larger the negative value of these terms, the more likely it would be that for a region with small values of ssT_{PDSL} and PP that negative MFB values could be predicted. By minimizing the absolute value of this term, where possible, we increase the predictive (real) range of the regression model.

6.2.3 Trophic Efficiency

Mesopelagic fish production (MFP: mg/m^2/year) can be calculated using the empirical relationship, taken from Gascuel et al. (2008):

$$\frac{\mathrm{MFP}}{MFB} = 20.19\mathrm{t}^{-3.26} \times \exp(0.041 \times ssT_{PDSL}) \quad (6.2)$$

where t is the trophic level. In this instance, the trophic level of mesopelagic fish is assumed to be 3.2 (www.fishbase.org) and by multiplying both sides by MFB and dividing both sides by PP, we arrive at the trophic efficiency between trophic levels 1 and 3.2:

$$TE_{1-3.2} = \frac{MFB}{PP} \times 0.455 \times exp(0.041 \times ssT_{PDSL}) \quad (6.3)$$

Where PP is converted to wet weight biomass from carbon weight by multiplying its value by 9 (Strathmann, 1967) and to a yearly rate (rather than a daily rate) by diving by 365.25.

6.2.4 NEMO-MEDUSA-2.0

Using data output from the NEMO-MEDUSA-2.0 ecosystem-climate coupled model (see 2.2 and Yool et al., 2013), we predicted how the values of Z_{PDSL}, MFB and TE within each MC may change by 2100. The data output from the model, for the period 2090 – 2100, had larger mean values of sub-surface temperatures, decreased wind stress and similar values of PP (Fig 6.2 and 6.7e & f). A measure of pelagic ecosystem resilience was derived by calculating the change in TE (ΔTE) per trophic level between the present state (represented by the 2005 – 2008 predictions) and the future state (2090 – 2100) of the pelagic ocean:

$$\Delta TE = \sqrt[2.2]{TE_{1-3.2}^{2090-2100}} - \sqrt[2.2]{TE_{1-3.2}^{2005-2008}} \quad (6.4)$$

Values of ΔTE were calculated for each gridded cell and binned into 5 classes, C1 representing cells that were predicted to experience the largest reduction in TE and C5, incorporated cells that incurred the largest increase in TE. The classes act as a proxy for pelagic ecosystem resilience, the larger the value or class index, the more efficient and therefore better prepared an ecosystem is, to cope with change.

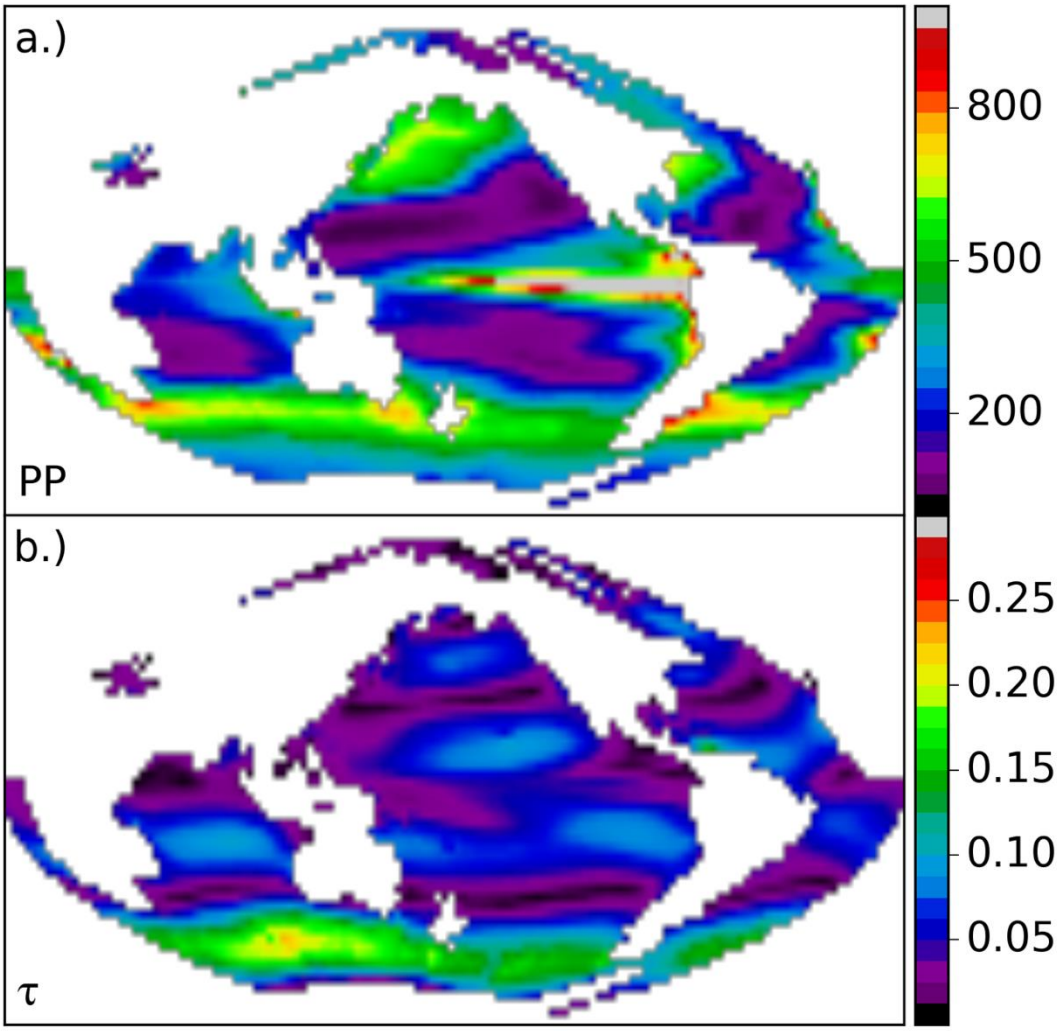

Figure 6.2: Mean values of primary production (PP: mg C/m^2/day) and wind stress (τ: N/m^2) for the period 2090 – 2100, output from the NEMO-MEDUSA-2.0 model.

6.3 Results

Weighted linear regression models (see 5.2.3), predicting values of MFB, were constructed for a range of cluster frequencies (3 – 35: 6.2.1/6.2.2), by averaging, for each cluster frequency, the explanatory variables over each individual cluster that data were available for, and using the values to explain the variation in MFB, calculated following section 5.2, in those clusters. The resultant R^2 values and regression constants were analysed (Fig 6.3) and used to select an appropriate number of clusters/mesopelagic classes (MCs) in order to form a mesopelagic biogeography (6.3.2). A model with 22 MCs, forming a biogeography for the period 2005-2008 was selected and a revised (in comparison to Equ 5.16) regression model to predict MFB was derived (6.3.1). Using data output from the NEMO-MEDUSA-2.0 model (2090 – 2100), a 24 MC K-means model was selected (using the same method) and the geographical distributions of the MCs for both time periods were plotted (6.3.3). Values for Z_{PDSL}, MFB and TE were predicted for both the current and future scenario (6.3.4) and their change analysed (6.3.5). The change in TE was used to act as a proxy for pelagic ecosystem resilience (PER) to stresses, such as over-fishing, in order to classify regions from 1 to 5, in increasing PER (6.3.6).

6.3.1 K-means model results and model selection

K-means models were run for a range of cluster frequencies (3 – 35) using gridded values of the two drivers of MFB, ssT_{PDSL} and PP. The BIC naturally increased when the cluster frequency was incremented, but the change in BIC (ΔBIC) varied considerably. Where ΔBIC reduced to a minimum (at a natural data well), the cluster arrangement provided a better than average fit to the data. Multiple K-means models, with cluster frequencies of 10, 14, 16, 19, 22, 27, 29 and 33 fell into natural data wells (Fig 6.3a). For each solution, a weighted linear regression (WLR) was performed, using mean values of PP and ssT_{PDSL} as explanatory variables, in order to explain the variance in MFB; using the clusters in each model that acoustic data were available for. Each regression produced an adjusted R^2 value (Fig 6.3b) which quantified the variance explained and a constant term (Fig 6.3c), giving the value of the y-intercept.

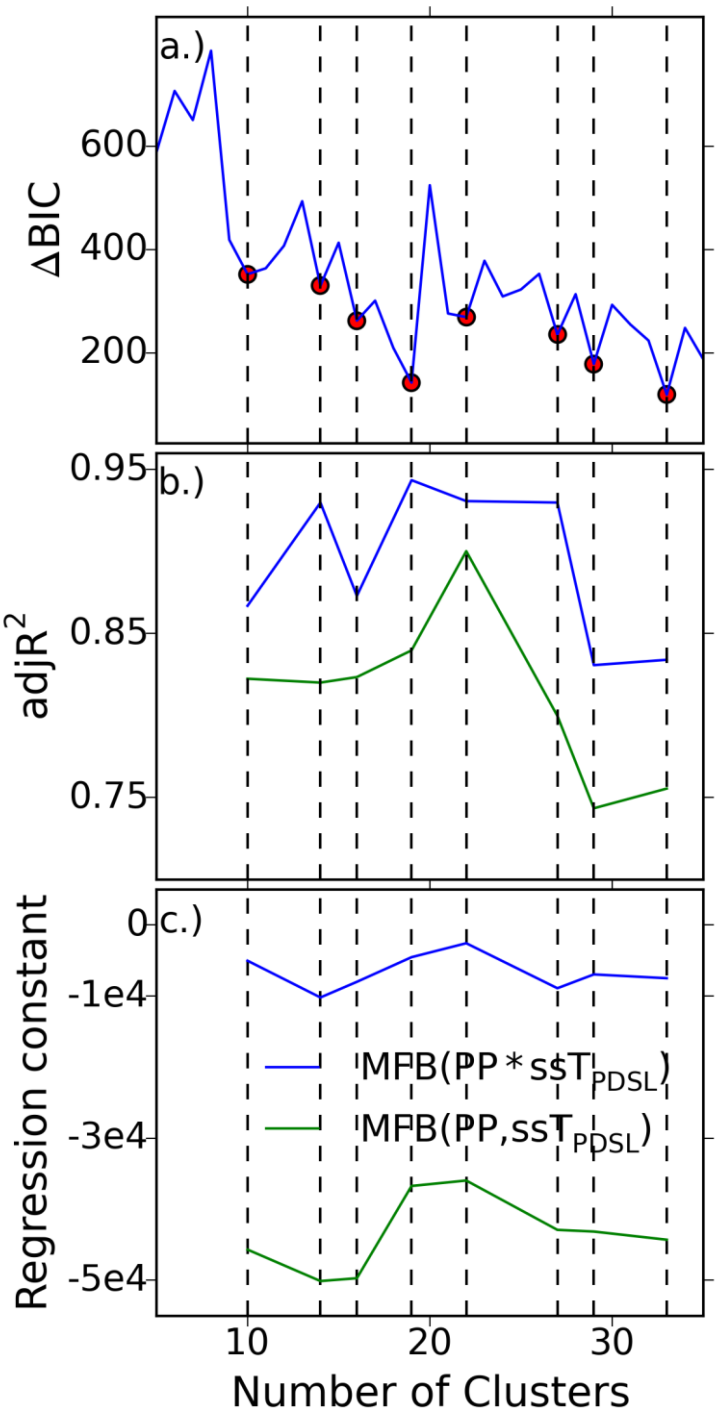

Figure 6.3: K-means and regression results for mesopelagic class frequencies. a.) The change in BIC (ΔBIC) is plotted for each cluster frequency and natural wells within the data are indicated (red circles and dashed lines) at bottom peaks; b.) Adjusted R^2 values are shown for two sets of weighted linear regressions (WLR) across the K-means models; c.) Regression constants are shown for the WLRs.

In addition to running the regressions using PP and ssT_{PDSL} as explanatory variables, they were also carried out using an interactive variable PP* ssT_{PDSL}, which yielded consistently higher values of R^2 and lower absolute regression constants (Fig 6.3). The model with 22 clusters (or MCs) was selected (Fig 6.3), due to its large R^2 value and small regression constant:

$$\widehat{MFB} = -2{,}567 + 13.76 \times (PP \times ssT) \quad (6.5)$$

The model (R^2 = 0.93, RMSE = 7,173 mg m^{-2}) outperformed the previous SP derived model (R^2 = 0.87, RMSE = 10,022 mg m^{-2}) for predicting MFB and was deemed to provide an improved global partitioning of the pelagic ocean (at large scales), compared with the SPs, when conducting analysis of the mesopelagic community.

In the above model, the single explanatory variable consisted of the product of PP and ssT_{PDSL}. The increased R^2 value of the regression model indicated that an increase in PP amplifies MFB by a factor equal to the increase multiplied by the value of ssT_{PDSL} (and vice-versa).

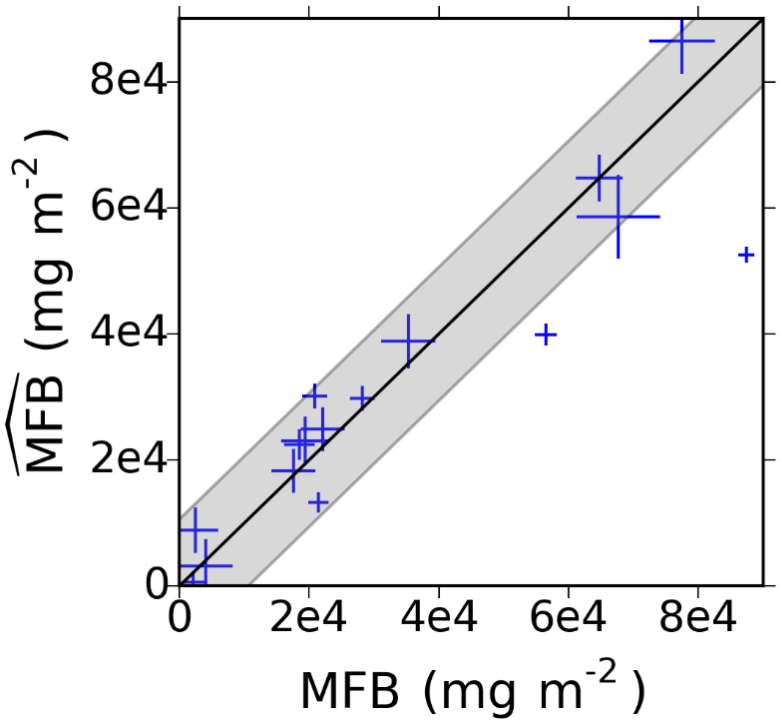

Figure 6.4: Weighted linear regressions (WLRs) predicting mesopelagic fish biomass (MFB) for each mesopelagic class (MC) in the 22 cluster arrangement. Grey regions indicate extent of RMSE for the regression. MFB was weighted by sample size (spatial coverage within each MC) and the weighting is indicated by marker-size. MFB: R^2= 0.93, RMSE = 7,173 mg m^{-2}. Cross size represents relative weighting between samples

6.3.2 Mesopelagic Biogeography

A mesopelagic biogeography was derived (6.2.1), consisting of 22 MCs (Fig 6.5a). The method was repeated using data output from the NEMO-MEDUSA-2.0 model for the period 2090-2100 and an arrangement of 24 MCs was selected (Fig 6.5b); in this case, no acoustic data were available and so the cluster frequency closest in number to the 2005-2008 model that also fell into a natural data well was chosen.

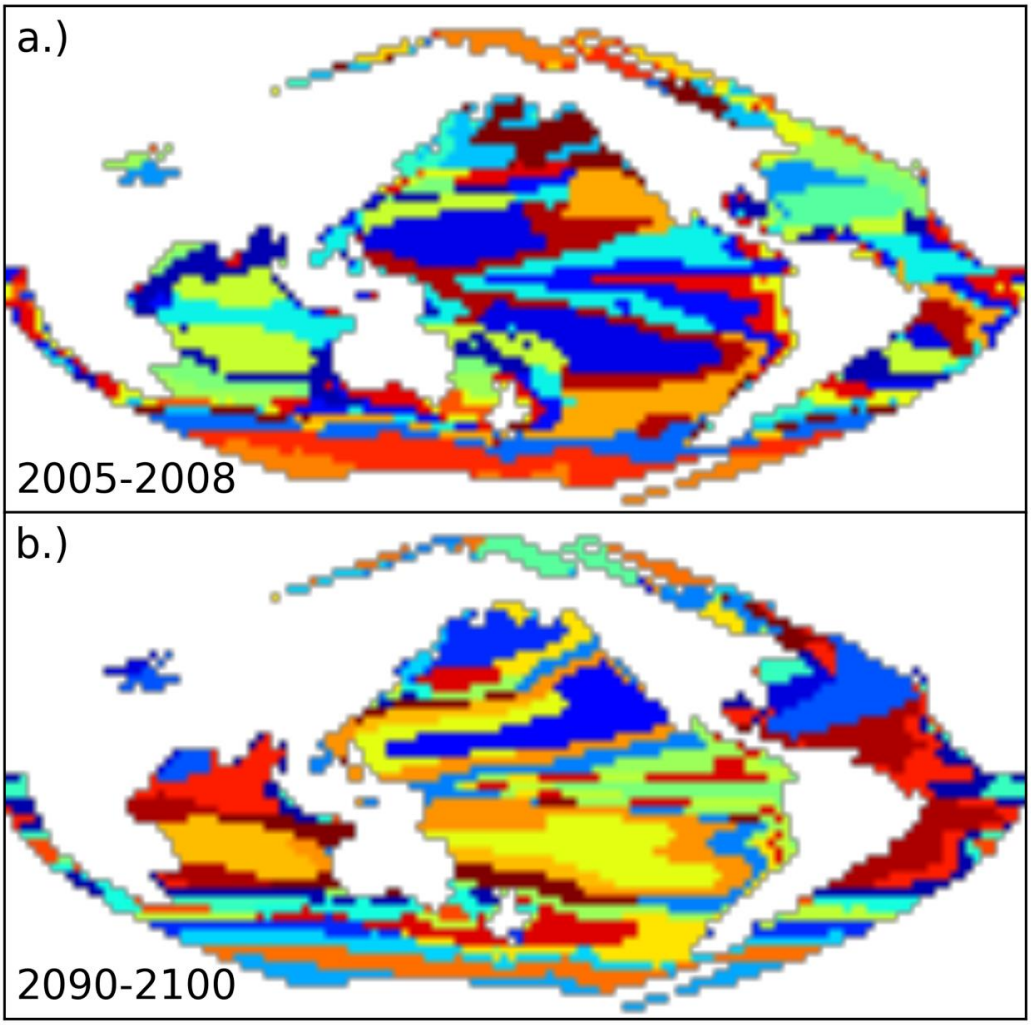

Figure 6.5: Mesopelagic biogeography derived from mesopelagic classes (MCs) based on PP and subsurface temperature at the depth of the primary deep scattering layer component. a.) 22 MCs, indicated by colour, for 2005-2008; b.) 24 MCs, indicated by colour, for 2090 – 2100.

The geographical partitions were based on two variables. The size of each province (isolated class member) gives some indication of the variance of the explanatory variables in that area;

where provinces are large, such as the two in the north and south pacific (Fig 6.5a dark blue), mean ssT_{PDSL} and PP values vary considerably less than in the provinces in the S. Atlantic for example. Interestingly, in the future scenario, the Atlantic becomes much more uniform, as opposed to the highly variable state in the present scenario. The MCs also reveal what parts of the pelagic ocean are similar to each other in terms of MFB. In order to understand how the MCs evolve through different spatial scales, the cluster arrangement for each data well (6.3.1) were plotted (Fig 6.6) forming biogeography's with between 3 and 33 MCs.

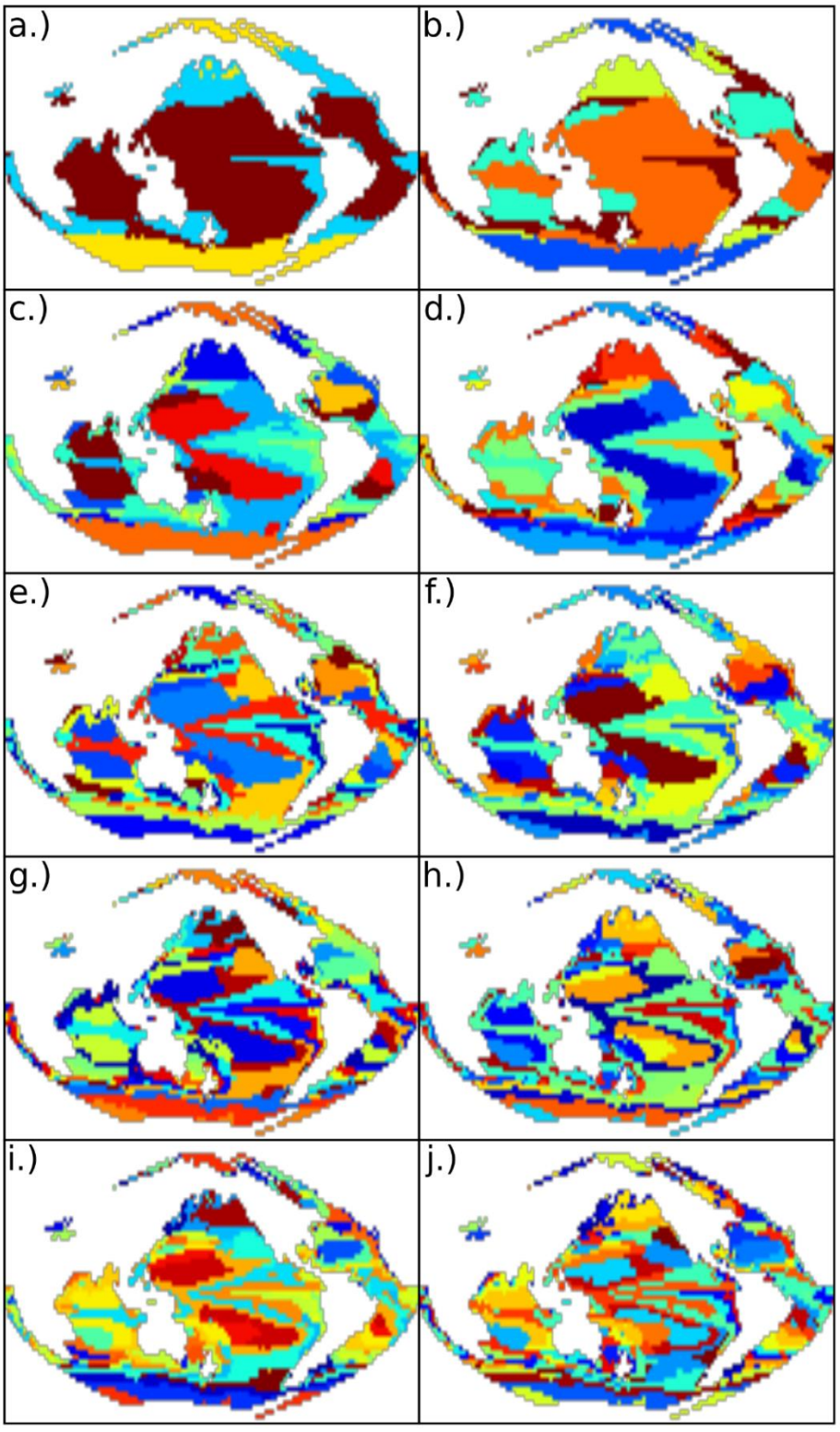

Figure 6.6: Mesopelagic biogeography's (MBs) at various spatial scales, produced by clustering drivers of MFB into different number of mesopelagic classes (MCs): a.) 3; b.) 5; c.) 10; d.) 14; e.) 16; f.) 19; g.) 22; h.) 27; i.) 29 and j.) 33 MCs.

The first partition into 3 MCs (Fig 6.6) is similar to Longhurst's (1998) biomes, the yellow class representing the Polar biome, the light blue class the Westerlies and the brown the Trades; the coastal class is not represented since these data were excluded. As the number of MCs is increased, the ocean breaks down naturally by the variation in the explanatory variables or descriptors of the mesopelagic community that drive DSL depth and biomass.

6.3.3 Global predictions of Z_{PDSL}, MFB and TE

The predicted values, along with the explanatory variables for MFB were plotted for the present (2005 – 2008) and future (2090 – 2100) scenario (Fig 6.7). The predicted mean Z_{PDSL} shallowed from 545m to 510m +/- 30m and the predicted ssT_{PDSL} increased from a mean of 7.2 +/- 0.28 to 8.5 +/- 0.37 °C (Fig 6.7). The PP remained fairly constant in the pelagic ocean, with mean values of 319 and 324 mg C/m^2/day, for the present and future scenario respectively, but changed significantly geographically, generally increasing in regions that presently displayed high PP values (frontal and equatorial) and decreasing in relatively low PP zones. Notably, the MFB, which globally was predicted to increase from 9,000 +/- 2,600 Mt to 11,050 +/- 2,750 Mt by 2100, was predicted to significantly decrease in the north Atlantic and either side of the equatorial pacific zone by 2100. The decrease in MFB in the Atlantic is surprising as the TE is predicted to increase due to increased sub-surface temperatures, but the predicted reduction in PP, limits the production of MFB. Mean TE values were predicted to increase from 15.7 +/- 2.15% to 17.35 +/- 2.1% per trophic level by 2100.

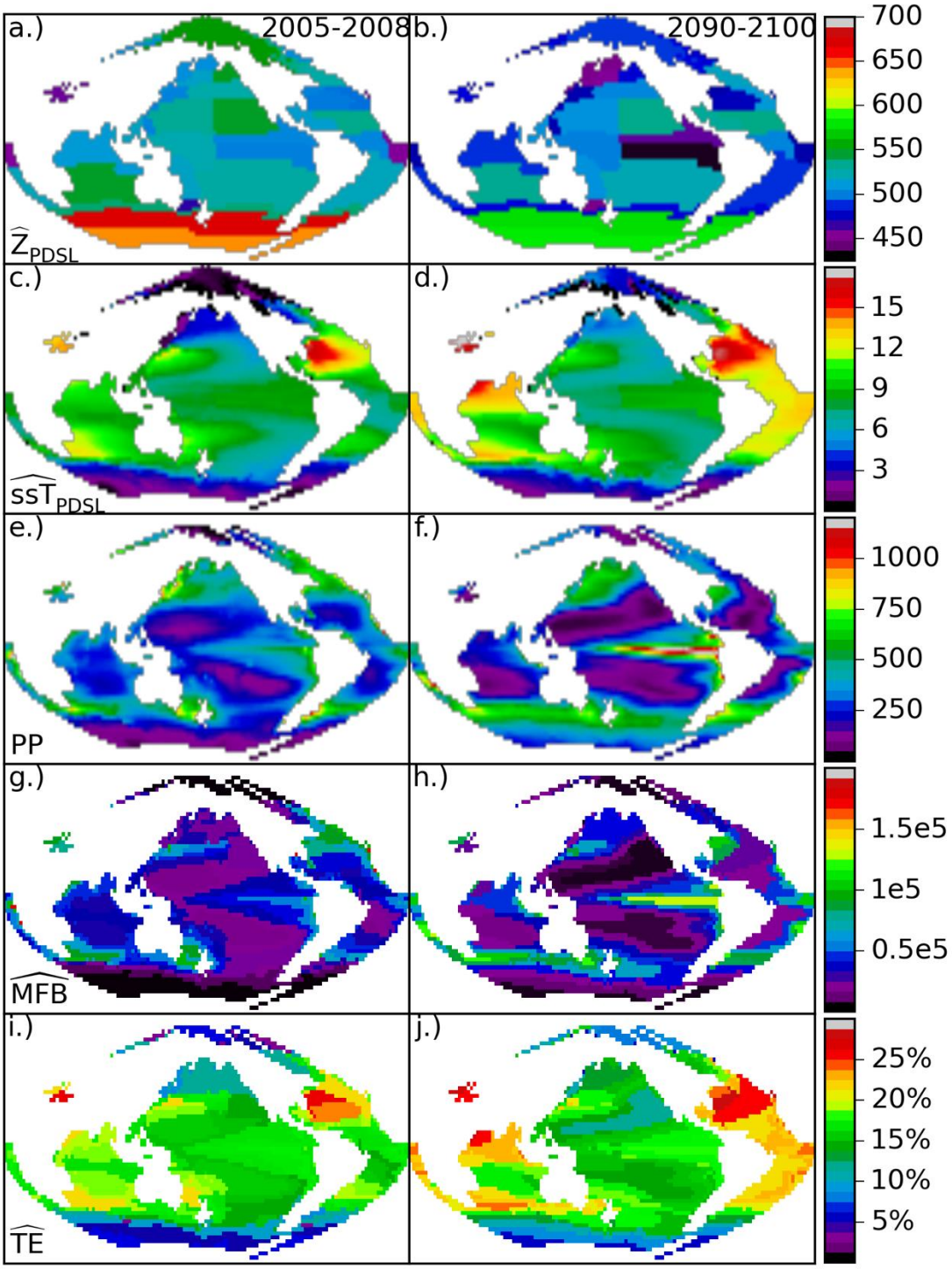

Figure 6.7: Globally predicted variables: a.) and b.) Deep scattering layer depth, Z_{PDSL} (m), predicted over surface provinces; c.) and d.) Temperature at DSL depth, ssT_{PDSL} (°C), predicted over gridded cells; e.) and f.) Primary production, PP (mg C day^{-1} m^{-2}) – calculated over gridded cells; g.) and h.) Mesopelagic fish biomass, MFB (mg m^{-2}), predicted for each mesopelagic class; i.) and j.) Trophic Efficiency, TE (% per trophic level), predicted for each mesopelagic class.

6.3.4 Global change in the pelagic ocean

Generally, DSLs were predicted to shallow, particularly in regions with increased PP (Fig 6.7c) but also deepen slightly in the central and north Atlantic (Fig 6.8a). Shallowing regions, particular towards the poles and in frontal zones show an increase in MFB, along with increases in TE; except for the equatorial pacific, where the increase in MFB is a direct consequence of much higher PP rates. The TE is predicted to increase in all regions apart from the southern Indian Ocean and the central pacific.

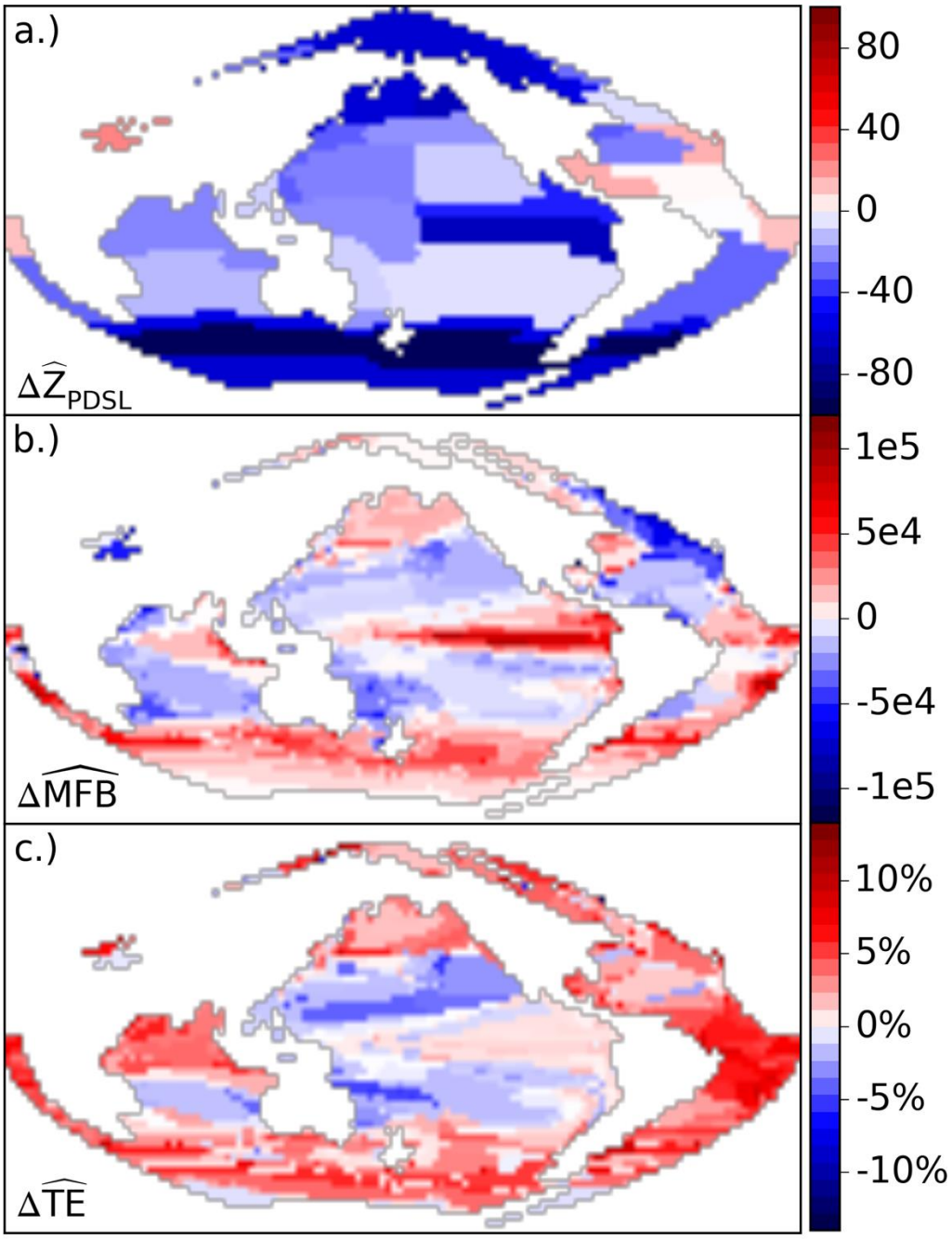

Figure 6.8: Globally predicted change in the depth of the primary deep scattering layer component (Z_{PDSL}, m), mesopelagic fish biomass (MFB, mg m^{-2}) and trophic efficiency (TE, % per trophic level). a.) Calculated over surface provinces; b.) & c.) Calculated using derived mesopelagic classes for both time periods (2005-2008 & 2090-2100).

6.3.5 Pelagic Ecosystem resilience

The estimated values of MFB will inherently include changes in biomass caused by anthropogenic impacts such as fishing, either directly or indirectly via trophic cascades. It follows that any predictions based on these relationships include those biases and as fishing pressure is likely to change over the next 100 years, it is worth considering the impact of this change, when interpreting the result. Regions that are predicted to increase in $TE_{1\text{-}3.2}$, are likely to be more resistant to such changes in fishing pressure and therefore by classifying regions based upon the predicted change in $TE_{1\text{-}3.2}$ between now and 2100, we grade areas, guided by the data (Fig 6.9), from 1 – 5 (C1: <-3%, C2: -3% - -0.3%, C3: -0.3% - 2.5%, C4: 2.5%-5.1%, C5: > 5.1%), in their resilience to anthropogenic impacts, producing an informative map for both fisheries and conservation management (Fig 6.10).

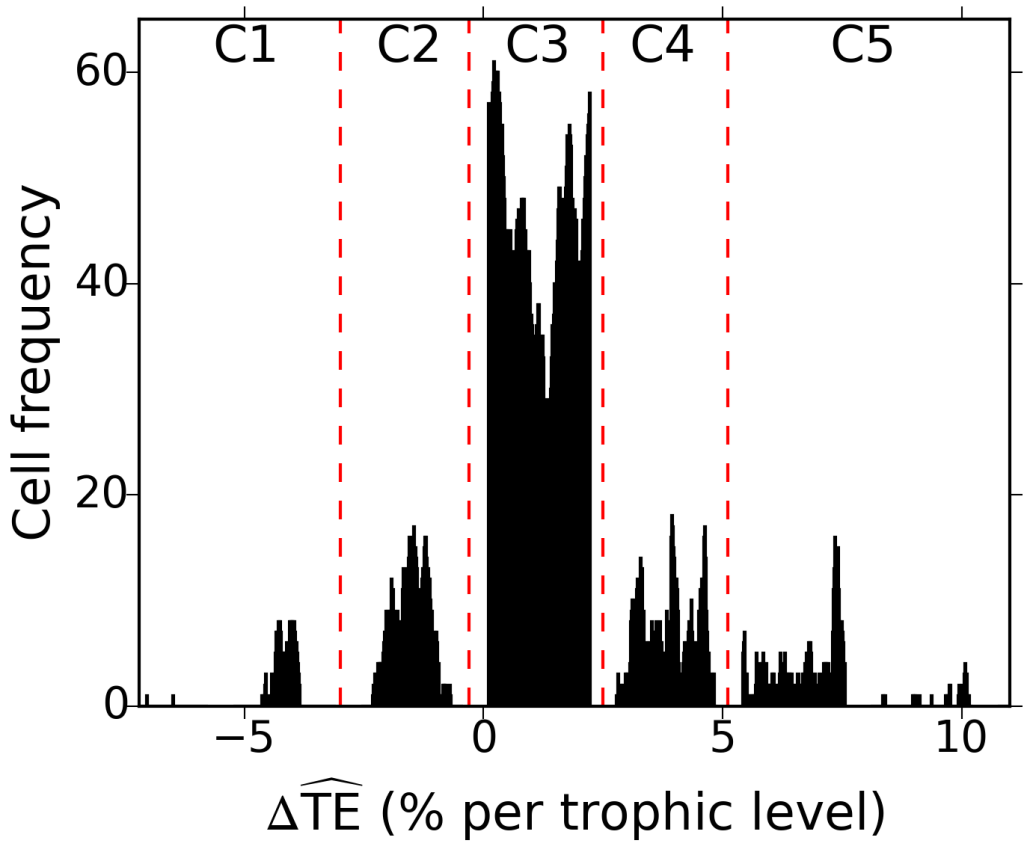

Figure 6.9. Pelagic ecosystem resilience (PER) classes based on change in predicted TE between 2005-2008 and 2090-2100.

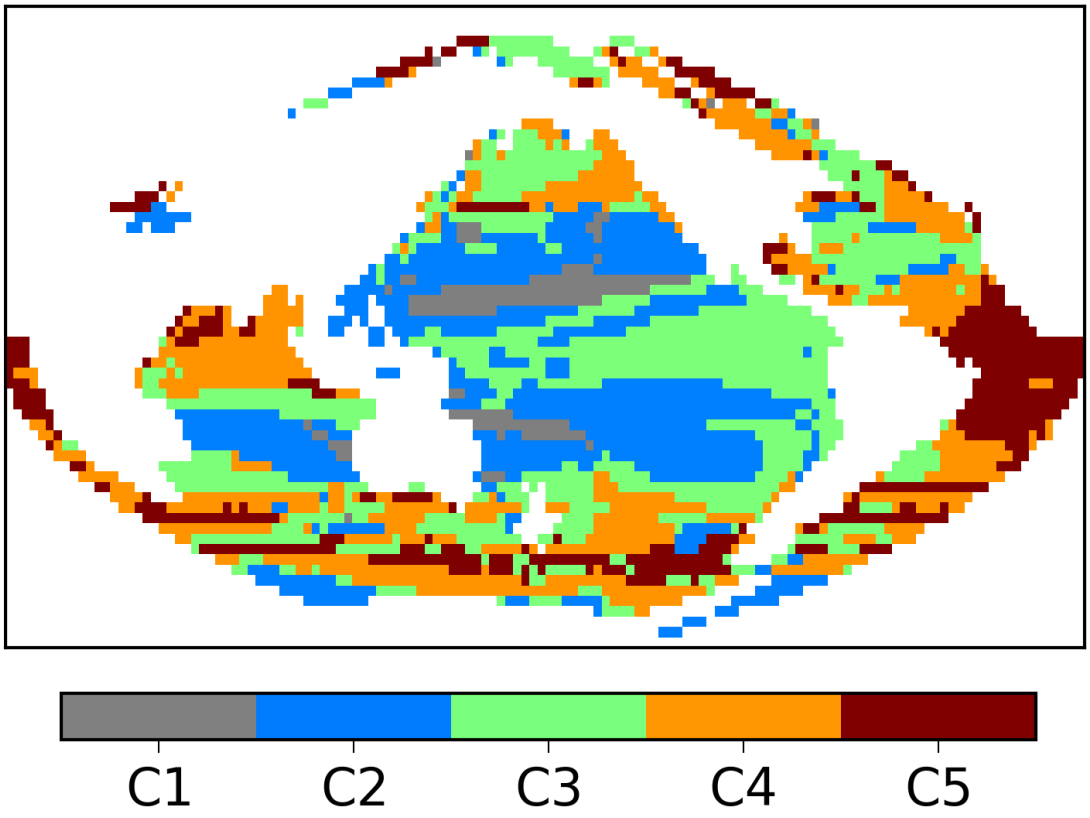

Figure 6.10: Pelagic ecosystem resilience (PER). Classes are numbered 1 (low resilience to change) to 5 (high resilience to change), change in trophic efficiency (ΔTE) by class: C1 (< -3%), C2 (-3% - -0.3%), C3 (-0.3% - 2.5%), C4 (2.5% - 5.1%), C5 (>5.1%).

The PER map highlights the Pacific, S. Indian Ocean and the N. Atlantic as regions that will potentially weaken in their resilience and therefore recovery to external stresses, such as those caused by increased fishing activity, but also include other climatically driven impacts, such as ocean acidification, that are expected to reduce production.

6.4 Discussion

The surface provinces (SPs) derived by Longhurst (1998) were deemed to not adequately partition the ocean into regions that were appropriate for mesopelagic study (Ch's 4 & 5). The reason for this is partly linked to large intra-province variance of the drivers of MFB: ssT_{PDSL} and PP; the higher the variance of these variables within a study region the larger the sample effort required in order to ascertain reliable results. These variables were clustered together using the K-means algorithm to determine a number of suitable cluster frequencies (Fig 6.3) that provided geographical partitioning at different scales (Fig 6.6). A mesopelagic biogeography was derived for a 22 cluster arrangement (Fig 6.5), as a large amount of the variance in MFB (93%) was explained by a WLR model using the MFB drivers as explanatory variables (Fig 6.3). The regression model (Fig 6.4), which outperformed both regression models derived for the SPs by the same method (see 5.3), allowed predictions of MFB and TE to be made in each mesopelagic cluster/class (MC), along with global estimates (6.3.4). Data output from NEMO-MEDUSA-2.0 was then used to predict how these values may change by 2100 (Fig 6.7 & 6.8) and a metric of pelagic ecosystem resilience (PER) was derived (6.3.6).

6.4.1 Mesopelagic biogeography

The mesopelagic biogeography derived here consisted of 22 mesopelagic classes, each one with a characteristic pair of PP and ssT_{PDSL} values. The biogeography is valid for a range of scales but the ability to predict changes in class properties reduces as the number of classes decreases for any given sample size. It follows that the required scale (or number of classes) is dependent upon your sample data. For data collected remotely by satellites where complete coverage is available, the scale is limited only by the resolution of the instrument, whereas for acoustic data, as in this study, a 22 class arrangement was optimum and class frequencies between 10 and 30 would have been acceptable (6.3.1).

Mesopelagic partitioning will improve mesopelagic study survey design, allowing for more focused studies of open-ocean communities. The mesopelagic classes will aid fisheries management at the regional scale by providing information concerning mesopelagic fish production and biomass. Estimated values of ecosystem trophic efficiency of these partitioned regions will be of particular interest to conservation management when assessing change in the marine environment and evaluating pelagic ecosystem health.

6.4.2 Predicted change in the ocean

Over the next 100 years, the mesopelagic community faces many challenges including, over-fishing, increased water temperatures, acidification and changes in nutrient and oxygen conditions (Yool et al., 2013). If fishing activity increases in the future and commercially important (subject to a species economic value) fish species populations are reduced to near extinction levels, fishers will be forced to catch other, probably smaller but more numerous fish species (Pauly et al., 1998). These could include the very abundant mesopelagic fish species of the Myctophidae and Stomatoid familes (St John et al., 2016); this would have dire consequences for pelagic ecosystems and the predicted increase in MFB and TE here, would not occur. However, if fishing activity is well managed and efforts are driven towards shifting the increased demand onto aquaculture, then the mesopelagic fish community could remain abundant and increase in line with increases in sub-surface temperature as long as their prey field remains intact. The ocean is predicated to become more acidic, affecting shell forming (made of $CaCO_3$) organisms such as the pteropods (Doney et al., 2009), a well-known prey-item of Myctophidae species (Pakhomov, 1996). This will be of little consequence for the mesopelagic fish as they feed on a variety of zooplankton, which in the majority is consistent of copepods (Pakhomov, 1996), the most abundant multi-celled organism on Earth, that feed on other smaller non-$CaCO_3$ forming microzooplankton. MFB and TE were predicted to increase by 2100 due to the shallowing of DSLs and increased water temperature of the sub-surface environment. PP increased in regions of high PP and decreased in regions of low PP, a form of ocean capitalism: the lipid rich get richer and the lipid poor get poorer. The Atlantic Ocean is predicted to change dramatically, with larger increases in ssT_{PDSL} but substantial reductions in PP, leading to increased TE but reduced biomass. The decrease in PP in the north and south pacific (low PP zones), reduce MFB to levels equivalent to what we experience now in the Polar Regions, effectively a polarisation of subtropical waters. Conversely, Polar Regions are predicted to increase in MFB and TE as the predicted shallowing of the DSL is most pronounced there.

6.4.3 NEMO_MEDUSA-2.0 predictions

The predictions of global MFB and TE for 2100 were based on the output from a single model, that was forced using the Representative Concentrative Pathways (RCP) 8.5 climate scenario, the highest carbon emissions scenario produced in the CMIP5 model suite, where atmospheric CO_2 levels increase to 1000 ppm by 2100 (Houghton et al., 2001). This climate scenario was

used to investigate the 'worst-case' scheme, in terms of emission reductions in the 21st century. It would be useful to examine other climate scenarios, such as RCP 2.6, where levels of CO_2 remain fairly constant, to determine if the global trends observed here (increases in MFB) are still apparent and to also compare regional variances. Further analysis of output from other CMIP5 models and climate scenarios were not considered in this study due to time restrictions. It would be expected however, that with reduced CO_2 levels and therefore lower temperatures, that, in accordance with equation 6.5, predicted future MFB values would also reduce. Generally, climate models predict an increase in levels of CO_2 in our atmosphere and therefore an increase in SST. Given that global PP does not reduce significantly, and that the mesopelagic temperature structure warms alongside increasing SST, an increase in MFB would still be expected.

6.4.4 Implications

The future success of fisheries and conservation management will rely heavily on our understanding of the ocean ecosystem, in a holistic sense, gained from marine science. In this study we concentrate on a single component, the mesopelagic community, which is comprised of mid-trophic level species. This component is perhaps currently the most poorly understood (Lehodey et al., 2010), but no less vital than any other. Changes in sub-surface communities affect the whole ecosystem and they need to be monitored. More work needs to be carried out in regards to the geographical partitioning of the mesopelagic community derived here, focusing on observed changes at ecologically important (or distinct) oceanic features, such as fronts, that are hot-spots of ocean production. Along with communication of this research amongst the science community through publications and conferences, the results need to permeate through into industry and policy. Currently, policy makers may only consider impacts based on predicted changes of surface communities and top predator populations that swamp the literature, when making important decisions regarding marine conservation, which will impact the entirety of the marine environment. This is of paramount importance right now, at a time of rapid climatic change (Yool et al., 2013), and should be highlighted without delay at a governmental level, underlining that fact that the mesopelagic environment is as important (if not more so, since it forms the centre of many food-webs) as other ecosystem components (PP and top predators). Due to the nature of the mesopelagic environment, it is out of sight, and so any impacts, directly/indirectly influenced by change in the mesopelagic to the ecosystem, are not fully understood or appreciated at present.

6.4.5 Conclusions

The pelagic ocean can be partitioned by mesopelagic community metrics, PP and sub-surface temperature (derived from DSL depth), to enable study of the pelagic ecosystem across a range of spatial scales. For the first time, characteristics of the mesopelagic community, known to be understudied due to the nature of the habitat (Webb et al., 2010), can be predicted using biophysical drivers that we can model. Open Ocean ecosystems are not currently protected (Game et al., 2009), as the majority of conservation lies close to coastlines and islands where impacts are more readily observed. In this study, we outline regions that may be less resilient to future stress, specifically in the north and south Pacific and the southern Indian Ocean. To improve our understanding of the relationships and global partitioning's derived here, a better insight into mesopelagic community structure and the acoustic response of mesopelagic fish is required. Currently, initiatives such as the Southern Ocean Network of Acoustics (SONA) and the Mesopelagic Southern Ocean Prey and Predators (MESOPP) project are seeking to obtain this knowledge.

Chapter 7: Conclusions

In deriving biophysical relationships of DSL depth and biomass and therefore providing a basis for a mesopelagic biogeography we have taken a substantial first step in understanding how the marine surface environment relates to sub-surface communities. Primary production at the surface and the temperature of the DSL environment underpin mesopelagic fish biomass and this result brings insight into mid-trophic level community dynamics and underlines the importance of the sub-surface temperature structure when considering ecosystem trophodynamics. The aim of this work was to provide an informative map for both conservation and fisheries management of distinct mesopelagic provinces, alike to the map produced by A. Longhurst (1998), which we have succeeded in doing (see Fig 6.5 and Fig 6.10). The geographical partition into mesopelagic classes, distinguishable by their mesopelagic fish biomass values, will aid in the future allocation of open-ocean marine protected areas and also in the management of mesopelagic fisheries, which are likely to be re-energised in the future (St John et al., 2016), fuelled by recent elevated estimations of global mesopelagic fish biomass (Irigoien et al., 2014).

7.1 Summary

More than 1 year's worth of 38 kHz echosounder data (Ch 2) covering 14 of the 32 pelagic surface provinces (SPs; Longhurst, 1998) have been used to examine sound scattering layers (SSLs). A subset of these data were used to develop a methodology, to identify and characterise sound scattering layers, SSLEM: Proud et al., 2015 & Ch. 3. Over 40,000 SSLs were extracted from the data, grouped together by region (300 by 300 km scale). The regional data were used to form local SSL probability distributions (SPDs) that estimated the probability of observing SSLs at different depths and backscatter levels. These SPDs were merged by likeness forming 6 distinct pelagic regimes (PRs), notably different in their deep scattering layer (DSL) metrics. The pelagic regimes naturally clustered together in space, regardless of temporal variations in data observations, revealing in some cases, overlap with the SPs and in others, complete disunity.

DSLs were found to typically have two global components, a relatively strong (in terms of backscatter strength) shallow primary DSL component, which was always present, at around 510 meters and a deeper, considerably weaker, secondary DSL component, that was sometimes absent, at between 700 and 900 meters. Other arrangements, consistent of more than 2 components were observed but were not statistically significant at the regional scale.

The assumption was made that the majority of mesopelagic fish reside at the depth of the primary component of the DSL (Z_{PDSL}). Primary production (PP) and wind-stress (a proxy for mixing) were found to explain the variation in Z_{PDSL} ($R^2 = 0.68$ for regression model, see 5.3.2). NASC values were determined for each SP and values of mesopelagic fish biomass (MFB) were inferred by estimating mean values of target strength and weight for mesopelagic fish from a pseudo-population of myctophids, based on the life-history traits obtained from the literature, of the ubiquitous Myctophidae sp. *Ceratoscopelus warmingii*. PP and sub-surface temperature (ssT_{PDSL}: sub–surface temperature at Z_{PDSL}) were found to explain the variability in MFB across the 14 SPs ($R^2 = 0.65$, see 5.3.2). The disunity between the SPs and the regions formed by the pelagic regimes was attributed to the non-linearity between surface and mesopelagic environments, primarily driven by the sea-surface and sub-surface temperature structure. A mesopelagic biogeography, formed of mesopelagic provinces, was constructed by clustering together geographical cells (300 by 300 km in size) based on their ssT_{PDSL} (estimated from predicted values of Z_{PDSL}) and PP values. Using these mid-water provinces, a more accurate regression model predicting variation in MFB ($R^2 = 0.93$, see 6.3.1) was derived. This

relationship was used to make a global estimate of MFB (9,000 +/- 2,600 Mt) and predict how this value may change by 2100 (11,050 +/- 2,750 Mt) using data output from the NEMO-MEDUSA-2.0 model. The increase in MFB was attributed to a global increase in trophic efficiency from 15.7 +/- 2.15% per trophic level to 17.35 +/- 2.1%. Although the resultant increase in MFB was determined from attributing the majority of backscatter from the mesopelagic to MFB (a likely overestimate) and only analysing output from a single coupled climate-ecosystem model, the implication remains the same, that for a warming ocean, the environment of the mesopelagic is also warming: if the DSL depth does not significantly deepen (dependent on PP and wind-stress) then TE is likely to increase as MFB is driven by ssT and PP. In this final chapter, implications of this work are explored in relation to fisheries management and marine conservation, including some recommendations for future research.

7.2 Implications of results

Here, I discuss the results of the data chapters, i.e. chapters 4 to 6, in a broader context, drawing in findings from recent publications and outlining implications to our understanding of management of pelagic ecosystems with an emphasis on fisheries management.

7.2.1 Pelagic regimes

The pelagic regimes (PR) were divided, in the first instance, by the sub-polar fronts, into the polar pelagic regime (PPR) and the 5 mid-to-low latitudinal ocean pelagic regimes (OPRs). The main difference between the two arises because in the PPR there are an abundance of DSLs that have very low levels of backscatter, which can be attributed to DSLs containing weakly scattering organisms such as zooplankton rather than mesopelagic fish. This polar trait could be related to evidence that suggests only expatriate populations of larger species of myctophids from sub-polar regions venture into higher latitudes, across the sub-polar fronts (Saunders pers. comm.), meaning that observations of mixed assemblages of fish and zooplankton would be spatially and temporally variable and dependent on some predator-prey parameter. Alternatively, polar mesopelagic fish populations may just be less abundant or more diffuse, such that they are not observed as frequently, owing to the natural reduction in diversity that comes with colder environments. The PPR is also highly variable in its depth arrangement of DSLs, suggesting that they either vary largely in space or time. Myctophids in the Southern Ocean have been observed to exhibit seasonal DSL depth changes along with vertical size stratification (Saunders et al., 2014; Saunders et al., 2015), which could explain the observations made here.

The OPRs take the form of what is likely to be the fundamental structure of the water-column, consisting of a surface component (0m – 200m), a migrant zone (MZ) (200m – 400m), a primary DSL component (400m – 700m) that is ubiquitous throughout the oceans and a secondary, deeper DSL component (700m – 900m) that is observed less frequently. These two DSL components are likely to be formed of organisms that are either linked to different predator-prey interactions or are separated by morphologically driven environmental responses.

Classification of the different types of water-column structures using PRs can act to inform open-ocean monitoring of pelagic ecosystems. This could be achieved by identifying shifts

between PR classes and inferring the consequences of changes in energy expenditure (through deepening/shallowing of DSL depths for example) and trophodynamics.

One such statistical approach could be to assign PR class membership probabilities, perhaps using a multinomial distribution. As additional data is added, changes in PR class membership could be tracked and inference made to determine the practical influence of environmental drivers such as temperature and PP.

Interestingly, migration dynamics of each PR varied significantly (Fig 4.5), visualised by the shift in backscatter in either a positive or negative direction within the MZ. The variation in MVBS with depth is a characteristic of the migrating assemblage, varying with organism, numerical density, orientation and swimbladder volume (Godø et al., 2009; Love et al., 2004). For example, an indication of an expatriate population of large older myctophids could be identified by a reduction in the change in MVBS in the MZ, since older fish are expected to be more heavily invested in lipids (Butler & Pearcy, 1972) and therefore change in the density of the swimbladder, and hence acoustic backscatter, will be smaller. The six PRs derived could also be broken down into sub-PRs that could allow for example, the polar region to be broken up, potentially into latitudinal bands following the frontal zones, thereby enabling water-column structure to be monitored at higher resolutions.

7.2.2 Biophysical drivers of DSL depth and biomass

The key difference between the epipelagic and mesopelagic environments is their relative temperature structures (Fig 5.2). Primary production (PP) is a carbon source for both environments and controls, to some extent, biomass across trophic levels. The mesopelagic fish biomass (MFB) values estimated here, driven by PP and sub-surface temperature, represent an estimate of the maximum MFB value.

The sources of error or uncertainty in the MFB model were the following: 1.) in order to estimate ssT_{PDSL}, the value of Z_{PDSL} was predicted. This value had an associated RMSE of 28m, which propagated through as an ssT_{PDSL} uncertainty (this was accounted for in MFB and TE estimates); 2.) Values of PP were estimated using the VGPM, the errors associated with this model were not accounted for in estimates of MFB and TE (quantifying these errors is currently a large area of study); 3.) Part of the acoustic response will have been produced from other sources: weakly scattering fluid-filled zooplankton (Stanton et al., 1996a), jellyfish (Kaartvedt et al., 2007; Klevjer et al., 2009) and squid (Brierley, 1992) along with stronger

acoustic targets such as physonects (Barham, 1966; Barham, 1963); 4.) mean target strength and weight values of mesopelagic fish were calculated from a pseudo-population, derived from the life-history traits of a single species. The relationships of age-to-length, age-to-abundance, length-to-weight and length-to-target strength, each have associated error values, however, since we are considering the entire population (in our global estimate), it was acceptable to use mean values of the population parameters.

One benefit of using acoustic data over net/trawl data is that you do not incur net avoidance errors, which are very hard to estimate and will likely vary with depth, species and geographical location (among other variables). The original estimate of MFB from ocean trawls of 1,000 Mt (Gjøsaeter & Kawaguchi, 1980; Lam & Pauly, 2005) incurred such uncertainties and is likely an underestimate.

Food availability and temperature are seemingly natural drivers of trophic flow and production, but a less obvious relationship is that between the depth of the primary DSL component (Z_{PDSL}) and wind-stress (5.3). This relationship refers to the depth of the most commonly observed DSL depth but the functional linear form will likely hold, for different regression coefficients, for the secondary DSL depth (when present); arguably, it is expected that a characteristic environment exists that promotes dual DSL component's over singular.

Wind stress increases mixing depth at the surface entraining nutrients from deeper colder waters, which in turn may increase PP. Any increase in production, is however, captured by the PP explanatory variable. Wind-stress also increases mixing in the surface layer, which could affect the locomotive energy expenditure of predator-prey interactions of organisms, especially those within the plankton. Increased wind stress deepens the primary DSL, meaning the relationship between Z_{PDSL} and wind stress is not linked to the penetration depth of light, which decreases with increased wind-driven mixing (Bone & Moore, 2008). An increase in Z_{PDSL} suggests that organisms themselves are bigger (Saunders et al., 2015) and so require lower light levels to hide from visual predation. Our model showed (see 6.3.1) that increased mixing significantly increases Z_{PDSL} such that the deepening overrides any shallowing effect related to a reduction in light penetration depth; this is not surprising since changes in light intensity in the open-ocean are principally affected by PP (Jerlov, 1976; Mobley, 1994).

A further consideration is that wind-stress is a proxy for some other variable, or variable combination. Recent studies have linked oxygen content to the depth of DSLs (Klevjer et al., 2016; Netburn & Koslow, 2015), observing a shallowing of DSLs where oxygen minimum zones

(OMZs) occur at depth. OMZs are found where non-utilized production increases microbial activity at the seabed or where mixing conditions are insufficient to enrich the water-column with oxygenated water regularly. A previous study linked the change in oxygen between the surface and mesopelagic, along with temperature change, PP and mixed-layer depth to migration depth of DSLs (Z_{DVM}: Bianchi et al., 2013).

An important driver of mid-water dissolved oxygen (DO) enrichment is increased surface wind-stress (Fig 7.1). Others drivers include increased PP, low salinity levels and cold temperatures (cold water can hold higher dissolved O_2 concentrations). Increased wind-stress therefore provides, in some cases, an oxygen pipeline for the mesopelagic community enabling the community to access deeper depths whilst, reduced light levels in deeper water reduce visual predation risk. I hypothesis that that organisms reside at the deepest depth at which they are not detectable by their predators – which is dependent upon their size – and has a suitable oxygen level for their survival. This hypothesis matches the results found here, that the deepest layers reside in cold, low salinity, intensely mixed waters (Southern Ocean) and the shallowest layers reside in warm, oxygen poor waters such as that is found in the Eastern Equatorial Pacific (Klevjer et al., 2016).

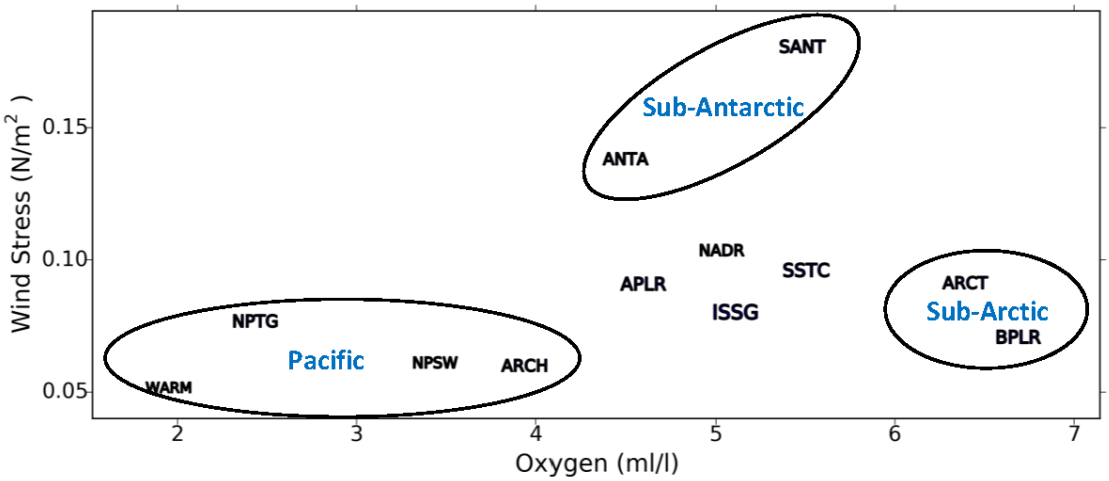

Figure 7.1: Wind stress (taken from SODA 2005 – 2008) versus dissolved oxygen content (averaged between 300 and 700m, taken from CTD profiles downloaded from the World Ocean Database: Boyer et al, 2013) for 12 ocean provinces (Longhurst, 1998). Short-names for provinces are indicated. Pacific, sub-Arctic and sub-Antarctic provinces circled.

Interestingly this doesn't seem to be the case in the Arctic (Fig 7.1: Arctic provinces BPLR and ARCT) where high values of DO and low values of wind stress are apparent. This result could be related to lower oxygen demands of the marine community or related to environment conditions such as ice cover, or decoupling of wind-driven mixing due to ice formation.

7.2.3 Mesopelagic biogeography

The mesopelagic biogeography defined here was based on the drivers of mesopelagic fish biomass (MFB) of which, the sub-surface temperature at the depth of the primary DSL (Z_{PDSL}), was estimated from predicted values of Z_{PDSL}. Unsurprisingly, the arrangement differed from Longhurst (1998) provinces which were based on PP regimes and oceanic boundaries.

The mesopelagic classes provide a partitioning of the pelagic ocean where water-column properties are such that they provide similar mesopelagic fish biomass values and are therefore useful when conducting large-scale studies that involve incomplete datasets (ship-borne as opposed to obtained from satellites). Since classes are produced by clustering pairs of PP and ssT_{PDSL} values over a gridded ocean (at some scale) into a predefined number of clusters, then a range of biogeography's exist, from the coarse, biome-like arrangement incorporating just 3 classes (Fig 6.6a) to a much more complex 33-class arrangement (Fig 6.6j) and beyond. The geographical partitioning that evolves with increasing class frequencies follows neatly the breakdown of the ocean into compartments that are associated with distinct features. At first, the polar biome is separated from regions of relatively high and low biomass. The regions of low productivity break down into the oligotrophic gyral systems of each ocean and the highly productive regions into oceanic fronts and currents systems. These areas in turn, breakdown into more specific features such as fragmented frontal zones and eddy fields that require greater temporal resolutions to resolve. The natural fractal-like structure of ocean communities exists because the environment is fractal and fluid in nature constantly evolving over time. Therefore, in reality, any derived biogeography of our ocean is dynamic and is in constant change. However, at the cost of losing some information, by taking averages over some temporal and spatial scale, a useful instance of that biogeography can be obtained and used to break down oceanic regions into spatially distinct classes, which ultimately aid in our analysis and interpretation of scientific observations.

Mesopelagic partitions are required due to the nature of the surface-to-mid-water disunity in temperature structure. As the ocean warms, it will become more stratified and currents may shift, meaning the disunity between the two environments will also change. This change will

impact trophic flow between the environments and have knock on effects to pelagic ecosystem resilience. The estimate of MFB made here (Ch 6) was likely an overestimate, yielding a large value of trophic efficiency (TE) between phytoplankton and mesopelagic fish of 15.6% per trophic level. Historically, literature suggests that this value should be around 10% which would reduce the biomass estimation from 9,000 Mt to 3,375 Mt, a value much closer to the estimate of MFB made by ocean trawls (Gjøsaeter & Kawaguchi, 1980; Lam & Pauly, 2005), but other studies have suggested that open-ocean TE may be closer to 20% (Calbet, 2000). The mesopelagic biogeography based on output from NEMO-MEDUSA-2.0, showed a shift in the arrangement and complexity of the mesopelagic provinces, harbouring a much more cohesive (larger provinces) Atlantic region, despite having 2 additional classes. Regional cohesion means that provinces may be less impacted by smaller scale effects, such as localised fishing effort or eddies. However, these regions have formed due to the change in the spatial arrangement of PP: regions of high productivity have continued to increase in their value of PP and low productivity regions have similarly, continued to decline, increasing the relative divide between the two (Fig 6.7e. & f.).

Province regional cohesion and increased PP values between high and low regions creates large areas north and south of the equator that are predicted to reduce substantially in mesopelagic fish production; which is true in all oceans except for in the N. Indian Ocean. In these areas, reductions in MFB, far outweigh the predicted increases in TE due to warming. This could mean that open-ocean ecosystems are more likely to be less resilient to fishing pressure and as of yet there are very few examples of open-ocean marine conservation (Game et al., 2009).

One recent example though, is the marine protected area (MPA) established in the Chagos archipelago (British Indian Ocean Territory) in the centre of the Indian Ocean. The archipelagic is believed to act as a sanctuary and breeding ground for commercially important/targeted migratory species such as Tuna (Koldewey et al., 2010) and a hotspot for pelagic fish production due to its shallow topography, geographical location and relatively high values of PP (Letessier et al., in press); although, recent modelling work has suggested otherwise (Dueri & Maury, 2012). By protecting Chagos/BIOT, the Indian Ocean ecosystem may be afforded some protection too; this MPA was established in 2010, ceasing all fishing activity, but it is still too early to tell what affect the MPA is having locally and also regionally. Conservations efforts,

in similar habitats to the Chagos archipelago, will need to be put into action in order to protect the other oceans, such as the Pacific, from mariculture demand.

The predicted change in mesopelagic community metrics found here were based on output from a single model, which predicted that levels of wind stress would decrease from the present to 2100 by almost 50%, but not all models predict such a change (Lee et al., 2013). From the regression model defined in Equation 5.15, the DSL deepens by 1m for every 0.0008 N/m^2 increase in wind stress, or 143m for a change of 0.1 N/m^2 which is experienced presently in the Southern Ocean across the zonal band at around -45° latitude (Fig 5.6b), changing significantly between the Indian Ocean and Pacific Ocean sectors. This implies that if wind stress values increase in the future then this could have large consequences on DSL depth and therefore, sub-surface temperature (affecting oxygen demands and therefore oxygen content) and energy expenditure of migrating organisms. Changes in global wind stress are controlled by air-density gradients and currents such as the Gulf Stream and continual improvements of our climate models, through projects such as the IPCC's Coupled Model Intercomparison Project (CMIP), will aid in our understanding of these physical processes, enabling us the ability to better predict how the underlying communities will change.

7.3 Future Directions

In order to gain a better understanding of the pelagic ecosystem, standard operating procedures need to be established for the collection and processing of mesopelagic data, specifically that pertaining to active acoustic data. To achieve this, international collaboration and data centralisation is required, alongside the development of metadata protocols (Ryan, 2011) and standardised and repeatable methodologies such as the sound scattering layer extraction method (SSLEM: Proud et al., 2015) developed during this project.

7.3.1 Data collaboration and SSLEM

International projects are already underway with the primary aims of collating and analysing acoustic data, including the Southern Ocean network of Acoustics (SONA) headed by the British Antarctic Survey (BAS) and also the Mesopelagic Southern Ocean Prey and Predators (MESOPP) project, which is a collaboration between France, Australia, Norway and the U.K funded by the European Commission. These projects will rely on data collected by institutes and those collated by data centres such as the British Oceanic Data Centre (BODC) and the Integrated Marine Observing System (IMOS). However, accessing data from these sources is not trivial and in some cases the published metadata does not correspond with the data actually stored. This is partly due to there being no standard protocol set in place for data collection parameters; although this is starting to change through initiatives setup via the working group of fisheries acoustics, science and technology (WGFAST) with respect to the protocols established by Ryan (2011) at IMOS. Research vessels are continually ploughing the ocean extending across vast regions of the pelagic environment, but too often is the case that there are not dedicated acousticians on board and echosounder data is not collected; an example of this are the Atlantic Meridional Transects (AMT), that have made 24 transects across the Atlantic since 1995 and from which, only 1 acoustic dataset exists held by the BODC, from which only 3 days' worth of data were recorded from a 30-day voyage. Echosounders, can simply be switched on and set to record and there is no reason why this should not be standard protocol on every research vessel; in fact, fisheries are starting to provide a better source of data (IMOS for example). One issue is the requirement of routine echosounder calibrations (Foote et al., 1983). These need to be carried out by personnel with expertise and training, requiring that at least one berth on any voyage should be reserved for an acoustician, although calibration can be accomplished by trained personnel visiting vessels when they are in suitable harbours or anchorages. Acoustic data, especially that which is collected by

multibeam or broadband echosounders, takes up a vast amount of storage space and requires extensive metadata to be provided. Therefore, it would be beneficial for a standalone centralised database to be established that provided collection and metadata protocols, similar to the Water Column Sonar Data Collection at the National Geophysical Data Center (NGDC).

7.3.2 Data analysis

A method of SSL identification and extraction (SSLEM: Ch 3) was developed during the project which provided a standardised analysis technique to characterise SSLs. The concept was to develop a method that was both objective, at least by frequency and scale, and automated. SSLEM was not fully automated in the sense that it required visual checks of the acoustic images in order to eliminate false bottoms (see 2.3). In order for more methods to be developed akin to SSLEM, better filtering and pre-processing tools need to be made available (freely), that are importantly, objective – most will fall over when given an image with multiple/complex sources of noise. SSLEM was designed to extract SSLs from water-column data and will naturally miss SSLs that are associated with the seabed, but could be applied to such images where the seabed is removed, using the bottom detection algorithm embedded in the ER60 (simrad) software for example. Since SSLEM is essentially an image processing technique, variants of the single beam method could easily be used to extract SSLs from ADCP, multi-beam and broadband acoustic data. By tracking SSLs using SSLEM, migration speeds can be estimated and these values could aid in migrant species identification, since swim speed is dependent upon size, species and swimbladder function. SSLEM also has applications in oceanography as SSLs can act as traces for physical changes in the water-column such as internal waves and eddies (Godø et al., 2012). Methods, similar to SSLEM in terms of its broad applicability and objectivity, need to be developed alongside advancements in technology (broadband acoustics) to allow us to take full advantage of the wealth of data that is now being collected and stored.

7.3.3 Mesopelagic fish distribution and Target Strength

The most widely distributed and diverse mesopelagic fish is that of the Myctophidae family, more commonly known as lanternfish, with 248 recorded species (www.fishbase.org) worldwide. The lanternfish is not currently a commercially ‘important’ species, probably because it’s small, often fatty and spends the daytime at depths of around 500 meters. After a

recent publication suggesting that there are ten times the previously expected quantity of mesopelagic fish in the seas (Irigoien et al., 2014), interests in the myctophid fishery are growing (St. John et al., 2016), particularly as a source of fishmeal for use in aquaculture. It seems slightly absurd to take the estimated value of MFB and use it in this context to potentially alter the direction of commercial fisheries. More knowledge is required of the variation in swimbladder growth across the 248 species (i.e intra-species Target Strength) and by extension, the proportion of scatter that can be attributed to the fish amongst different background communities. Recent studies have shown a high degree of variance in TS-length relationships of myctophids due to the variation in intra-species swimbladder morphology and growth (Scoulding et al., 2015; Yasuma et al., 2009). Resolving individual relationships by species, which are likely to vary seasonally and annually, for regions like the tropics where over 100 species have been recorded (www.fishbase.org), seems unrealistic at present. A better approach, following the one taken here and by Irigoien et al. (2014), is to consider populations as mixed assemblages, but instead of using mean or median TS values, derive TS distributions. Myctophids are perhaps arguably more ecologically important, than they are commercially as a food source for our ever-expanding population. They reside at the centre of the biomass pyramid, providing a food source for top predators and mediating, via DVM, the flux of carbon and nutrients in the water-column. As the ocean warms it is likely that more species will populate the Polar Regions, specifically the myctophid poor Arctic (www.fishbase.org), bolstering polar food-webs. Along with routine echosounder observations, DSLs should be fished and morphological and life-history traits of these fish should be ascertained and used to make better estimates of regional fish production and trophic efficiency using similar analysis methods as used in this study.

7.3.4 Future work

This project focused on delivering specific goals, i.e. determining biophysical drivers of DSL depth and biomass and deriving a mesopelagic biogeography, and so others avenues of study outside of these aims were not followed, but should be considered for future research. This study looked at long-term trends in ocean variables and DSL characteristics, but recent work has indicated that there is large seasonal variance in DSL depth in the Southern Ocean (Saunders et al., 2015), which supports the findings here (highly variable Polar regime: see Fig 4.5a). By concentrating on a single region, or by obtaining a larger dataset, a seasonal analysis could be conducted. It is likely that for some regions, seasonal variance will be low, but for

others, they will be significant (see Fig 4.7). Only daytime DSLs were analysed since they contain both the resident and migratory mass of the community. A further study could investigate night-time DSLs, answering such questions as: what proportion of the community is resident/migrant? How does the DSL change day-to-night and how does this change vary seasonally and annually? It is likely that the resident population will increase when there is an abundance of prey at the surface and predation risk is high, reducing the need for, and increasing the risk of, daily migrations; alternatively, fish may feed for shorter time periods at the surface. A further question concerns the occurrence of multiple DSLs in the mesopelagic and why certain arrangements exist (see Fig 4.5). Here we have looked primarily at the strongest and broadest of the DSLs when estimating depth, but further work could be instigated to separate out DSL formations into groups of organisms by fishing specific depth ranges. This would aid in determining if there is a single mechanism (i.e. light level) behind daytime depth stratification or if there are multiple mechanisms responsible (light level, fish density, oxygen concentration etc.) occurring simultaneously.

7.4 Concluding remarks

Political and social pressures, are forcing fisheries to become more sustainable, but regional variances in ecosystem properties such as production and trophic efficiency, coupled with regulations that are broadly invoked make the task a difficult one (Roberts et al., 2005). The human population, despite being faced with global food and water shortages, is predicted to continue to rapidly increase, prompting the need for new methods of food acquisition and security. With predictive models indicating decreases in wind-driven mixing (reducing nutrient recycling into the mixed layer) and primary production, it has generally been thought that ocean biomass pyramids will follow suit and that we should prepare accordingly, by bolstering anthropogenic fish production.

Here we provide evidence that this may not be the case and predict that fish production will increase into the future. This was accomplished by the collation of a global dataset of echosounder data, the development of a multi-platform, single frequency, sound scattering layer extraction method (SSLEM) and the derivation of biophysical drivers of deep scattering layers, leading to a description of a mesopelagic biogeography. We suggest that with careful management of fisheries and increased efforts in open-ocean marine conservation, informed by regional trophodynamics, we will be able to achieve global food security, even in light of a growing population and a rapidly changing climate and perhaps enable us to avoid a future of increasing reliance on farmed fish.

Bibliography

Ainslie, M. A., & McColm, J. G. (1998). A simplified formula for viscous and chemical absorption in seawater. *Journal of the Acoustical Society of America*, 103, 1671–1672.

Anderson, C. I. H., Brierley, A. S., & Armstrong, F. (2005). Spatio-temporal variability in the distribution of epi- and meso-pelagic acoustic backscatter in the Irminger Sea, North Atlantic, with implications for predation on Calanus finmarchicus. *Marine Biology*, *146*(6), 1177–1188.

Alexander, R. (1966). Physical aspects of swimbladder function. *Biological Reviews*, *41*(1), 141-176.

Alvarino, A. (1965). Chaetonaths. *Oceanography* and *Marine Biology*: An *Annual* Review, 3, 115-194.

Anderson, C. I. H., Horne, J. K., & Boyle, J. (2007). Classifying multi-frequency fisheries acoustic data using a robust probabilistic classification technique. *The Journal of the Acoustical Society of America*, *121*(6), EL230–7.

Andreeva, I. B. (1964). Scattering of sound by air bladders of fish in deep sound-scattering ocean layers. *Sov. Phys. Acoust*, *10*(1), 17-20.

Andreeva, I. B., Galybin, N. N., & Tarasov, L. L. (2000). Vertical structure of the acoustic characteristics of deep scattering layers in the ocean. *Acoustical Physics*, *46*(5), 505–510.

Ariza, A., Landeira, J. M., Escánez, A., Wienerroither, R., de Soto, N. A., Røstad, A., Kaartvedt, S. and Hernández-León, S., (2016). Vertical distribution, composition and migratory patterns of acoustic scattering layers in the Canary Islands. *Journal of Marine Systems*.

Auster, P. J., Griswold, C. A., Youngbluth, M. J., & Bailey, T. G. (1992). Aggregations of myctophid fishes with other pelagic fauna. *Environmental Biology of Fishes*, *35*(2), 133–139.

Backus, R., & Barnes, H. (1958). Television-echo sounder observations of midwater sound scatteres. *Deep Sea Research (1953)*, 116–119.

Backus, R. H. (1986). Biogeographic boundaries in the open ocean. In – Pelagic Biogeography, *UNESCO Technical Paper* in *Marine Science*, 49, 9 – 13.

Baird, R. C., Wilson, D. F., Beckett, R. C., & Hopkins, T. L. (1974). Diaphius-Taaningi Norman, principal component of a shallow sound-scattering layer in Cariaco trench, Venezuela. *Journal of Marine Research*, *32*(2), 301-312.

Balls, R. (1948). Herring fishing with the echometer. *Journal Du Conseil*, (ii).

Barange, M., Hampton, I., Pillar, S. C., & Soule, M. A. (1994). Determination of composition and vertical structure of fish communities using in situ measurements of acoustic target strength. *Canadian Journal of Fisheries and Aquatic Sciences*, 51, 99–109.

Barham, E. (1963). Siphonophores and the Deep Scattering Layer. *Science*, *140*(3568), 826–828.

Barham, E. G. (1966). Deep scattering layer migration and composition: observations from a diving saucer. *Science (New York, N.Y.)*, *151*(3716), 1399–1403.

Bary, B. (1967). Diel vertical migrations of underwater scattering, mostly in Saanich inlet, British Columbia. *Deep Sea Research and Oceanographic Abstracts*, *14*, 35–50.

Behrenfeld, M. J., Boss, E., Siegel, D. A., & Shea, D. M. (2005). Carbon-based ocean productivity and phytoplankton physiology from space. *Global Biogeochemical Cycles*, *19*(1), 1–14.

Behrenfeld, M. J., & Falkowski, P. G. (1997). Photosynthetic rates derived from satellite-based chlorophyll concentration. *Limnology and Oceanography*, *42*(1), 1–20.

Beklemishev, K. V. (1964). Concerning the phytogeographic division of the Antarctic pelagic region. *Information Bulletin*, *2*, 272.

Beklemishev, K. V. (1976). *Ekologiya i biogeografiya pelagiali (Ecology and Biogeography of the Open Ocean)* (No. NOO-T-25). Naval Oceanographic Office Washington DC.

Benfield, M. C., Lavery, A. C., Wiebe, P. H., Greene, C. H., Stanton, T. K., & Copley, N. J. (2003). Distributions of physonect siphonulae in the Gulf of Maine and their potential as important sources of acoustic scattering. *Canadian Journal of Fisheries and Aquatic Sciences*, *60*, 759–772.

Benoit, D., Simard, Y., & Fortier, L. (2008). Hydroacoustic detection of large winter aggregations of Arctic cod (Boreogadus saida) at depth in ice-covered Franklin Bay (Beaufort Sea). *Journal of Geophysical Research*, *113*(C6), C06S90.

Berge, J., Cottier, F., Varpe, Ø., Renaud, P. E., Falk-Petersen, S., Kwasniewski, S., Griffiths, C., Søreide, J.E., Johnsen, G., Aubert, A., Bjaerke, O., Hovinen, J., Jung-Madsen, S., Tveit, M. & Majaneva, S. (2014). Arctic complexity: a case study on diel vertical migration of zooplankton. *Journal of plankton research*, 36(5), 1279-1297.

Bertignac, M., Lehodey, P., & Hampton, J. (1998). A spatial population dynamics simulation model of tropical tunas using a habitat index based on environmental parameters. *Fisheries Oceanography*, 7(3-4), 326-334.

Bianchi, D., Galbraith, E. D., Carozza, D. A., Mislan, K. A. S., & Stock, C. A. (2013). Intensification of open-ocean oxygen depletion by vertically migrating animals. *Nature Geoscience*, *6*(7), 545–548.

Bierregaard, R. O., Lovejoy, T. E., Kapos, V., dos Santos, A. A., & Hutchings, R. W. (1992). The biological dynamics of tropical rainforest fragments. *BioScience*, 42, 859–866.

Boden, B. P. (1962). Plankton and sonic scattering. *Cons. Perm. int. Explor. Mer, Rapp. Process-Ver. Reu*, *153*, 171-77.

Boden, B. P., & Kampa, E. M. (1967). The influence of natural light on the vertical migrations of an animal community in the sea. In Symposia of the Zoological Society of London, 19, 15-26.

Boersch-Supan, P., Boehme, L., Read, J., Rogers, A., & Brierley, A. (2012). Elephant seal foraging dives track prey distribution, not temperature: Comment on McIntyre et al. (2011). *Marine Ecology Progress Series*, *461*(4), 293–298.

Bone, Q., & Moore, R. (2008). *Biology of fishes*. Taylor & Francis.

Bost, C. A., Cotté, C., Terray, P., Barbraud, C., Bon, C., Delord, K., Gimenez, O., Handrich, Y., Naito, Y., Guinet, C. and Weimerskirch, H. (2015). Large-scale climatic anomalies affect marine predator foraging behaviour and demography. *Nature Communications*, *6*, 8220.

Boyce, D. G., Lewis, M. R., & Worm, B. (2010). Global phytoplankton decline over the past century. *Nature*, *466*(7306), 591–596.

Boyce, D. G., Lewis, M., & Worm, B. (2012). Integrating global chlorophyll data from 1890 to 2010. *Limnology and Oceanography: Methods*, *10*(11), 840–852.

Boyer, T. P., J. I. Antonov, O. K. Baranova, C. Coleman, H. E. Garcia, A. Grodsky, D. R. Johnson, R. A. Locarnini, A. V. Mishonov, T. D. O'Brien, C. R. Paver, J. R. Reagan, D. Seidov, I. V. Smolyar, & M. M. Zweng, (2013). World Ocean Database 2013, NOAA Atlas NESDIS 72, S. Levitus, Ed., A. Mishonov, Technical Ed.; Silver Spring, MD, 209.

Brander, K. M. (2007). Global fish production and climate change. *Proceedings of the National Academy of Sciences of the United States of America*, *104*(50), 19709–19714.

Brierley, A. S. (1992). *Aspects of genetic diversity and population structure of squid*. Diss. University College of North Wales.

Brierley, A. S. (2014). Diel vertical migration. *Current Biology*, *24*(22), R1074–R1076.

Brierley, A., Watkins, J., & Murray, A. (1997). Interannual variability in krill abundance at South Georgia. *Marine Ecology Progress Series*, *150*, 87–98.

Briggs, J. (1974). Marine Zoogeograpghy. McGraw-Hill, New York.

Brinton, E. (1962). The distribution of Pacific euphausiids. *Scripps Institution of Oceanography*. 8, 51-270.

Burd, A., & Lee, A. (1951). The sonic scattering layer in the sea. *Nature*, *167*, 624–626.

Butler, J. L., & Pearcy, W. G. (1972). Swimbladder Morphology and Specific Gravity of Myctophids off Oregon. *Journal of the Fisheries Research Board of Canada*, *29*(8), 1145–1150.

Cade, D. E. & Benoit-Bird, K. J. (2014). An automatic and quantitative approach to the detection and tracking of acoustic scattering layers (supplemental code). Oregon State University Libraries. Software.

Calbet, A. (2000). Mesozooplankton grazing effect on primary production : A global comparative analysis in marine ecosystems. *Fisheries Science*, *46*(7), 1824–1830.

Carey, F. G., & Robinson, B. H. (1981). Daily patterns in the activities of swordfish, Xiphias gladius, observed by acoustic telemetry. *Fishery bulletin-United States, National Marine Fisheries Service*.

Carton, J. A., Chepurin, G., Cao, X., & Giese, B. (2000). A simple ocean data assimilation analysis of the global upper ocean 1950-95. Part I: Methodology. *Journal of Physical Oceanography*, *30*(2), 294-309.

Change, C. (2001). The scientific basis, intergovernmental panel on climate change, *by JT Houghton, Y. Ding, DJ Griggs, et al*.

Chapman, R., Bluy, O., Adlington, R., & Robison, A. (1974). Deep scattering layer spectra in the Atlantic and Pacific Oceans and adjacent seas. *The Journal of the Acoustical Society of America*, *56*(6), 1722–1734.

Chapman, R., & Marshall, J. (1966). Reverberation from Deep Scattering Layers in the Western North Atlantic*. *The Journal of the Acoustical Society of America*, *40*(2), 405–411.

Clarke, G. L., & Backus, R. H. (1964). Interrelations between the vertical migration of deep scattering layers, bioluminescence, and changes in daylight in the sea. Bulletin de l'Institut océanographique de Monaco, *64*(1318), 1-36.

Coetzee, J. (2000). Use of a shoal analysis and patch estimation system (SHAPES) to characterise sardine schools. *Aquatic Living Resources*, *13*(1), 1–10.

Conte, M., Bishop, J., & Backus, R. (1986). Nonmigratory, 12-kHz, deep scattering layers of Sargasso Sea origin in warm-core rings. *Deep Sea Research Part I: Oceanographic Research Papers*, *33*(11/12), 1869–1884.

Cox, M. J., Watkins, J. L., Reid, K., & Brierley, A. S. (2011). Spatial and temporal variability in the structure of aggregations of Antarctic krill (Euphausia superba) around South Georgia, 1997-1999. *ICES Journal of Marine Science*, *68*(3), 489–498.

Croxall, J. P., Everson, I., Kooyman, G. L., Ricketts, C., & Davis, R. W. (1985). Fur seal diving behaviour in relation to vertical distribution of krill. *The Journal of Animal Ecology*, 1-8.

Cushing, D. (1951). The vertical migration of planktonic crustacea. *Biological Reviews*, (1828), 158–192.

Cushing, D., & Richardson, I. (1956). A Record of Plankton on the Echo-sounder. *Journal of the Marine Biology Association of the UK*, *35*, 231–240.

Cury, P., Shannon, L., & Shin, Y. J. (2003). The functioning of marine ecosystems: a fisheries perspective. *Responsible fisheries in the marine ecosystem*, 103-123.

Cushing, D. H. (1955). Some experiments on the vertical migration of zooplankton. *The Journal of Animal Ecology*, 137-166.

Cushing, D. H., & Richardson, I. D. (1955). *Echo sounding experiments on fish*. HM Stationery Office.

Dagorn, L., Bach, P., & Josse, E. (2000). Movement patterns of large bigeye tuna (Thunnus obesus) in the open ocean, determined using ultrasonic telemetry. *Marine Biology*, *136*(2), 361–371.

Davies, I. (1977). Acoustic volume reverberation in the eastern tropical Pacific Ocean and its relationship to oceanographic features. *Deep Sea Research Part I: Oceanographic Research Papers*, *24*, 1049–1053.

De Busserolles, F., Fitzpatrick, J. L., Paxton, J. R., Marshall, N. J., & Collin, S. P. (2013). Eye-Size Variability in Deep-Sea Lanternfishes (Myctophidae): An Ecological and Phylogenetic Study. *PLoS ONE*, *8*(3), e58519.

De Robertis, A., & Higginbottom, I. (2007). A post-processing technique to estimate the signal-to-noise ratio and remove echosounder background noise. *ICES Journal of Marine Science: Journal du Conseil*, *64*(6), 1282-1291.

Demer, D. A, & Renfree, J. S. (2008). Variations in echosounder – transducer performance with water temperature. *ICES Journal of Marine Science*, *65*, 1021–1035.

Dickson, R. (1972). On the relationship between ocean transparency and the depth of sonic scattering layers in the North Atlantic. *Journal Du Conseil*, *34*(3), 416–422.

Dietz, R. S. (1948). Deep scattering layer in the Pacific and Antarctic Oceans. Journal of *Marine* Research, *7*(3), 430-442.

Doney, S. C., Fabry, V. J., Feely, R. A., & Kleypas, J. A. (2009). Ocean Acidification: The Other CO 2Problem. *Annual Review of Marine Science*, *1*(1), 169–192.

Doray, M., Josse, E., Gervain, P., Reynal, L., & Chantrel, J. (2006). Acoustic characterisation of pelagic fish aggregations around moored fish aggregating devices in Martinique (Lesser Antilles). *Fisheries Research*, *82*(1-3), 162–175.

Doray, M., Josse, E., Gervain, P., Reynal, L., & Chantrel, J. (2007). Joint use of echosounding, fishing and video techniques to assess the structure of fish aggregations around moored Fish Aggregating Devices in Martinique (Lesser Antilles). *Aquatic Living Resources*, *20*(4), 357–366.

Dueri, S., & Maury, O. (2012). Modelling the effect of marine protected areas on the population of skipjack tuna in the Indian Ocean. *Aquatic Living Resources*, *26*(02), 171-178.

Duvall, G. E., & Christensen, R. J. (1946). Stratification of sound scatterers in the ocean. *The Journal of the Acoustical Society of America*, *18*(1), 254-254.

Edwards, M., Beaugrand, G., Hays, G. C., Koslow, J. A., & Richardson, A. J. (2010). Multi-decadal oceanic ecological datasets and their application in marine policy and management. *Trends in Ecology & Evolution*, *25*(10), 602–610.

Eyring, C., Christensen, R., & Raitt, R. (1948). Reverberation in the Sea. *The Journal of the Acoustical Society of America*, *20*(4), 1948.

Fennell, S., & Rose, G. (2015). Oceanographic influences on Deep Scattering Layers across the North Atlantic. *Deep Sea Research Part I: Oceanographic Research Papers*, *105*, 132-141.

Fiksen, Ø., & Carlotti, F. (1998). A model of optimal life history and diel vertical migration in Calanus finmarchicus. *Sarsia*, *83*(2), 129–147.

Fischer, J., & Visbeck, M. (1993). Seasonal variation of the daily zooplankton migration in the Greenland Sea. *Deep Sea Research Part I: Oceanographic Research Papers*, *40*(8), 1547–1557.

Foote, K. G. (1983a). Linearity of fisheries acoustics, with addition theorems. *The Journal of the Acoustical Society of America*, *73*(6), 1932–1940.

Foote, K. G. (1983b). Maintaining precision calibrations with optimal copper spheres. *The Journal of the Acoustical Society of America*, *73*(3), 1054.

Foote, K. G. (1987). Fish target strengths for use in echo integrator surveys. *The Journal of the Acoustical Society of America*, *82*(September), 981–987.

Foote, K. G., Knudsen, H. P., & Vestnes, G. (1983). Standard calibration of echo sounders and integrators with optimal copper spheres. *Fiskeridirektoratet, Havforskningsinstituttet*, *17*, 335–346.

Francois, R. E. & Garrison, G. R. (1982). Sound absorption based on ocean measurements. Part I: Pure Water and magnesium sulfate contributions. *The Journal of the Acoustical Society of America*, 72(3), 896–907.

Fulton, E., Smith, A, & Punt, A. (2005). Which ecological indicators can robustly detect effects of fishing? *ICES Journal of Marine Science*, *62*(3), 540–551.

Gajate, J., Ponce, R., Peña, M., Iglesias, M., Fernandes, P., & Alvarez, F. (2004). The SIMFAMI database: a library of ground truthed acoustic survey data. In *Annual Science ICES Conference, ICES ASC*.

Game, E. T., Grantham, H. S., Hobday, A. J., Pressey, R. L., Lombard, A. T., Beckley, L. E., Gjerde, K., Bustamante, R., Possingham, H. P. & Richardson, A. J. (2009). Pelagic protected areas: the missing dimension in ocean conservation. *Trends in Ecology and Evolution*, *24*(7), 360–369.

Gartner, J. V. (1991). Life histories of three species of lanternfishes (Pisces: Myctophidae) from the eastern Gulf of Mexico - I. Morphological and microstructural analysis of sagittal otoliths. *Marine Biology*, *111*(1), 11–20.

Gascuel, D. (2005). The trophic-level based model: A theoretical approach of fishing effects on marine ecosystems. *Ecological Modelling*, *189*, 315–332.

Gascuel, D., Morissette, L., Palomares, M. L. D., & Christensen, V. (2008). Trophic flow kinetics in marine ecosystems: Toward a theoretical approach to ecosystem functioning. *Ecological Modelling*, *217*(1-2), 33–47.

Genin, A., Haury, L., & Greenblatt, P. (1988). Interactions of migrating zooplankton with shallow topography: predation by rockfishes and intensification of patchiness. *Deep Sea Research Part A. Oceanographic Research Papers*, *35*(2), 151-175.

Gjøsaeter, J., & Kawaguchi, K. (1980). *A review of the world resources of mesopelagic fish* (No. 193-199). Food & Agriculture Org.

Giske, J., Aksnes, D., Baliño, B., Kaartvedt, S., & Lie, U. (1990). Vertical Distribution and trophic interactions of zooplankton and fish in Masfjorden, Norway. *Sarsia*, 65–81.

Godø, O. R., Patel, R., & Pedersen, G. (2009). Diel migration and swimbladder resonance of small fish : some implications for analyses of multifrequency echo data. *ICES Journal of Marine Science*, *66*, 1143–1148.

Godø, O. R., Samuelsen, A., Macaulay, G. J., Patel, R., Hjøllo, S. S., Horne, J., Kaartvedt, S. and Johannessen, J. A., (2012). Mesoscale eddies are oases for higher trophic marine life. *PloS One*, *7*(1), e30161.

Greenlaw, C. (1979). Acoustical estimation of zooplankton populations. *Limnology and Oceanography*, *24*(2), 226–242.

Greenlaw, C. F., & Pearcy, W. G. (1985). Acoustical patchiness of mesopelagic micronekton. *Journal of Marine Research*, *43*(1), 163–178.

Griffiths, S. P., Young, J. W., Lansdell, M. J., Campbell, R. A., Hampton, J., Hoyle, S. D., Langley, A., Bromhead, D. and Hinton, M. G., (2010). Ecological effects of longline fishing and climate change on the pelagic ecosystem off eastern Australia. *Reviews in Fish Biology and Fisheries*, *20*(2), 239–272.

Haigh, K. K. R. (1970). Geographic, seasonal, and annual patterns of midwater scatterers between latitudes 10 and 68 degrees north in the Atlantic. In *Proceedings of an International Symposium on Biological Sound Scattering in the Ocean. Department of the Navy, Washington, DC*, 278-290.

Hardy, A. C. (1936). Plankton ecology and the hypothesis of animal exclusion. In *Proceedings of the Linnean Society of London*, 148(2), 64-70.

Handegard, N. O., Buisson, L. D., Brehmer, P., Chalmers, S. J., Robertis, A., Huse, G., Kloser, R., Macaulay, G., Maury, O., Ressler, P. H., Stenseth, N. C. & Godø, O. R. (2013). Towards an acoustic-based coupled observation and modelling system for monitoring and predicting ecosystem dynamics of the open ocean. *Fish and Fisheries*, *14*(4), 605-615.

Hayashi, A., Watanabe, H., Ishida, M., & Kawaguchi, K. (2001). Growth of Myctophum asperum (Pisces: Myctophidae) in the Kuroshio and transitional waters. *Fisheries Science*, *67*(5), 983–984.

Hays, G. C. (1995). Zooplankton avoidance activity. *Nature*, *376*(6542), 650-650.

Hays, G. C. (2003). A review of the adaptive significance and ecosystem consequences of zooplankton diel vertical migrations. *Hydrobiologia*, *503*(1-3), 163–170.

Hays, L. M., Crowe, J. H., Wolkers, W., & Rudenko, S. (2001). Factors affecting leakage of trapped solutes from phospholipid vesicles during thermotropic phase transitions. *Cryobiology*, *42*(2), 88–102.

Heath, M. R., Astthorsson, O. S., Dunn, J., Ellertsen, B., Gaard, E., Gislason, A., Gurney, W. S. C., Hind, A. T., Irigoien, X., Melle, W., et al. (2000). Comparative analysis of Calanus finmarchicus demography at locations around the Northeast Atlantic. *ICES Journal of Marine Science: Journal du Conseil*, *57*(6), 1562-1580.

Herdman, H. (1953). The deep scattering layer in the sea: association with density layering. *Nature*, *172*(4372), 275–276.

Hersey, J. B, & Backus, R. H. (1954). New evidence that migrating gas bubbles, probably the swimbladders of fish, are largely responsible for scattering layers on the continental rise south of New England. *Deep Sea Research (1953)*, 190–191.

Hersey, J. B., & Backus, R. H. (1962). Sound scattering by marine organisms. *The sea*, *1*, 498-539.

Hersey, J. B, Backus, R. H., & Hellwig, J. (1962). Sound-scattering spectra of deep scattering layers in the western North Atlantic Ocean. *Deep Sea Research Part I: Oceanographic Research Papers*, *8*, 196–210.

Hersey, J. B., Johnson, H. R., & Davis, L. C. (1952). Recent findings about the deep scattering layer. *Journal of Marine Research*, *11*(1), 1-9.

Hersey, J. B., & Moore, H. B. (1948). Progress report on scattering layer observations in the Atlantic Ocean. *Eos, Transactions American Geophysical Union*, *29*(3), 341-354.

Hewitt, R.P., Watkins, J.L., Naganobu, M., Tshernyshkov, P., Brierley, A.S., Demer, D.A., Kasatkina, S., Takao, Y., Goss, C., Malyshko, A., et al. (2002). Setting a precautionary catch limit for Antarctic krill Setting a Precautionary Catch Limit for Antarctic Krill. *Oceanography*, *15*(3), 26–33.

Hewitt, R. P., Watkins, J., Naganobu, M., Sushin, V., Brierley, A. S., Demer, D., Kasatkina, S., Takao, Y., Goss, C., Malyshko, A., et al. (2004). Biomass of Antarctic krill in the Scotia Sea in January/February 2000 and its use in revising an estimate of precautionary yield. *Deep Sea Research Part II: Topical Studies in Oceanography*, *51*(12-13), 1215–1236.

Holliday, D. V, Donaghay, P. L., Greenlaw, C. F., Mcgehee, D. E., Mcmanus, M. M., Sullivan, J. M., & Miksis, J. L. (2003). Advances in defining fine- and micro-scale pattern in marine plankton. *Aquatic Living Resources*, *16*, 131–136.

Holliday, D. V., McCoy, J. J., Beran, M. J., Bratkovich, A. W., & Reader, W. T. (1987). *High Frequency Forward Acoustic Volume Scattering and Its Relation to Oceanic Fine Structure*. Tracor Applied Sciences Inc. San Diego CA.

Holton, A. (1969). Feeding Behavior of a Vertically Migrating Lanternfish. *Pacific Science*, *23*, 325–331.

ICES. (2015). Second Interim Report of the Working Group on Fisheries Acoustics, Science and Technology (WGFAST), 29 May 2015, Nantes, France. ICES CM 2015/SSGIEOM: 21, 16.

ICES WGTC: CRR 238 (2000). Editor: Dave Reid, Report on Echo Trace Classification.

IMOS (2013). IMOS BASOOP sub-facility, imos.org.au [accessed 1st June 2013].

IPCC (2013). Climate Change 2013: The Physical Science Basis. Contribution of Working Group I to the Fifth Assessment Report of the Intergovernmental Panel on Climate Change, Cambridge University Press, Cambridge, United Kingdom and New York, NY, USA, 1535.

Irigoien, X., Klevjer, T. A., Røstad, A., Martinez, U., Boyra, G., Acuña, J. L., Bode, A., Echevarria, F., Gonzalez-Gordillo, J. I., Hernandez-Leon, S. & Agusti, S. (2014). Large mesopelagic fishes biomass and trophic efficiency in the open ocean. *Nature Communications*, *5*.

Isaacs, J., & Schwartzlose, R. (1965). Migrant Sound Scatterers : Interaction with the Sea Floor. *Science (New York, NY)*, *150*(3705), 1810–1813.

Isaacs, J., Tont, S., & Wick, G. (1974). Deep Scattering Layers: vertical migration as a tactic for finding food. *Deep Sea Research and Oceanographic Abstracts*, *21*, 651–656.

Jarvis, T., Kelly, N., Kawaguchi, S., van Wijk, E., & Nicol, S. (2010). Acoustic characterisation of the broad-scale distribution and abundance of Antarctic krill (Euphausia superba) off East Antarctica (30-80°E) in January-March 2006. *Deep Sea Research Part II: Topical Studies in Oceanography*, *57*(9-10), 916–933.

Jerlov, N. G. (1976). *Marine optics* (Vol. 14). Elsevier.

Johnsen, S. (2014). Hide and seek in the open sea: pelagic camouflage and visual countermeasures. *Annual review of marine science*, *6*, 369-392.

Johnson, M. W. (1948). Sound as a tool in marine ecology, from data on biological noises and the deep scattering layer. Journal of *Marine* Research, *7*(3), 443-458.

Johnson, H., Backus, R., Hersey, J., & Owen, D. (1956). Suspended echo-sounder and camera studies of midwater sound scatterers. *Deep Sea Research (1953)*, *8*(1955), 266–272.

Johnson, R. K. (1976). Volume scattering regions in the eastern tropical Pacific. *Deep Sea Research and Oceanographic Abstracts*, *23*, 769–772.

Johnson, R. K. (1977). Acoustic estimation of scattering-layer composition. *The Journal of the Acoustical Society of America*, *61*(6), 1636.

Johnson, H. R., Backus, R. H., Hersey, J. B., & Owen, D. M. (1956). Suspended echo-sounder and camera studies of midwater sound scatterers. *Deep Sea Research (1953)*, *3*(4), 266IN7269-268IN13272.

Jones, F. H., & Marshall, N. B. (1953). The structure and functions of the theleostean swembladder. *Biological Reviews*, *28*(1), 16-82.

Kaartvedt, S., Klevjer, T. A., Torgersen, T., Sørnes, T. A., & Røstad, A. (2007). Diel vertical migration of individual jellyfish (Periphylla periphylla). *Limnology and Oceanography*, *52*(3), 975–983.

Kanwisher, J., & Volkmann, G. (1955). A Scattering Layer Observation. *SCIENCE*, *121*(3134), 108–109.

Kawaguchi, S., Nicol, S., Virtue, P., Davenport, S. R., Casper, R., Swadling, K. M., & Hosie, G. W. (2010). Krill demography and large-scale distribution in the Western Indian Ocean sector of the Southern Ocean (CCAMLR Division 58.4.2) in Austral summer of 2006. *Deep Sea Research Part II: Topical Studies in Oceanography*, *57*(9-10), 934–947.

Key, R. M., Kozyr, A., Sabine, C. L., Lee, K., Wanninkhof, R., Bullister, J. L., Feely, R. A., Millero, F. J., Mordy, C. and Peng, T. H. (2004). A global ocean carbon climatology: Results from Global Data Analysis Project (GLODAP). *Global Biogeochemical Cycles*, *18*(4), 1–23.

Kinzer, J. (1969). On the quantitative distribution of zooplankton in deep scattering layers. *Deep Sea Research and Oceanographic Abstracts*, *16*, 117–125.

Klevjer, T. A., Irigoien, X., Røstad, A., Fraile-Nuez, E., Benítez-Barrios, V. M., & Kaartvedt, S. (2016). Large scale patterns in vertical distribution and behaviour of mesopelagic scattering layers. *Scientific Reports*, *6*, 19873.

Klevjer, T. A., Kaartvedt, S., & Båmstedt, U. (2009). In situ behaviour and acoustic properties of the deep living jellyfish periphylla periphylla. *Journal of Plankton Research*, *31*(8), 793–803. 6

Klevjer, T. A., Torres, D. J., & Kaartvedt, S. (2012). Distribution and diel vertical movements of mesopelagic scattering layers in the Red Sea. *Marine Biology*, *159*(8), 1833–1841.

Kloser, R. J., Ryan, T. E., Young, J. W., & Lewis, M. E. (2009). Acoustic observations of micronekton fish on the scale of an ocean basin : potential and challenges. *ICES Journal of Marine Science*, *66*, 998–1006.

Kloser, R. J., Ryan, T., Sakov, P., Williams, A., & Koslow, J. A. (2002). Species identification in deep water using multiple acoustic frequencies. *Canadian Journal of Fisheries and Aquatic Sciences*, *59*(6), 1065–1077.

Kloser, R. J., Williams, A, & Koslow, J. A. (1997). Problems with acoustic target strength measurements of a deepwater fish , orange roughy (Hoplostethus atlanticus , Collett). *ICES Journal of Marine Science*, *54*(1989), 60–71.

Knox, G. A. (2006). *Biology of the southern ocean*. CRC Press.

Koldewey, H. J., Curnick, D., Harding, S., Harrison, L. R., & Gollock, M. (2010). Potential benefits to fisheries and biodiversity of the Chagos Archipelago/British Indian Ocean Territory as a no-take marine reserve. *Marine Pollution Bulletin*, *60*(11), 1906–1915.

Koppelmann, R., & Frost, J. (2008). The ecological role of zooplankton in the twilight and dark zones of the ocean. *Biological Oceanography Research Trends. Nova Science Publishers, Inc., New York*, 67-130.

Korneliussen, R. J., Ona, E., Eliassen, I., Heggelund, Y., Patel, R., Godø, O. R., Giertsen, C., Patel, D., Nornes, E., Bekkvik, T., Knudsen, H.P. & Lien, G. (2006). THE LARGE SCALE SURVEY SYSTEM - LSSS. *Proceedings of the 29th Scandinavian Symposium on Physical Acoustics*, (February).

Lam, V., & Pauly, D. (2005). Mapping the global biomass of mesopelagic fishes. *Sea Around Us Project Newsletter*, *30*(4).

Lawson, G. (2001). Species identification of pelagic fish schools on the South African continental shelf using acoustic descriptors and ancillary information. *ICES Journal of Marine Science*, *58*(1), 275–287.

Lee, T., Waliser, D. E., Li, J. L. F., Landerer, F. W., & Gierach, M. M. (2013). Evaluation of CMIP3 and CMIP5 wind stress climatology using satellite measurements and atmospheric reanalysis products. *Journal of Climate*, *26*(16), 5810-5826.

Lehodey, P. (2004). A Spatial Ecosystem And Populations Dynamics Model (SEAPODYM) for tuna and associated oceanic top-predator species: Part II – Tuna populations and fisheries. *17th Meeting of the Standing Committee on Tuna and Billfish, Majuro, Marshall Islands*, (August), 1–36.

Lehodey, P., Andre, J. M., Bertignac, M., Hampton, J., Stoens, A., Menkès, C., Memery, L. & Grima, N. (1998). Predicting skipjack tuna forage distributions in the equatorial Pacific using a coupled dynamical bio-geochemical model. *Fisheries Oceanography*, 7(3-4), 317-325.

Lehodey, P., Chai, F., & Hampton, J. (2003). Modelling climate-related variability of tuna populations from a coupled ocean–biogeochemical-populations dynamics model. *Fisheries Oceanography*, 12(4-5), 483-494.

Lehodey, P., Murtugudde, R. & Senina, I. (2010). Bridging the gap from ocean models to population dynamics of large marine predators: a model of mid- trophic functional groups. *Progress in Oceanography*, 84, 69–84.

Lehodey, P., Senina, I., & Murtugudde, R. (2008). A spatial ecosystem and populations dynamics model (SEAPODYM) – Modeling of tuna and tuna-like populations. *Progress in Oceanography*, *78*(4), 304–318.

Letessier, T. B.**,** Cox, M. J., Meeuwig, J. J., Boersch-Supan, P. H., & Brierley, A. S. In press. Enhanced pelagic biomass around coral atolls. *Marine Ecology Progress Series*.

Longhurst, A. (1998). Ecological Geography of the Sea, Academic Press, San Diego.

Longhurst, A., Sathyendranath, S., Platt, T., & Caverhill, C. (1995). an Estimate of Global Primary Production in the Ocean From Satellite Radiometer Data. *Journal of Plankton Research*, *17*(6), 1245–1271.

Love, R. H., Fisher, R. A., Wilson, M. A., & Nero, R. W. (2004). Unusual swimbladder behavior of fish in the Cariaco Trench. *Deep Sea Research Part I: Oceanographic Research Papers*, *51*(1), 1–16.

Lyman, J. (1948). The sea's phantom bottom. *The Scientific Monthly*, *66*(1), 87–88.

Macaulay, M. C., English, T. S., & Mathisen, O. A. (1984). Acoustic characterization of swarms of Antarctic krill (Euphausia superba) from Elephant Island and Bransfield Strait. *Journal of Crustacean Biology*, *4*(5), 16-44.

Mackas, D., & Bohrer, R. (1976). Fluorescence analysis of zooplankton gut contents and an investigation of diel feeding patterns. *Journal of experimental marine biology and ecology*, *25*(1), 77-85.

Maclennan, D. (2002). A consistent approach to definitions and symbols in fisheries acoustics. *ICES Journal of Marine Science*, *59*(2), 365–369.

MacLennan, D., & Simmonds, E. (2005). *Fisheries acoustics*. Blackwell Science Ltd.

Malhi, Y., Phillips, O. L., Lloyd, J., Baker, T., Wright, J., Almeida, S., Arroyo, L., Frederiksen, T., Grace, J., Higuchi, N., et al. (2002). An international network to monitor the structure, composition and dynamics of Amazonian forests (RAINFOR). *Journal of Vegetation Science,* 13(3), 439-450.

Magnússon, J. (1996). The deep scattering layers in the Irminger Sea. *Journal of Fish Biology*, *49*, 182–191.

Margalef, R. (1997). Our Biosphere. Inter-Research, Oldendorf, Germany.

Marshall, N. B. (1951). Bathypelagic fishes as sound scatterers in the ocean. *Journal of Marine Research*, *10*(1), 1-17.

Mcclatchie, S., Thorne, R. E., Grimes, P., & Hanchet, S. (2000). Ground truth and target identification for fisheries acoustics. *Small*, *47*, 173–191.

McElroy, P. (1974). Geographic patterns in volume-reverberation spectra in the North Atlantic between 33N and 63N*. *The Journal of the Acoustical Society of America*, 394–407.

McGowan, J. A. (1971). Oceanic biogeography of the Pacific. In – The Micropaleontology of the Oceans (S.M. Funnell and W.R. Riedl, Eds.), pp. 3-74. Cambridge University Press, Cambridge.

McManus, M. A., Alldredge, A. L., Barnard, A. H., Boss, E., Case, J. F., Cowles, T. J., Donaghay, P. L., Eisner, L.B., Gifford, D. J., Greenlaw, C. F. and Herren, C. M. (2003). Characteristics, distribution and persistence of thin layers over a 48 hour period. *Marine Ecology Progress Series*, *261*, 1.

McManus, M. A., Cheriton, O., Drake, P., Holliday, D., Storlazzi, C., Donaghay, P. L., & Greenlaw, C. F. (2005). Effects of physical processes on structure and transport of thin zooplankton layers in the coastal ocean. *Marine Ecology Progress Series*, *301*, 199–215.

McNab, B. K. (1971). On the ecological significance of Bergmann's rule. *Ecology*, 845-854.
Menon, N., & Devi, P. (1990). First Workshop on scientific results of forv sagar sampada. *Proceedings of the First Workshop on Scientific Results of FORV Sagar Sampada*, 257–271.

Mobley, C. D. (1994). *Light and water: radiative transfer in natural waters*. Academic press.

Moore, H. B. (1948). *Report on the biological interpretation of the deep scattering layer in the North Atlantic*. Woods Hole Oceanographic Institution.

Moore, H. B. (1950). The relation between the scattering layer and the Euphausiacea. *The Biological Bulletin*, 181–212.

Morel, A. (1991). Light and marine photosynthesis: a spectral model with geochemical and climatological implications. *Progress in oceanography*, *26*(3), 263-306.

Morel, A., & Berthon, J. F. (1989). Surface pigments, algal biomass profiles, and potential production of the euphotic layer: Relationships reinvestigated in view of remote-sensing applications. *Limnology and Oceanography*, *34*(8), 1545–1562.

Neighbors, M. A., & Nafpaktitis, B. G. (1982). Lipid compositions, water contents, swimbladder morphologies and buoyancies of nineteen species of midwater fishes (18 myctophids and 1 neoscopelid). *Marine Biology*, *66*, 207–215.

Nicol, S., Pauly, T., Bindoff, N. L., Wright, S., Thiele, D., Hosie, G. W., Strutton, P. G. and Woehler, E. (2000). Ocean circulation off east Antarctica affects ecosystem structure and sea-ice extent. *Nature*, *406*(August), 504–507.

Nelson, D. R., McKibben, J. N., Strong Jr, W. R., Lowe, C. G., Sisneros, J. A., Schroeder, D. M., & Lavenberg, R. J. (1997). An acoustic tracking of a megamouth shark, Megachasma pelagios: a crepuscular vertical migrator. *Environmental Biology of Fishes*, *49*(4), 389-399.

Nelson, J. S. (2006). *Fishes of the World*. John Wiley & Sons.

Netburn, A. N., & Koslow, J. A. (2015). Dissolved oxygen as a constraint on daytime deep scattering layer depth in the southern California current ecosystem. *Deep Sea Research Part I: Oceanographic Research Papers*, *104*, 149-158.

Odum, E.P. (1971). Fundamental of Ecology. Saunders, Philadephia.

Orr, J. C., Fabry, V. J., Aumont, O., Bopp, L., Doney, S. C., Feely, R. A., Gnanadesikan, A., Gruber, N., Ishida, A., Joos, F., et al. (2005). Anthropogenic ocean acidification over the twenty-first century and its impact on calcifying organisms. *Nature*, *437*(7059), 681–6.

Page, E. S. (1954). Continuous inspection schemes. *Biometrika*, 100-115.

Pakhomov, E. A., Perissinotto, R., & McQuaid, C. D. (1996). Prey composition and daily rations of myctophid fishes in the Southern Ocean. *Marine Ecology Progress Series*, *134*(1-3), 1–14.

Pauly, D., Christensen, V., Dalsgaard, J., Froese, R., & Torres, F. (1998). Fishing down marine food webs. *Science*, *279*(5352), 860-863.

Pieper, R. E. (1979). Euphausiid distribution and biomass determined acoustically at 102 kHz. *Deep Sea Research Part A. Oceanographic Research Papers*, *26*(6), 687-702.

Pitcher, T., & Cochrane, K. (2002). The use of ecosystem models to investigate multispecies management strategies for capture fisheries.

Phleger, C. F., Nichols, P. D., & Virtue, P. (1997). The lipid, fatty acid and fatty alcohol composition of the myctophid fish Electrona antarctica: high level of wax esters and food-chain implications. *Antarctic Science*, *9*(3), 258–265.

Proud, R., Cox, M. J., Wotherspoon, S., & Brierley, A. S. (2015). A method for identifying Sound Scattering Layers and extracting key characteristics. *Methods in Ecology and Evolution*, *6*(10), 1190–1198.

Rabindranath, A., Daase, M., Falk-Petersen, S., Wold, A., Wallace, M. I., Berge, J., & Brierley, A. S. (2010). Seasonal and diel vertical migration of zooplankton in the High Arctic during the autumn midnight sun of 2008. *Marine Biodiversity*, *41*(3), 365–382.

Rasmussen, O. I., & Giske, J. (1994). Life-history parameters and vertical distribution of Maurolicus muelleri in Masfjorden in summer. *Marine Biology*, *120*(4), 649-664.

Reid, J. L., Brinton, E., Fleminger, A., Venrick, E. L. and McGowan, J. A., (1978). Ocean circulation and marine life. In *Advances in oceanography* (pp. 65-130). Springer US.

Reid, D. G. & Simmonds, E. J. (1993). Image analysis techniques for the study of fish school structure from acoustic survey data. *Canadian Journal of Fisheries and Aquatic Sciences*, 50, 886–893.

Renfree, J. and Demer, D. (2015). Optimizing transmit interval and logging rate while avoiding aliased seabed echoes. In the 7th ICES sponsored Symposium on Fisheries Acoustics and Technology investigating aquatic ecosystems, Nantes, May, 2015.

Ressler, P. H., De Robertis, A., Warren, J. D., Smith, J. N., & Kotwicki, S. (2012). Developing an acoustic survey of euphausiids to understand trophic interactions in the Bering Sea ecosystem. *Deep Sea Research Part II: Topical Studies in Oceanography*, *65-70*, 184–195.

Ringelberg, J. (1999). The photobehaviour of Daphnia spp. as a model to explain diel vertical migration in zooplankton. *Biological Reviews of the Cambridge Philosophical Society*, *74*(04), 397–423.

Robertis, A. De, Higginbottom, I., De Robertis, A., & Higginbottom, I. (2007). A post-processing technique to estimate the signal-to-noise ratio and remove echosounder background noise. *ICES Journal of Marine Science*, *64*(6), 1282–1291.

Robertis, A. De, Jaffe, J. S., & Ohman, M. D. (2000). Size-dependent Predation Risk and the Timing of Vertical Migration in Zooplankton, 1838–1844.

Roberts, C. M., Hawkins, J. P., & Gell, F. R. (2005). The role of marine reserves in achieving sustainable fisheries. *Philosophical Transactions of the Royal Society of London B: Biological Sciences*, *360*(1453), 123-132.

Robinson, C., Steinberg, D.K., Anderson, T.R., Arístegui, J., Carlson, C.A., Frost, J.R., Ghiglione, J.F., Hernández-León, S., Jackson, G.A., Koppelmann, R., et al. (2010). Mesopelagic zone ecology and biogeochemistry - A synthesis. *Deep-Sea Research Part II: Topical Studies in Oceanography*, *57*(16), 1504–1518.

Robison, B. H. (1984). Herbivory by the myctophid fish Ceratoscopelus warmingii. *Marine Biology*, *84*(2), 119-123.

Robison, B. H. (2009). Conservation of deep pelagic biodiversity. *Conservation Biology : The Journal of the Society for Conservation Biology*, *23*(4), 847–58.

Roquet, F., Madec, G., McDougall, T. J., & Barker, P. M. (2015). Accurate polynomial expressions for the density and specific volume of seawater using the TEOS-10 standard. *Ocean Modelling*, *90*(0), 29–43.

Ryan, T. (2011). Overview of Data Collection, Management and Processing Procedures of Underway Acoustic Data–IMOS BASOOP Sub-Facility.

Ryan, T. E., & Kloser, R. J. (2004). Improving the precision of ES60 and EK60 echosounder applications. *Report of the Working Group on Fisheries Acoustic Science and Technology (WGFAST)*, 20-23.

Sameoto, D. D. (1976). Distribution of sound scattering layers caused by euphausiids and their relationship to chlorophyll a concentrations in the Gulf of St. Lawrence Estuary. *Journal of the Fisheries Board of Canada*, *33*(4), 681-687.

Sameoto, D. D. (1983). Euphausiid distribution in acoustic scattering layers and its significance to surface swarms. *Journal of Plankton Research*, *5*(2), 129-143.

Saunders, R. A., Collins, M. A., Foster, E., Shreeve, R., Stowasser, G., Ward, P., & Tarling, G. A. (2014). The trophodynamics of Southern Ocean Electrona (Myctophidae) in the Scotia Sea. *Polar biology*, *37*(6), 789-807.

Saunders, R. A., Collins, M. A., Ward, P., Stowasser, G., Shreeve, R., & Tarling, G. A. (2015). Distribution, population structure and trophodynamics of Southern Ocean Gymnoscopelus (Myctophidae) in the Scotia Sea. *Polar Biology*, *38*(3), 287-308.

Schnetzer, A., & Steinberg, D. K. (2002). Active transport of particulate organic carbon and nitrogen by vertically migrating zooplankton in the Sargasso Sea. *Marine Ecology Progress Series*, *234*, 71–84.

Schüler, F., & Krefft, G. (1951). Zur Frage der Verwendung des Echographen in der Loggerfischerei (An investigation of the application of echograms in the lugger fishery). Fischereiwelt (Fisheries World), 3(4). 63 pp. (In German).

Scoulding, B., Chu, D., Ona, E., & Fernandes, P. G. (2015). Target strengths of two abundant mesopelagic fish species. *The Journal of the Acoustical Society of America*, *137*(2), 989-1000.

Sekino, T. & Yoshioka., T. (1995). The relationship between nutritional condition and diel vertical migration of Daphnia galeata. *Japanese* Journal of *Limnology*. 56, 145–150.

Sekino, T., & Yamamura, N. (1999). Diel vertical migration of zooplankton: Optimum migrating schedule based on energy accumulation. *Evolutionary Ecology*, *13*, 267–282.

Semina, H. J. (1997). An outline of the geographical distribution of oceanic phytoplankton. *Advances in marine biology*, *32*, 527-563.

Shelford, V. E. (1963). *Ecology of North America*. University of Illinois.

Simard, Y., Lacroix, G., & Legendre, L. (1985). In situ twilight grazing rhythm during diel vertical migrations of a scattering layer of Calanus finmarchicus. *Limnology and Oceanography*, *30*(3), 598–606.

Smith, P., Ohman, M., & Eber, L. (1989). Analysis of the patterns of distribution of zooplankton aggregations from an acoustic doppler current profiler. *CalCOFI Report*, *30*, 88–103.

Strathmann, R. R., (1967). Estimating the organic carbon content of phytoplankton from cell volume or plasma volume. *Limnology and Oceanography*, 12(3), 411–418.

St John, M. A., Borja, A., Chust, G., Heath, M., Grigorov, I., Martin, A. P., Serrão Santos, R. and Mariani, P. (2016). A Dark Hole in our Understanding of Marine Ecosystems and their Services: Perspectives from the mesopelagic community. *Frontiers in Marine Science*, *3*, 31.

Stanton T.K. (2009). Broadband acoustic sensing of the ocean. The Journal of the Marine Acoustics Society of Japan. 36, 95-97.

Stanton, T. K., & Chu, D. (2000). Review and recommendations for the modelling of acoustic scattering by fluid-like elongated zooplankton: euphausiids and copepods. *ICES Journal of Marine Science*, *57*(4), 793–807.

Stanton, T. K., Chu, D., & Wiebe, P. (1996a). Acoustic scattering characteristics of several zooplankton groups. *ICES Journal of Marine Science*, *53*, 289–295.

Stanton, T. K, Chu, D., & Wiebe, P. (1996b). Sound scattering by several zooplankton groups. II. Scattering models. *The Journal of the Acoustical Society of America*, *103*(January), 236–253.

Stanton, T. K., Sellers, C. J., & Jech, J. M. (2012). Resonance classification of mixed assemblages of fish with swimbladders using a modified commercial broadband acoustic echosounder at 1–6 kHz. *Canadian Journal of Fisheries and Aquatic Sciences*, *69*(5), 854–868.

Nielsen, E. S. (1952). The use of radio-active carbon (C14) for measuring organic production in the sea. *Journal du Conseil*, *18*(2), 117-140.

Steuer, A. (1933). Zur planmässigen Erforschung der geographischen Verbreitung des Haliplanktons, besonders. der Copepoden. *Zoogeographica*, *1*(3), 269-302.

Takagi, K., Yatsu, A., Moku, M., & Sassa, C. (2006). Age and growth of lanternfishes, Symbolophorus californiensis and Ceratoscopelus warmingii (Myctophidae), in the Kuroshio-Oyashio Transition Zone. *Ichthyological Research*, *53*(3), 281–289.

Tarasov, L. L. (2002). Deep scattering layers in the northwestern pacific. *Acoustical Physics*, *48*(1), 81–86.

Tarling, G. A., Matthews, J. B. L., David, P., Guerin, O., & Buchholz, F. (2001). The swarm dynamics of northern krill (Meganyctiphanes norvegica) and pteropods (Cavolinia inflexa) during vertical migration in the Ligurian Sea observed by an acoustic Doppler current profiler. *Deep Sea Research Part I: Oceanographic Research Papers*, *48*(7), 1671-1686.

Tchernia, P. (1949). Observations d'oceanographie biologique faites par l'aviso polaire'Commandant Charcot'pendant la campagne 1948-9'. *Bull. Inf. Com. Centre. Oceanographie et d'Etudes des Cotes I*, *50 (In French)*.

Torgersen, T. (2001). In situ swimming behaviour of individual mesopelagic fish studied by split-beam echo target tracking. *ICES Journal of Marine Science*, *58*(1), 346–354.

Trout, G. C., Lee, A. J., Richardson, I. D., & Jones, F. H. (1952). Recent echo sounder studies. Nature. 71-72.

Tucker, G. H. (1951). Relation of fishes and other organisms to the scattering of underwater sound. *Journal of marine research*, *10*(2), 215-238.

Urmy, S. S., Horne, J. K., & Barbee, D. H. (2012). Measuring the vertical distributional variability of pelagic fauna in Monterey Bay. *ICES Journal of Marine Science*, *69*(2), 184–196.

UNESCO. (2009). Global Open Oceans and Deep Seabed (GOODS) – Biogeographic Classification. Paris, UNESCO-IOC. (IOC Technical Series, 84.)

van Minnen, J. G., Goldewijk, K. K., Stehfest, E., Eickhout, B., van Drecht, G., & Leemans, R. (2009). The importance of three centuries of land-use change for the global and regional terrestrial carbon cycle. *Climatic Change*, *97*(1), 123–144.

Walters, C., Christensen, V., & Pauly, D. (1997). Structuring dynamic models of exploited ecosystems from trophic mass-balance assessments. *Reviews in fish biology and fisheries*, *7*(2), 139-172.

Walters, A., Lea, M. A., van den Hoff, J., Field, I. C., Virtue, P., Sokolov, S., Pinkerton, M. H. & Hindell, M. A. (2014). Spatially Explicit Estimates of Prey Consumption Reveal a New Krill Predator in the Southern Ocean. *PloS one*, *9*(1), e86452.

Watkins, J. L., & Brierley, A. S. (1996). A post-processing technique to remove background noise from echo integration data. *ICES Journal of Marine Science*, *53*, 339–344.

Watkins, J. L., Morris, D. J., Ricketts, C., & Murray, A. W. A. (1990). Sampling biological characteristics of krill: effect of heterogeneous nature of swarms. *Marine Biology*, *107*(3), 409-415.

Watkins, J. L., & Murray, A. W. A. (1998). Layers of Antarctic krill, Euphausia superba: are they just long krill swarms? *Marine Biology*, *131*(2), 237-247.

Webb, T. J., Berghe, E. V., & O'Dor, R. (2010). Biodiversity's big wet secret: the global distribution of marine biological records reveals chronic under-exploration of the deep pelagic ocean. *PLoS One*, *5*(8), e10223.

Webster, C. N., Hansson, S., Didrikas, T., Gorokhova, E., Peltonen, H., Brierley, A. S., & Lehtiniemi, M. (2015). Stuck between a rock and a hard place: zooplankton vertical distribution and hypoxia in the Gulf of Finland, Baltic Sea. *Marine Biology*, *162*(7), 1429-1440.

Weston, D. (1958). Observations on a scattering layer at the thermocline. *Deep Sea Research (1953)*, *5*, 44–50.

Wilson, E.O. (1994). Biodiversity: Challenge, science, opportunity. *American Zoologist*, 34, 5–11.

Witek, Z., Kalinowski, J., Grelowski, A., & Wolnomiejski, N. (1981). Studies of aggregations of krill (*euphausia-superba*). Meeresforschung-reports on marine research, *28*(4), 228-243.

Yasuma, H., Sawada, K., Ohshima, T., Miyashita, K., & Aoki, I. (2003). Target strength of mesopelagic lanternfishes (family Myctophidae) based on swimbladder morphology. *ICES Journal of Marine Science*, *60*(3), 584–591.

Yasuma, H., Sawada, K., Takao, Y., Miyashita, K., & Aoki, I. (2009). Swimbladder condition and target strength of myctophid fish in the temperate zone of the Northwest Pacific. *ICES Journal of Marine Science*, *67*(1), 135–144.

Yasuma, H., Takao, Y., Sawada, K., Miyashita, K., & Aoki, I. (2006). Target strength of the lanternfish, Stenobrachius leucopsarus (family Myctophidae), a fish without an airbladder, measured in the Bering Sea. *ICES Journal of Marine Science*, *63*(4), 683–692.

Yool, A., Popova, E. E., Coward, A. C., Bernie, D., & Anderson, T. R. (2013). Climate change and ocean acidification impacts on lower trophic levels and the export of organic carbon to the deep ocean. *Biogeosciences*, *10*(9), 5831-5854.

Young, J. W., Bulman, C. M., Blaber, S. J. M., & Wayte, S. E. (1988). Age and growth of the lanternfish Lampanyctodes hectoris (Myctophidae) from eastern Tasmania, Australia. *Marine Biology*, *99*(4), 569–576.

Appendix A: Disclaimer of collaborative contributions

Chapter 3

The work presented in this chapter has been published:

Proud, R., Cox, M.J., Wotherspoon, S. & Brierley, A.S. *A method for identifying Sound Scattering Layers and extracting key characteristics.* Methods in Ecology and Evolution, 2015. **6**(10): p. 1190-1198.

Data were downloaded from the Integrated Marine Observing System (IMOS) and processed by myself.

Chapter 4, 5 & 6

The work presented in these chapters is currently being prepared for publication as

Proud, R., Cox, M.J., & Brierley, A.S. TBD in Current Biology.

Acoustic data were collected on board the R/V Polarstern and obtained from British Oceanographic Data Centre (BODC, 2014) the Integrated Marine Observing System (IMOS, 2013), British Antarctic Survey (BAS), the Pelagic Ecology Research Group (PERG) and from a recent cruise on the RRS James Clark Ross, Surface Mixed Layer Evolution at Sub-mesoscales Cruise (SMILES, 2015). Ocean variables were obtained from Simple Ocean Data Assimilation (SODA) product (Carton et al., 2000), Ocean Productivity website (http://www.science.oregonstate.edu/ocean.productivity/index.php) and output from NEMO-MEDUSA-2.0 was provided by Andrew Yool.

Appendix B: Derivation and definition of acoustic variables

Derivation of backscatter variables

The backscatter cross section of a single target (σ_b) is

$$\sigma_{bs} = R^2 I_b / I_i$$

where σ_{bs}can be conceived as the area of the incident wave (I_i) intercepted by the target of which the power is then retransmitted as the backscattered wave (I_b). R is the distance from the target.

and the **Target Strength** (TS) is then

$$TS = 10\log(\sigma_{bs})$$

with units of dB re 1m^2.

For many targets within a volume the **volume backscattering coefficient** ($\mathbf{s_v}$) is

$$s_v = \sum \sigma_{bs} / V_0$$

where V_0 is the minimum sample volume that is dependent on pulse duration and beam angle of the transducer.

For the energy returned by a layer over a depth range, the **area backscattering coefficient** (s_a) is:

$$s_a = \int_{z2}^{z1} s_v dz$$

with units m^2/m^2

Where z1 and z2 are the two depths marking the extent of the layer range. The **nautical area scattering coefficient** (NASC - s_A) is then

$$s_A = 4\pi(1852)^2 s_a$$

with units m^2/nmi^2

The 4π term is added to calculate the total energy scattered (spherical as opposed to backscattered wave) and remains there purely due to historical reasons (MacLennan & Simmonds, 2005).

The **volume backscattering strength** (S_v) is then

$$S_v = 10log(s_v)$$

with units of dB re 1m^{-1},

and the **Mean Volume Backscattering Strength** (MVBS) for many pings over a certain depth range is

$$MVBS = 10log(\bar{s}_v)$$

with units of dB re 1m^{-1}.

Appendix C: Deep Scattering Layers: A history

Deep scattering layers (DSLs) were discovered during WWII. They were observed in the Pacific Ocean and the data was analysed and published by the University of California (1942-1946). The phenomenon was originally conceived to be of a physical origin and a lot of the early work (1946-1950) reflected that (Duvall and Christensen, 1946; Hersey & Moore, 1948; Moore, 1948; Eyring et al., 1948; Dietz, 1948; Johnson, 1948). During the following decade, DSL observations were made consistently throughout the Atlantic and Pacific Oceans, within shallower regions, namely the English Channel, Barents Sea and the North Sea (Burd & Lee, 1951) but very few in the Polar Regions (Dietz, 1948). Tchernia (1949) believed DSLs to be universal, but the concept was not generally accepted until much later. At the time, low frequency echosounders were in use, that exhibited large near-field ranges and poor resolution; the success of Tchernia was owed to his use of a relatively high frequency instrument, which enabled him to observe smaller organisms. Throughout the next 50 years two chains of study were developed, the first concerning the composition of DSLs, and the other, its changing structure as a consequence of the physical environment; important milestones in the history of DSLs are shown in chronological order in Fig C1.

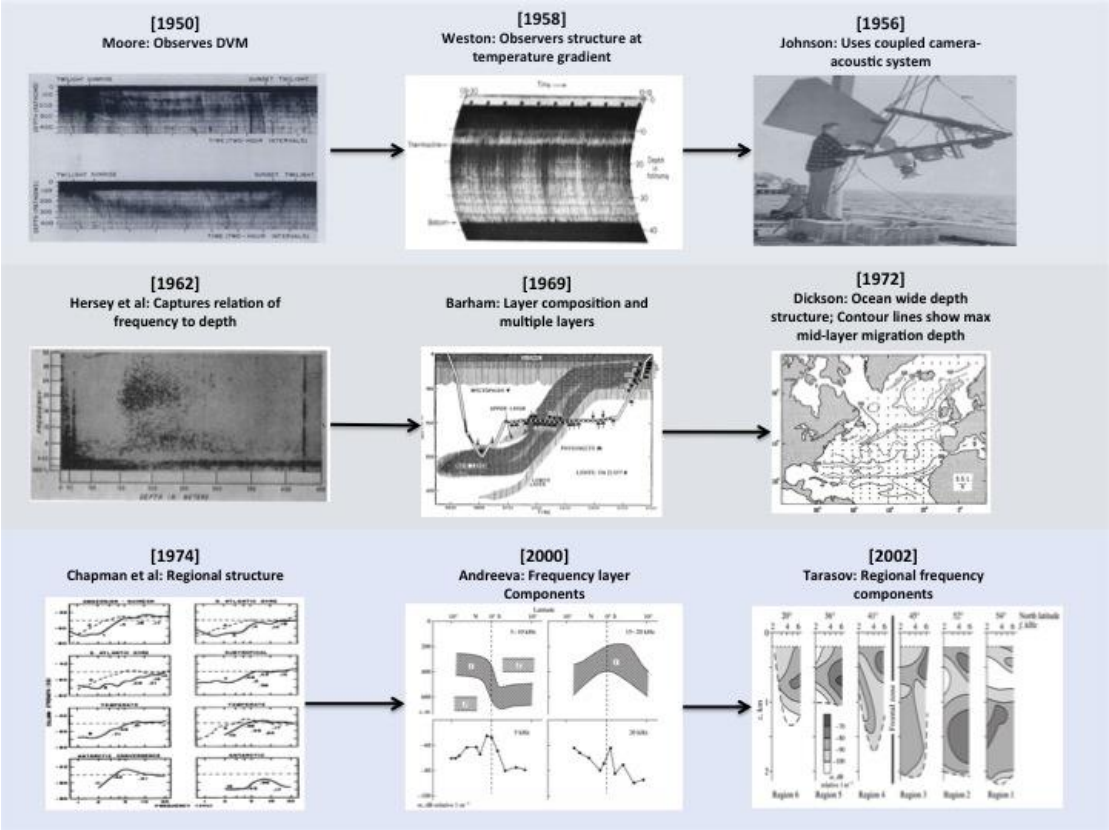

Figure C1: Important milestones in Deep Scattering Layer history

DSL Composition

Lyman, (1948) linked DSLs to a biological origin and made the connection to diel vertical migration (DVM), hypothesizing that DSLs or 'the sea's phantom bottom' (as it was then named by the Hydrographic Office) were made up primarily of squid; based on the observed ascent speeds and the ubiquitous nature of the organism. DVM was a well-known concept at the time, but had only previously been observed using well-timed in-situ trawls - see Cushing (1951) for a review. In fact, an English sea captain named Ronald Balls, observed DVM acoustically in the thirties, however, Balls was no scientist and was unable to make the connection to DVM (Balls, 1948). Moore (1950) gave a comprehensive description of the layer, when he observed a more diverse DSL constituting of fish, squid and crustacea, which exhibited a species relation with depth. The presence of fish was also observed by Marshall (1951) and Tucker (1951) but was not confirmed until the first camera (Johnson et al., 1956) and television (Backus & Barnes, 1958) assisted acoustic studies, the quality of which was far too poor to notice any zooplankton. Hersey & Backus (1954), identified the swimbladder as a strong source of reverberation (previously suggested by Burd & Lee, 1951) when tracking

organism's resonant frequencies within DSLs as they migrated, much like that of a gas bubble under varying pressure. This was later confirmed by Hersey et al. (1962) and also by the first observation of fish tracks, using at depth acoustic measurements (Kanwisher & Volkmann, 1955). The majority of early observations used low frequency sounders and as a result were not generally picking up layers of zooplankton; euphausiids, that are now considered major contributors to DSLs worldwide, were ruled out by Boden (1962) and Hersey & Bachus (1962). Barham (1963) claimed that siphonophores were the main contributor but later corrected himself in 1966 after observing vast quantities of myctophids in an underwater submersible. In the late sixties, higher frequency echo sounders were starting to become more popular. High concentrations of zooplankton were observed in DSLs (Kinzer, 1969; Sameoto, 1976; 1983; Pieper, 1979; Witek et al, 1981; Macaulay et al, 1984) showing consistently that aggregations within the layer were orders of magnitude higher, than anywhere outside. In the late seventies, a lot of work was carried out concerning the frequency response of DSLs (e.g. Greenlaw, 1979; Johnson, 1977) relating resonant frequency to animal size (Andreeva, 1964).

Acoustic observations were becoming increasingly more accurate, aided by key advances in calibration techniques made by Foote (1983, 1987): the once mysterious layers were becoming more transparent. In the early nineties, it was under general acceptance that DSLs were diverse (Magnússon, 1996) and were made up of mainly zooplankton species (Giske et al, 1990) and mesopelagic fish (Ramussen & Giske, 1994), which had important implications for predator-prey interactions (Carey & Robison, 1981; Giske et al, 1990; Nelson et al, 1997; Dagorn et al, 2000).

DSL Structure

It is more useful to divide the history of DSL structure into four subcategories: microstructure; topographical influence; oceanic features and temporal change.

The physical properties of the water-column limit the spatial structure of DSLs in a complicated way. The depth range and daily duration of the photic zone is thought to be a key driver in DVM and DSL structure. Early studies observed how isolumes and isotherms greatly controlled migration patterns and timings and also the depth structure of DSLs (Moore, 1950; Schuler & Kreff, 1951; Tucker, 1951; Trout et al, 1952; Cushing, 1955; Cushing & Richardson, 1956; Weston, 1958; Boden & Kampa, 1967). In 1972, Dickson was able to relate ocean transparency to the maximum depth of DSLs across the North Atlantic Ocean, showing that in turbid waters, DSLs appear shallower. This work was important, it countered the earlier hypothesis that

organisms maintained deep migration to transport great horizontal distances to more favourable conditions with little effort (Isaacs et al., 1974). DSLs were also found to be limited by oxygen minimum zones (OMZs) (Chapman & Marshall, 1966) but then were controversially shown to have no effect on zooplankton (Kinzer, 1969); It is the case that OMZs will generally restrict DSLs (Johnson, 1976) but in some cases, these extreme conditions provide additional protection from predation to organisms that can survive in these hostile environments (Klevjer et al., 2012).

DSLs exhibit different characteristics over shallow seabed topograpghy to that of open sea. Increased biomass within DSLs was first observed over seamounts and close to islands by Isaacs & Schwartzlose (1965). These bulges in the layer were shown to be driven by currents that force biota and nutrient rich waters at these systems effectively providing a constant stream of food for any inhabiting species. This mechanism was observed a decade later at a shelf break where deep upwellings of nutrient rich waters fed a dense scattering layer, at the front dividing the inshore continental shelf and open ocean species (Baird et al, 1974; Genin et al, 1988; Holliday, 1987; Pieper et al, 1979; Smith et al., 1989). These studies outlined the interactions between DSLs, the seabed and the continental shelf, underlining the importance of faunal fronts in DSL structure.

Moore (1950) suggested that geographical regions could by classified by the depth structure of DSLs. He also pointed out that the physical properties of the surrounding environment restricted this structure. Herdman (1953) was the first to observe this variance when observing sharp changes in the DSLs around the Antarctic convergence. At the time, broadband technologies were not available and so explosives were employed, covering a low frequency bandwidth up to about 30kHz. Region-to-region variability was demonstrated in the work by Hersey & Backus (1962) when they observed similarities between local areas in the North Atlantic and stark changes in the equatorial regions north of the Bahamas. In 1966, Chapman & Marshall used the total backscatter from the water-column, to compute a single value for each frequency considered, thereby producing a spectral plot associated with each studied site. These column spectra were to become a standard when assessing the similarities between regions and boundaries (Beklenishev, 1964). A large-scale project that studied the structure of DSLs using this metric was carried out between 1953 and 1963 at sites across the Pacific, Atlantic, in the Caribbean, Labrador, Norwegian and Mediterreanean Seas and in Baffin Bay (Chapman et al, 1974). The project included broadband comparison across vast latitudes

and longitudes (including both polar and equatorial sites) across Gyres, currents and fronts and over vast slopes and plains. The study encountered all manner of oceanic features including seamounts and eddies, but such small-scale disturbances would have been dissolved into the larger regional structure. This work categorically demonstrated that acoustic regions and boundaries existed in the world ocean. A similar, but all be it smaller scale study, took place in 1972 in the North Atlantic by McElroy (1974) in which column spectra were compared quantitatively. McElroy, effectively provided an index of similarity (by sum of squares) between the 34 sites studied and grouped values that were similar in value and proximity. In the study, fronts were easily classified owing to their characteristic sharp faunal and physical gradients whereas more gradual variations observed in Gyre systems were less well defined. During the next thirty years of study there was little progress in DSL regional classification. Interesting studies concerning currents in the Eastern tropical Pacific (Davies, 1977) and Greenland Sea are noteworthy and also the ephemeral micro-fronts created by eddies (Owen, 1981; Conte et al., 1986) showing up as small-scale structural changes in DSLs. But the real advances were made by Andreeva et al. (2000) and Tarasov (2002) who characterized regions of the Atlantic and North Western Pacific, respectively, using the depth-frequency structure of the volume scattering strength; an idea which was originally suggested by Moore (1950). Andreeva (2000) split the water column into a number of sheets (up to 3), which represented distinct regions of the DSLs for low and high frequency bands (3-20kHz). Tarasov selected nine depths (down to 1050m) and 4 frequencies (3.15, 4.2, 5.2 and 6.2 kHz) and used a simple clustering technique to divide the region by a backscattering coefficient. Both studies highlighted the potential of dividing the ocean into regions and boundaries using depth structure.

DSLs vary widely on spatial scales but also exhibit variance at temporal scales too. A key driver of DVM and hence DSL structure is light and so there are strong shifts in structure at dusk and dawn. This was recognized almost straight away, but seasonal and annual variances of DSLs where not observed to much later (Haigh, 1970). Mackas and Bohrer (1976) hypothesized that feeding strategy would affect the acoustic response of fauna during the night, this was later confirmed by Simard et al. (1985) who observed 'Twilight grazing', where biota exhibited a second migration at twilight to feed once more before descending to depth. Day-to-day changes were observed at coarse scales (1-100km) showing up as micro-patches within DSLs (Greenlaw & Pearcy, 1985; Smith et al., 1989). In the early nineties a lot more work was carried out to measure seasonal changes, notably Menon & Devi (1990) within the Indian Exclusive

Economic Zone, observing peaks in the months of April and December whereas Fischer & Visbeck (1993) observed weak migrations in the Greenland Sea during the summer and the polar night. Importantly, diapause was indicated by Heath et al. (2000) as a key reason for reductions in DSL biomass over winter periods. Inter- annual events such as the El-Nino Southern Oscillation (ENSO) have not been assessed in terms of DSL structure to date. It would be expected however that the large-scale anomalies associated with such events would contribute to the annual variance of DSL structure.

Appendix D: Myctophidae relationships

Below are available length-weight, Target Strength-length and length-age relationships for lanternfish obtained from the literature.

Myctophidae species	Mean length (mm)	a	b	DW	mean DW as a % of WW	Min (mm)	Max (mm)	Source
Electrona antarctica	52.8	0.0002	3.706	Yes	25.3	25	85	1
Gymnoscopelus nicholsi	115.3	0.0009	3.296	Yes	40	69.1	139	1
Gymnoscopelus opisthopterus	113.1	0.00003	3.873	Yes	20.2	64	153.5	1
Electrona paucirastra	58.1	0.0008	3.312	Yes	26	48.5	65.8	1
Metelectrona herwigi	49.7	0.0011	3.363	Yes	34.6	46.3	57	1
Gymnoscopelus bolini	56.6	0.0004	3.377	Yes	24.4	24.3	98.1	1
Protomyctophum normani	29.3	0.0032	2.99	Yes	25.9	17.5	55.5	1
Diaphus taaningi	40.5	0.0006	3.332	Yes	22.8	12.4	59.5	1
Diaphus hudsoni	40.4	0.0012	3.236	Yes	29.3	15	47.3	1
Ceratoscopelus warmingi	51.3	0.0004	3.361	Yes	21.7	16.5	74.6	1
Symbolophorus boops	74.7	0.0002	3.517	Yes	24.6	25	96.1	1
Diaphus dumerilii		3.00E-06	3.181	No		25	95	2
Diaphus garmani		2.00E-05	2.72	No		26	50	2
Diaphus perspicillatus		4.00E-06	3.195	No		47	104	2
Hygophum hygomii		4.00E-06	3.21	No		34	77	2
Lepidophanes guentheri		2.00E-06	3.218	No		25	80	2
Myctophum affine		3.00E-06	3.178	No		24	60	2
Notoscopelus caudispinosus		3.00E-06	3.213	No		27	70	2
Scolopsis multipunctatus		7.00E-07	3.534	No		34	91	2

Table D1: Length-weight relationships (dry weight (mg) = a*length (mm)^{b}) of Myctophidae species. Where DW is dry weight, WW, wet weight and the source references are: 1 - Pakhomov et al., 1996; 2 - Bernardes and Rossi-Wongtschowski, 2000.

Myctophidae species	swimbladder	a	b	source
Ceratoscopelus warmingii	No	49.4	112.2	1
Diaphus chrysorhyncus	No	30.5	96.3	1
Diaphus garmani	No	54	113.5	1
Myctophum punctatum	No	52.7	108.3	1
Notoscopelus japonicus	No	20	86.7	2
Symbolophorus californiensis	No	20	85.7	3
Ceratoscopelus warmingii	Yes	26.3	78.1	1
Diaphus garmani	Yes	34.5	83.5	1
Diaphus theta	Yes	11.8	63.5	2
Myctophum asperum	Yes	45.4	88.6	1

Table D2: Target Strength (TS)-length (L) relationships of Myctophidae species (TS (dB re 1m^2) = a*log$_{10}$(L(cm)) - b) with and without swimbladders. Source references: 1 - Yasuma et al., 2009; 2 - Yasuma et al., 2003; 3 - Yasuma et al., 2006.

Myctophidae species	Length-Age relationship	Reference
Engraulis japonicus	$L = 148.2(1 - 0.9153e^{(-0.004733A)})$	Hayashi and Kondo, 1957
Sardinops melanostictus	$L = 223.9(1 - e^{(-0.87(A-17.63))})$	Nakai and Hayashi, 1962
Symbolophorus californiensis	$L = 128(1 - e^{(0.003(A-1.52))})$	Takagi et al, 2006
Ceratoscopelus warmingii	$L = 80.8(1 - e^{(-0.00769(A-34.4))})$	Takagi et al, 2006*
Diaphus dumerilii	$L = 74.86(1 - e^{(-0.005(A+1.82))})$	Gartner,1991
Myctophum asperum	$L = 85e^{(-1.886e^{(-0.01A)})}$	Hayashi et al, 2001**
Diaphus theta	$L = 3.54 + 0.129A$	Moku et al, 2001***

Table D3: Length (L, mm) - age (A, days) relationships of Myctophidae species. *specimens larger than 20mm **assuming 60 days for larval and metamorphoses stage ***juveniles only.

Appendix E: Ocean Phenomenon

The deep ocean remains the most unexplored environment on Earth. Below are some deep ocean phenomena captured by echosounders.

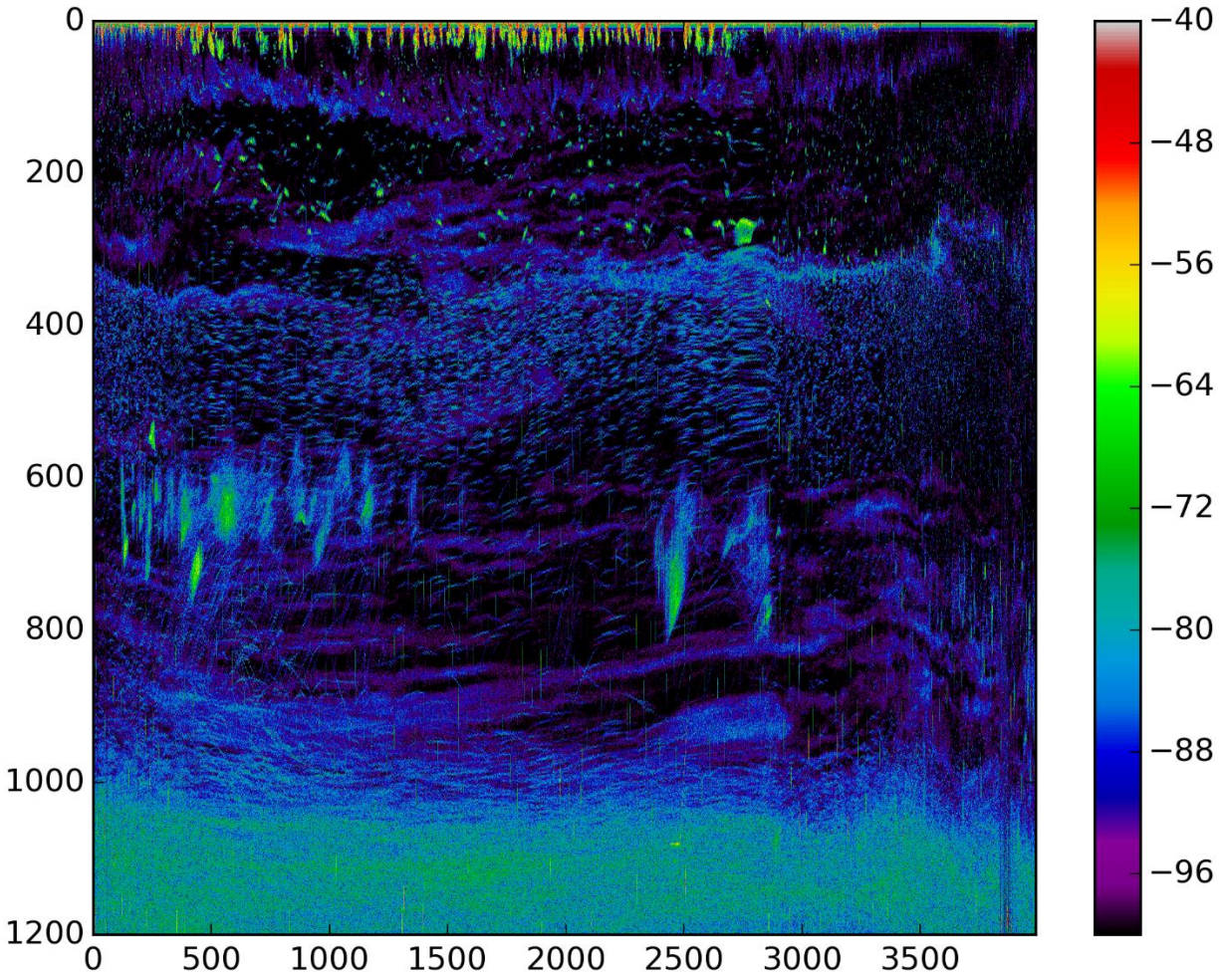

Figure E1: Biological Chaos in the Ocean. Reminiscent of a Van Gogh night-time piece. A very deep scattering layer dwells at 1000m.